Optically Stimulated Luminescence dating of ice-marginal palaeosandar from the last Irish Sea Ice-Stream

Thesis submitted in accordance with the requirements of the University of Liverpool for the degree of Doctor in Philosophy by *Ian Mark Thrasher*

November 2008

In memory of *Grandad,*
Uncle John and *Laura.*

Optically Stimulated Luminescence dating of ice-marginal palaeosandar from the last Irish Sea Ice-Stream

IM Thrasher

In the British and Irish Isles there has been considerable research effort expended in improving understanding of the expansion and retreat of the last ice-sheet (Marine Isotope Stage 2) but the chronological control for the Last Glacial Maximum (LGM) extent and subsequent retreat phases of the British and Irish Ice-sheet (BIIS) is poor. Based on results from extensive sedimentological and stratigraphic studies of fossil ice-marginal sandar at *Orrisdale* (Isle of Man), *Co. Wexford* (south-eastern Ireland) and *Porth Dinllaen* (north-western Wales), a suite of glaciofluvial lithofacies were identified and sampled for OSL analysis, with the ultimate aim of dating the retreat of the Irish Sea Ice-Stream (ISIS) during the last deglaciation of the Irish Sea basin. Complete bar-form fining-up sequences were targeted as they are typically indicative of waning or shallow water flow, allowing sufficient opportunity for bleaching of quartz grains within these glaciofluvial deposits.

Different grain size fractions of quartz were extracted and the SAR protocol applied using small aliquots (~30 grains) to identify which depositional environments and grain size fractions were best suited for optical dating. Equivalent dose (D_e) distributions for all samples showed wide and positively skewed characteristics with overdispersion values >40%, indicative of heterogeneous bleaching. The 'age' model decision-protocol of Bailey and Arnold (2006) was used to choose the most applicable 'age' model (i.e. Minimum Age Model; MAM, Central Age Model; CAM or Lowest 5% Model; L5%) by analysing the D_e distribution via weighted skewness, kurtosis and overdispersion. This enabled a statistically informed choice to be made as to which 'age' model was appropriate for burial dose estimation.

No observable difference was evident between the ages calculated for different grain size fractions of the same sample; agreement within 2σ errors was observed. Glaciofluvial sandur systems appear to act as an efficient 'mixer' of sediment grains, allowing some to be well-bleached and others to be poorly-bleached, with no bias towards preferential bleaching of a particular grain size fraction. However differences between ice-proximal and ice-distal depositional sub-environments were more evident. The ice-distal Orrisdale and Porth Dinllaen samples showed better bleaching characteristics (as observed from skewness and overdispersion parameters) than the ice-proximal Wexford samples. Age overestimation was observed for the Wexford samples, even using the MAM. The only obvious lithofacies difference observed was that of the trough cross-bedded sample (laterally extensive deep sandur palaeo-channel) taken from Orrisdale which showed very poor bleaching characteristics in comparison to the other samples taken from this field site, once again, resulting in significant age overestimation.

Ages of ~ 23 ka were calculated for Wexford samples, indicative of almost immediate retreat of the ice-stream margin from its LGM extent off the north coast of the Scilly Isles and the Celtic Sea to the present-day coastline of Co. Wexford. The OSL age from Porth Dinllaen is ~21 ka, indicative of continued northwards retreat, albeit in a slower and more oscillatory manner, due to the stabilisation of the ice-stream as it was constrained by the narrow corridor of land between Wales and Ireland. Ages in the range of 17-14 ka were calculated for the Orrisdale samples, coincident with the Heinrich Event 1/Killard Point stadial readvance in north-eastern Ireland. In combination with previously published ages, a detailed Bayesian model-derived retreat sequence for the ISIS was established which allowed estimated retreat rates to be calculated for different ice-marginal phases.

ACKNOWLEDGEMENTS

Firstly I would like to thank my supervisors; Richard Chiverrell, Barbara Mauz and Andreas Lang for their time, encouragement and critical insight. Thanks also for your help in the field – those sections would have been very intimidating without you to guide me through. I owe a huge depth of gratitude to Geoff Thomas for fuelling my interest in glacial environments from undergraduate level with his endless enthusiasm. The undergraduate dissertation trip to Norway really did capture my interest! Thanks for all your help and wisdom in the field – especially in those huge quarries in Ireland – quite intimidating to a novice sedimentologist!

Many thanks to Susan Packman and Zhixiong Shen; Susan, thanks for making sure I was able to use the Risø machines when I really needed to and for your encouragement and helpful insights. Thanks also to Zhixiong for your help with the seemingly endless LM- and CW-OSL curve fitting in OriginPro– without you I would still be sat here trying to figure out how to do it in SigmaPlot!

Over the past three years I have had many helpful discussions with people in the research community which have helped me to develop academically, and so many thanks go to; Ed Rhodes, Helena Rodnight, Mark Bateman, Ruth Robinson, Rex Galbraith, Claire Boulter, Lee Arnold and Ashok Singhvi. Thanks are also extended to Uwe Reiser at Victoria University of Wellington in New Zealand for undertaking additional gamma spectrometric analysis on Wexford and Porth Dinllaen samples.

I would like to thank all the lab technicians at the University of Liverpool; Hilda, Irene, Alan and Bob. Special thanks are extended to Irene to her help and patience with HF preparation – thanks for stepping in to help me many a time! The Cartographics staff have also been of great help with the preparation and printing of conference posters, and all their hard work in helping us to organise the QRA Postgraduate Conference 2008; thanks Sandra, Suzanne and Ian! Tinho, you have also been a huge help to us in organising the conference; you stopped us from panicking and undertook a great deal of effort on our behalf – thank you! The secretarial and administrative staff have also been of great assistance throughout the past three years; Andrea, Jayne, Mary and Claire – thank you!

Thanks to all the geography staff and postgrads who have been of great encouragement, from including me in 5-a-side football (as horrifically rubbish as I am) to keeping me company at coffee-time; Katharine (my office buddy), Lee, Claire, Mary, Hayley, Lynda, Anthony, Ivo, Andy, Ashley, Liz & Greg and Angel. My friends from home and away have successfully been able to distract me from the PhD; thanks to Kate, Ellen, Hannah, Olly, Biggs, James, Sweeney (my PT!), Laura & Simon, Charlotte & Becky, Sarah K, Jarlath & Sarah C, Nic & Terry, Kathryn and Nad.

Finally, I owe my Mum, Dad and Eric an endless number of thank yous! Mum and Dad you have always supported me in whatever I have done. You are always there for me, encouraging me and keeping me fed and watered on Friday evenings! Eric, what would I have done without you over the past two years? You have kept me completely happy and been able to encourage me and keep me motivated with weekends camping and holidays to more exotic locations! Thank you so much for your encouragement and patience when I was stressed!

CONTENTS

Front cover photographs:
Top centre: A view over the northern plain of the Isle of Man with the Bride Moraine visible in the distance.
Bottom centre: The Blackwater sand and gravel pit in Co. Wexford, south-eastern Ireland.

LIST OF FIGURES

Appendix A

Appendix B

LIST OF TABLES

Appendix C

LIST OF ACRONYMS

AEA	Architectural Element Analysis
AMS	Accelerator Mass Spectrometry
BIC	Bayesian Information Criterion
BIIS	British and Irish Ice-Sheet
BP	years Before Present (AD. 1950)
CW-OSL	Continuous-Wave OSL
CAM	Central Age Model
D_e	Equivalent Dose
FMM	Finite Mixture Model
IR	Infra-Red
IRSL	Infra-Red Stimulated Luminescence
ISB	Irish Sea Basin
ISIS	Irish Sea Ice Stream
L5%	Lowest 5% Model
LED	Light Emitting Diode
LGM	Last Glacial Maximum
LM-OSL	Linearly-Modulated OSL
MAM-3	Minimum Age Model (3 parameters)
MAM-4	Minimum Age Model (4 parameters)
MIS	Marine Isotope Stage
OD	Ordnance Datum
OSL	Optically Stimulated Luminescence
PH_1	Preheat (that applied before natural and regenerated signals)
PH_2	Cutheat (that applied before test dose signal)
RR	Recycling Ratio
SAAD	Single-Aliquot Additive-Dose protocol
SAR	Single-Aliquot Regenerative-Dose protocol
SIEM	Southern Ireland End Moraine
SSC	Suspended Sediment Concentration
TL	Thermoluminescence
TT	Thermal Transfer
UV	Ultra-Violet

Chapter 1

GENERAL INTRODUCTION

In the British and Irish Isles there has been considerable research effort expended in improving understanding of the expansion and retreat of the last ice-sheet (Marine Isotope Stage 2) (Evans and Ó Cofaigh, 2003a; Clark, et al., 2004a; Ó Cofaigh and Evans, 2007), but the chronological control for the timing of the Last Glacial Maximum (LGM) extent and subsequent retreat stages of the British and Irish Ice-Sheet (BIIS) is poor when compared to the Laurentide Ice-sheet (Miller, et al., 1999; Marsella, et al., 2000; England, et al., 2006; Carlson, et al., 2007). In part, this problem reflects the paucity of material dateable by radiocarbon techniques; however considerable strides have and are being made by applying optical (Duller, 1994; Olley, et al., 2004; Duller, 2006) and cosmogenic (Ballantyne, et al., 2006, 2007; Golledge, et al., 2007; Ballantyne, et al., 2008) dating techniques to glacigenic sediments.

The attraction of optical dating lies in that it directly dates the time of deposition using the quartz and feldspars that dominate the *glaciofluvial* sediments of interest in this research. The optical dating signal itself is acquired by individual minerals through exposure to environmental radiation within sedimentary bodies. The signal is reset or bleached through exposure to daylight during transportation processes. Thus Optically Stimulated Luminescence (OSL) dating of sediments attempts to determine the time elapsed since burial. Optical dating techniques have been used to date sediments successfully from a wide range of depositional environments; however the

application of this technique to glacigenic sediments has proven to be more challenging due to issues relating to the lack of opportunity for sufficient bleaching of minerals in glacial environments. A detailed review of the challenges faced when undertaking OSL dating of glacial sediments is given in Chapter 2.

This research focuses upon the development of OSL dating for application with glaciofluvial deposits. The primary aim is to develop a better understanding as to the rate of retreat of the Irish Sea Ice-Stream (ISIS) during late MIS 2. This is achieved by using OSL dating to provide a chronology as to when the ISIS deposited ice-marginal glaciofluvial sediments at three locations around the perimeter of the present-day Irish Sea Basin. These locations are *Orrisdale* on the Isle of Man (Thomas, 1977, 1985; Thomas, et al., 1985; Chiverrell, et al., 2001; Chiverrell, et al., 2004; Thomas, et al., 2006; Roberts, et al., 2007), *Wexford* in south-eastern Ireland (Summers, 1981; Thomas and Summers, 1982; 1983; Thomas and Kerr, 1987), and *Porth Dinllaen* on the Llŷn peninsula in North Wales (Thomas, et al., 1998; Thomas and Chiverrell, 2007).

Here a directed approach to sediment sampling was undertaken to evaluate which ice-marginal sandur sub-environments (e.g. channel, bar-top, back-bar, bar-growth, overbank) were most likely to produce assemblages of quartz grains that had been sufficiently bleached. Within these depositional sub-environments different grain size fractions within individual samples were targeted to tighten the sediment/process characterised and explore any grain size dependence upon OSL resetting.

A range of methodological techniques and statistical 'age' models were used to deal with heterogeneous bleaching and poor quartz luminescence characteristics. Several 'age' models have been published which address the problem of deriving the best single-valued estimate of the burial dose from such heterogeneously-bleached equivalent dose (D_e) distributions (e.g. Galbraith and Green, 1990; Olley, et al., 1998; Galbraith, et al., 1999) further explanation of which is given in Chapters 2 and 5. Bailey and Arnold (2006) produced the first statistically-based decision-protocols to enable the appropriate 'age' model to be chosen and used for equivalent dose (D_e) and subsequent age determination. This decision-protocol was derived for single-grains of heterogeneously-bleached fluvial sediments and this research assesses the appropriateness of the decision-protocol of Bailey and Arnold (2006) for its application to small aliquots (~30 grains) of the glaciofluvial samples investigated here.

1.1 Research context

1.1.1 The British and Irish Ice-sheet (BIIS) and the Irish Sea Ice-Stream (ISIS)

The time period focussed upon in this research is the Last Glacial Maximum (LGM) of MIS 2, defined by EPILOG (Environmental Processes of the Ice age: Land, Oceans, Glaciers) as the most recent interval during MIS 2 when global ice-sheets reached their maximum integrated volume and is currently identified as centred around 21 cal. ka BP (Mix, et al., 2001). Thomas and Chiverrell (submitted) reviewed evidence for the LGM in Britain and Ireland and found an increasingly repeatable two phase sequence, with ice advance broadly after 30 cal. ka BP and maximum extension reached early between 30 and 24 cal. ka BP, with a retreat and subsequent readvance in the period 24-20 cal. ka BP. However, this is not to say that

all sectors of the BIIS reached maximum volume at the same time. Indeed there is a plethora of evidence, reviewed in Thomas and Chiverrell (submitted) that suggests asynchrony of the timing of maximum extent between different sectors within the BIIS.

The late MIS 2 glaciation in Britain began after ~30 ka with extensive growth of glaciers in the mountains of the Western Highlands and Southern Uplands of Scotland. These centres of ice accumulation expanded until the dominant ice from the Highlands became confluent with Southern Upland, Lake District and Northern Irish ice in a large stream moving southwards through the northern Irish Sea Basin creating the Irish Sea Ice-Stream (ISIS). At its maximum at around 28-22 ka, this lobe extended as far south as the Celtic Sea (Scourse, et al., 1990; Scourse, 1991a; Scourse, et al., 1991; Scourse and Furze, 2001; Hiemstra, et al., 2006) as it became confluent with Welsh and southern Irish ice caps, adding to its volume (Thomas, 1985). However, this maximum ice limit is still under debate (Bowen, et al., 2002; Knight, 2004). The controversy is mainly due to the lack of absolute dating control on the age of the tills in the Celtic Sea and in southern Ireland, especially that which would constrain the timing of the advance of the ISIS to its overall maximum limit in the Celtic Sea.

Ice-sheet modelling (Boulton, et al., 1977; Boulton, et al., 1991; Boulton and Hagdorn, 2006) (Figure 1.1) resulted in the construction of both a minimum and maximum extent model for the LGM BIIS. The maximum extent model was based on ideas that the Scottish and Scandinavian ice-sheets were confluent in the North Sea. Recent work by Bowen et al. (2002) also agreed with this proposed ice margin

based on the terrestrial record and cosmogenic nuclide surface-exposure dating, aminostratigraphy of 'shelly' glacial deposits, AMS radiocarbon dating and evidence from continental margin marine cores (Figure 1.1). Bowen et al. (2002) concluded that new data have shown that the BIIS was a long lived feature that probably evolved for much of the Devensian as a mobile and sensitive ice-sheet, in which the Last Glacial Maximum was but one important event at about 22 ka.

However, the maximum extent of the ISIS in particular, and the conditions during deglaciation remain poorly understood and strongly contested. Many reconstructions (Boulton, et al., 1991; Lambeck, 1993a; Bowen, et al., 2002) place the limit of the ice across the Irish Sea between Pembrokeshire and Wexford at about 52°N. However, there is onshore sedimentary evidence that the ISIS extended around the south coast of Ireland, almost as far as Cork (Evans and Ó Cofaigh, 2003a; Ó Cofaigh and Evans, 2007), and on the basis of offshore evidence, Scourse and Furze (2001) suggested that grounded ice deposited subglacial till as far south as the Scilly Isles (Figure 1.1). Scourse and Furze (2001) argue that glaciomarine deposits occur to the south of this glacial limit, where the basin is deep enough to remain flooded even during time of low eustatic sea level.

Eyles and McCabe (1989) argued that glaciomarine deposits are evident and indeed widespread all around the perimeter of the Irish Sea Basin, extending to well above the present sea level, with local relative sea levels controlled by seemingly excessive isostatic depression. Conversely, Thomas (1985) suggested that Eyles & Eyles (1984) ignore the geomorphology, the presence of intraformational ground-ice structures, kettle basin subsidence, and the rich terrestrial organic sequences.

Although the glaciomarine hypothesis received support during the 1990s it has also attracted much criticism and is now regarded as generally unsupported by the evidence (e.g. Huddart, 1977; Thomas, et al., 1985; Thomas and Dackombe, 1985; Harris, 1991; McCarroll, 1991; Scourse, 1991a; Scourse, et al., 1991; Scourse, 1991b; Austin and McCarroll, 1992; McCarroll and Harris, 1992; Mejdahl and Christiansen, 1994; McCarroll, 1995; Harris, et al., 1997; Thomas, et al., 1998; Merritt and Auton, 2000; Hambrey, et al., 2001; McCarroll, 2001; Ó Cofaigh and Evans, 2001a; Scourse and Furze, 2001; Evans and Ó Cofaigh, 2003a; Glasser, et al., 2004; Thomas, et al., 2004; McCarroll, 2005; Etienne, et al., 2006; Scourse, et al., 2006; Thomas, et al., 2006; Ó Cofaigh and Evans, 2007).

For over a century the extent of the BIIS during the MIS 2 in the Celtic Sea and onshore in southern Ireland has been debated. In Ireland a large swath of land across the southern part of the island, beyond the limit of the South Ireland End Moraine (SIEM), was interpreted as having been unglaciated during the MIS2 based on the subdued morphology of the surficial drifts, their deep calcification and cryoturbated nature (Charlesworth, 1928; Synge, 1981; McCabe, 1987). These deposits were assigned to a penultimate 'Munsterian Glaciation' and were contrasted to the fresh glacial topography inside the SIEM, which was regarded as having been glaciated during MIS 2.

However, recent AMS radiocarbon dates upon glacially transported marine shells from the Irish Sea till at sites along the south coast of Ireland, beyond the limits of the SIEM (Ó Cofaigh and Evans, 2007), provided conflicting evidence for the limits of the last glaciation in south-eastern Ireland. Many of the shells were reworked

marine macro- and micro-fauna enclosed within sediments that were either subglacially or glaciotectonically stacked to produce the Irish Sea Till by a grounded ISIS during its advance into the Celtic Sea. The reworked shell fragments from the till gave maximum ages, with the youngest of these dates expected to be most instructive with respect to the timing of their deposition. Six dates of between 28,072-23,931 cal. a BP[1] demonstrated that the last advance of the ISIS into the Celtic Sea, which deposited the Irish Sea Till along the south coast of Ireland occurred during MIS 2. The three youngest dates constrained the precise timing of this advance to after ~23,000 cal. a BP. This interpretation is supported by radiocarbon dates of 41,508-38,200 cal. a BP and 27,948-23,612 cal. a BP from organic sediments below the Scilly Member, the stratigraphic correlative of the Irish Sea Till, on the Scilly Isles (Scourse, et al., 1991; Hiemstra, et al., 2006). The dated samples were well constrained stratigraphically, being collected from coastal outcrops in which shell-rich Irish Sea Till was overlain by inland till. The dates indicated that the inland tills record ice advance from the Irish Midlands and south-west onto the continental shelf during the MIS 2. Therefore, the SIEM which was thought to have represented the last glacial limit was reinterpreted as a recessional feature formed during ice-sheet retreat from LGM extent (Ó Cofaigh and Evans, 2007).

In the Celtic Sea, the Irish Sea Till records the southward advance of the largest outlet of the BIIS to as far south as 49°30'N (Ó Cofaigh and Evans, 2007). Several studies have now argued that the BIIS was extensive during MIS 2, covering most of

[1] *All radiocarbon ages are calibrated to the Reimer et al. (2004) (for ages of <20,000 ^{14}C a BP) or Fairbanks et al. (2005) (for ages of >20,000 ^{14}C a BP) curves where appropriate using either the OxCal (Bronk Ramsey, C. (2001). Development of the radiocarbon calibration program OxCal. Radiocarbon 43, 355-363.) or Fairbanks et al. (2005) software (Fairbanks, R. G., Mortlock, R. A., Chiu, T.-C., Cao, L., Kaplan, A., Guilderson, T. P., Fairbanks, T. W. and Bloom, A. L. (2005). Marine Radiocarbon Calibration Curve Spanning 0 to 50,000 Years B.P. Based on Paired $^{230}Th/^{234}U/^{238}U$ and ^{14}C Dates on Pristine Corals. Quaternary Science Reviews 24, 1781-1796.). The 2σ radiocarbon ages are suffixed by cal. a BP with present defined as AD 1950. For all other geochronological methodologies the ages are clearly identified and suffixed with ka.*

Ireland and extending far south into the Celtic Sea (Warren, 1985; Scourse, 1991a; Scourse, et al., 1991; Ó Cofaigh and Evans, 2001a; Ó Cofaigh and Evans, 2001b; Hiemstra, et al., 2006; Thomas and Chiverrell, submitted). This unstable and short-lived ice advance to its overall maximum in the Celtic Sea was facilitated by a saturated substrate of marine mud (Scourse, et al., 1990; Scourse, et al., 1991; Ó Cofaigh and Evans, 2001a; Ó Cofaigh and Evans, 2001b; Scourse and Furze, 2001; Evans and Ó Cofaigh, 2003a; Hiemstra, et al., 2006). Further north in the Irish Sea Basin at sites such as the Screen Hills in southeastern Ireland and Dinas Dinlle in northwestern Wales, major deglacial sediment accumulations and stacked tills mark stillstands and oscillations of the ice-stream during overall recession (Thomas and Summers, 1983; McCabe, 1987; Evans and Ó Cofaigh, 2003a; Thomas, et al., 2004; Thomas and Chiverrell, 2007). These first major stillstands are thought to reflect stabilisation of the ice-stream as it reached the narrow corridor of St. Georges Channel, between the coasts of Wales and Ireland (Ó Cofaigh and Evans, 2007).

Recently there have been attempts to map glacial landforms and features related to the last British Ice-sheet on a comprehensive country-wide basis as part of the BRITICE programme (Clark, et al., 2004a; Evans, et al., 2005; Greenwood, et al., 2007). Emphasis was placed upon the compilation of evidence that would help constrain the Devensian ice-sheet, primarily its extent (e.g. moraines, drift limits, nunataks) and flow geometry (drumlins, erratic dispersal) to help inform future models of ice extent. The GIS output from this vast research base clearly indicates appropriate landforms and therefore helps to demarcate the limits of the MIS 2 BIIS. The remote mapping of drumlins and mega-scale glacial lineations, using satellite and flight path laser technology has also helped to identify areas that have been

subject to ice-streaming. Evidence of landforms existing in Scotland and the Lake District have also helped to map the extent of glaciation and ice cap formation relating to the Loch Lomond stadial (Younger Dryas) approximately 12.5-11.5 ka. This information, together with chronological data mentioned previously is a powerful tool for reconstruction of LGM limits and retreat stages of the BIIS.

Although the timing of the LGM limits for the ISIS have been constrained somewhat by the combination of AMS radiocarbon dates mentioned above (Ó Cofaigh and Evans, 2007), and large-scale remote mapping, the timing of subsequent retreat stages is severely lacking. This lack of chronology is often the driver for such controversy about the dynamic nature of the ISIS, how rapidly it retreated and implications that this may have for sea level reconstructions for the Irish Sea Basin (Lambeck, 1991; Lambeck and Purcell, 2001; Shennan, et al., 2006; Brooks, et al., 2008; Edwards, et al., 2008; McCabe, 2008a). The application of OSL dating techniques to sediments deposited as a direct result of the retreat of the ISIS should therefore enable the retreat chronology to be constrained further.

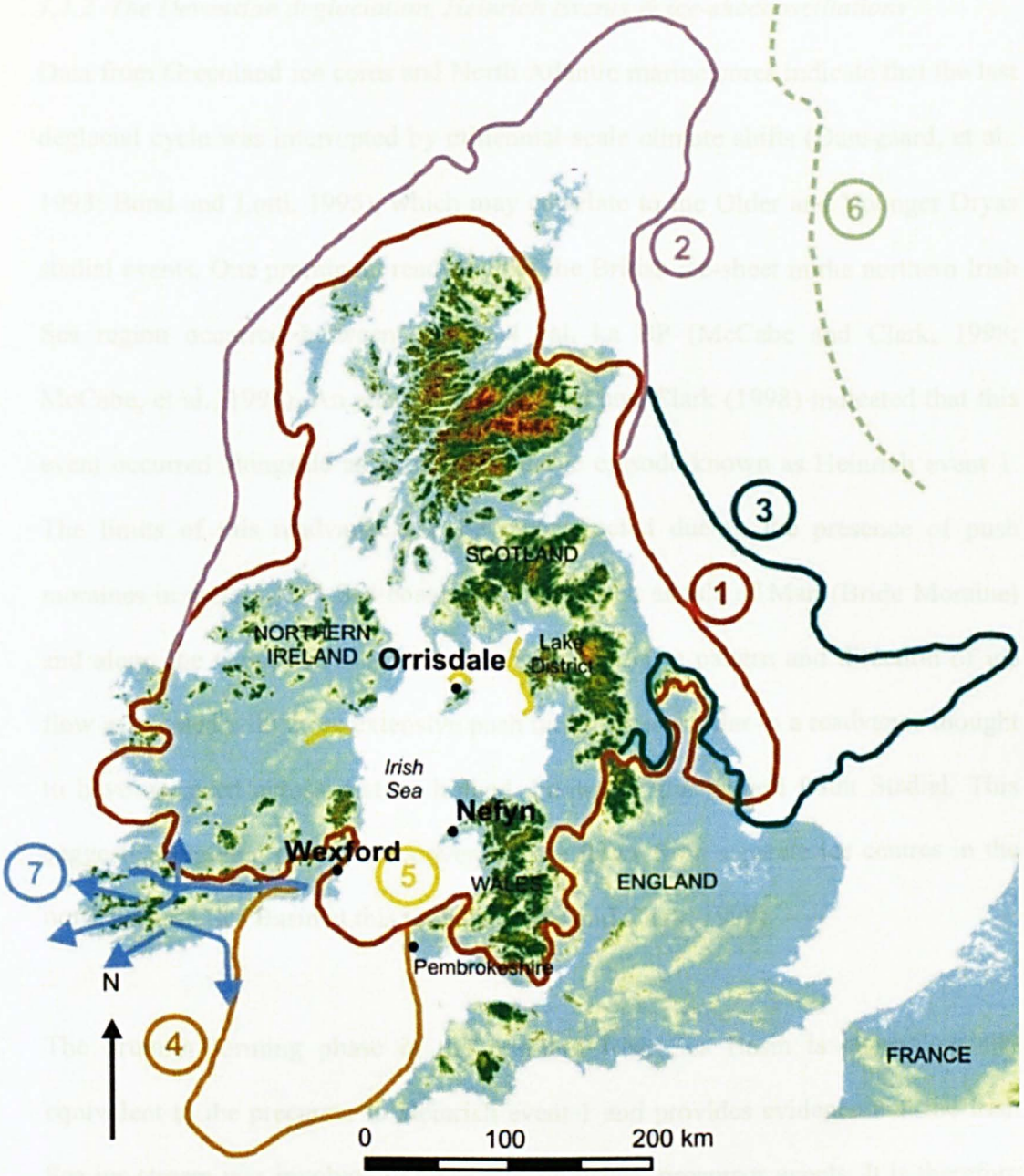

Figure 1.1 *Recent reconstructions of the maximum extent of the MIS 2 ice-sheet over the British Isles, showing the uncertainties associated with currently submarine evidence. (1 = Bowen et al. (2002); 2 = Hall (1997); 3 = Balson and Jeffrey (1991) & Boulton et al. (1977) & Boulton et al. (1991); 4 = Scourse and Furze, 2001 & Hiemstra et al. 2006. Lines marked 5 show the extent of readvances in the Irish Sea Basin (Ireland –Synge (1978); Isle of Man – Dackombe & Thomas (1991); Cumbria – Huddart, 1991). 6 = possible western margin of the Scandinavian ice-sheet at the LGM (Hall, 1997). 7 = Ó Cofaigh & Evans (2007).*

1.1.2 The Devensian deglaciation, Heinrich Events & ice-sheet oscillations

Data from Greenland ice cores and North Atlantic marine cores indicate that the last deglacial cycle was interrupted by millennial-scale climate shifts (Dansgaard, et al., 1993; Bond and Lotti, 1995), which may correlate to the Older and Younger Dryas stadial events. One prominent readvance of the British ice-sheet in the northern Irish Sea region occurred between 18.8-16.4 cal. ka BP (McCabe and Clark, 1998; McCabe, et al., 1998). An analysis by McCabe and Clark (1998) indicated that this event occurred alongside an iceberg discharge episode known as Heinrich event 1. The limits of this readvance can be reconstructed due to the presence of push moraines in certain Irish Sea coastal locations such as Isle of Man (Bride Moraine) and along the Cumbrian coast (St. Bee's, Drigg). The pattern and direction of ice flow associated with these extensive push moraines is similar to a readvance thought to have occurred across eastern Ireland, known as the Killard Point Stadial. This suggests a regional pattern of convergent ice flows from separate ice centres in the northern Irish Sea Basin at this time (McCabe and Clark, 1998).

The drumlin forming phase in the northern Irish Sea Basin is chronologically equivalent to the precursor to Heinrich event 1 and provides evidence that the Irish Sea ice-stream was involved in these climate-driven precursor events. It is therefore probable that these events, reflecting ice-sheet variability are an oscillator driven by climate upon unstable ice rather than any internal ice-sheet mechanism. In this respect, it is also significant that field evidence for oscillations within the deglacial stratigraphy are predominantly marked along the most active and sensitive ice-streams which drained the last ice-sheet [e.g. Irish Sea ice-stream (Eyles and McCabe, 1989)] (McCabe, 1996). The deglacial stratigraphy is clearly witnessed in

the geological record in areas such as the Isle of Man (Orrisdale), Wexford (south-eastern Ireland), and Llŷn Peninsula (North Wales) and provides evidence for an active and sensitive ice-stream which underwent many small scale ice-marginal oscillations.

1.1.3 Sedimentary stratigraphy

Due to the dynamism of the glacial environment (continual advance/retreat cycles superimposed upon minor snout oscillations), glacial sediments are rarely deposited in a "layer cake" manner, which makes stratigraphic interpretation difficult. Glacial sediments are more likely to be deposited in a series of interlocking lenses or discontinuous layers, which relate to different processes. Debris that passes through the glacial system can have a complex transport history which means that on final deposition, individual debris elements may contain different data superimposed upon one another (Hart, 1999).

The frequent oscillations of the ISIS margin during the period of deglaciation resulted in a suite of proglacial sediments being deposited one on top of the other. There are locations around the Irish Sea Basin where such sediments are exposed in cliff sections e.g. Isle of Man (Thomas, 1977; 1985; Thomas, et al., 1985; Chiverrell, et al., 2001; Chiverrell, et al., 2004; Thomas, et al., 2006), Wexford (Summers, 1981; Thomas and Summers, 1982; 1983; Thomas and Kerr, 1987) and the Llŷn Peninsula (Thomas, et al., 1998; Thomas and Chiverrell, 2007). These locations, at the time of deposition, were on the margin of the ISIS during various retreat stages. Their sediments yield information concerning any changes in glacial sediment deposition,

which, in turn helps identify the extent and duration of ice-sheet fluctuations at the particular locality.

Oscillations in the ice-sheet margin allowed deposition of sandur sediments on the continental shelf adjacent to the Irish Sea Basin. In many areas, glacial till, deposited as a result of the MIS 2 ice-sheet advance underlies these sandur deposits, illustrating a neat stratigraphic chronology of deglaciation and ice-sheet retreat. However, their lack of organic material (due to the cold and ice-covered depositional environment) limits their use for radiocarbon dating. New dating techniques such as optically stimulated luminescence (OSL) and recent advances in such techniques, offer an opportunity to date the sediment directly, with no need for chance occurrence of organic material as required for radiocarbon dating techniques. This would add a valuable chronology to the retreat of the ISIS.

Sedimentary stratigraphy and lithofacies analysis in combination with analyses of local and regional geomorphology are powerful techniques for reconstructing palaeo-environments of sediment deposition and enable inferences to be made concerning sedimentary processes and ice-sheet oscillations.

1.1.4 Lithofacies analysis

Lithofacies analysis refers to the identification of lithological components, sedimentary structures and the vertical and lateral relationships between them for a sedimentary sequence (Miall, 2006). Understanding the architectural relationships between lithofacies (or architectural element analysis: AEA) can subdivide sedimentary basin fills into elements (or facies assemblages) on the basis of

sedimentary body geometry and lithological composition (Miall, 1985; Brookfield and Martini, 1999; Boyce and Eyles, 2000). These approaches help geologists to constrain the nature of past depositional environments and processes.

Much of the work on lithofacies models for braided rivers is concentrated upon modern sedimentation processes that produce typical river morphology (Smith, 1974; Hein and Walker, 1977; Miall, 1977; 1978; Bryant, 1983; Hammer and Smith, 1983; Sambrook Smith, 2000). Glacial outwash environments are well described both in terms of the spatial distribution of sediments in present systems and in terms of vertical sequences from older deposits. Neither of these perspectives provides a wholly satisfactory model to predict the internal organisation of sediments within bodies of glacial outwash, since the sediments most easily observed in modern environments have the lowest preservation potential, whereas the vertical sequence of facies in one section has limited application to the description of later variation (Dawson and Bryant, 1987). When looking at ancient river sediments, preservability must therefore be questioned. The problem of preservability hangs over any study of modern rivers, because it cannot be known with much certainty what fragments of the most recent deposits in the river will survive erosion long enough to enter the geological record (Miall, 1977). This is especially the case where terrestrial ice-sheets are concerned, with a greater fluctuation in meltwater release and a high potential reservoir of flood water, any vast release of meltwater has the potential to destroy braided river facies and wipe away part of the geological record.

Braided stream activity dominates the sandur depositional environment. This is due to the association of high slopes, variable discharges and coarse grain sizes (Miall,

1977). Proglacial fluvial environments are typically characterised by large and rapid discharge fluctuations, abundance of easily eroded debris, and high rates of sediment transport and deposition (Hammer and Smith, 1983).

Large scale fluctuations in meltwater and sediment supplies to sandar reflect not only seasonal, diurnal and episodic events, but also vary in response to long-term climatic changes reflected in advance or retreat cycles of the source ice mass. Glacier advance or retreat can act to release lower or higher volumes of meltwater, and modify the availability of sediment to the proglacial system. Hence, lithofacies sequences within glacial outwash may well reflect major changes in meltwater and sediment supply regimes resulting from fluctuations in the rates and patterns of glacier movement and melting (Maizels, 1993). It is often the case that lithofacies sequences can illustrate a switch from distal to proximal sedimentation due to ice advance or retreat.

The first step in an analysis of a stratigraphic succession is the recognition of the suite of lithofacies types of which the succession is composed. For some depositional environments a limited range of lithofacies types cover virtually all the variability present in modern and ancient deposits. This permits the establishment of standard lithofacies schemes which may be formally defined and coded for field application (Eyles, et al., 1983). A lithofacies coding concept proposed by Miall (1977, 1978, and 1996) classifies primary sedimentary features (Table 1.1). This scheme was extended for glacial deposits by Eyles et al. (1983) and specific features for glaciofluvial deposits were added by Siegenthaler and Huggenberger (1993).

Table 1.1 *Lithofacies and sedimentary structures of modern and ancient braided stream deposits (modified from Miall, 1996).*

Facies Code	Lithofacies	Sedimentary Structures	Interpretation
Gmm	matrix-supported, massive gravel	weak grading	plastic debris flow (high-strength, viscous)
Gmg	matrix-supported gravel	inverse to normal grading	pseudoplastic debris flow (low strength, visous)
Gci	clast-supported gravel	inverse grading	clast-rich debris flow (high strength) or pseudoplastic debris flow (low strength)
Gcm	clast-supported massive gravel	-	pseudoplastic debris flow (inertial bedload, turbulent flow)
Gh	clast-supported crudely bedded gravel	horizontal bedding, imbrication	longitudinal bedforms, lad deposits, sieve deposits
Gt	gravel, stratified	trough cross-beds	minor channel fills
Gp	gravel, stratified	planar cross-beds	transverse bedforms, deltaic growth from older bar remnants
St	sand, fine to very coarse, may be pebbly	solitary or grouped trough cross-beds	sinuous-crested and linguoid (3-D dunes)
Sp	sand, fine to very coarse, may be pebbly	solitary of grouped planar cross-beds	transverse and linguoid bedforms (2-D dunes)
Sr	sand, very fine to coarse	ripple cross-lamination	ripples (lower flow regime)
Sh	sand, very fine to coarse, may be pebbly	horizontal lamination parting or streaming lineation	plane-bed flow (critical flow)
Sl	sand, very fine to coarse, may be pebbly	low-angle (<15°) cross-beds	scour fills, humpback or washed-out dunes, antidunes
Ss	sand, fine to very coarse, may be pebbly	broad, shallow scours	scour fill
Sm	sand, fine to coarse	massive, or faint lamination	sediment-gravity flow deposits
Fl	sand, silt, mud	fine lamination, very small ripples	overbank, abandoned channel, or waning flood deposits
Fsm	silt, mud	massive	backswamp or abandoned channel deposits
Fm	mud, silt	massive, desiccation cracks	overbank, abandoned channel or drape deposits
Fr	mud, silt	massive, roots, bioturbation	root bed, incipient soil
C	coal, carbonaceous mud	plant, mud films	vegetated swamp deposits
P	paleosol carbonate (calcite, siderite)	pedogenic features: nodules, filaments	soil with chemical preparation

In a lithofacies code that is employed by fluvial sedimentologists, Miall (1977, 1978 and 1996) showed that the majority of fluvial deposits, including glaciofluvial outwash deposits, can be described using a set of 20 standard lithofacies types. Each type has been assigned code letters for convenience in logging. The codes are in two parts; the first is a capital letter *G*, *S* or *F* which represents gravel, sand, or fines. The second part of the code consists of one or two letters to describe the most characteristic internal feature of the lithofacies e.g. *Gms* for matrix-supported gravel, *Sp* for planar cross-bedded sand, etc. The principal lithofacies are listed in Table 1.1 with notes on their composition, structure and brief interpretation. The key to a positive identification of the environment of deposition, therefore, lies in the nature of the facies assemblage, including the vertical and lateral lithologic variability and extent.

Four vertical profile models for braided rivers, using this lithofacies code were erected by Miall (1977) on the basis of a survey of information on modern sedimentary processes and ancient deposits. The most appropriate facies types in relation to glaciofluvial lithofacies are the Scott, Donjek and South Saskatchewan type vertical profile models (Figure 1.2).

The Scott model, named after the Scott outwash river, Alaska (Boothroyd and Ashley, 1975) was erected for proximal braided stream deposits where gravel is the dominant facies, particularly facies *Gm*, with rare units of *Gp* and *Gt*, and some interbedded sandy channel-fill deposits (Figure 1.2). The Scott type consists of small-scale gravel-sand cycles of waning-flood origin, and intervals of superimposed longitudinal-bar deposits. The assemblage is located in a fan environment beyond the

limit of debris flows. Other facies types may occur to a lesser extent as a response to waning flow. They represent small scale upward-fining sequences in abandoned channels or the development of small scale wedges.

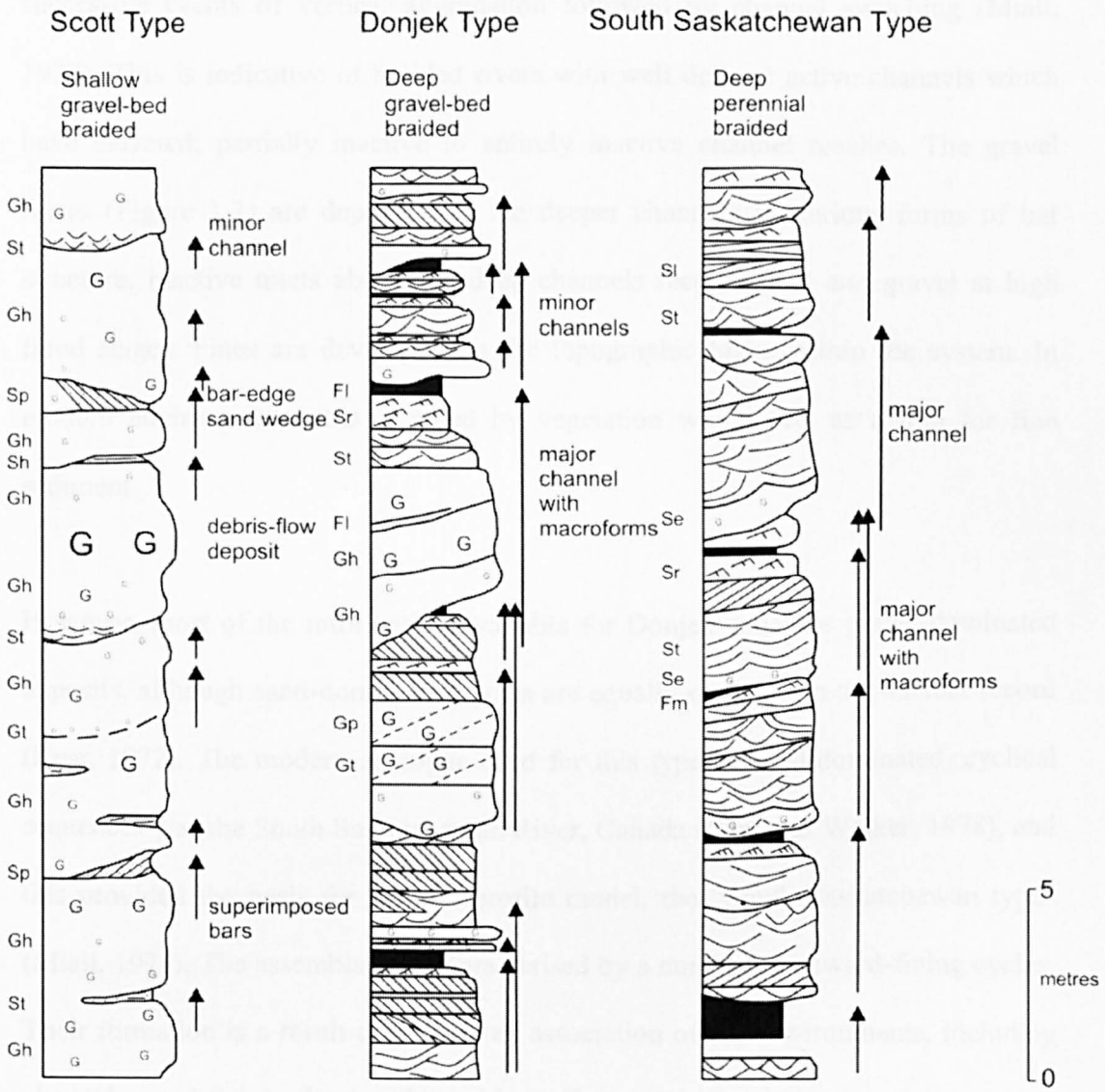

Figure 1.2 *Typical fluvial lithofacies assemblages and vertical profiles for the three fluvial styles discussed below. Vertical arrows indicate cyclic sequences of various types, showing direction of fining and bed thinning. Lithofacies codes are given at left of column. Redrafted from Miall, 1996.*

The Donjek model, named after the Donjek river, Yukon (Williams and Rust, 1969) was established to encompass most types of cyclic braided river deposit. Fining-upward cycles of several scales were present, the thicker cycles reflecting sedimentation at different topographic levels within the channel system, or successive events of vertical aggradation followed by channel switching (Miall, 1977). This is indicative of braided rivers with well defined active channels which have elevated; partially inactive to entirely inactive channel reaches. The gravel facies (Figure 1.2) are deposited in the deeper channels as various forms of bar structure, inactive tracts above the deep channels receive sand and gravel at high flood stages. Fines are developed on the topographic highs within the system. In modern environments, this is aided by vegetation which acts as a trap for fine sediment.

However, most of the information available for Donjek concerns gravel-dominated deposits, although sand-dominated cycles are equally common in the ancient record (Rust, 1972). The modern analogue used for this type of sand-dominated, cyclical sequences was the South Saskatchewan River, Canada (Cant and Walker, 1978), and this provided the basis for another profile model, the "South Saskatchewan type" (Miall, 1978). The assemblage is characterised by a number of upward-fining cycles. Their formation is a result of a complex association of sub-environments, including channels, sand flats and cross-channel bars. Topographic variation across the system also has a control upon the deposition, and bedforms in the deeper channels tend to be sinuous crested dunes (*St*) whilst in shallower reaches sand waves are more common (*Sr*). Large sand flats are formed by cross-channel bars building around a nucleus. On the wane of the flood facies types *Sr* and *Sh* may form on bar tops and

fines may accumulate in overbank inactive areas (Cant and Walker, 1978). In most cases, facies *St* is the dominant component, with a varying proportion of *Sp, Sr, Sh, Se, Gm, Fl* and *Fm* arranged within thinning and fining-up sequences.

The Scott, Donjek and South Saskatchewan profile types form a gradational proximal-distal sequence in some ancient braided river deposits reflecting a downstream increase in sand/gravel ratio (Miall, 1978) along with reduction in flow velocity, turbidity and competence. Bar morphology and the types of internal stratification are dependent on grain size and therefore, these also show downstream changes. There is no doubt that vertical profile models act as a framework within the ancient record but departures occur as a result of varied architectural control upon the depositional system.

Connaughton (1986) showed, in a case study of a Late Pleistocene sandur from the Isle of Man, that sandur deposition at the margins of large continental ice-sheets is significantly different in character than proglacial valley sandur systems, which display well organised proximal-distal facies transitions. Attributing certain facies assemblages to locations within a proximal-distal relationship may result in an incorrect assessment of the overall depositional environment. This is particularly the case where channel systems are influenced by ice stagnation topography and where glacio-dynamic deformation act as a control on subsequent outwash (Connaughton, 1986). Lithofacies assemblages for an ice-marginal proglacial sandur were devised by Thomas (1985) and more detail and explanation is provided in Chapter 2.

1.2 Research aims and objectives

The primary aim of this research is to define a chronological model for the deglacial history of the ISIS. In order to do this, accessible and well-documented sites were identified along the flowline of the ISIS which display evidence of glaciofluvial sedimentary facies to which OSL dating can be applied.

A detailed lithofacies analysis of the glaciofluvial sediments of the Bishop's Court Member, an ice-marginal palaeosandur sequence, on the west coast of the Isle of Man (see Figure 1.1 for location details) has already been carried out by Thomas (1977, 1984, 1985) and Thomas et al. (2006) and this information was used to target a suite of lithofacies for luminescence sampling. Detailed lithofacies logs of the Bishop's Court Member were analysed and fining-upwards sequences noted, in both proximal and distal palaeo-sandur locations. A variety of lithofacies types were sampled (*Sp, Sh, Sr, St, Fl*) as a detailed comparison of the luminescence bleaching properties of each was needed to direct subsequent field sampling towards the lithofacies type that was more favourable for luminescence dating.

The most successful lithofacies for OSL dating of the ice-marginal palaeosandur from the Isle of Man were then targeted at two other field sites which display in-section evidence of ice-marginal glaciofluvial sedimentation as a direct result of the retreating ISIS; Porth Dinllaen, northwestern Wales and Wexford, southeastern Ireland (see Figure 1.1 for location details and Chapter 5 for detailed site investigations). At Porth Dinllaen, depositional evidence for a lower fan, distal sandur environment is present within cliff section exposure (see Thomas and Chiverrell, 2007). In comparison, ice-contact proximal glaciofluvial sedimentation

was observed within quarry sections at Wexford (see Thomas and Summers, 1982; 1983; 1984; Thomas and Kerr, 1987). A less exhaustive field sampling technique was required for these additional sites.

The successful application of OSL dating at each of the sites mentioned above, allowed a time-stepped retreat of the Irish Sea ice-stream to be reconstructed with the aid of Bayesian modelling techniques. This is the first time such a comprehensive chronology has been achieved for this area, and so providing valuable data for the research community. A variety of objectives were fulfilled to achieve the main aim:

1. *The present day exposed lithofacies of the Bishop's Court Member at Orrisdale in the Isle of Man were analysed and specific lithofacies were selected, based upon their hypothesised depositional environment (and inferred bleaching potential) for luminescence sampling.*

2. *Luminescence techniques (preheat tests, linearly-modulated OSL curve fitting, constant-wave OSL decay curve fitting) were used to characterise the quartz grains in terms of determining a 'safe' preheat temperature and characterising the fast component (its relative intensity and photoionisation cross-section).*

3. *An appropriate single-aliquot regenerative-dose (SAR) protocol (based on results from quartz characterisation) was applied using small aliquots (~30 grains) to generate a distribution of equivalent dose (D_e) values. The*

resulting D_e distribution allowed the extent of heterogeneous-bleaching to be evaluated (via skewness, kurtosis and overdispersion calculations).

4. *The number of D_e values required to ensure a reproducible distribution for each sample was evaluated and the statistical 'age' model most appropriate to calculate the D_e value used for age calculation was determined via a previously published, statistically-based decision-making protocol (Bailey and Arnold, 2006).*

5. *Ages were then calculated for all sand sized lithofacies types (Sh, St, Sr, Fl) from the Bishop's Court Member, Isle of Man and any discrepancies in terms of lithofacies and grain size were compared.*

6. *The information obtained at the Isle of Man was used to inform sampling of appropriate lithofacies at two other sites on the perimeter of the Irish Sea Basin which were subject to terrestrial proglacial sandur sedimentation as a result of the retreating Irish Sea ice-stream i.e Wexford (S.E. Ireland) and the Porth Dinllaen, Llŷn Peninsula (N.W. Wales).*

7. *The same luminescence and statistical analysis techniques were applied to samples from Wexford and Porth Dinllaen and an investigation into the applicability of the decision-protocol for choosing the most appropriate statistical 'age' model for D_e distributions derived from these samples was undertaken.*

8. ***All chronological data (derived from this research and from previously published papers) was reviewed to reconstruct a time-stepped retreat of the Irish Sea ice-stream with the aid of Bayesian modelling techniques.***

1.3 Thesis structure

In line with the objectives specified above, the main body of this research is concerned with developing the successful application of OSL dating to glaciofluvial deposits associated with the retreat of the ISIS.

In **Chapter 2**, a review of previous applications of luminescence dating techniques to glacigenic sediments is given. Details concerning the intricacies of the OSL technique are discussed together with previous investigations into problems concerning the bleaching of glaciofluvial quartz.

Chapter 3 covers the derivation of environmental dose-rate for each sample, giving one half of the age equation (see Chapter 2).

Chapter 4 details the series of tests used to investigate quartz luminescence characteristics (thermal transfer, sensitivity, fast component analysis), as well as determining an appropriate preheat temperature to use during the SAR protocol for each sample.

Chapters 5 is the main OSL dating results chapter concerning the application of quartz luminescence characterisation and D_e determination methodology to the Isle of Man, Porth Dinllaen and Wexford samples. It details how the appropriate

statistical 'age' model was selected for D_e determination via the use of a statistically-based decision-making protocol (Bailey and Arnold, 2006). Results for OSL ages are given and interpreted in terms of lithofacies and grain size differences and how these optical ages sit within previously published ages derived via various chronological techniques.

Chapter 6 is the main discussion chapter and brings all chronological data together in an attempt to reconstruct the retreat of the ISIS with the aid of Bayesian modelling techniques. It discusses the wider implications of this research in relation to sea-level modelling and its contribution to the glaciomarine/terrestrial ISIS debate.

Chapter 7 summarises the main findings, evaluates the wider implications of this research and considers future research priorities.

Chapter 2

Luminescence dating of glacigenic deposits: a review

2.1 Introduction

There are a number of chronological techniques that can establish the age of sediments, with radiocarbon being most routinely used. In most circumstances, radiocarbon dating is useful only from a few hundred years to ~ 45 000 years and obviously requires the presence of fossil organic matter. There is often a severe lack of organic matter within glacigenic sediments due to the very nature of the depositional environment; cold and ice-covered environments are not conducive to the presence of abundant flora or fauna. Furthermore, for radiocarbon years to be compared to calendar years, then detailed knowledge about past variations in the concentration of radiocarbon in the atmosphere is needed (Bronk Ramsey, 2008; Lian and Roberts, 2006; Smart and Frances, 1991). Linkages between a radiocarbon age and the surrounding sediment matrix are made by assuming that the organic material being dated, died at the same (or approximately the same) time as the sediment in the surrounding matrix was deposited, which is often not the case. Other methods such as potassium-argon, argon-argon, uranium-series and fission track dating require the presence of in situ volcanic or carbonate deposits (Smart and Frances, 1991; Lian and Roberts, 2006). Dendrochronology, amino acid racemisation and palaeomagnetic techniques only give relative ages unless age patterns can be matched with independently dated sequences.

There are relatively few techniques for the direct dating of the time of deposition of sediments (Aitken, 1998). There are clear advantages to chronological techniques that use the abundant and ubiquitous constituents of the sediment itself such as quartz and feldspar. The luminescence methods are dominant in this respect and thermoluminescence (TL) and optically stimulated luminescence (OSL) present an opportunity to date the dominant constituents of the sediment itself. The history of the exposure to environmental radiation over time is carried by electrons (charge) trapped within defects in the lattice structure of mineral grains; the total number of electrons in these traps will increase with burial time, but the charge is released when the mineral grains are exposed to daylight during depositional processes. This process of detrapping charge by light exposure is referred to as *bleaching*. The amount of trapped charge forms a clock that starts ticking at the moment the mineral is buried and shielded from light (Aitken, 1998; Wallinga, 2002). The luminescence signal used for dating reflects the amount of charge trapped, and hence the irradiation dose the sample has received since burial, also known as the palaeodose. The equivalent dose (D_e) equates to the laboratory irradiation dose required to induce a luminescence signal equal to that acquired since the most recent bleaching event. The equivalent dose is routinely determined for a sample that ranges in size from individual grain (single-grain) to small sub-samples (30-200 grains). These sub-samples are known as *aliquots*. The optical age is then determined by dividing the D_e (Gy) by the environmental dose-rate (Gy/year).

OSL techniques have been used to successfully date sediments from a wide range of depositional environments, especially aeolian dunes (Huntley, et al., 1985; Stokes, 1992; Ollerhead, et al., 1994; Fitzsimmons, et al., 2007; Telfer, et al., 2008; Zhou, et

al., 2008) and loess deposits (e.g. Wintle, 1990; Lang, et al., 2003; Roberts, et al., 2003; Lai, et al., 2007; Buylaert, et al., 2008; Demuro, et al., 2008). These types of sediments are lain down in environments conducive to grains having been sufficiently bleached upon exposure to daylight during aeolian transport processes to remove any pre-existing trapped charge. The application of this technique to glacigenic sediments has proven to be more challenging due to the lack of opportunity for minerals to be exposed to daylight as the majority of glacigenic sediments are transported and deposited by a glacier or ice-sheet or are deposited in turbid proglacial sandur environments.

This chapter reviews the application of OSL dating techniques to establish accurate chronologies for glacigenic, and in particular, glaciofluvial deposits. Glacigenic sediments encompass a variety of depositional environments from subglacial diamict to glaciofluvial outwash, each of which can experience different bleaching conditions. The literature suggests that proglacial glaciofluvial depositional environments offer the greatest opportunity for a proportion of mineral grains to be completely bleached upon deposition. However, problems such as insensitive quartz, the lack of a dating 'signal' (fast component – see Section 2.2.4) and the incomplete bleaching of some mineral grains still remain. Recent literature is used to illustrate how problems such as heterogeneous-bleaching have been overcome through advances in measurement methodology (Duller, 2004; 2006), such as the movement towards analysis of 'populations' of aliquots and using single-aliquot and single-grain analysis techniques. This single-aliquot/grain approach and the measurement of numerous D_e values for a sample has permitted the use of robust statistical D_e analysis methodologies (Galbraith and Green, 1990; Olley, et al., 1998; Galbraith, et

al., 1999) to identify the extent of heterogeneous-bleaching and bleaching history for the composite quartz grains. Linking the extent of heterogeneous-bleaching to certain sedimentary environments and lithofacies types could then direct luminescence sampling of glacigenic sediments towards those depositional environments that are more likely to yield mineral grains that are well-bleached.

2.2 The Optically Stimulated Luminescence technique

The basic concept of the luminescence technique is to use naturally occurring minerals, principally quartz and various feldspars, as dosimeters, which record their exposure to ionising radiation from the environment (mainly produced by the U and Th series and ^{40}K) and a small contribution from cosmic rays. During exposure to ionising radiation, free charge carriers (electrons and holes) are produced and some of them are trapped at defects in the crystal lattice as shown in Figure 2.1. The charge retained in the OSL traps targeted for dating are stable over long periods of time (>1 Ma) and either heat or light can release the trapped electrons. Under such stimuli, some of these released electrons will recombine with electron holes in recombination centres and emit light. This light is called luminescence and is referred to as optically stimulated luminescence (OSL) and thermoluminescence (TL) when the stimulation is via visible light and heat respectively (Aitken, et al., 1964; Aitken, et al., 1968; Aitken, 1998). The following sections review some key methodological issues integral to the luminescence dating technique and its application to glacigenic sediments.

2.2.1 The 'age' equation

The luminescence age of a sample is given by the following equation, where the dose rate is the irradiation dose flux experienced in the natural environment, per annum (Aitken, 1998).

$$!" \quad \#\$\%"\&'() * \#\frac{+,-./\&0"12 \quad \#34(" \quad \#\$5\%)}{64(" \quad \# \&2'\#\$5\%7\%"\&')}$$

The equivalent dose (D_e) equates to the laboratory irradiation dose required to induce a luminescence signal equal to that acquired since the most recent bleaching event (palaeodose). The dose rate represents the rate at which energy is absorbed from the flux of naturally occurring nuclear radiation; it is evaluated by assessment of the radioactivity of the sediment, and can be carried out both in the laboratory and on-site through field gamma spectrometry (Aitken, 1998). Thus the sample age is the total dose accumulated by the mineral grain (D_e) over its period of burial divided by the rate at which it accumulates (the environmental dose-rate).

2.2.2 The single-aliquot regenerative-dose (SAR) protocol

For quartz, the most rigorous and commonly used method for measuring the D_e is the single-aliquot regenerative-dose (SAR) protocol (Murray and Roberts, 1998; Murray and Wintle, 2000). Before this was established, the main problem concerning the measurement of OSL was that repeat stimulation, preheat and irradiation of quartz causes the grain to change sensitivity i.e. the quartz gives a higher/lower OSL response with repeated dosing and stimulation. The SAR protocol (Murray and Wintle, 2000) was devised to account and compensate for *sensitivity change.*

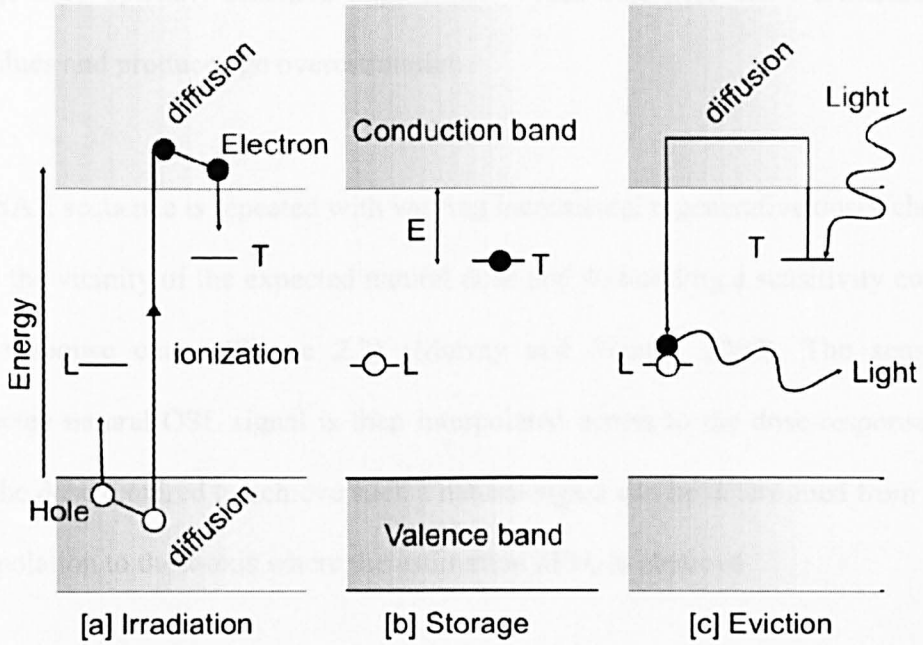

Figure 2.1 *Energy-level representation of the OSL process (based on Aitken, 1998, redrafted from Wallinga, 2002). (A) Ionisation (detachment) due to exposure of the crystal to nuclear radiation, with trapping of electrons and holes at defects, T and L respectively. (B) Storage during time; in order that leakage is negligible the lifetime of electrons in traps needs to be much longer than the age span of the sample. This lifetime is determined by depth E of the trap below the conduction band and for dating purposes we are interested in those deep enough for the lifetime to be at least several million years. (C) By shining light of appropriate wavelength onto the sample, electrons are evicted from traps and some of these reach luminescence centres; if so, light (i.e. OSL) is emitted in the process of combining into these centres. The TL process is similar except that stimulation is by heat: a temperature is reached at which the thermal vibrations of the crystal lattice are sufficient to cause eviction; the deeper the trap the higher the temperature necessary.*

The SAR protocol detailed in Table 2.1 uses the response to a fixed test dose, applied after each regeneration dose, to monitor for changes in sensitivity. The fundamental assumption is that the response (T) to the test dose provides an appropriate measure of the sensitivity that pertained during measurement of the main OSL signal (L) (Murray and Wintle, 2003). If this is not the case, sensitivity changes cannot be accounted for throughout each cycle of the SAR and an invalid estimate of D_e will result. Preheats are given during each cycle (Table 2.1) to remove thermally unstable

charge from optically-sensitive traps which would otherwise cause artificially high D_e values and produce age overestimation.

The SAR sequence is repeated with varying incremental regenerative doses chosen to be in the vicinity of the expected natural dose and so building a sensitivity corrected dose-response curve (Figure 2.2) (Murray and Wintle, 2000). The sensitivity-corrected natural-OSL signal is then interpolated across to the dose-response curve and the dose required to achieve such a natural signal can be determined from further interpolation to the *x*-axis where the estimation of D_e is obtained.

Table 2.1 *Generalised quartz SAR protocol (after Murray and Wintle, 2000, 2003).*
[a] *For the natural sample, $i = 0$ and D_0 is the natural dose.*
[b] *Aliquot cooled to < 60°C after heating. In step 5, the TL signal from the test dose can be observed.*
[c] *The stimulation time is dependent on the stimulation light intensity and wavelength (e.g. 40 s for blue light diodes, 100-125 s for lamp-based green-light sources).*
[d] *L_i and T_i are derived from the stimulation curve, typically the first 1-10 s of initial OSL signal, minus a background estimated from the last part of the stimulation curve.*

Step	Treatment	Observed
1	Give dose[a], D_i	
2	Preheat[b] (usually between 160-280°C for 10s)	
3	Optical stimulation[c] at 125°C for 40s	L_i[d]
4	Give test dose, D_t	
5	Heat[b] (160-280°C)	
6	Optical stimulation[c] at 125°C for 40s	T_i[d]
7	Return to 1	

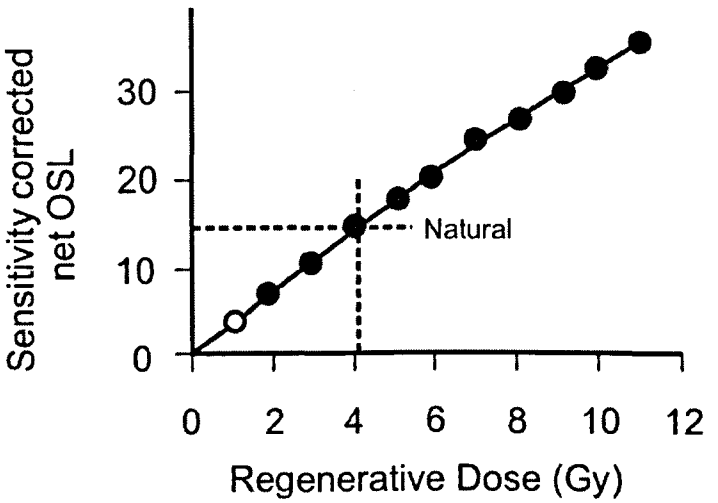

Figure 2.2 *Dose-response curve illustrating linear growth in OSL with regenerated dose. Graph highlights how interpolation allows the equivalent dose to be estimated (redrafted from Murray & Wintle, 2000).*

2.2.3 Single-aliquot and single-grain analysis

Originally, TL procedures involved the measurement of TL from individual aliquots of sediment which had been subjected to different laboratory irradiation and optical bleaching regimes prior to measurement. This involved heating grains to 500°C, thereby removing all information concerning trapped electron populations giving rise to the TL signal. Therefore, TL dating involved the preparation and measurement of numerous aliquots of the same sample that were assumed to be identical in relation to luminescence response and sensitivity (Murray, et al., 1997). A composite dose-response curve is then created which was thought to be representative of the entire sample. This is unlikely to be the case for glacigenic sediments where variation in the extent of bleaching and in the sensitivity of each individual grain would be masked by the multiple-aliquot approach, often resulting in age overestimation. The multiple-aliquot approach was extended to optical dating methods where *different* aliquots of the same sample are once again used to construct a single dose-response curve for D_e determination. The accuracy and precision of the D_e is controlled by the

appropriateness of the dose-response curve and aliquot-to-aliquot scatter in the luminescence signal which results in large uncertainties in D_e estimates (Jain, et al., 2003a).

The development of the SAR protocol (Murray and Wintle, 2000; Murray and Olley, 2002) which uses only a single aliquot to determine a D_e has allowed higher precision and improved accuracy (Jain, et al., 2003a) as a dose-response curve is derived for each individual aliquot. When single-aliquots are analysed often more than 50 D_e values and dose-response curves are obtained per sample (Olley, et al., 1998; Lepper, et al., 2000) to ensure that a D_e representative of the entire sample is achieved. For single-grain analysis, often thousands of quartz grains are measured individually to allow an acceptable number of D_e values to be determined (many are rejected on an individual basis due to poor luminescence characteristics). This allows a D_e distribution to be analysed, and for a sample that is well-bleached (a simple unimodal distribution), the average D_e can be taken and used for age determination. For glacigenic samples that are often poorly- or heterogeneously-bleached, more complex statistical treatments of D_e distributions are required (see Section 2.6).

2.2.4 The 'fast' component

Quartz shows a complicated natural-OSL decay curve as shown in Figure 2.3 where different components are identified as easy to bleach and hard to bleach. Bailey et al. (1997) suggest that the OSL decay curve from quartz can be approximated using three first-order decay components (these components were referred to as the "fast", "medium" and "slow" components) each with different detrapping rates reflecting how easily bleached they are. The most probable explanation is that the OSL signal

originates from three physically distinct traps (fast, medium and slow) (Bailey, 1997) with different rates of charge loss due to different trap depths and trap photoionisation cross-sections (Singarayer and Bailey, 2003). The fast component has a larger trap photoionisation cross-section and therefore empties quickly in relation to traps with smaller photoionisation cross-sections, which yield the medium and slow components (Kuhns, et al., 2000).

The *fast component* is suitable for luminescence dating as it is quick to bleach under optical stimulation and should give a low residual signal after exposure to sunlight during transport. This is especially important in glacigenic sediments where opportunity for exposure to sunlight is limited. The SAR protocol (Murray and Wintle, 2000) was developed on a sample that had a dominant fast component. Although Jain et al. (2003b) found that the majority of quartz samples have optical signals that are dominated by the fast component, in some samples this is not the case. In studies where the optical signal was dominated by other components (medium/slow) (Choi, et al., 2003a; Tsukamoto, et al., 2003) the standard SAR protocol does not work as effectively. It is therefore important to assess whether the samples are dominated by the fast component.

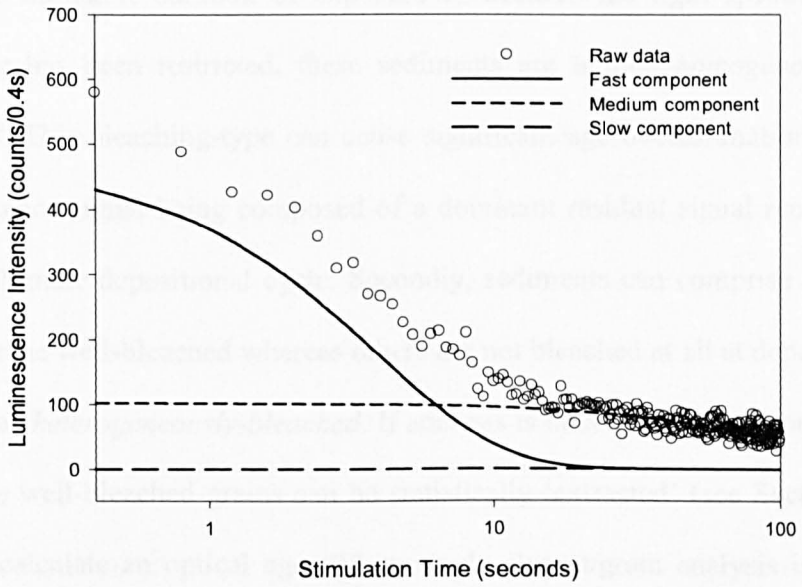

Figure 2.3 *Natural-OSL decay curve for a small aliquot (~30 quartz grains) of a glaciofluvial palaeo-sandur sample from Wexford, south-eastern Ireland (Chapter 5). Illustrated are the fast, medium and slow components which comprise the natural-OSL decay curve, extracted via curve fitting procedures. The slow component is likely to represent the background signal rather than a 'real' slow component.*

2.2.5 Bleaching

An implicit assumption when dating sediments is that the mineral grains in question were exposed to daylight during transport and deposition and that this exposure removed any remnant optical luminescence signal they may have carried. Thus, when grains are first deposited, they have a minimal luminescence signal and their equivalent dose (D_e) is approximately zero. In glacigenic sediments, this is often not the case due to a lack of opportunity for mineral grains to be sufficiently bleached in the glacial depositional environment, resulting in a poorly-bleached composite of mineral grains.

Theoretically, poor bleaching can take two forms (Duller, et al., 1995); firstly, sediments where all the grains have been equally, but poorly-bleached at deposition,

owing to the short duration of exposure or because the light spectrum used for bleaching has been restricted, these sediments are termed *homogenously poorly-bleached.* This bleaching-type can cause significant age overestimations due to the luminescence signal being composed of a dominant residual signal remaining from the penultimate depositional cycle. Secondly, sediments can comprise a mixture of grains, some well-bleached whereas others are not bleached at all at deposition, these are termed *heterogeneously-bleached.* If analysis is on a small aliquot or single-grain level, the well-bleached grains can be statistically 'extracted' (see Section 2.6) and used to calculate an optical age. When single aliquot/grain analysis is used, most glacial sediments appear to be heterogeneously bleached albeit to differing degrees.

2.3 Glacigenic sediments and their potential for bleaching

Glacigenic sediments are composed of grain sizes ranging from boulders to fine silts and clay and can be transported and deposited on top of (*supraglacial*), beneath (*subglacial*) or within (*englacial*) a glacier or ice-sheet. The finer-grained material is then released from the ice as it melts and transported in deep, turbid and fast flowing subaqueous environments (*proglacial*). Duller et al. (1995) suggested that light penetration through either the body of ice or the turbid water column is minimal and the degree of resetting of the OSL signal in mineral grains is often homogenously-poor.

2.3.1 Subglacial deposition

At the bed of the glacier, sediment can be incorporated into the ice by a variety of mechanisms (Boulton, 1974). In some cases, the sediment can be brought up to the surface of the glacier along dirt bands or thrust planes within the ice and

subsequently can melt out at the surface to release the sediment (Gemmell, 1988b). However, the dominant proportion of mineral grains transported in a subglacial environment emerge from the glacial system as deformation till and subglacial meltout tills (Tsukamoto, et al., 2002). Sediment transport and deposition in this manner occurs beneath a glacier or ice-sheet and hence sediments are unlikely to have been exposed to daylight during transport or deposition. Basal till in particular very rarely shows any trace of bleaching prior to deposition as illustrated by a number of TL (Punning and Raukas, 1983; Berger, 1984; Wintle and Catt, 1985; Gemmell, 1988b) and OSL (Tsukamoto, et al., 2002; Zhou, et al., 2008) investigations. Tsukamoto et al. (2002) observed that deformation tills sampled in the Kanchenjunga Himal, eastern Nepal gave age overestimations of ~ 29 ka (38.8 ± 6.3 ka and 36.5 ± 2.8 ka) in comparison to glaciofluvial and supraglacial meltout tills (8.1 ± 0.7 ka, 9.8 ± 0.6 ka and 9.0 ± 1.4 ka) which, in contrast appeared to be well-bleached upon deposition and gave ages in agreement with each other. The luminescence signal observed in such deformation tills is likely to be composed of a dominant residual OSL signal relating to the timing of the penultimate depositional cycle. A homogenously poorly-bleached OSL signal will result and the calculated optical age will not reflect the time elapsed since deposition as a subglacial till but will give an age overestimate which relates to the timing of the previous depositional event. Investigations into a range of subglacial waterlain depositional environments (eskers, fluviokames) have also suggested that their chaotic depositional setting is not conducive to satisfactory bleaching of mineral grains (Raukas and Stankowski, 2005).

2.3.2 Supraglacial deposition

For supraglacial deposits, the chance of bleaching is much greater as the sediment is transported on the glacier surface, therefore the sediment at the surface of the deposit is subsequently exposed to daylight and should be completely bleached (Tsukamoto, et al., 2002). Some mineral grains may be subject to supraglacial stream flow and transported in this manner across the glacier surface. The mixing of the sediment as it is transported in this way gives a greater opportunity for more mineral grains to be sufficiently bleached.

The dominant method of transport on to the glacier surface is via slump or fall from the valley sides. If the sediment lands on the glacier above the firn line, it is likely to be buried by further snowfall and moved downwards within the ice and so limiting the likelihood of complete bleaching (Gemmell, 1988b). If the sediment is deposited below the firn line it could then be transported to the glacier margin with the movement of the glacier ice and deposited as a flow or supraglacial meltout till. Such mass-movement of sediment is not conducive to satisfactory bleaching of mineral grains as the deposit has not been sufficiently mixed upon transport and deposition for the majority of mineral grains to be exposed to daylight.

2.3.3 Proglacial outwash deposition

The greatest chance of sufficient bleaching of mineral grains in the glacial system is likely to occur in proglacial outwash streams (Richards, 2000) (i.e. a sandur) and this is where the majority of research into OSL dating of glacigenic sediments has been directed (e.g. Gemmell, 1988a; b; Hütt and Jungner, 1992; Rhodes and Pownall, 1994; Duller, et al., 1995; Owen, et al., 1997; Rhodes and Bailey, 1997; Duller,

2006; Klasen, et al., 2006; Alexanderson and Murray, 2007; Bøe, et al., 2007; Gemmell, et al., 2007; Lukas, et al., 2007; Pawley, et al., 2008). This is due to the greater transport distance between glacier margin and point of deposition, which increases the probability of grains having undergone sufficient exposure to sunlight (Richards, 2000). Proglacial outwash streams can transport grains originating from on, in or beneath the glacier for many kilometres beyond the glacier margin. The subsequent mixing and cycling of sediment in the sandur system should allow a dominant 'population' of mineral grains to be sufficiently bleached. Distal sandur sediments are more likely to yield mineral grains that have been satisfactorily bleached in comparison to proximal sandur sediments. Sediments in distal environments are transported a greater distance and have been subject to many depositional and erosional cycles (for example, deposited on a bar top during waning flow but subsequently eroded and deposited further downstream during rising flow) (Richards, 2000).

Although glaciofluvial sandur systems offer greater opportunity for bleaching than the aforementioned glacial environments, their turbulence and turbidity means that some grains are not sufficiently exposed to daylight to enable the optical signal to be *completely* reset (Ditlefsen, 1992; Rendell, et al., 1994; Sanderson, et al., 2007), whereas other grains (those transported at the top of the water column) may have been well-bleached, producing a heterogeneously-bleached population of grains.

In exposed proglacial forelands during low water flow, when a large proportion of the sandur is subaerially exposed, aeolian transport via dust storms can occur frequently (McGowan, et al., 1996; McGowan and Sturman, 1997) and so enhancing

the opportunity for sufficient bleaching (Richards, 2000). These grains can be redeposited across the entire sandur system and reincorporated into glaciofluvial transport. They can also be transported great distances and deposited supraglacially or as coversands in periglacial environments extending from a few km^2 to thousands of km^2 and have been successfully dated using TL and OSL techniques (e.g. Bateman, 1995; 1998; Murton, et al., 2003; Bateman and Murton, 2006) due to their well-bleached nature. The redistribution of aeolian sediments across the proglacial foreland allows them to be incorporated into glaciofluvial sedimentary stratigraphy. Although difficult to identify, it enhances the chance of sampling well-bleached mineral grains across the full range of glaciofluvial depositional environments.

Despite problems concerning poor-bleaching many authors have applied luminescence dating techniques to constrain the timing of deposition of glacigenic sediments with some being more successful (e.g. Owen, et al., 2002; Duller, 2006; Alexanderson and Murray, 2007; Bøe, et al., 2007; Gemmell, et al., 2007; Klasen, et al., 2007) than others (e.g. Duller, et al., 1995; Raukas and Stankowski, 2005).

2.4. Problems associated with OSL dating of glaciofluvial sediments

2.4.1 Quartz or feldspar?

For quartz, optical stimulation in the laboratory is with blue light (wavelength 470Δ30 nm). For most feldspars, infrared stimulation (IRSL) in the region of 800-900 nm is used (Hütt, et al., 1988). There is a mineral dependency upon how easily the luminescence signal is bleached, with quartz being more easily bleached in full daylight than potassium feldspars as illustrated in Figure 2.4 (Godfrey-Smith, et al., 1988; Wintle, 1997). Hansen et al. (1999) report feldspar IRSL ages a factor of two

greater than quartz OSL ages for early Holocene glaciofluvial sediments from East Greenland illustrating that in turbid environments, quartz can be preferentially bleached over feldspar minerals.

This view was supported by Spencer and Owen (2004) who compared the outcome of applying optical dating techniques to quartz and feldspar from the same samples taken from numerous glacigenic sedimentary environments (glaciolacustrine, fluvial, glaciofluvial, supraglacial lacustrine, glaciotectonised glaciofluvial and diamict moraine deposits) from the Upper Hunza Valley of the Himalayas. The D_e for quartz samples was determined using the SAR protocol whereas for feldspars IRSL was used and D_e was determined using the single-aliquot additive dose (SAAD) protocol (Spencer and Owen, 2004). The results showed that the onset of luminescence saturation with increasing dose occurred much earlier in their feldspars in comparison to quartz and so constraining their use. They interpreted this as reflecting the presence of large remnant geological luminescence signals, suggesting inadequate bleaching of the infrared signal before deposition and, therefore, overestimation of the feldspar ages (Owen, et al., 2002; Spencer and Owen, 2004).

Feldspar is also known to display other problems such as anomalous fading (Wintle, 1973; Spooner, 1994; Lamothe and Auclair, 1999; Huntley and Lamothe, 2001; Auclair, et al., 2003; Kars, et al., 2008) and changes in trapping probability (Wallinga, et al., 2000) which are challenging to account for and overcome. Other investigations (Duller, et al., 1995; Owen, et al., 2002; Spencer and Owen, 2004; Lukas, et al., 2007) also show failure of IRSL on K-feldspars from different parts of the world, confirming their unfavourable characteristics for dating glacigenic

sediments. Due to the limitations of using the IRSL signal from feldspars in glacial settings most recent work has concentrated on quartz measurements using the SAR method (Duller, 2006; Alexanderson and Murray, 2007; Bøe, et al., 2007).

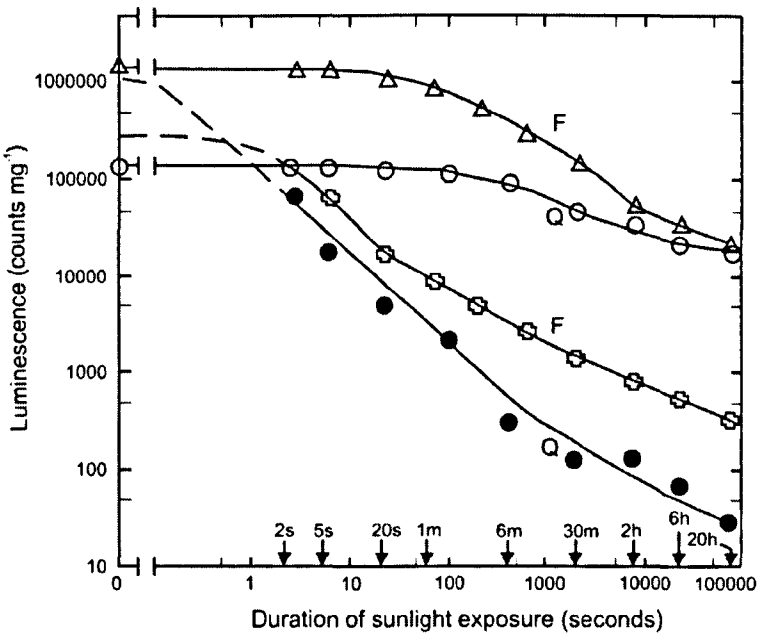

Figure 2.4 *Sunlight bleaching of natural TL and of natural OSL (based on Godfrey-Smith et al, 1988, redrafted from Wallinga, 2002). Quartz grains (Q) and K-feldspar grains (F) were used; the unbleached luminescence levels are shown on the vertical axis. The graph shows that the OSL of the minerals (• and +) is reset more readily than the TL (○ and Δ). It is also shown that the quartz OSL is reset more readily than the feldspar OSL.*

2.4.2 Poor quartz luminescence sensitivity and an absent fast component

Poor quartz luminescence sensitivity has been reported from glacially-derived sediments (Rhodes and Pownall, 1994; Rhodes and Bailey, 1997; Rhodes, 2000; Richards, 2000; Spencer and Owen, 2004; Lukas, et al., 2007) and has been attributed to geologically-young non-sedimentary bedrock sources, a lack of subaerial weathering of grains (Rhodes and Pownall, 1994) or an insufficient number of bleaching and dosing cycles prior to deposition (Pietsch, et al., 2008).

Lukas et al. (2007) observed that quartz from the north-western Scottish Highlands had a weak or absent fast component which was thought to be linked to the poor sensitivity of this quartz. The bedrock of the surrounding area was dominantly metamorphic schistose rocks which had not been through previous cycles of erosion and deposition and lacked opportunity to build up luminescence sensitivity. This is in contrast to the work of Gemmell et al. (2007) and Duller (2006) who observed adequately bleached quartz with reasonable luminescence sensitivity characteristics from the Buchan area in north-eastern Scotland, although a fast component was not always dominant. This could be explained by the greater lithological variety found in Buchan, including Devonian sandstones which may have been subject to previous bleaching and dosing cycles in Devonian desert environments, allowing luminescence sensitivity to build up (Gemmell, et al., 2007; Lukas, et al., 2007).

More recent short-duration episodes of deposition and reworking during the transport of grains through an ephemeral fluvial system have been shown to increase quartz luminescence sensitivity with distance travelled downstream. This was investigated by Pietsch et al. (2008) for the Castlereagh River in New South Wales, Australia. As grains were transported and subsequently deposited, their exposure to intense sunlight either on bar-tops or dry river beds allowed complete bleaching. Repeated erosion, transport and deposition cycles allowed quartz luminescence sensitivity to increase with each bleaching and dosing (burial) cycle as grains were transported further downstream (Pietsch, et al., 2008). This could be equally applicable to glaciofluvial environments where mineral grains undergo numerous episodes of deposition and reworking during transport through the sandur system. The depth and

turbidity of the water column which prevents sufficient bleaching in glaciofluvial environments could somewhat hinder this process.

The problem of quartz luminescence sensitivity and the lack of a fast component seem therefore to be related to bedrock provenance, the quartz type that is dominant within that bedrock lithology and the number of episodes of deposition and reworking that the quartz grain has undergone. To overcome this problem, detailed investigations into the provenance of the sediment being sampled for luminescence dating should be undertaken. An evaluation of whether quartz grains may have undergone previous cycles of erosion and deposition and hence multiple dosing cycles can then be made; for example, Permo-Triassic sandstones will have been subject to cycles of both aeolian and fluvial transport and deposition in Permo-Triassic desert environments, allowing quartz luminescence sensitivity to build up.

2.4.3 Turbidity of the water column

Under turbid water in a glaciofluvial environment, the intensity of the light is greatly reduced, and the spectrum of the light is restricted, slowing the average rate of bleaching for grains in transport (Gemmell, 1997). The highly turbid flows in glaciofluvial rivers imply that long transport distances and repeated deposition/erosion cycles may be needed to effectively bleach a high proportion of sediment grains in glaciofluvial environments (Richards, 2000).

Gemmell (1985) suggested that the turbidity of glaciofluvial sandur systems along with their high flow velocity combine to create an environment unsuitable for sufficient bleaching of mineral grains, especially when using TL measurements. This

was supported by field evidence from Western Norway (Gemmell, 1988a). The TL signal is reset much more slowly than the 'fast' component targeted in OSL dating, as shown in Figure 2.4 (Godfrey-Smith, et al., 1988) and so the use of OSL would therefore increase the opportunity for fully and partially bleached grains to dominate the sediment composition.

A particular factor needing to be considered is the presence of suspended sediment within the water column which, through selective absorption shifts the peak wavelengths of light penetrating the water towards the red part of the spectrum (Gemmell, 1988a). This wavelength is less effective at bleaching the remnant TL/OSL signal within quartz mineral grains. Shorter and longer wavelengths are attenuated and this attenuation effect increases with sediment concentration (Berger, 1990). The potential for underwater bleaching of the TL and OSL signals has been tested at different depths through a calm water column for both quartz and feldspar grains (Rendell, et al., 1994). The results indicated that a three hour light exposure is sufficient to bleach the optical signals down to water depths of 10 metres for feldspar IRSL and 12-14 metres for quartz OSL in the English Channel with visibility of 15 metres (Ditlefsen, 1992; Rendell, et al., 1994). This does not account for varying turbidity of water as observed in glaciofluvial environments (Clifford, et al., 1995; Hodson and Ferguson, 1999) and so partial bleaching is much more prevalent in quartz and feldspar from such deposits.

Sanderson et al. (2007) undertook underwater bleaching experiments upon canal sediments from Vietnam which provided an important insight into the effect of turbidity upon bleaching of the optical signal. The results showed that both

illumination intensities and spectral distributions are severely altered by as little as 1.5 m of turbid water and that OSL bleaching rates for both quartz and feldspars are reduced. At peak daylight wavelengths (~400-700 nm) intensities are reduced to ~5% of surface levels through 150 cm of moderately turbid water. By contrast the UV wavelengths and some IR components are attenuated more severely leaving less than 1% of surface intensities over the same depth range. Residual OSL signals for quartz minerals at depth under a moderately turbid water column were much greater than for feldspar minerals. It appeared that feldspars may therefore be more rapidly bleached than quartz under conditions of severe daylight attenuation and the shift to longer wavelengths of the moderately turbid underwater environment. However, the other challenges associated with optical dating of feldspar minerals as listed in Section 2.4.1 still hinder the widespread use of feldspars for optical dating of glacigenic sediments. The data implied that the assumption that quartz will normally be completely reset may not be satisfied under conditions of turbid water (Sanderson, et al., 2007). Although the water column in this research was described as "moderately turbid", an exact value for turbidity is not given. It could be assumed that the glaciofluvial water column is likely to be more turbid than that of a canal, resulting in further attenuation of daylight in the water column.

The results of Sanderson et al. (2007) support those of Ditlefsen (1992) where bleaching studies of potassium feldspars in turbid water suspensions showed that the IRSL signal bleached very slowly once suspended sediment concentrations reached greater than 200 mg/l. Investigations by Clifford et al. (1995) and Hodson and Ferguson (1999) show that suspended sediment concentrations (SSC) of glacial meltwater streams from glaciers of different thermal states can vary from as low as

200 mg/l to as high as 30 000 mg/l measured during one pulsing event (Clifford, et al., 1995; Hodson and Ferguson, 1999). When compared to the SSC mentioned by Ditlefsen (1992) the problem of poor bleaching of quartz and feldspar grains in such depositional environments becomes more apparent.

Although these SSC figures are high, they are recorded for main channel turbulent flow immediately downstream from the glacier terminus. There are sandur sub-environments (for example; overbank, bar top and back bar) where sediment can rain-out of suspension under lower SSC's and so increasing the opportunity for complete bleaching. The potential for successful optical dating of Pleistocene glaciofluvial and glacigenic samples is high, particularly if finer grains sizes and lower energy environments are sampled in the field (Rhodes and Bailey, 1997).

2.4.4 Diurnal and annual flow regime

The flow regime of glacier-fed rivers is strongly diurnal with maximum flow occurring in the afternoon (Ferguson, 1984; Collins, 1996; Benn and Evans, 1998) shortly after peak temperature and insolation and during maximum melting of the ice. The mineral grains transported/deposited during hours of darkness are unlikely to be bleached, creating a heterogeneously-bleached sediment when mixed with material transported, deposited and satisfactorily bleached during daylight (Gemmell, 1999). Repeated deposition and remobilisation of mineral grains as a result of the multiple diurnal flow cycles is likely to result in satisfactory bleaching to give near zero Gy equivalent doses (e.g. Bøe, et al., 2007). Thus many grains undergo numerous transport events and some may experience periods of subaerial exposure early in the day before water flow maximum. Both of these factors increase the

likelihood of effective bleaching (Richards, 2000) and bleaching potential increases with distance transported.

Ferguson (1984) investigated the influence of annual flow regime in relation to sediments from the Himalayas and observed that over 95% of glaciofluvial sediment transport in the Himalaya occurs in the summer, coinciding with highest insolation intensity. The higher insolation and average temperature in summer months associated with the annual flow regime of glacial outwash should therefore aid the bleaching of mineral grains although the related high sediment loads may mitigate against this point (Richards, 2000).

Diurnal and annual flow regime of glaciofluvial sediments could in theory aid the bleaching of mineral grains. Large fluctuations in sediment and water supply cause mineral grains to be cycled repeatedly throughout transport in the sandur system. This creates multiple transport events for each mineral grain and so enhancing the chance for sufficient bleaching. It also allows for subaerial exposure.

2.5 Techniques used to detect and account for heterogeneous bleaching

Several different schemes have been devised with the aim of detecting heterogeneous bleaching and these can be broadly separated into two groups; 'signal analyses' and 'distribution methods'. Signal analysis methods allow a comparison of various parts of the OSL signal to detect heterogeneous bleaching whereas distribution methods rely upon the analysis and interpretation of the form of a distribution of D_e values. This section details each of these methods.

2.5.1 Signal analysis; $D_e(t)$ plots

The investigation of D_e as a function of stimulation time; $D_e(t)$ plots, was first suggested by Huntley et al. (1985). In this method, the D_e is calculated using successive intervals of the decaying OSL signal. A requirement for this test is that the OSL signal must be composed of at least two thermally stable components of differing bleachability (Bailey, et al., 2003). Significant evidence exists to suggest that the quartz OSL signal does indeed comprise of several thermally stable components that each decay at different rates under stimulation (Bailey, et al., 1997; Bulur, et al., 2000; Jain, et al., 2003b); see also Section 2.2.4. A flat $D_e(t)$ plot suggests that all components were equally reset prior to burial and that the same age was obtained for all portions of the OSL signal i.e. a fully bleached sample. A rising $D_e(t)$ plot may indicate insufficient signal resetting prior to deposition as the more slowly bleached components are expected to retain a larger residual signal and would therefore yield a greater age upon measurement i.e. a heterogeneously bleached sample (Bailey, 2000a; Bailey, et al., 2003).

Bailey et al. (2003) compared the $D_e(t)$ plots of two samples types; aeolian and fluvial (Figure 2.5 a & b respectively). The young (<1000 years) aeolian gave a constant $D_e(t)$ which suggested that the sample was well bleached whereas the modern-age fluvial sample showed a consistently rising $D_e(t)$ plot indicative of heterogeneous bleaching. There are, however, a number of complications with this technique outlined in Bailey et al. (2003) and summarised here. A thermally unstable slow component can yield a falling $D_e(t)$ plot and thermal transfer of charge to the medium component can cause a rising $D_e(t)$ plot, both of which are unrelated to how well bleached the sample is.

2.5.2 Distribution methods

Empirical studies of glaciofluvial and fluvial sediments (Murray, et al., 1995; Olley, et al., 1998; Olley, et al., 1999; Lepper, et al., 2000; Olley, et al., 2004; Rodnight, 2006) have reported evidence of asymmetric D_e distributions based on single-aliquot and single-grain approaches, where the larger D_e values are attributed to the presence of poorly-bleached grains in the sample. Olley et al. (1999) analysed D_e distributions (Figure 2.5) of fluvial samples from New South Wales in Australia. Figure 2.5 shows the measured D_e's from small aliquots (60-100 grains) of quartz from one sample. The distribution is clearly asymmetric and positively skewed, with a dominance of well-bleached grains and a population of poorly-bleached grains that contribute to the long 'tail' on the D_e distribution towards higher D_e values.

Overdispersion is a parameter which can be used to detect heterogeneous bleaching. It can be calculated for each D_e distribution and is described as the spread in the D_e population that is in addition to the spread expected from the error on each D_e value (Galbraith, et al., 1999). Jacobs et al. (2006) and Duller and Augustinus (2006) found overdispersion values of 10-12% for single-grain and small aliquot datasets from well-bleached aeolian sand. This natural variation in D_e values could be related to non-uniform emptying of optically-sensitive traps and thermal transfer (Galbraith, et al., 2005). Therefore, any overdispersion value of >10% for single-grain/small aliquot D_e distributions is indicative of heterogeneous bleaching, assuming that no other post-depositional disturbance or beta-dose heterogeneity has occurred within the samples. In fluvial samples from South Africa, Rodnight et al. (2006) observed overdispersion values of between 35-101% which was illustrative of partial bleaching within these sediments.

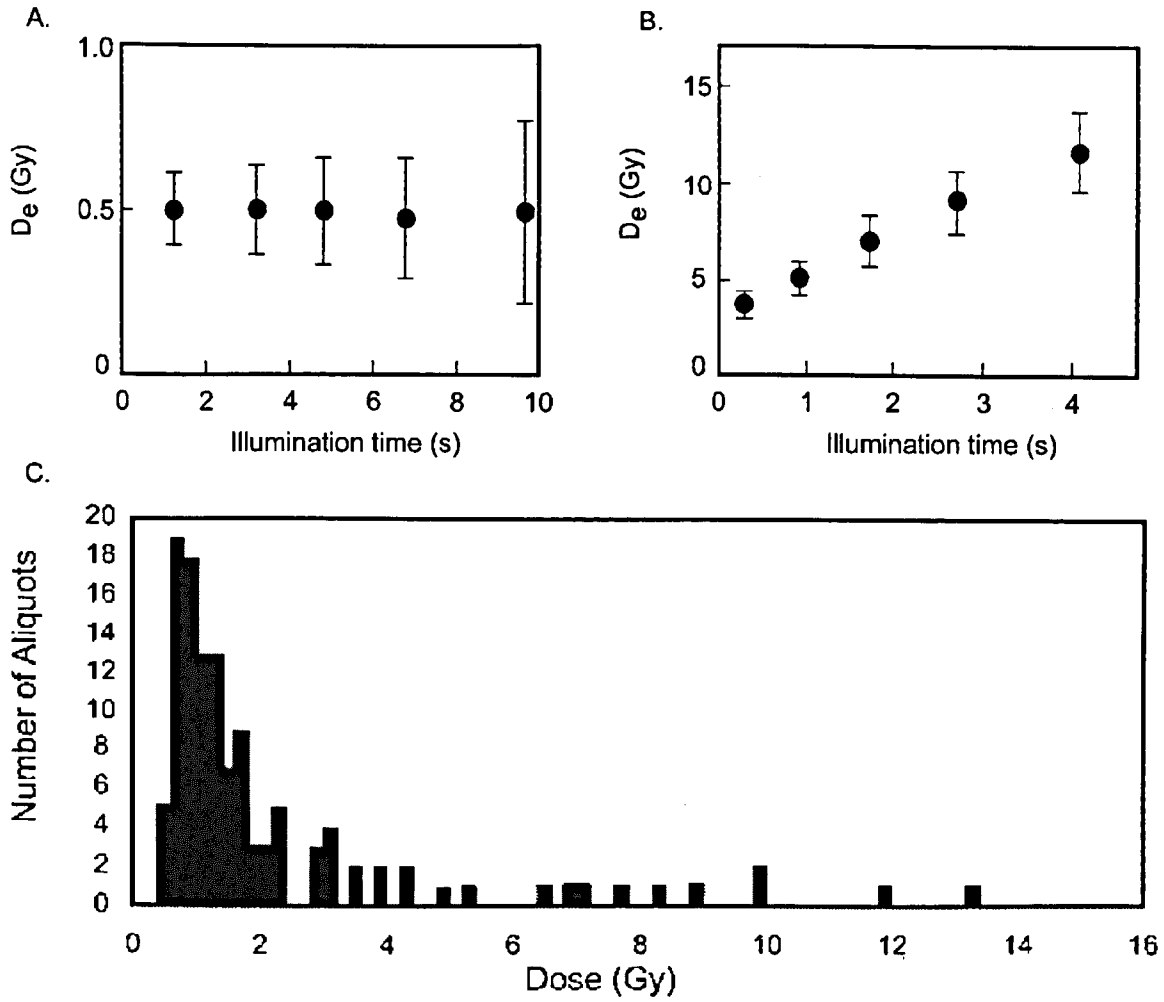

Figure 2.5 *(a) $D_e(t)$ plot for a young aeolian sediment (redrafted from Bailey et al., 2003) (b) $D_e(t)$ plot for a modern-age fluvial sample (redrafted from Bailey et al, 2003) (c) D_e distribution obtained from small aliquots (60-100 grains) of fluvial quartz from New South Wales, Australia. The distributions are skewed to higher doses as a result of contamination of the sample by a small number of poorly-bleached quartz grains (redrafted from Olley et al. 1999).*

2.5.3 Deriving a D_e from a heterogeneously-bleached quartz; statistical 'age' models

Several schemes have been published which address the problem of deriving a single-value estimate of the burial dose from such positively skewed and overdispersed D_e distributions, some of which are described below:

1. *The Minimum Age Models (MAM)* of Galbraith et al. (1999) attempt to define the minimum D_e acquired by the fully bleached proportion of grains within a heterogeneously-bleached D_e distribution. The distribution of D_e values is approximated by a truncated log-normal distribution, with the truncation point giving the estimate of palaeodose (Galbraith, et al., 1999).

2. *The mean of the lowest 5%* (L5%) of D_e values (Olley, et al., 1998) are expected to represent the well-bleached portion of a sample that shows evidence of heterogeneous-bleaching. This was used upon partially bleached fluvial samples from Australia (Olley, et al., 1998). By calculating the mean of the lowest 5% of D_e values, age estimates were obtained that were stratigraphically consistent.

3. *The Finite Mixture Model (FMM)* of Galbraith and Green (1990) identifies 'populations' (or clusters) of aliquots/single grains within the entire heterogeneously-bleached D_e distribution. Each component population of aliquots/single grains has its own D_e and error associated with it. Additionally, the Bayesian Information Criterion (BIC) is given, which is used to assess the 'best fit' number of populations to fit a dataset. BIC

reduces to a minimum at the optimum number of component populations (Rodnight, 2006). The *lowest* D_e population identified through this process is thought to reflect the well-bleached proportion of the sample.

The decision protocols of Bailey and Arnold (2006) enable a robust statistically-informed choice to be made as to which statistical 'age' model is most appropriate for a particular shaped D_e distribution. These protocols were based upon a set of real and modelled D_e distributions from fluvial samples using overdispersion, weighted skewness and kurtosis to characterise the D_e distribution (see Bailey and Arnold, 2006; Arnold et al., 2007 for decision protocols). This decision process was then tested on empirical data (Arnold, et al., 2007) for samples for which there was independent age control (Bailey and Arnold, 2006).

2.5.4 Overcoming heterogeneous bleaching

Duller *et al* (1995) applied OSL techniques to large aliquots of potassium-rich feldspars of pre-late Devensian sites in Scotland, the majority of which were glacigenic in origin. A number of glaciofluvial sediments from Scottish sites had been sampled including: Howe of Byth, Burn of Bigholm and Mains of Cardno (Duller, et al., 1995). At Howe of Byth a series of meltwater gravels were sampled from a horizontally-laminated sand (*Sh*) overlying imbricate cobble-gravels (Duller, et al., 1995; Hall and Connell, 2000) representing deposition of sheet flow sand over a gravel-bedded channel in a ice-proximal, fast flowing environment. At Burn of Bigholm the presence of imbricate gravel horizons and cross- and flat-bedded sand lenses from which the luminescence sample was taken indicates a braided stream

deposit undergoing ice-proximal sheet-flow. The Mains of Cardno sample was taken from a bar-edge sand lens within braided outwash gravels.

The Howe of Byth sample from the horizontally laminated sand gave IRSL ages of 45.5 ± 3.8 and 36.8 ± 3.6 ka, much older than their hypothesised Late Devensian age. The Burn of Bigholm sample gave a multiple grain IRSL age of 21.3 ± 4.6 ka, also much older than the postulated age defined by a series of four calibrated radiocarbon ages (13.3-11.0 ka) and the Mains of Cardno sample also gave a significant age overestimate of 120 ± 10 ka and 108 ± 13 ka. These age overestimations were likely to have been a result of the ice-proximal environment in which all samples were hypothesised to have been deposited allowing few feldspar grains to be completely-bleached upon deposition. The results from such samples led Duller *et al* (1995) to conclude that these sediments, deposited a few kilometres from an ice margin were unsuitable for OSL dating purposes. This multiple-grain IRSL approach demonstrated that such sediments showed incomplete bleaching of grains (Duller, et al., 1995; Hall and Connell, 2000).

Due to advances in protocols (Murray and Wintle, 2000) and equipment (Bøtter-Jensen and Duller, 1992; Bøtter-Jensen, et al., 1999; Duller, et al., 1999; Bøtter-Jensen, et al., 2000; Bøtter-Jensen, et al., 2003) it is now feasible to measure the D_e of single mineral grains. *Quartz single-grain* OSL dating of Duller's Scottish glacial sediments (Duller, 2006) showed much more encouraging results. The use of the FMM allowed the identification of clusters or 'populations' of D_e values within the distribution with the lowest D_e cluster representing the well-bleached portion of the sample. The approach to applying the FMM as used by Duller (2006) was to choose

the dose population with the lowest D_e but which contains at least 10% of the grains (or D_e values) to enable the rejection of outlying low D_e values (after Rodnight, et al., 2006). For the Burn of Bigholm and Mains of Cardno samples, three D_e components were fitted to each D_e distribution (Duller, 2006).

The Burn of Bigholm sample, whose multiple grain IRSL age overestimated the independent age control by ~10 ka, was measured once again using single grains of quartz and an age of 10.8 ± 1.0 ka was calculated which was in agreement with the 11.0-13.3 ka radiocarbon ages (Duller, 2006). The Mains of Cardno sample which originally overestimated the hypothesised age by a factor of five, gave a single-grain OSL age 17.3 ± 1.5 ka. A significant reduction in the calculated ages is observed. The radial plot for the Mains of Cardno sample shown in Figure 2.6 allows the different D_e clusters to be observed clearly. A population of grains with higher D_e values is apparent, centred on ~250 Gy (~145 ka). This relates to a dominant proportion of grains that have not been completely bleached.

Both Burn of Bigholm and Mains of Cardno samples were taken from ice-proximal gravelly-lithofacies with intercalating sand layers, but clearly there were grains within the sediment matrix that still had the opportunity to be well-bleached upon deposition. The single-grain approach and the use of the appropriate 'age' model (FMM) then allowed these well-bleached grains to be identified within the D_e distribution and an optical age to be calculated as a result. This illustrates the impact that recent technique and statistical analysis development has had upon the ability to date sediments that were once thought impossible to date due to poor luminescence characteristics and partial bleaching.

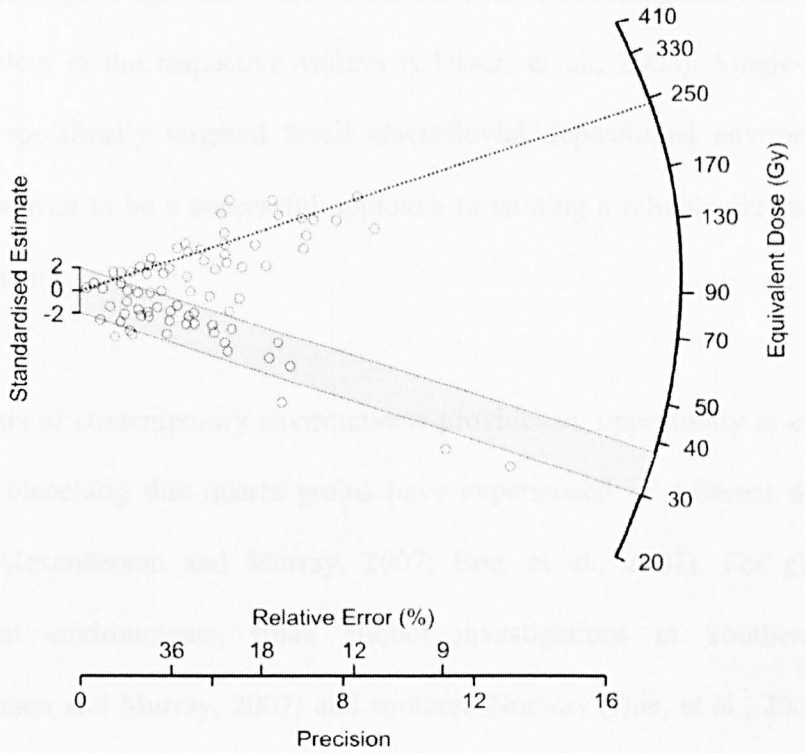

Figure 2.6 *Radial plot of single-grain D_e values for Scottish Mains of Cardno sample. The grey shading denotes the D_e value obtained from fitting the Finite Mixture Model. A higher D_e cluster is also indicated by the dashed line. This cluster is hypothesised to be related to unbleached grains in the sample. Redrawn and adapted from Duller (2006).*

2.6 Recent successful applications of OSL dating of glaciofluvial sediments

The use of single-grain and small aliquot methodologies (Duller, 2006; Alexanderson and Murray, 2007; Bøe, et al., 2007) has improved understanding of the bleaching history of a sample. These 'population'-based approaches reveal significant differences in bleaching between depositional environments. Duller (2006) attempted to produce an absolute chronology for glacigenic deposits of Exploradores and Leones valleys, Chile. Single-grain optical dating was applied to ice-contact glaciofluvial deposits along the margins of the former glacier purposely avoiding glacial diamicts. Applying the FMM identified a D_e component that, together with

dose-rate data, gave ages that were consistent with the cosmogenic chronology data from boulders in the respective valleys (Glasser, et al., 2006). Single-grain OSL dating of specifically targeted fossil glaciofluvial depositional environments has therefore proven to be a successful approach to gaining a reliable chronology from such sediments.

The analysis of contemporary environments provides an opportunity to evaluate the degree of bleaching that quartz grains have experienced in different depositional settings (Alexanderson and Murray, 2007; Bøe, et al., 2007). For glaciofluvial depositional environments, small aliquot investigations in Southern Sweden (Alexanderson and Murray, 2007) and southern Norway (Bøe, et al., 2007) showed that D_e's of modern samples taken from both deep-channelled stream and ripple and laminated structures deposited in shallow water were <5% of the average for the fossil sandur sediments of interest. This strongly suggested that the sediment sampled was readily bleached by the prevailing conditions at the time of deposition (Bøe, et al., 2007).

Optical ages of the fossil sandur sediments as determined by Alexanderson and Murray (2007), taken from similar depositional environments as the 'contemporary' environments, were stratigraphically consistent and they also agreed between sites kilometres apart. Those obtained by Bøe et al. (2007) agreed with independent age information (^{14}C and ^{10}Be) and so emphasising the reliability of the OSL chronological data for the deposition of glaciofluvial sediments as a result of the melting of a lobe of the regional LGM ice-sheet in Norway.

These investigations (Duller, 2006; Alexanderson and Murray, 2007; Bøe, et al., 2007) have shown that reliable quartz OSL chronologies can be successfully obtained from glacigenic sediments, but suggest that sampling needs to be directed towards depositional environments that are conducive to yielding well-bleached quartz grains. For example, distal glaciofluvial sub-environments have been proven to yield well-bleached quartz grains (Alexanderson and Murray, 2007; Bøe, et al., 2007), due to deposition within a shallow and non-turbid water column allowing exposure to sufficient daylight bleach the optical signal upon deposition.

2.7 Directions for future research; a lithofacies-based approach

2.7.1 The lithofacies concept

Lithofacies analysis refers to the identification of lithological components, sedimentary structures and the vertical and lateral relationships between them for a sedimentary sequence (Miall, 2006). Understanding the architectural relationships between lithofacies (or architectural element analysis (AEA)) assists the subdivision of sedimentary basin fills into elements (or facies assemblages) on the basis of sedimentary body geometry and lithological composition (Miall, 1985; Brookfield and Martini, 1999; Boyce and Eyles, 2000). These approaches help to constrain the nature of past depositional environments and processes.

Contemporary glaciofluvial environments are typically braided systems and characterised by large and rapid discharge fluctuations, abundance of easily erodible material, and high rates of sediment transport and deposition (Hammer and Smith, 1983). Fluctuations in meltwater and sediment supply to sandar reflect seasonal, diurnal and stochastic changes, as well as responses to advance or retreat cycles of

the source ice masses. All these factors result in a spatially and temporally variable pattern of sediment grain size and structure which is then preserved in the fossil record as complicated laterally and vertically variable sequences of lithofacies (Thomas, et al., 1985).

An example of a typical glaciofluvial lithofacies succession is given in Figure 2.7 which illustrates the construction of a facies model for lithofacies assemblages found in a palaeosandur at Orrisdale in the Isle of Man. This Facies Relation Diagram (Thomas, et al., 1985; Connaughton, 1986) illustrates an idealised progression from one lithofacies to another for two different glaciofluvial depositional environments. Lithofacies assemblage A shows an idealised assemblage deposited in a high energy, ice-proximal environment where gravel bars (*Gm/Gp*) dominate the assemblage and from a luminescence perspective the bleaching potential is thought to be minimal. The number of potentially well-bleached lithofacies in ice-proximal depositional environments is reduced and is perhaps limited to bar-top and back-bar ripple and laminated sands (*Sr/Fl*) that reflect waning flow conditions as part of the diurnal/annual flow cycle. Lithofacies assemblage B shows a sand-dominated stratigraphy related to a more ice-distal depositional environment. Although there is sandy bar-growth lithofacies (*Sp*) present, there is evidence of fining-up sequences indicating waning flow and therefore greater potential for bleaching, especially if bar tops (*Fl*) are subsequently subaerially exposed.

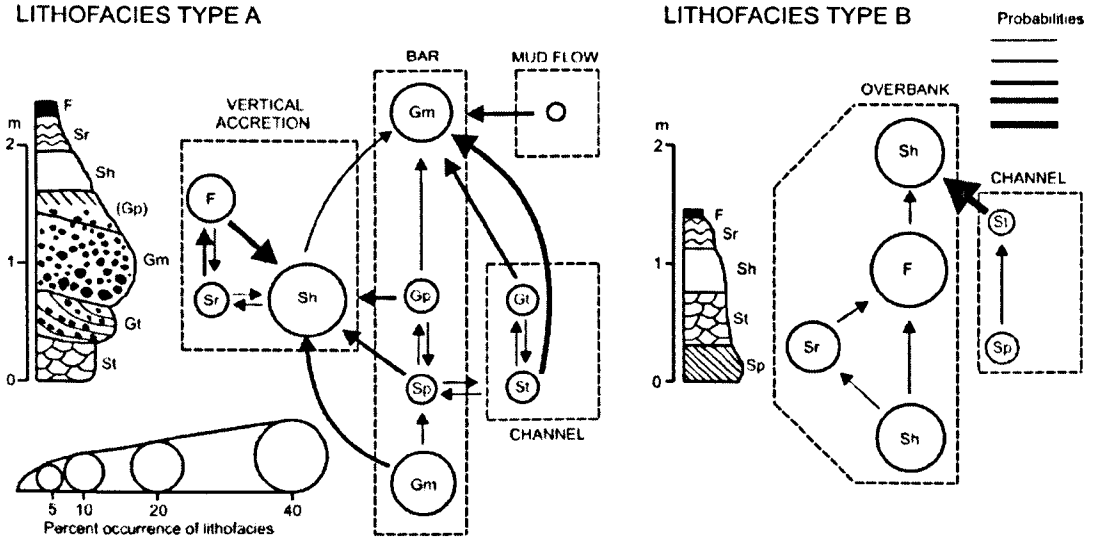

Figure 2.7 *Facies Relation Diagram for each of the Assemblages A and B. Idealised facies sequences for each assemblage, based on the Facies Relation Diagram and average thickness are also given (redrafted from Thomas, 1985).*

2.7.2 A conceptual method for targeting well-bleached glaciofluvial sediments

Figure 2.8 shows a flow diagram of the main routeways, storage and depositional environments of a proglacial sandur, identifying the transport and storage mechanisms (and associated lithofacies) that provide enhanced opportunities for bleaching of mineral grains. Those lithofacies with low bleaching potential are deposited in turbid environments proximal to the ice margin such as bar core (massive gravels; *Gm*) and bar growth (planar cross bedded sands/gravels; *Sp/Gp*) lithofacies. Those deposited during waning flow in shallow, slow flowing or stagnant water columns were sediment can settle out of suspension under relatively clear water have the highest chance of bleaching such as bar-top and back-bar deposits (rippled sands; *Sr*, horizontally-laminated sands; *Sh* and finely-laminated sands; *Fl*). Subsequent subaerial exposure of these deposits presents an opportunity for these

bar-top and back-bar deposits to be subject to aeolian transport under daylight (McGowan, et al., 1996; McGowan and Sturman, 1997) further enhancing their potential to be sufficiently bleached. Research from Lake Tekapo in New Zealand's South Island (McGowan, et al., 1996; McGowan and Sturman, 1997) has suggested that aeolian transport in cold environments is a significant transport mechanism for sand across exposed proglacial areas. Such dust storms occur where ice marginal temperature differences encourage wind circulation and strong gusts to initiate dust storms on exposed areas of the proglacial sandur. The exposure of such sediments to sunlight during these dust storms adds further opportunity for sufficient bleaching and re-deposition across the entire sandur surface.

Undertaking a targeted lithofacies-based approach to sampling for optical dating maximises the opportunity of extracting quartz that has been well-bleached. A comprehensive knowledge of proglacial glaciofluvial transport and depositional processes is therefore required to identify the lithofacies most likely to yield such well-bleached quartz grains (Duller, 2006; Alexanderson and Murray, 2007; Bøe, et al., 2007) . If samples prove to be problematic in relation to bleaching status, single aliquot/grain analysis methodologies allow the few well-bleached grains to be identified. The use of appropriate statistical 'age' models then allows the grains assumed to be well-bleached to be used for D_e determination and age calculation (Duller, 2006).

Figure 2.8 *Flow diagram illustrating the main routeways, storage and deposition of proglacial sandur sediments along with identifying those processes which provide an enhanced opportunity for material to be bleached.*

2.8 Conclusions

This review has identified a series of key issues that have implications for future OSL dating of glacigenic sediments which are summarised below:

- Quartz is the preferred mineral for optical dating of glacigenic sediments due to the luminescence signal of some grains being more readily bleached than feldspar minerals even under turbid water columns. Additional problems associated with optical dating of feldspars including anomalous fading and changes in trapping sensitivity further hinders their use with glacigenic sediments.
- Problems related to quartz luminescence sensitivity and the lack of a fast component in glacigenic sediments seem to be related to quartz bedrock provenance and sedimentary history and are physical characteristics of the quartz itself that, at present cannot be overcome. Therefore a detailed evaluation of quartz provenance is necessary to ensure that the surrounding bedrock lithology is composed of mineral grains that may have been subject to previous dosing cycles.
- It is clear that heterogeneous-bleaching is always likely to be an issue during OSL dating of glacigenic sediments due to the very nature of their depositional environments. Improvements in sampling methodology such as using a lithofacies-based approach has improved the analysis of depositional environments which should in turn guide the researcher to sample such areas where satisfactory bleaching is most likely to have occurred. Proglacial glaciofluvial sediments offer the greatest chance for sufficient bleaching of quartz grains and should be targeted for future research.

- Methodological improvements for the analysis of luminescence such as the advent of the SAR protocol (Murray and Wintle, 2000) together with a critical understanding of quartz bleaching history and regime and the ability to measure the optical signal of individual grains of quartz (Duller, 2004) and small aliquots, has enhanced the likelihood of obtaining a population of well-bleached grains within a D_e distribution, from which the depositional age can be derived.
- A product of the move to population based approaches to collecting D_e measurements requires the use of statistical 'age' models such as the Minimum Age Model (Galbraith, et al., 1999) and the Finite Mixture Model (Galbraith and Green, 1990) for heterogeneously-bleached deposits. These have enabled the nature of heterogeneously-bleached D_e distributions to be analysed in greater detail, allowing the well-bleached D_e population to be statistically extracted from those that are poorly-bleached.

Chapter 3

Dosimetry

3.1 Introduction

The measurement of natural radioactivity and its evaluation in terms of natural dose-rate received by the sample is of equal importance to the measurement of OSL and the derivation of D_e. For the majority of samples, nearly the entire natural dose-rate is provided by the radioactive decay of isotopes in the uranium series, thorium series (shown in Figure 3.1) and potassium-40. A small contribution comes from the decay of rubidium-87 and cosmic rays (Aitken, 1985). Natural uranium has three isotopes, ^{238}U, ^{235}U and ^{234}U and their relative atom abundances are 99.2745%, 0.7200% and 0.0055% respectively. The decay of these uranium isotopes, along with ^{232}Th series isotopes results in the emission of alpha and beta particles and photons. ^{40}K represents 0.0117% of the natural potassium and emits beta particles and photons whereas ^{87}Rb emits only beta particles on decay (Aitken, 1985). The half-lives of the U and Th parent isotopes, and of ^{40}K, are in the order of 10^9 years. Thus the natural abundance of these remains constant over the period of time that OSL dating is feasible (up to 10^5 years).

Minerals accumulate dose gradually from this natural irradiation from alpha, beta and gamma emitters. A fundamental assumption is that the number of trapped electrons in the crystal lattice is related to the dose that the crystal receives from natural irradiation. This dose is equivalent to the laboratory irradiation that can create the same number of trapped electrons as natural irradiation. Therefore, the length of

time that the mineral was exposed to natural irradiation can be determined if the environmental dose-rate can be found. However, there is an assumption that the dose-rate is equal to the rate of energy emission per unit mass, implying that there is homogeneity in radioactive content in the sediment surrounding the dosimeter and in absorption coefficient (Adamiec and Aitken, 1998).

However, secular disequilibrium of the decay chain can occur when a radioisotope is added to or removed from a system (Osmond and Cowart, 1982). If due to some process an excess amount of daughter is present, the rate of decay will exceed the rate of production and the amount will decrease until the equilibrium condition is reached. In this case, the daughter is *supported* by the parent. If by some process the parent is removed, then the daughter becomes *unsupported* and its amount decreases exponentially with time as determined by its half-life (Aitken, 1985). Therefore, the activity of daughter products will change through time and thus the environmental dose-rate cannot be calculated from the concentrations of the parent isotopes alone. The activity of a number of daughter radionuclides in the decay series should be compared to allow a full picture of the decay series to be achieved.

Studies investigating sediments with disequilibrium have been performed using high-resolution gamma spectrometry (Olley, et al., 1996) or a combination of alpha spectrometry and gamma spectrometry (Krbetschek, et al., 1994; Olley, et al., 1997). These techniques are able to determine the activity of various nuclides in the decay chains, enabling an assessment of equilibrium status to be made. In this research, high-resolution gamma spectrometry was performed on samples to estimate the environmental dose-rate and to assess the equilibrium status of the ^{238}U decay chain.

Uranium-238 Series			Uranium-235 Series			Thorium-232 Series		
Nuclide	*Decay mode*	*Half-life*	*Nuclide*	*Decay mode*	*Half-life*	*Nuclide*	*Decay mode*	*Half-life*
^{238}U		4.47×10^{9} a	^{235}U		7.04×10^{8} a	^{232}Th		1.39×10^{10} a
↓	α		↓	α		↓	α	
^{234}Th		24.10 d	^{231}Th		25.52 h	^{228}Ra		5.75 a
↓	β		↓	β		↓	β	
^{234}Pa		1.17 m	^{231}Pa		3.28×10^{4} a	^{228}Ac		6.13 h
↓	β		↓	α		↓	β	
^{234}U		2.45×10^{5} a	^{227}Ac		21.77 a	^{228}Th		1.91 a
↓	α		↓	β		↓	α	
^{230}Th		7.54×10^{4} a	^{227}Th		18.72 d	^{224}Ra		3.66 d
↓	α		↓	α		↓	α	
^{226}Ra		1.60×10^{3} a	^{223}Ra		11.43 d	^{220}Rn		55.60 s
↓	α		↓	α		↓	α	
^{222}Rn		3.80 d	^{219}Rn		3.96 s	^{216}Po		0.15 s
↓	α		↓	α		↓	α	
^{218}Po		3.11 m	^{215}Po		1.78×10^{-3} s	^{212}Pb		10.64 h
↓	α		↓	α		↓	β	
^{214}Pb		26.80 m	^{211}Pb		36.10 m	^{212}Bi		60.50 m
↓	β		↓	β		↓	β	
^{214}Bi		19.90 m	^{211}Bi		2.14 m	^{212}Po		3.04×10^{-7} s
↓	β		↓	α		↓	α	
^{214}Po		163.69 μs	^{207}Tl		4.77 m	^{208}Tl		3.10 m
↓	α		↓	β		↓	β	
^{210}Pb		22.26 a	^{207}Pb		Stable	^{208}Pb		Stable
↓	β							
^{210}Bi		5.01 d						
↓	β							
^{210}Po		138.38 d.						
↓	α							
^{206}Pb		Stable						

Figure 3.1 *Decay series for ^{238}U, ^{235}U and ^{232}Th. The decay mode and half life of each isotope are also indicated.*

3.2 Internal dose-rate

The D_e values in this work were obtained from measurements on quartz grains. If K was present in significant quantities in the grains then the ^{87}Rb contribution to the internal dose-rate should be taken into account (Mejdahl, 1987). Quartz grains contain very low levels of U, Th and K and hence whilst the grains may have some alpha activity, it is thought that one is able to assume that the internal dose-rate of the

grains is negligible (Aitken, 1998). However, for particularly low-activity samples, the contribution of internal dose-rate to total dose-rate becomes increasingly significant and so for all samples, an internal dose-rate of 0.035 ± 0.010 Gy/ka was assumed (Mejdahl, 1987; Murray and Funder, 2003).

3.3 External dose-rate

The external beta and gamma dose-rates and the cosmic dose-rate are summed with the internal dose to derive the environmental dose-rate for a sample. The external alpha dose-rate does not need to be taken into account because alpha particles only penetrate the outer rind of a quartz grain; the alpha particles are attenuated before reaching the inner core and the HF acid treatment used in sample preparation is assumed to etch away the alpha irradiated skin (the outer 10 μm of the quartz grain).

3.3.1 Cosmic ray contribution

Cosmic radiation usually contributes a few percent to annual dose (Aitken, 1985) and varies with altitude, latitude, longitude and burial depth (Prescott and Hutton, 1994). Prescott and Hutton (1994) calculated the long-term variation of cosmic radiation and concluded that the variation is negligible for the natural dose-rate calculation. The dependence of cosmic dose-rate on latitude is due to the change of the magnetic field of the earth. However, for latitudes above 40°, the cosmic dose-rate is not significantly affected by latitude and is constant at the same altitude (Prescott and Hutton, 1994). The total cosmic dose-rate under 0.5 m depth and 110g/cm^2 density is approximately 185 ± 11 mGy/ka and 280 ± 14 mGy/ka at the surface (Aitken, 1985). The natural dose-rate that the sediments received is the sum of the dose-rate calculated from radioactive decay and cosmic radiation.

Due to both rapid sediment accumulation during the period of deposition (as typical of a glaciofluvial sandur system) and the depth of sampling locations beneath the present day land surface (10-20 metres) the contribution of cosmic radiation (Prescott and Hutton, 1994) was minimal (0.0281 ± 0.0014 Gy/ka) but the proportional contribution to the total dose rate is larger for low activity samples (see Chapter 5 for more detailed site-specific depositional environment information).

3.4 Factors affecting the accuracy of determination of the natural dose-rate

There are a number of factors that can affect the accuracy of natural dose-rate determination, including radiation equilibrium status, water content, organic content and alpha radiation efficiency (only for the analysis of fine grained samples i.e. <63 μm).

3.4.1 Radioactive disequilibrium

Secular disequilibrium in the ^{232}Th series is not significant for optical dating since the longest half-life of the decay daughters in this series is no more than 6 years (Aitken, 1985) and secular equilibrium can be achieved after around 40 years of burial. Disequilibrium in the ^{235}U series is also not important due to its limited contribution to the total natural dose-rate. However, disequilibrium in the ^{238}U chain is a prominent contributor to inaccurate dose-rate values. Several members of the ^{238}U decay series have relatively long half-lives and, therefore, once equilibrium is broken, a relatively long time is needed before equilibrium can be re-established (Olley, et al., 1996; Olley, et al., 1997).

Disequilibrium can result from geochemical sorting, whereby a process acts to move a parent or daughter into or out of the system at a rate which is significant relative to the half-life of the daughter. The decay chains in deeply buried, unweathered materials are generally in equilibrium (Olley, et al., 1996). However, weathering processes that occur at or near the earth's surface operate on a sufficiently short time-scale for disequilibrium to result. Weathering processes in surficial environments can cause disequilibrium by two main processes. Firstly, dissolution and precipitation reactions occur as a result of the presence of water; for example, radium may be leached out by groundwater and then all subsequent members of the series are also depleted (Aitken, 1985). This process is more likely to occur in waterlain sediments, and thus for a glaciofluvial environment it is important to assess if a decay chain is in secular equilibrium. Secondly, emanation of radon isotopes via diffusion (Olley, et al., 1996) can occur as a result of physical disturbance to the depositional sediment matrix. This escape is most likely if the sample is porous rather than compact and so is unable to retain radon gas due to its loose and unconsolidated nature.

Olley et al. (1996) investigated young fluvial samples for disequilibria in both the U and Th decay chains. Their results showed significant disequilibrium for various parent-daughter ratios of the ^{238}U decay chain, although this rarely exceeded 50% (i.e. activity concentration ratios for relevant parent-daughter pairs of 0.5-1.5). The ^{232}Th decay chain was generally near secular equilibrium. In a number of samples, however, an excess of ^{228}Ra was present; this was attributed to rapid, significant, radium redistribution. Due to the short half-lives of radionuclides in the ^{232}Th decay chain (the longest lived daughter product is ^{228}Ra with a half-life of 5.75 years), disequilibrium in the ^{232}Th decay chain is unlikely to be important and thus the ^{228}Ra

excess should not be a problem in dose-rate calculation. The findings from these studies indicate that it is important to assess if disequilibrium particularly in the U decay series is present.

3.4.2 Water content

Another factor affecting the accuracy of dose-rate determination is water content. For the calculation of natural dose-rate, an important assumption is that the matrix is homogeneous as to the radiation mass stopping powers (for beta particles) and mass absorption coefficient (for photons). However, water and organic materials which may be present within the sediment have different mass stopping powers and mass absorption coefficients compared to minerals, resulting in attenuation of alpha and beta particles and photons. This must be accounted for by using the equations given in Section 3.6.2.

The water content of each sample was measured in the laboratory. The sampling bags were completely sealed at the time of sampling and so the laboratory measured water content was a good representation of the field value. The water content measured in the laboratory was calculated as the mass of water divided by the mass of the dry sediment multiplied by 100. The mass of water was calculated by weighing the wet sediment and then weighing once again after drying for at least 24 hours at 100°C. The mass of water was determined by subtracting the weight of the dry sediment from the weight of the wet sediment. A good estimate of the water content was necessary for calculation of the appropriate environmental dose-rate because water absorbs a significant amount of radiation that would otherwise reach the mineral grains.

3.4.3 Organic content

In highly organic sediments, disequilibrium in the U decay chain is possible since organic matter takes up U from groundwater (Lian, et al., 1995). Although disequilibrium could occur at several points in the decay chain, the main concern is with the decay of ^{234}U to ^{230}Th, which has a half-life of ~75 ka, much longer than that of the other decay products. An equation allowing for the correction of dose-rate according to organic content (Divigalpitiya, 1982) is given in Lian et al. (1995).

A correction for organic content was *not* necessary for these samples as they were laid down in an environment which was not conducive to organic growth and therefore are devoid of any form of organic material.

3.5 High-resolution gamma spectrometry

High-resolution low-background gamma spectrometry was used to determine the activities of various isotopes of the uranium and thorium decay chains and of ^{40}K and also to enable the detection of disequilibrium within the decay series. Two gamma detectors were used for these measurements to allow a comparison to be made (to check for reproducibility of results) and to allow an assessment of any secular disequilibrium within the ^{238}U decay chain to be made.

3.5.1 University of Liverpool

For samples measured at the University of Liverpool (*all samples*) the gamma spectrometer uses a coaxial HPGe detector (Pop Top type) with relative efficiency at 1.33 MeV of 32%. The detector has a size of ~70 mm in diameter and ~33 mm in height and is shielded with 15 mm copper and a 10 cm low activity lead castle. The

entrance window is mylar placed at around 5 mm distance from the Ge-crystal. A Perspex bar guarantees exact positioning of the sample onto the detector to ensure that measurement geometry was the same for each measurement enabling a direct comparison to be made with the reference material (*Nussi*) with regard to activity ratios. Samples were packed into air-tight plastic containers holding approximately 120 g and stored for around four weeks in order to achieve secular equilibrium between ^{226}Ra and ^{222}Rn (half-life of 3.90 days) (Mauz, et al., 2002). The increasing background together with the increasing self-absorption reduces the precision of counting in the low energy range (~<100 keV) and a precise assessment of secular disequilibrium requires long measurement times.

3.5.2 Victoria University of Wellington

In addition, selected samples (BLA1, BLA3, OR14) were measured at Victoria University of Wellington, New Zealand using an Ultralow-level Canberra BE5030 detector (Broad Energy 50 cm^2 area 30 mm thickness) J-style configuration, shielded with 6 inches of low level lead with electrolytic copper on the inside (Figure 3.2 and 3.3). Between the lead and the copper there is also a layer of tin. The sample was stored for four weeks and measured in a reusable airtight plastic container (Figure 3.3), which has a 0.5mm perspex window and the maximum filling height is 14mm. The area of the container approximately matches the area of the detector, so they are sitting face to face as in a planar detector. The use of this machine resulted in higher relative efficiency at 1.33 MeV of 50% (Figure 3.4) and quicker measurement time for low-activity samples. Due to the higher precision of counting in the low energy range associated with this machine (due to higher nominal efficiency), detection of secular disequilibrium in the ^{238}U decay chain is possible (Section 3.5.4) via

measurement and comparison of ^{234}Th (~63 and 92 keV), ^{226}Ra (~186 keV, taking into account the contribution of ^{235}U at this energy level, this was only used for a qualitative assessment) and ^{210}Pb (~46 keV) daughter radionuclide activities (Rieser, *pers. comm.).*

Figure 3.2 *Photograph showing the Ultralow-level Canberra BE50 detector used for samples OR14, BLA1 and BLA3. The electrolytic copper on the inside of the detector can also be seen (Photograph courtesy of Dr Uwe Reiser, Victoria University of Wellington, New Zealand).*

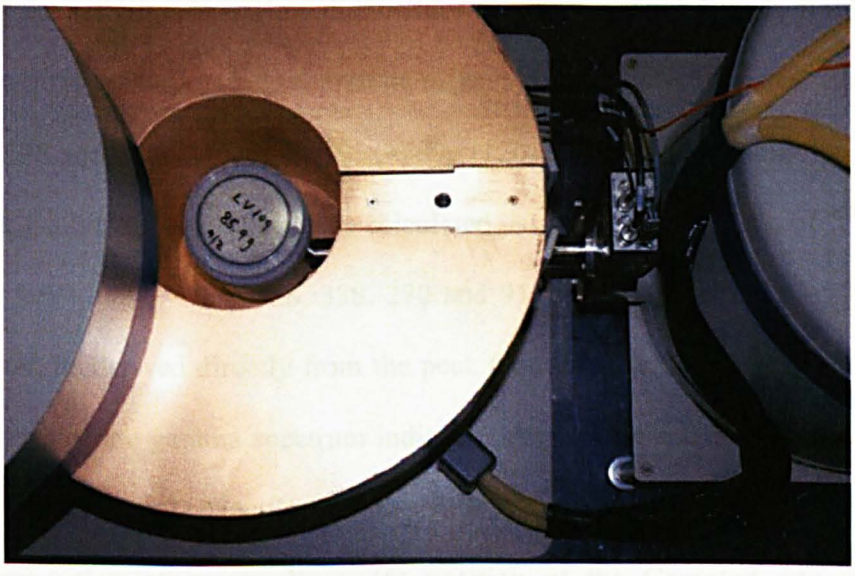

Figure 3.3 *Photograph showing the Ultralow-level Canberra BE50 detector together with the airtight plastic container used for sample storage and measurement (Photograph courtesy of Dr Uwe Reiser, Victoria University of Wellington, New Zealand).*

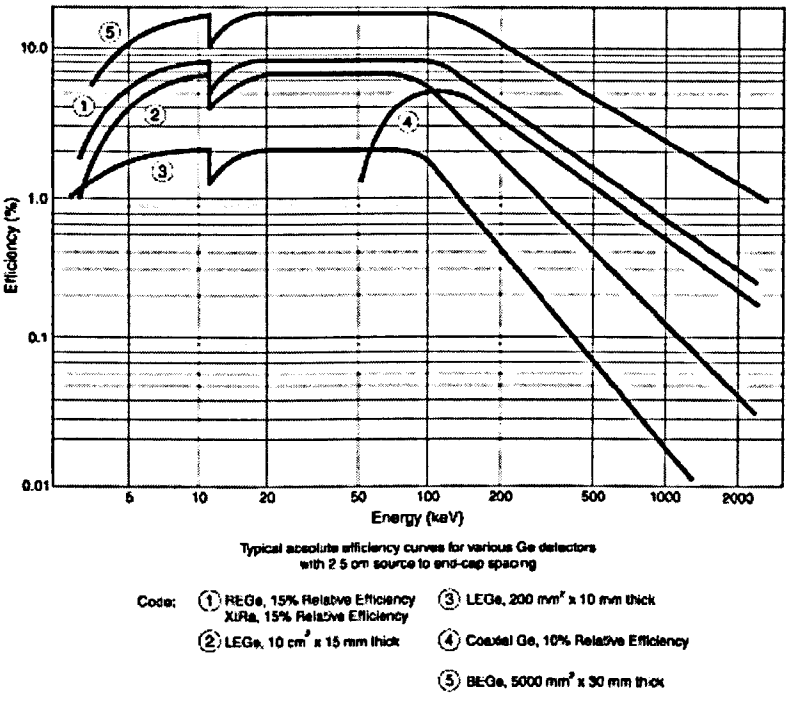

Figure 3.4 *Graph illustrating the absolute efficiency achieved by the Ultralow-level Canberra BE50 detector (line number 5) in comparison to other detectors (graphic courtesy of Dr Uwe Reiser, Victoria University of Wellington, New Zealand).*

3.5.3 Calculation of activities

Using high-resolution gamma spectrometry at the University of Liverpool (all samples) the activity of certain radionuclides can be measured directly from peaks in the gamma ray spectrum. ^{238}U cannot be measured directly but was derived from the ^{214}Pb (~295 and 352 keV) and ^{214}Bi (~609, 1120 and 1764 keV) activity. ^{232}Th has no direct gamma emission, but was calculated as the weighted mean of ^{208}Tl (~585 and 860 keV) and ^{228}Ac (~328, 338, 270 and 911 keV). The activity of ^{40}K in the sample can be derived directly from the peak associated with ^{40}K at 1461 keV. The energy lines of the gamma spectrum indicated above were selected according to (1) detector efficiency, (2) specific line intensities, (3) expected nuclide concentrations, (4) superposition of energy lines, (5) position of the Compton edge, (6) self-absorption of the sample (Mauz, et al., 2002).

For samples BLA1, BLA3 and OR14 radionuclide activity data was additionally provided by Victoria University of Wellington using the Ultralow-level Canberra BE5030 detector to allow the reproducibility of results to be checked. For these samples, ^{238}U activity was determined via the weighted mean of activities from ^{214}Pb (~295 and 352 keV) and ^{214}Bi (609 keV). For ^{234}Th, activity was determined via the weighted mean of ^{212}Pb, ^{208}Tl and ^{228}Ac energy lines.

The specific activities [$A_s(t)$], given in Bq kg^{-1} were subsequently transformed into concentration (ppm) using the following equation:

$$8_9\ \$2) * \#\frac{\ldots\ ;\ \#<_=}{>?_@}\#\ _9\$2)$$

where A^*_s = concentration (ppm and wt %), N_A = Avogadro constant, m_a = atomic weight (n) and $\lambda = \tau^{-1}$ (decay constant) (Mauz, et al., 2002).

This data was then compared directly to data from the University of Liverpool HPGe detector to ensure reproducibility. No significant disagreement in radionuclide activity (within 2σ errors) between the two gamma detectors was evident (Table 3.1).

Table 3.1 *A comparison of radionuclide activities measured by two different gamma detectors (Liverpool – HPGe and Wellington – BE5030). Activity data for different radionuclides of the ^{238}U decay chain are given. Errors indicated are 2σ values. Note the higher errors on the data derived from the HPGe detector compared to those measured using the higher efficiency Ultralow-level Canberra BE50 detector.*

Sample	^{238}U (Bq/kg)[1]	^{234}Th (Bq/kg)[2]	^{226}Ra (Bq/kg)[3]	^{210}Pb (Bq/kg)[4]
OR14 (BE5030)	**9.52 ± 0.49**	**9.27 ± 2.72**	**11.87 ± 1.73**	**12.11 ± 2.47**
OR14 (HPGe)	**10.81 ± 0.72**	**10.44 ± 4.81**	**10.36 ± 3.02**	**11.81 ± 5.76**
OR15 (HPGe)	**16.99 ± 1.00**	**13.48 ± 5.52**	**12.08 ± 3.38**	**16.57 ± 6.36**
OR22 (HPGe)	**15.92 ± 0.92**	**13.81 ± 4.78**	**11.14 ± 2.94**	**14.65 ± 5.60**
OR26 (HPGe)	**13.78 ± 0.90**	**14.21 ± 4.41**	**10.48 ± 2.74**	**11.89 ± 4.40**
BLA1 (BE5030)	**8.78 0.23**	**8.53 ± 2.22**	**10.01 ± 1.48**	**9.02 ± 1.98**
BLA1 (HPGe)	**7.55 ± 0.89**	**6.47 ± 3.48**	**7.49 ± 2.26**	**6.17 ± 3.16**
BLA3 (BE5030)	**5.19 ± 0.25**	**5.69 ± 1.73**	**5.93 ± 1.24**	**5.19 ± 1.48**
BLA3 (HPGe)	**4.98 ± 0.37**	**6.87 ± 2.88**	**5.17 ± 1.70**	**4.72 ± 2.46**
NEF4 (HPGe)	**14.85 ± 0.88**	**12.24 ± 4.74**	**11.56 ± 2.94**	**17.06 ± 6.18**

1 ^{238}U activity derived from energy lines associated with ^{214}Pb and ^{214}Bi (295, 352, 609 keV)
2 ^{234}Th activity is derived from the 63.29 keV energy line
3 ^{226}Ra activity is derived from the 186.11 keV energy line
4 ^{210}Pb activity is derived from the 46.52 keV energy line

Table 3.2 *Details of values and measurements used in calculating the environmental dose-rate (errors shown at the 1σ level).*

Sample	Lithofacies	Grain size (μm)	Water content (%)	Potassium (%)	Uranium (ppm)	Thorium (ppm)	Beta dose-rate (Gy/ka)	Gamma dose-rate (Gy/ka)	Environmental dose-rate (Gy/ka)
OR14*	*Sr*	90-125	5	1.23 ± 0.03	0.77 ± 0.02	2.59 ± 0.04	1.04 ± 0.07	0.48 ± 0.01	**1.59 ± 0.07**
OR14*	*Sr*	200-250	5	1.23 ± 0.03	0.77 ± 0.02	2.59 ± 0.04	0.99 ± 0.06	0.48 ± 0.01	**1.54 ± 0.06**
OR15	*Fl*	90-125	16	1.31 ± 0.03	1.37 ± 0.04	4.10 ± 0.12	1.07 ± 0.07	0.57 ± 0.02	**1.70 ± 0.07**
OR22	*Sh*	90-125	9	1.23 ± 0.03	1.28 ± 0.04	4.01 ± 0.11	1.09 ± 0.07	0.58 ± 0.02	**1.73 ± 0.08**
OR22	*Sh*	150-180	9	1.23 ± 0.03	1.28 ± 0.04	4.01 ± 0.11	1.06 ± 0.07	0.58 ± 0.02	**1.70 ± 0.07**
OR26	*St*	90-125	10	1.13 ± 0.03	1.10 ± 0.03	3.50 ± 0.10	0.97 ± 0.06	0.51 ± 0.01	**1.54 ± 0.06**
BLA1*	*Fl*	90-125	10	0.68 ± 0.01	0.71 ± 0.01	2.39 ± 0.04	0.60 ± 0.02	0.32 ± 0.01	**0.98 ± 0.02**
BLA1*	*Fl*	180-212	10	0.68 ± 0.01	0.71 ± 0.01	2.39 ± 0.04	0.58 ± 0.02	0.32 ± 0.01	**0.96 ± 0.02**
BLA3*	*Sr*	90-125	6	0.44 ± 0.01	0.42 ± 0.01	1.42 ± 0.03	0.40 ± 0.01	0.21 ± 0.01	**0.67 ± 0.01**
BLA3*	*Sr*	212-250	6	0.44 ± 0.01	0.42 ± 0.01	1.42 ± 0.03	0.38 ± 0.01	0.21 ± 0.01	**0.65 ± 0.01**
NEF4	*Sr*	90-125	12	1.00 ± 0.03	1.19 ± 0.04	3.73 ± 0.10	0.88 ± 0.05	0.49 ± 0.01	**1.43 ± 0.05**

* denotes those samples (and results shown here) which underwent gamma spectrometric analysis at the Victoria University of Wellington (for comparison of results see Table 3.1).

3.5.4 Investigations into radioactive disequilibrium

Disequilibrium in the ^{238}U decay chain has been shown to cause a problem in estimating the environmental dose-rate for fluvial sediments (Olley, et al., 1996) and so this needed to be investigated for the glaciofluvial sediments studied here. For samples measured via the Ultralow-level Canberra BE50 detector, an assessment into radioactive disequilibrium could be undertaken as the higher relative efficiency of the machine allowed greater precision within the lower energy lines.

As mentioned in Section 3.4.1, disequilibrium in the ^{235}U and ^{232}Th is unimportant and so was not investigated or corrected for in this research. Disequilibrium within the ^{238}U decay chain is assessed by analysing the activity ratios for ^{238}U, ^{234}Th, ^{230}Th and ^{226}Ra (this radionuclide shares a gamma emission energy line with ^{235}U and so it was used for a qualitative assessment only). However, the values for ^{234}U and ^{230}Th are based on the activities of ^{238}U and ^{226}Ra and so only ^{238}U and ^{226}Ra can be compared. ^{210}Pb can also be measured directly, allowing an analysis into the state of equilibrium at the latter end of the decay chain to be undertaken. Table 3.1 gives the radionuclide activity data (Bq/kg) for ^{234}Th, ^{226}Ra, ^{210}Pb for each of the three samples (BLA1, BLA3 and OR14) measured using the BE5030 detector, all values for each radionuclide activity overlap within 2σ suggesting that radioactive disequilibrium in the ^{238}U decay chain was not an issue in these samples.

The same radionuclide activities were also measured using the HPGe detector and are also shown in Table 3.1. However, the lower counting efficiency associated with the coaxial HPGe detector resulted in higher error values for activity data. It must be noted, however, that the activities for these radionuclides do overlap within 2σ errors

for all samples, suggesting that radioactive disequilibrium was not an issue within these samples (Table 3.1).

3.6 Calculation of environmental dose-rate

The concentrations of the radioelements (in ppm for U and Th, and % for K – Table 3.2) derived from high-resolution gamma spectrometry were converted to dose-rates (in Gy/ka) by using the conversion factors in Adamiec and Aitken (1998) shown in Table 3.3. The emission values (from nuclear data tables) for the three radioactive decay series were converted to dose-rate by assuming an infinite matrix where the rate of energy emission is equal to the rate of energy absorption in a volume with dimensions greater than the ranges of the radiation (Roesch and Attix, 1968; Aitken, 1985).

3.6.1 Attenuation of the beta dose

The energy of the beta particle when interacting with matter needs to be corrected both for attenuation within the grains and for attenuation from the water content of the sediment (Bell, 1979; Mejdahl, 1979). The degree of attenuation within the grain is dependent on the energy of the beta particle. Mejdahl (1979) provides tabulated figures for the absorbed beta-dose in quartz grains over a range of diameters (5-10,000 μm); from these, the appropriate values for the grain size of quartz used for OSL analysis can be selected to correct the absorbed beta-dose due to attenuation.

The HF etching performed on the quartz grains will have a disproportionate effect on the beta dose-rate. This is because the exterior of the grain will have a higher absorbed dose fraction than the centre of the grain (Mejdahl, 1979). The values are taken from Bell (1979), who calculated the effect of etching on the absorbed beta-

dose from the U, Th and K chains, and thus the attenuation factors take into account the distribution of dose within the grain arising from the different energies of the beta emissions.

Table 3.3 *Dose-rate conversion factors for converting potassium, rubidium, thorium and uranium concentration to dose-rate (Adamiec and Aitken, 1998).*

		Alpha	Beta	Gamma
^{238}U	Full chain	2.685	0.143	0.112
	Pre-radon	1.145	0.057	0.0025
^{235}U	Full chain	16.6	0.515	0.269
	Pre-radon	(16.6)	0.515	0.269
^{232}Th	Full chain	0.732	0.0273	0.0476
	Pre-radon	0.305	0.0091	0.0178
^{40}K		-	0.782	0.243
^{87}Rb		-	0.019	-

Notes:

1. Concentration for uranium and thorium is 1 ppm, for potassium it is 1% natural K_2O and for rubidium it is 50 ppm.
2. The rows labelled 'pre-radon' give the values for 100% escape of radon in the case of the ^{232}Th and ^{238}U series, but because of the short half-life of ^{219}Rn the values given for ^{235}U include contributions of that gas and its daughters.
3. Full chain indicates radioactive equilibrium.
4. Unit is Gy/ka.

3.6.2 Correcting for water content

Conventional dose-rate estimates consider air and water as a constant pore-filling substance and account for the attenuation effect of water using correction factors (Zimmerman, 1971; Aitken, 1985; Aitken and Xie, 1990; Nathan and Mauz, 2008). Water has a much higher absorption coefficient than minerals for alpha, beta and gamma radiation. Therefore, the dose-rate calculated using dry materials must be adjusted (Aitken, 1985).

Recently, Nathan and Mauz (2008) produced alternative correction factors for carbonate-cemented deposits which experience accumulation and dissolution of carbonate as a pore-filling substance over time. Zimmerman's method did not explicitly take into account the variability of the degraded energy spectra of the beta and gamma radiations as the composition of the interstitial material changes (Nathan and Mauz, 2008). Nathan and Mauz (2008) derived beta- and gamma-dose correction factors for carbonate-rich sediments for varying carbonate and water contents using dose-rate modelling, based upon primary energy spectra of U, Th and K from Evaluated Nuclear Structure Data File (ENSDF).

For the samples researched here, carbonate content is assumed to be zero (no significant carbonate) and water content between 5-16% (see Table 3.2). Using these values, the correction factors used for water content as derived by Nathan and Mauz (2008) are shown below:

$$\dot{D}_{\beta} = \dot{D}_{\beta,dry}/(1+1.19W)$$

$$\dot{D}_{\gamma} = \dot{D}_{\gamma,dry}/(1+1.02W)$$

Where W is the water content in the sediments expressed as (weight of water)/(weight of dry material). $\dot{D}_{\beta}$, and $\dot{D}_{\gamma}$ are the β and γ dose-rates corrected for water absorption and $\dot{D}_{\beta.dry}$ and $\dot{D}_{\gamma.dry}$ are the β and γ dose-rates of the dry sample.

However, it should be noted that in natural environments, the water content of sediments is not always constant but fluctuates with climate and weather change, ground water variation and compaction. Therefore, an appropriate estimate of past water content variation and suitable correction was necessary for accurate dose-rate determination. Table 3.2 shows that the moisture content for all samples varied from 5-16%. Although this reflects the present day water content, the sediments are free-draining sand and gravel, thus temporal variation in water content is thought to be minimal. An appropriate error of ±5% was given to each value to account for possible post-depositional variations in water content.

3.7 Conclusions

- In this chapter, the high-resolution gamma spectrometry method used to calculate the U, Th and K concentrations from the Orrisdale, Wexford and Porth Dinllaen samples has been outlined. The use of two different gamma detectors, the coaxial HPGe detector and the Ultralow-level Canberra BE50 detector allowed reproducibility of radionuclide activities and concentrations to be assessed. The results suggested that there was no systematic deviation in radionuclide activity/concentration between the two gamma detectors. For the samples where the Ultralow-level Canberra BE50 detector was used (OR14, BLA1, BLA3), results from this detector were used for dose-rate calculation due to the higher precision output from this higher efficiency detector.
- The gamma spectrometry technique allowed an assessment of disequilibrium within the samples to be made. Activity values for radionuclides of the ^{238}U decay chain showed agreement within 2σ errors. Therefore, disequilibrium within these samples is not an issue. Corrections were made for beta dose attenuation both within the grains (Bell, 1979; Mejdahl, 1979) and for water content (Zimmerman, 1971; Aitken, 1985; Aitken and Xie, 1990; Nathan and Mauz, 2008).
- Assessment of the correct environmental dose-rate is vital to allow the correct age to be calculated for a sample using OSL dating as it forms one half of the age equation. The dose-rates shown in Table 3.2 are used for final age calculation together with appropriate D_e values.

Chapter 4

Quartz Luminescence Characterisation

4.1 Introduction

In settings such as formerly glaciated environments the provenance of materials can be extremely variable, thus a luminescence dating approach should include characterisation of quartz luminescence. This ensures that a picture concerning variation of quartz behaviour within samples and between samples from different field sites is gained. Although the quartz at all field sites has originated from the Irish Sea Basin, the Southern Uplands of Scotland, the Lake District and Northern Ireland, such a large geographical source area means the ice overran bedrock lithologies composed of different types of quartz grains (e.g. Triassic sandstones, Permo-Triassic sandstones, Carboniferous material; see Figure 4.9). The dominance of certain quartz types within the glacial deposit will influence its luminescence properties. The quartz under analysis was characterised to ensure that the most appropriate SAR protocol was applied to each sample (in terms of preheat temperature applied), and also to confirm that the dating protocol was targeting a dominant 'fast' component (Bailey, et al., 1997). This is the fast, easy to bleach optical trap that the original SAR protocol targets (Murray and Wintle, 2000).

Preheat tests which allowed an appropriate preheat range to be defined were undertaken and recycling ratios and thermal transfer were calculated for each preheat temperature. Linearly-Modulated (LM) and Constant-Wave (CW) OSL decay curve fitting allowed an assessment be made of the presence and dominance of certain

optical components within the quartz. The fast component could then be defined in terms of its photoionisation cross-section and compared to other components that may be present.

Tests were applied to one sample from each field site, Orrisdale (*OR*), Porth Dinllaen (*NEF*) and Wexford (*BLA*). These samples were taken as representative of the quartz at each field site due to the close proximity of samples to one another. The short-term processes and rapid sediment accumulation which occurred during the period of glaciofluvial deposition also ensures that the quartz type is similar for each sample from the same field site. The glaciofluvial stratigraphy within each field site is *not* thought to be a result of multiple glacial events occurring at different times with changing quartz provenance. This chapter outlines the concepts, methodology and results for each quartz characterisation test. It also discusses luminescence characteristics in relation to quartz provenance. For details concerning field site investigations, field sampling methodologies and sample laboratory preparation procedures see Chapter 5.

4.2 Concepts and Methodology

4.2.1 Measurement details

All luminescence measurements were performed using automated Risø DA-15 readers, equipped with diodes emitting 470Δ30 nm and an EMI 9235QB photomultiplier. The optical stimulation units delivered ~30 mW cm^{-2} at 90% power of blue diodes. The OSL, IRSL and TL emissions were detected through an optical filter (Hoya U340, 7.5 mm) transmitting 260 nm to 390 nm wavelengths. Risø 1 had a beta source with a dose-rate of 0.09714 ± 0.00194 Gy/s (calibrated 16.01.07) and

Risø 2 had a beta-source with a dose rate of 0.13099 ± 0.00262 Gy/s (calibrated 16.01.07). For simplicity, irradiation doses will be given in Gray (Gy).

The OSL and signal depletion measurements were carried out at 125°C to prevent retrapping of charge in the trap corresponding to the 110°C TL peak (Murray and Wintle, 1998; Wintle and Murray, 2000). The optical stimulation time used for all the OSL measurements was 40 seconds (unless otherwise stated) with counts in 250 channels each lasting 0.16 seconds. This was to ensure good counting statistics. The sensitivity-corrected regenerated (L_x) and test dose (T_x) values were derived from the OSL signal counts obtained from the initial 0.8 seconds of the OSL decay curves, minus a background estimate obtained in the last 8 seconds consisting of instrument 'noise' and any remaining slower bleaching signal components.

4.2.2 The Single-Aliquot Regenerative-dose (SAR) protocol

The SAR procedure for quartz was described by Murray and Roberts (1998) and developed further by Murray and Wintle (2000). The basic details of the SAR protocol are outlined in Chapter 2. As luminescence efficiency per unit trapped charge and the rate of trap filling per unit ionisation can change between measurement of natural-OSL and subsequent regenerated signals it was necessary for sensitivity to be monitored for each OSL measurement (Murray and Wintle, 2000). In the SAR procedure, sensitivity changes were monitored by measuring the OSL signal response to a test dose (T_x) given immediately after the natural (L_n) or regenerated (L_x) OSL signal. By calculating a number of sensitivity corrected regenerative luminescence intensities (L_x/T_x) it was possible to produce a dose-response (or 'growth') curve that brackets the expected sensitivity corrected natural

intensity (L_n/T_n). D_e estimates could then be derived by interpolation of the L_n/T_n values onto their respective growth curves (See Chapter 2).

The growth curves obtained in the single-aliquot analysis were all fitted with a function comprised of a single saturating exponential term in the form:

$$\%^{*}\ \&A\ B\ "CDB\frac{\$CF\ G}{H}IJ$$

Where x is the laboratory dose, a is the saturation level, the level to which the OSL tends for large x, c is the y-intercept, and b is a dose parameter indicative of the onset of saturation.

The fundamental assumption of the SAR protocol is that the response to the test dose provides an appropriate measure of the sensitivity that pertained during measurement of the main OSL signal (Murray and Wintle, 2003). This allows sensitivity to be corrected for in both natural and regenerated cycles. For the response to the test dose to monitor the luminescence sensitivity, the assumption is made that the electron traps that are being probed are the same as the responsible for the main signal.

4.2.3 Assessing the suitability of the SAR protocol

The present assessment of the SAR procedure aims to (i) investigate whether the assumptions inherent to the SAR protocol are upheld for these samples and (ii) assess the general suitability of the particular SAR measurement conditions adopted in the analysis of D_e. This is achieved using a number of 'internal checks' on the SAR protocol performance, along with the tests of SAR reliability suggested by Murray

and Wintle (2000) (namely preheat plateau, thermal transfer, recycling ratio and dose recovery tests). The tests outlined below have the aim of helping to design a SAR protocol which is tailored to the samples in terms of selecting appropriate regeneration doses, preheat temperatures and deciding whether additional recycling ratio, OSL-IR depletion ratio (Duller, 2003), and thermal transfer tests are required. Furthermore, confirmation that the SAR protocol was targeting a dominant 'fast' component was also obtained (Bailey, et al., 1997; Murray and Wintle, 2000; Murray and Wintle, 2003).

4.2.4 D_e as a function of preheat temperature; the preheat 'plateau' test

Preheat temperatures are an essential part of the SAR protocol as they are required to empty any thermally-unstable light-sensitive shallow traps, particularly those filled by laboratory irradiations. If preheat temperature is too low, then the light-sensitive shallow traps are not effectively emptied and their electron populations will contribute towards the dating signal, giving a measureable D_e. If preheat temperature is too high, the optically sensitive traps used for dosimetry may be thermally eroded, resulting in a lower than expected D_e as the signal has been erased by the application of a high preheat temperature (Wintle and Murray, 2006).

The influence of SAR preheating conditions on D_e can be investigated by determining a series of D_e's across different preheat temperatures. Samples showing no preheat dependence will have mean D_e estimates that are consistent with each other over a range of preheat temperatures, forming a 'preheat plateau'. Indeed, Murray and Wintle (2000) suggest that the presence of a preheat plateau is a fundamental criterion for the acceptance of a D_e value as it is an indication that D_e

estimates in this range are derived from a thermally-stable OSL signal. The D_e estimates obtained using preheat temperatures within these plateau ranges are generally regarded as being accurate (Murray and Wintle, 2000) .

The preheat temperature under analysis was that which occurred before the measurement of the natural and regenerated signals and from hereon will be denoted PH_1. PH_1 temperatures were varied in 10°C increments between 180-280°C and D_e measurements were made on four aliquots per PH_1 temperature. The PH_1 durations were kept constant at 10 seconds as were the PH_2 (preheat treatment before the test dose OSL is measured) conditions (200°C cutheat). The PH_2 temperature is less severe to minimise sensitivity change between the measurement of natural/regenerative and subsequent test dose signals. Medium sized aliquots were used for this test (3 mm diameter).

The SAR protocol used between seven and nine regeneration doses to characterise the single saturating exponential growth of luminescence signal with given dose (see Appendix B for dose-response curves). A test dose was used to allow monitoring of sensitivity change. This test dose was chosen to be relatively high (19.6 Gy) due to the inherently insensitive nature of the quartz grains. It required a high test dose to ensure that a measureable OSL response was achieved allowing improved counting statistics and reduced errors. The given test dose was chosen to be in the linear range of growth in OSL with given dose.

To assess whether the test dose was accurately correcting for sensitivity change a recycling ratio test was undertaken (Wintle and Murray, 2006). A repeated low-dose

(chosen to be identical to the first regenerative dose) was given at the end of the SAR protocol and the ratio between the sensitivity-corrected OSL of the first and last dose was calculated, giving the *recycling ratio*. A zero dose point was also included once all regeneration doses had been given to enable thermal transfer to be monitored and calculated (as a percentage of the natural signal). An outline of the protocol used for sample OR22; 90-125 μm is shown in Table 4.1.

Rejection criteria were used to identify aliquots containing quartz that had no natural signal, had a 'weak' fast component or dominant 'medium' component and high thermal transfer. Aliquots showing slower decay of luminescence intensity with time (OSL signal had not reached background by >10 seconds of stimulation with blue LEDs at 90% power), indicative of a dominant medium component, were rejected. This analysis was undertaken via simple visual inspection of each OSL decay curve. Aliquots were rejected if the criteria for recycling ratios (1.0 ± 10%; *recycling ratio must overlap this range within 1σ errors*) and thermal transfer (must be <5% of the natural signal) were not met (Murray and Wintle, 2000). Additionally, if the dose-response was not described by a single saturating exponential function, the aliquot was also rejected.

Table 4.1 SAR protocol for the preheat 'plateau' test as applied to sample OR22; 90-125 μm.

Step	Treatment	Observed
1	PH_1 temperature of 180°C	
2	OSL at 125°C for 40s	Natural/regenerated signal
3	Give a test dose of 19.6 Gy	
4	Cutheat of 200°C	
5	OSL at 125°C for 40s	Test signal
6	Give next regenerated dose (from 7.8-188.6 Gy) and repeat steps 1-5, followed by zero dose, and repeat low dose of 7.8 Gy (recycling ratio).	
7	Repeat step 1, increasing the PH_1 temperature by 10°C up to a maximum of 280°C.	

4.2.5 The combined preheat dose-recovery test

A test was designed which should rule out the impact that heterogeneously-bleached grains have upon dose distribution, and make it easier to define the appropriate PH_1 range. This test is named the *combined preheat dose-recovery test* as it combines the elements of two commonly used tests. The first step was to remove the natural signal from all grains using the Risø blue LED's at 90% optical power for 40 seconds at room temperature. This treatment should be sufficient to completely bleach the optical signal in the quartz grains. The aliquots were then stored for 10,000 seconds (~2¾ hours) at room temperature, so that any charge transferred into the 110°C TL trap had time to thermally decay, and then the second half of the protocol was applied. The quartz grains were bleached once again under the same conditions as the first bleach treatment to ensure OSL traps were empty. A dose, which was close to the postulated natural dose, was then given to the aliquot. Different preheat treatments in the range 180-280°C in 10°C increments (each preheat temperature being held for 10 seconds) were then applied to four aliquots per PH_1 temperature.

The remaining SAR protocol was then applied, with regeneration doses characterising the saturating exponential growth of the luminescence signal with given dose, followed by a zero dose point and a repeated low and high dose to enable both *low* and *high* dose recycling ratios to be calculated. The repeated high dose (chosen to be the same as the highest regenerative dose) was incorporated to ensure that the test dose was able to account for dose-related sensitivity change. At high irradiation doses given during the SAR protocol it is important to ensure that sensitivity changes which may have been induced by such high doses can be accounted for.

A further repeat-dose was then given to all aliquots, followed by a PH_1 temperature of 230°C and then IR stimulation (90% power) at room temperature (to avoid thermal assistance) for 100 seconds, followed by optical stimulation and the subsequent test dose cycle. The IR stimulation should bleach certain feldspar components (the IR-stimulated signal) within the sample as micro-inclusions or remnant grains (Jain and Singhvi, 2001), and so the subsequent luminescence signal detected during optical stimulation should be purely from quartz. This luminescence signal was then compared to the original dose point during the main SAR protocol (which was measured without IR stimulation). An OSL-IR depletion ratio (Duller, 2003) was then calculated. If the sample was not contaminated with feldspar that contains an IR stimulated signal, then this ratio should be unity. There are a *small minority* of feldspars that contain a blue/green-stimulated signal and so these cannot be detected by using the IR simulation technique. As IRSL was only used to *detect* if feldspar contamination was a potential issue, this method was satisfactory. Tables 4.2a, b and c summarises the protocol used for each sample.

D_e's were calculated for all aliquots at each PH_1 temperature. Aliquots were rejected according to the established criteria detailed in Section 4.2.4. Additionally, if the OSL-IR depletion ratio was <0.90 the aliquot was rejected. The OSL-IR depletion ratio was looked upon cautiously, as it was sometimes the case that the ratio could be >1. This often corresponded to aliquots where the OSL decay curve was poorly defined and had a low signal to noise ratio, meaning errors were high, and ratios could not be calculated precisely.

As an outcome of the preheat-dose recovery test an assessment could be made to determine if aliquots that would *usually* be accepted, according to the rejection criteria (Section 4.2.4) were accurately recovering the known given dose.

Table 4.2a *The measurement protocol carried out during the combined preheat dose-recovery test for sample OR22; 90-125 μm.*

Step	Treatment
1	Bleach at room temperature for 40s using blue LEDs at 90% power
2	Pause for 10,000s
3	Bleach at room temperature for 40s using blue LEDs at 90% power
4	Give a dose of 35.1 Gy
5	PH_1 temperature of 180 °C. Increase in 10°C increments up to a maximum of 280°C with each successive SAR.
6	OSL at 125°C for 40s
7	Give a test dose of 10.5 Gy
8	Cutheat of 200°C
9	OSL at 125°C for 40s
10	Give next regenerated dose (from 7.8-188.6 Gy) and repeat steps 5-9, followed by zero dose, and repeat low (7.8 Gy) and high (188.6 Gy) dose.
11	Repeat steps 4-9 with a repeated regenerated dose and IR stimulation at room temperature for 100s.

Table 4.2b *The measurement protocol carried out during the combined preheat dose-recovery test for sample BLA1; 90-125 μm.*

Step	Treatment
1	Bleach at room temperature for 40s using blue LEDs at 90% power
2	Pause for 10,000s
3	Bleach at room temperature for 40s using blue LEDs at 90% power
4	Give a dose of 29.1 Gy
5	PH_I temperature of 180 °C. Increase in 10°C increments up to a maximum of 280°C with each successive SAR.
6	OSL at 125°C for 40s
7	Give a test dose of 14.6 Gy
8	Cutheat of 200°C
9	OSL at 125°C for 40s
10	Give next regenerated dose (from 5.8-155.4 Gy) and repeat steps 5-9, followed by zero dose, and repeat low (5.8 Gy) and high (155.4 Gy) dose.
11	Repeat steps 4-9 with a repeated regenerated dose and IR stimulation at room temperature for 100s.

Table 4.2c *The measurement protocol carried out during the combined preheat dose-recovery test for sample NEF4; 90-125 μm.*

Step	Treatment
1	Bleach at room temperature for 40s using blue LEDs at 90% power
2	Pause for 10,000s
3	Bleach at room temperature for 40s using blue LEDs at 90% power
4	Give a dose of 26.2 Gy
5	PH_I temperature of 180 °C. Increase in 10°C increments up to a maximum of 280°C with each successive SAR.
6	OSL at 125°C for 40s
7	Give a test dose of 14.6 Gy
8	Cutheat of 200°C
9	OSL at 125°C for 40s
10	Give next regenerated dose (from 5.8-139.9 Gy) and repeat steps 5-9, followed by zero dose, and repeat low (5.8 Gy) and high (139.9 Gy) dose.
11	Repeat steps 4-9 with a repeated regenerated dose and IR stimulation at room temperature for 100s.

4.2.5.1 Thermal transfer as a function of preheat temperature

Phenomena known as thermal transfer and recuperation need to be accounted for in order to achieve an accurate D_e. If an aliquot is optically bleached either in nature or in the laboratory and then the OSL is measured, zero signal is expected to be observed. In fact, an observable OSL signal is seen in many samples and this is often related to the preheat that is applied prior to stimulation whereby charge is thermally released from a relatively shallow but optically-sensitive trap during preheating and subsequently recaptured in a deeper OSL trap (Murray and Wintle, 2000).

The preheat-dose recovery test enabled thermal transfer to be calculated, as a percentage of the natural signal, for every aliquot at each PH_1 temperature, to enable a PH_1 temperature to be chosen that induces low thermal transfer. Low thermal transfer is desirable as it enables more accurate D_e values to be determined rather than artificially high D_e values. A background 'noise' signal should be observed at the end of a SAR sequence after a zero dose is given, however if a luminescence decay signal is observed, then this can be attributed to the preheat applied prior to optical stimulation, due to thermal transfer of charge from light-insensitive but thermally stable traps to the main OSL trap (associated with the 325°C TL peak) (Jain, et al., 2002). This thermal transfer signal is then calculated as a percentage of the natural signal. Murray and Wintle (2000) suggest that this value should not exceed 5% of the natural signal, to avoid it having a significant impact upon values calculated for D_e determination.

4.2.6 Thermal transfer calculated according to Jain et al. (2002)

A further test was carried out after Jain *et al.* (2002) which allowed thermal transfer to be measured as a function of the PH_I temperature by incremental heating of the aliquot (Jain, et al., 2002). Firstly, the aliquot was bleached and then PH_I temperatures in the range 180-280°C were applied in 10°C increments to enable a signal which was purely from thermal transfer to be generated (Table 4.3). A dose-response curve was then created via a SAR protocol. This allowed thermal transfer to be interpolated to the dose-response curve enabling it to be calculated in Gy instead of a percentage of the natural signal. As thermal transfer was in Gy, this allowed potential offsets in D_e as a direct result of thermal transfer to be calculated.

Potential D_e offsets as a result of thermal transfer were then calculated as follows (see Table 4.3 for the meaning of each parameter):

Step 1: Corrected thermal transfer signal (corrected for sensitivity change):

$$N_i' = \frac{N_i}{\alpha} \text{ where, } \alpha = \frac{T_i}{T_{180}}, i = 180\text{-}280°C$$

Step 2: Corrected thermal transfer signal:

$$TT_i' = \frac{(N_i')}{T_{180}}, \text{ where } i = 180\text{-}280°C$$

The corrected signal TT_i' was then interpolated onto the dose-response curve to give the apparent dose due to thermal transfer at each PH_I temperature i.e. TT_i (Gy).

Table 4.3 *Measurement protocol applied to sample OR22; 90-125 μm to calculate potential D_e offsets due to thermal transfer in Gy. Eight regeneration doses in the range 5.8-138.2 Gy were used to enable a dose-response curve to be constructed, onto which the signal due to thermal transfer (step 3) could be interpolated.*

Step	Treatment
1	Bleach at room temperature for 40s using blue LEDs at 90% power
2	PH_1 temperature, increase in 10°C increments from (180-280 °C)
3	OSL at 125°C for 40s (N_i)
4	Give a test dose of 8.6 Gy
5	Cutheat of 160°C
6	OSL at 125°C for 40s (T_i)
7	Give next regenerated dose (ranging from 5.8-138.2 Gy)
8	PH_1 (temperature fixed at 180°C for 10s)
9	OSL at 125°C for 40s
10	Give a test dose of 8.6 Gy
11	Cutheat of 160°C
12	OSL at 125°C for 40s
13	Repeat steps 7-12 until all regeneration doses have been given.

4.2.7 Fast component analysis; OSL decay curve fitting

Quartz shows a complicated OSL decay curve where different components have been identified as easy to bleach and hard to bleach (Bailey, et al., 1997). Bailey et al. (1997) have suggested that the OSL decay curve from quartz can be approximated using three first-order decay components. These components were referred to as the 'fast', 'medium' and 'slow' components according to their respective detrapping rates. It was demonstrated that the most probable explanation is that the OSL signal originates from three physically distinct traps with different rates of charge loss due to different trap depths and photoionisation cross-sections (Singarayer and Bailey, 2003). The slow component has been observed to have a higher saturation limit than the fast component, and a decay-rate dependence on initial charge concentration (Jain, et al., 2003b). Studies on multiple quartz grains using LM-OSL have indicated

three (Kuhns, et al., 2000), four (Bulur, et al., 2000) or five OSL components (Singarayer and Bailey, 2003).

The fast component is suitable for luminescence dating as it is quick to bleach under optical stimulation and should give a low residual signal after exposure to sunlight during transport. The SAR protocol (Murray and Wintle, 2000) was developed on a sample that had a dominant fast component. Although Jain et al. (2003b) found that the majority of quartz samples have optical signals that are dominated by the fast component, in some samples this is not the case. In studies where the optical signal was dominated by other components (ultrafast/medium/slow) the standard SAR protocol did not work as effectively (Choi, et al., 2003a; Choi, et al., 2003b; Tsukamoto, et al., 2003). It is therefore important to assess whether the samples are dominated by a true fast component as defined by its photoionisation cross-section.

4.2.7.1 Linearly-Modulated OSL (LM-OSL) curve fitting

Bulur (1996) introduced an innovative method of measuring OSL, which is now widely known as LM-OSL. Measurement of the OSL signal during linear ramping of the stimulation power (LM-OSL) is a useful and efficient method for separating constituent OSL components, and for detailed investigation of the luminescence properties of each component (Choi, et al., 2006a). By ramping the stimulation power from zero to a particular value (usually the maximum power of the light source), the OSL signal appears as a series of peaks; each peak represents a component of the OSL signal with a particular luminescence parameter, namely the photoionisation cross section and trap depth. The LM-OSL curve, therefore, gives a luminescence curve, which shows a spectrum of the net detrapping rates; these are

proportional to the photoionisation cross-sections (Bulur, et al., 2000). The LM-OSL signal allows effective characterisation of each OSL component, and thus, can be used as an essential tool for understanding processes giving rise to OSL (Choi, et al., 2006a). The aim of this process is to ensure that the component targeted for dating purposes is indeed the fast component (not ultra fast or medium) and to determine its relative strength, compared to other components that may be present.

Assuming a single trap model, with a single recombination centre, and quasi-equilibrium conditions (i.e. the number of free electrons is much smaller than trapped electrons and the rate of change of free electron concentration is much smaller than the rate of trapped electrons) analytical expressions for the LM-OSL curve can be obtained (Bulur, 1996). The parameters of the luminescence curve (the peak height L_{max} and the peak position t_{max}) are related to the physical parameters of the trap involved in stimulated luminescence production (Bulur, et al., 2000) i.e. the trap population (n_0) and the detrapping rate (b) which is proportional to the stimulation light intensity (I_0) and the photoionisation cross-section (σ) ($b=\sigma I_0$) (Bulur, et al., 2002). For first order kinetics (i.e. negligible retrapping), Bulur (1996) has shown that the OSL output with linearly increasing stimulation power can be written as:

$$L(t) = n_0 \frac{b}{P} t \exp\left[-\frac{bt^2}{2P}\right]$$

Where $L(t)$ is the luminescence intensity, n_0 is the number of trapped electrons and P is the stimulation time. The parameters of the curve are:

$$t_{max} = \sqrt{\frac{P}{b}} \text{ and } L_{max} = n_0 \sqrt{\frac{b}{P}} \frac{1}{\sqrt{e}} = \frac{n_0}{t_{max}} \frac{1}{\sqrt{e}}$$

Where t_{max} is the time at which the OSL curve reaches the maximum (L_{max}) (Bulur, et al., 2002).

LM-OSL curves can be separated into their component parts using the equation from Bulur (1996) and the different values for detrapping probability and photoionisation cross-section of each OSL component (ultra fast, fast, medium, slow 1, slow 2, slow 3 and slow 4) from Jain et al. (2003b), see Table 4.4. These values were based upon the number of components observed from twelve different samples of quartz from Australia, Denmark, India, Korea, Morocco, Scotland, Sweden and Tanzania. In total, seven LM-OSL components were identified and between three and six components were required to fit any single quartz sample.

Table 4.4 *Trap parameters from nine different quartz samples for blue stimulation light (470 ± 30 nm light). Redrawn from Jain et al. (2003b).*

	Ultra fast	Fast	Medium	Slow 1	Slow 2	Slow 3	Slow 4
Detrapping probability; b (s^{-1})	32	2.5 ± 0.2	0.62 ± 0.05	0.15 ± 0.03	0.023 ± 0.002	0.0022 ± 0.0002	0.00030 ± 0.00001
Photoionisation cross-section (cm^2)	2.9×10^{-16}	$2.32 \pm 0.16\times10^{-17}$	$5.59 \pm 0.44\times10^{-18}$	$1.33 \pm 0.26\times10^{-18}$	$2.08 \pm 0.46\times10^{-19}$	$2.06 \pm 0.16\times10^{-20}$	$2.76 \pm 0.17\times10^{-21}$
Relative cross-section	13	1	0.2	0.06	0.01	0.001	0.0001

In this research, LM-OSL curves were obtained by stimulating small aliquots (~30 grains) of quartz with increasing stimulation light intensity from 0 to 92% power for 4000 seconds at 125°C. The natural LM-OSL was measured and followed by a

regenerated LM-OSL after a given dose. Preheats of 250°C for OR22 and 240°C (for 10 seconds) for BLA1 and NEF4 were applied before both the natural and regenerated LM-OSL were measured. The data was collected in 2000 bins, each containing the photon counts for 2 seconds. Both natural and regenerated LM-OSL signals were measured to observe if a fast component could be generated after artificial irradiation. If this had happened, it would point towards accidental bleaching of the natural fast component; fortunately, this was not the case in any of the aliquots measured. The regenerated LM-OSL was also measured to ensure that after irradiation additional components could not be generated. The background LM-OSL count over 4000 seconds (calculated from the average of three blank discs that were measured under the same conditions as the samples) was subtracted from each of the LM-OSL curves.

Small aliquots were used to reduce the impact of 'averaging' different components from hundreds of grains. The photon count data sets were then transferred to OriginPro 7.5 and the LM-OSL versus time plots were then used for curve fitting. The simplest form of the equation governing the LM-OSL curve has been given above. The number of OSL components has been shown to vary from sample to sample and so it was necessary to find the number of components that provided the best fit for each sample i.e. the highest r^2 value and the lowest Chi-squared/degrees of freedom value. In some instances however, the same r^2 value was obtained for fits of different numbers of components; these instances occurred when a single component was fitted as two components with identical b values. In these cases, the fit with the lesser number of components was selected to be the best fit.

Component fitting was carried out using the "Non Linear Curve Fit" "Advanced Fitting Tool" option in OriginPro 7.5. The equation was entered by listing the parameters involved i.e. $n_1, n_2, n_3, b_1, b_2, b_3$ & P for a three component fit. The initial n_N values were set to be 100,000 (after Choi, et al., 2006) and the initial values for b_N were based on the values of σ (photoionisation cross-section) given by Jain et al. (2003b). A maximum stimulation power of 30.67 $mW.cm^{-2}$ was used for this experiment. For N=3 components, photoionisation cross sections were σ_F, σ_M, σ_{S1} for the fast, medium and slow 1 components, with initial values of 2.32×10^{-17}, 5.59×10^{-18} and 1.33×10^{-18} (cm^2) (see Table 4.4). This led to b values (using the equation $b=\sigma I_0$, where $I_0 = 7.3 \times 10^{16}.s^{-1}.cm^{-2}$, based on a maximum stimulation light intensity of 30.67 $mW.cm^{-2}$) of $b_1 = 1.69\ s^{-1}$, $b_2 = 0.408\ s^{-1}$ and $b_3 = 0.0971\ s^{-1}$. The value of P in the equation was fixed at 4000 seconds. 100 iterations were carried out until the Chi-squared value remained the same after each set of 100 iterations. The entire process was repeated for 4, 5 and 6 components, n_N values remained the same (100000) and the values for b_4, b_5 and b_6 were derived from Jain et al. (2003b), with P remaining fixed at 4000 seconds. Individual LM-OSL growth curves were calculated for each component, using the values for n_N and b_N and P. This then allowed a visual analysis of each individual component and the calculation of photoionisation cross-section to see if the 'fast' component extracted agreed with other published work concerning calculation of fast component photoionisation cross-sections.

4.2.7.2 Continuous-Wave OSL (CW-OSL) decay curve fitting.

An alternative method for component analysis and in particular the characterisation of the fast component is to fit the CW-OSL decay curve with different components.

This is a similar process to that mentioned above for LM-OSL. However, the advantages of using the CW-OSL decay curve for component analysis are the reduction in measurement and component fitting time together with a constant background signal that can be easily accounted for (Huntley, 2006). Investigations concerning the shape of OSL decay curves (Smith and Rhodes, 1994; Bailey, et al., 1997; Bailey, 2000b; Adamiec, 2005) have shown that OSL emission at a constant stimulation power (continuous-wave or CW-OSL) can be fitted by the sum of three exponential components; the fast, medium and slow components (Smith and Rhodes, 1994)

The quartz OSL decay curve can be mathematically decomposed into its rapid and slow components. In this research the CW-OSL decay curves were fitted with the exponential function (Bailey, et al., 1997):

K$2) * #1 L H L MNC$B2H L) F #1 P H P MNC$B2H P) F #Q IR

Where $L(t)$ is the luminescence intensity as a function of time, t is time, n_n is the number of trapped electrons for a particular component, b_n is the detrapping rate of a particular component, which is proportional to the stimulation light intensity (I_0) and the photoionisation cross-section (σ) ($b=\sigma I_0$).

In this experiment, blue LED stimulation was at 10% of total power to enable the fast component to decay much slower than at full power. The aliquots were stimulated for a total of 100 seconds. This allowed the fast and medium components to be seen at higher resolution, as the luminescence decayed much slower, over a longer period

of time, therefore achieving characterisation of the fast component in higher detail. The slow component would not be observed during such stimulation time and power. However, initial LM-OSL experiments demonstrated that no slow component was present in all samples and so the CW-OSL method allowed more rapid characterisation of the fast and any medium component due to the lower measurement and component fitting time required. Small aliquots (~30 grains) were used for this experiment to reduce the impact of 'averaging' different components from hundreds of grains.

Component fitting was carried out following procedures suggested by Choi et al. (2006). The 'Non Linear Curve Fit' and 'Advanced Fitting Tool' options in OriginPro 7.5 were used for computational fitting. Before this commenced, initial values for number of trapped electrons (n) and detrapping rate (b) were input into the programme. The initial values for n_n were set at 100,000 (Choi, et al., 2006a) and the initial values for b_n were calculated using the equation $b = \sigma I_0$. Values for photoionisation cross-section of each component (fast, medium and slow) from Jain et al. (2003) were used to calculate detrapping rate and a stimulation light intensity of 8.06×10^{15} $s^{-1}.cm^{-2}$ (10% power) was used. 100 iterations were carried out until the Chi-squared/degrees of freedom value remained the same after each set of 100 iterations. The entire process was repeated for 3, 4 and 5 components (to evaluate if multiple medium components existed). The fast component from the 'best fit' number of components (Chi-squared/degrees of freedom) was calculated and used for comparison with other aliquots of the same sample and for comparison with results achieved via the LM-OSL technique.

4.3 Results

4.3.1 D_e as a function of preheat temperature; preheat 'plateau' test

The dependence of D_e on preheat temperature was investigated for sample OR22; 90-125 μm. Figure 4.1 shows the results for D_e (Gy) plotted against PH_1 temperature. The graph includes all *accepted* aliquots for which a D_e could be derived. Those aliquots that were rejected are not included in analysis (see Section 4.2.4 for rejection criteria). Figure 4.1 shows a distinct lack of D_e dependence on preheat temperature. There is such wide spread in the data that it is difficult to identify any existing preheat plateau as required by Murray and Wintle (2000). This variation is thought to result from heterogeneous bleaching creating a wide spread in D_e. This is unrelated to preheat temperature. Due to the inconclusiveness of this test upon such heterogeneously-bleached glaciofluvial sediments, it was abandoned and not carried out upon any other samples.

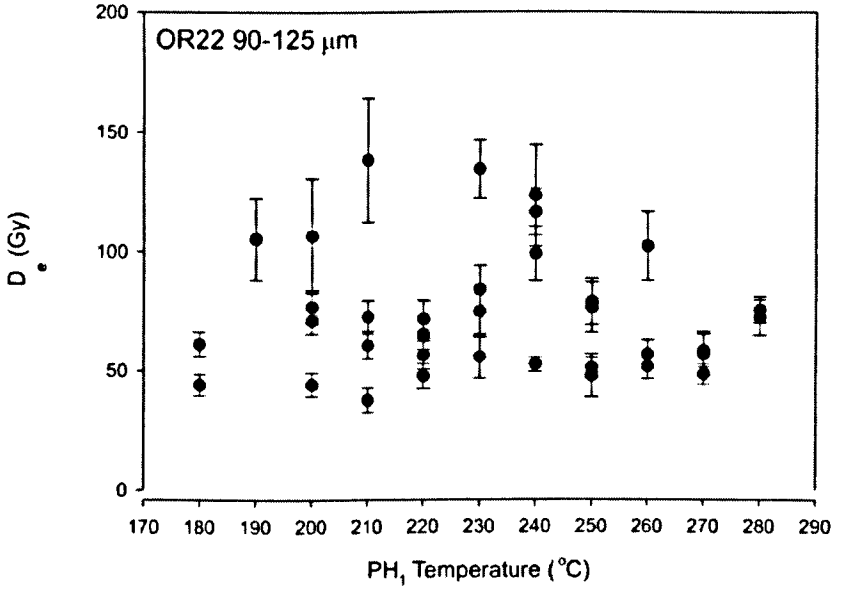

Figure 4.1 *D_e plotted against PH_1 temperature for sample OR22; 90-125 μm showing accepted aliquots only. Individual aliquot D_e values are shown as filled circles. Errors are shown at the 1σ level.*

4.3.2 The combined preheat-dose recovery test

Due to the limited conclusiveness of the traditional preheat test outlined previously, the *preheat dose-recovery test* was carried out on samples OR22; 90-125 μm, BLA1; 90-125 μm and NEF4; 90-125 μm. The results are shown in Figure 4.2 where the ratio of given dose to recovered dose for each accepted aliquot is plotted across the range of PH_1 temperatures.

For OR22; 90-125 μm, the rejection criterion (Section 4.2.5) led to 22 out of the 44 aliquots being discarded across the full range of PH_1 temperatures. For samples BLA3; 90-125 μm and NEF4; 90-125 μm, fewer aliquots were rejected (3 aliquots rejected for BLA1 and 2 aliquots rejected for NEF4). Tables 4.5a, b and c summarise how many aliquots were rejected at each PH_1 temperature (out of a total of 4 aliquots) and the reason for rejection.

For sample OR22; 90-125 μm, accepted aliquots could accurately recover the given dose (± 10%) within 1σ errors at all PH_1 temperatures up to 260°C. Using a PH_1 temperature in this range should allow an accurate D_e to be obtained, once the aliquot is known to meet the acceptance criteria outlined in Section 4.2.4. At temperatures above 260°C, accepted aliquots begin to become unreliable in accurately recovering a known given dose.

Table 4.5a Number of aliquots rejected and their reason for rejection at each PH_I temperature for sample OR22; 90-125 μm.

PH_I temperature (°C)	Number of aliquots rejected	Aliquot number and reason for rejection
180	2	AL5: TT[1] AL7: RR[2] (*low & high*)
190	2	AL11: RR (*low*) AL13: RR (*low*)
200	1	AL23: RR (*high*)
210	1	AL25: RR (*low*)
220	3	AL33: RR (*high*) AL37: TT AL39: RR (*low*)
230	3	AL41: RR (*low*) AL45: RR (*high*) AL47: RR (*low*)
240	2	AL49: RR (*low*) AL55: TT
250	2	AL57: RR (*low*) AL63: TT
260	2	AL67: TT AL71: TT
270	2	AL73: TT AL77: IR[3]
280	2	AL83: TT AL85: RR (*low*)
TOTAL	**22**	

[1] TT = rejected due to high thermal transfer i.e. >5%
[2] RR = rejected due to unacceptable recycling ratios. *Italics* indicates which recycling ratio was unacceptable
[3] IR = rejected due to unacceptable OSL-IR ratio indicative of feldspar contamination

Table 4.5b Number of aliquots rejected and their reason for rejection at each PH_I temperature for sample BLA1; 90-125 μm.

PH_I temperature (°C)	Number of aliquots rejected	Aliquot number and reason for rejection
180	0	n/a
190	0	n/a
200	1	AL23: TT
210	0	n/a
220	0	n/a
230	1	AL43: TT
240	0	n/a
250	1	AL59: TT
260	0	n/a
270	0	n/a
280	0	n/a
TOTAL	**3**	

Table 4.5c *Number of aliquots rejected and their reason for rejection at each PH_I temperature for sample NEF4; 90-125 μm.*

PH_I temperature (°C)	**Number of aliquots rejected**	**Aliquot number and reason for rejection**
180	0	n/a
190	0	n/a
200	1	AL21: RR (*low*)
210	0	n/a
220	0	n/a
230	1	n/a
240	0	n/a
250	1	n/a
260	0	n/a
270	0	n/a
280	0	AL85: RR (*low*)
TOTAL	**2**	

For samples BLA1; 90-125 μm and NEF; 90-125 μm coherence between given and recovered dose is observed across the full range of PH_I temperatures. Of the accepted aliquots for BLA1; 90-125 μm an accurate dose is recovered (±10%) at all PH_I temperatures up to and including 270°C, whereas for NEF4; 90-125 μm this is 260°C. At temperatures above 260°C, accepted aliquots for NEF4; 90-125 μm become more unreliable in accurately recovering a known given dose. The rejection criteria appears to work sufficiently as all accepted aliquots accurately recover a known dose at PH_I temperatures up to 260°C.

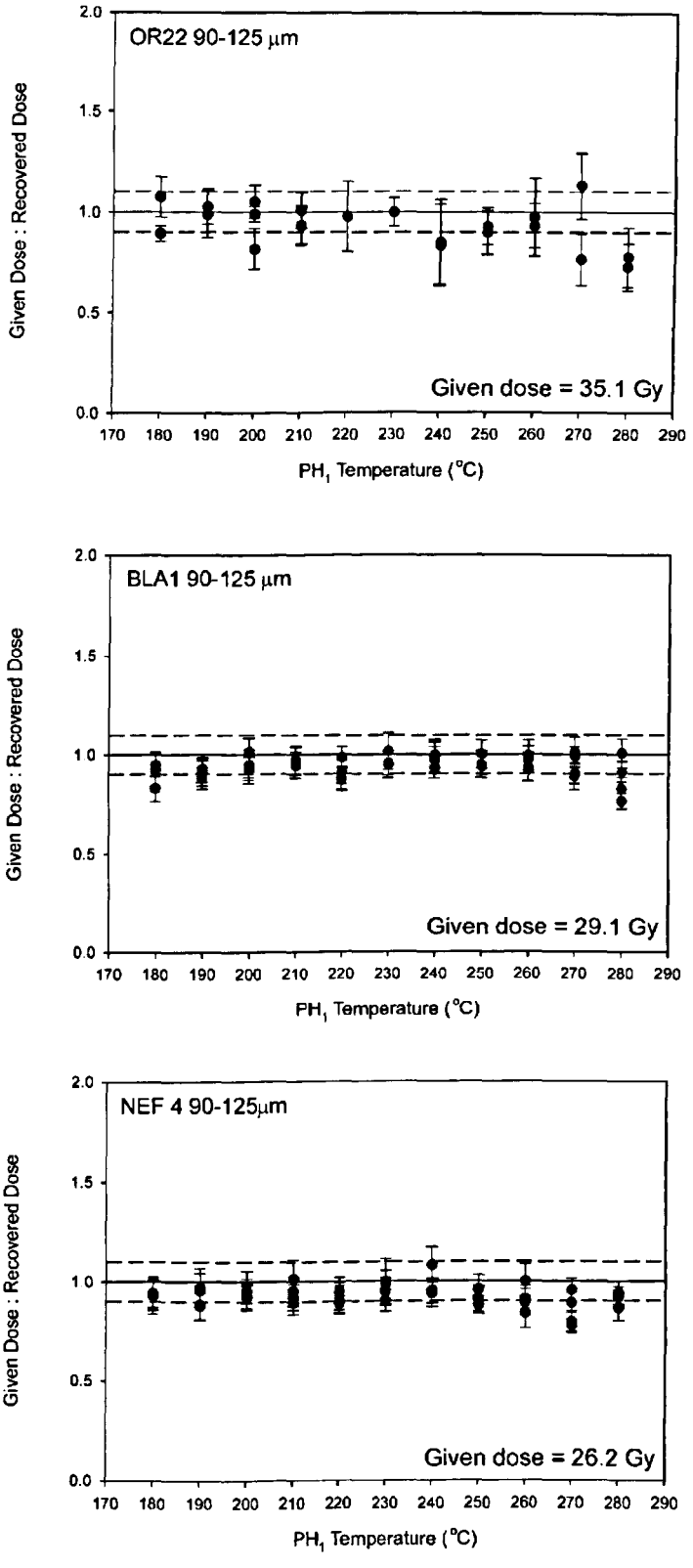

Figure 4.2 *Ratio of given dose to recovered dose (accepted aliquots only) plotted against PH_1 temperature for samples from all field sites. Filled circles indicate ratios for each individual aliquot, errors shown at the 1σ level. The solid horizontal reference line indicates unity, whereas the dashed lines indicate the ± 10% boundary.*

4.3.2.1 Recycling ratios as a function of preheat temperature

Figure 4.3 shows both low and high repeat-dose recycling ratios as a function of PH_1 temperature for aliquots of each sample. For OR22; 90-125 μm, large variation in both low and high repeat-dose recycling ratio is observed at all PH_1 temperatures. At PH_1 temperatures of ≥240°C the variation in recycling ratios decreases and both low and high repeat dose recycling ratios overlap with unity (±10%) within errors. The individual aliquots whose recycling ratios lay outside the acceptance boundary of 1 ± 10% (within 1σ errors) would be rejected as part of the standard rejection criteria established in this research. For the BLA and NEF samples, both low and high repeat dose recycling ratios for most aliquots at all PH_1 temperatures were at unity (±10%) within 1σ errors.

4.3.2.2 Thermal transfer as a function of preheat temperature

Thermal transfer was calculated for every aliquot at each PH_1 temperature. Figure 4.4 shows thermal transfer as a percentage of the natural signal, plotted against PH_1 temperature for *all* aliquots. For sample OR22; 90-125 μm, all PH_1 temperatures have the potential to induce thermal transfer of >5% (of the natural signal), this becomes more apparent at temperatures of 210°C and above. However, there are aliquots at all PH_1 temperatures where thermal transfer is below the 5% rejection criteria of Murray and Wintle (2000). For BLA1; 90-125 μm, the majority of aliquots at all PH_1 temperatures induce thermal transfer of <5% of the natural signal. There are, however, aliquots at PH_1 temperatures of 200°C and above that induce thermal transfer of above 5% of the natural signal. For NEF4; 90-125 μm, all aliquots have thermal transfer of ≤ 5% of the natural signal at PH_1 temperatures up to 280°C.

Therefore, thermal transfer does not seem to be a problem in the quartz at this locality but should still to be monitored and enforced as part of the rejection criteria.

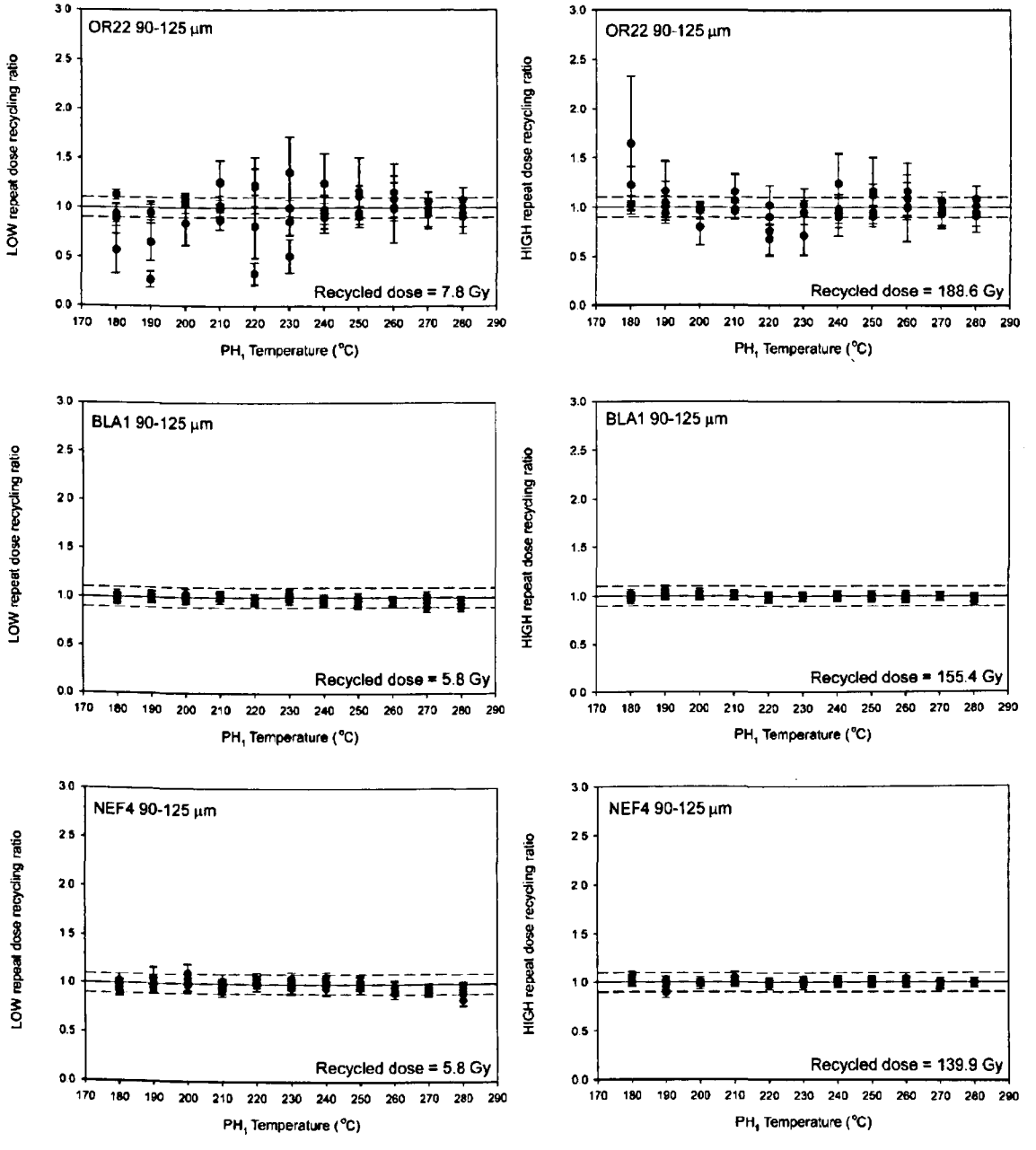

Figure 4.3 *Low and high repeat dose recycling ratios plotted against PH_1 temperature for samples from all field sites. Individual aliquot recycling ratios are shown as filled circles along with their associated 1σ error bars. The solid line indicates unity and the dashed line delimits the ± 10% limits (Murray & Wintle, 2000).*

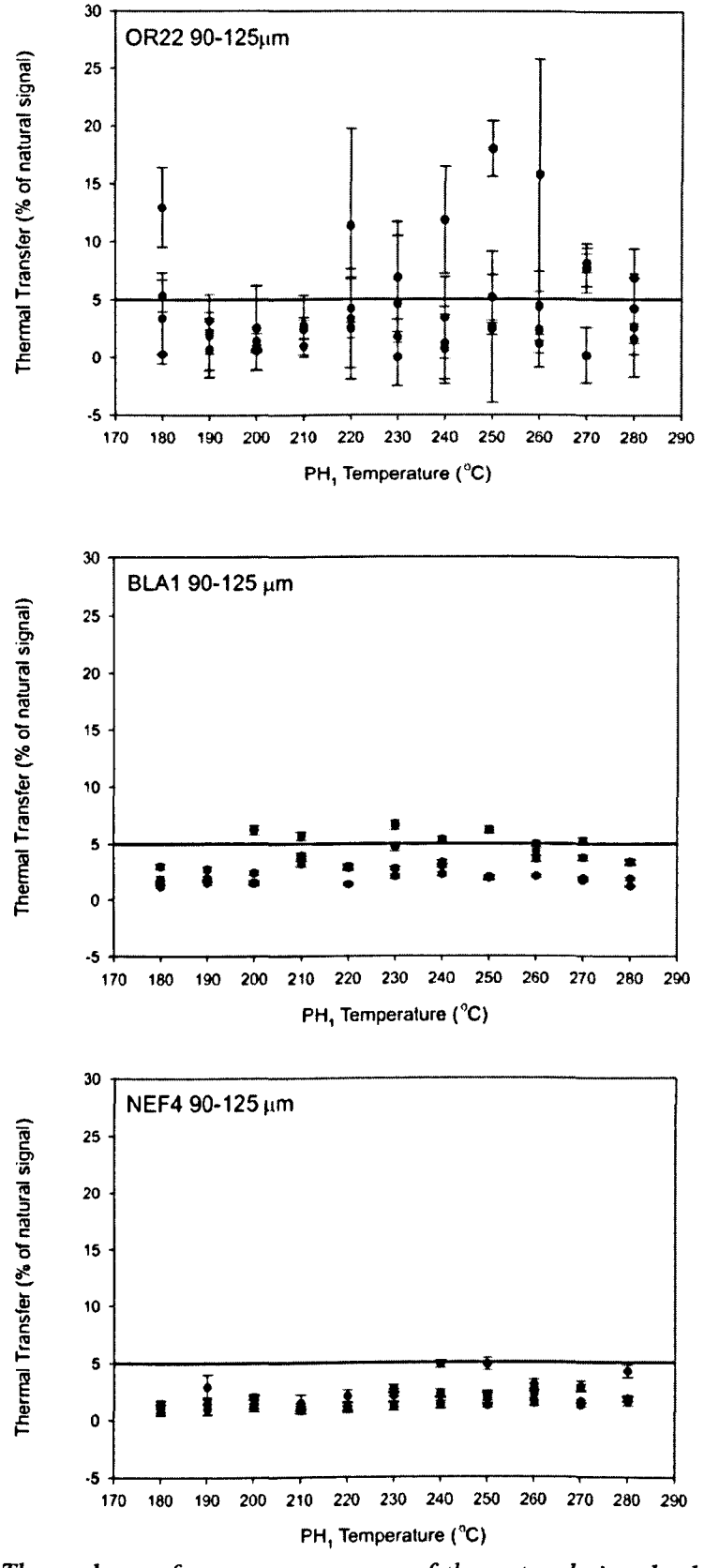

Figure 4.4 *Thermal transfer as a percentage of the natural signal, plotted against PH_1 temperature for samples from all field sites. Filled circles show individual aliquot thermal transfer (% of the natural signal) and 1σ errors. The 5% rejection line (Murray and Wintle, 2000) is also indicated on the graph.*

4.3.3 Thermal transfer calculated according to Jain et al. (2002)

Results of this test are illustrated for two aliquots of OR22; 90-125 μm in Figure 4.5 where the thermal transfer phenomenon is observed rather well, with thermal transfer (Gy) rising with PH_I temperature for aliquot 23, although the actual quantity of thermal transfer in Gy is low. Aliquot 19 however shows no discernable increase in thermal transfer (Gy) with PH_I temperature, although the quantity of thermal transfer in Gy is much higher than that in aliquot 23. Aliquot 23 would therefore be preferential for OSL dating. It can be deduced that there are aliquots where thermal transfer does not pose a problem if an appropriate preheat temperature is chosen.

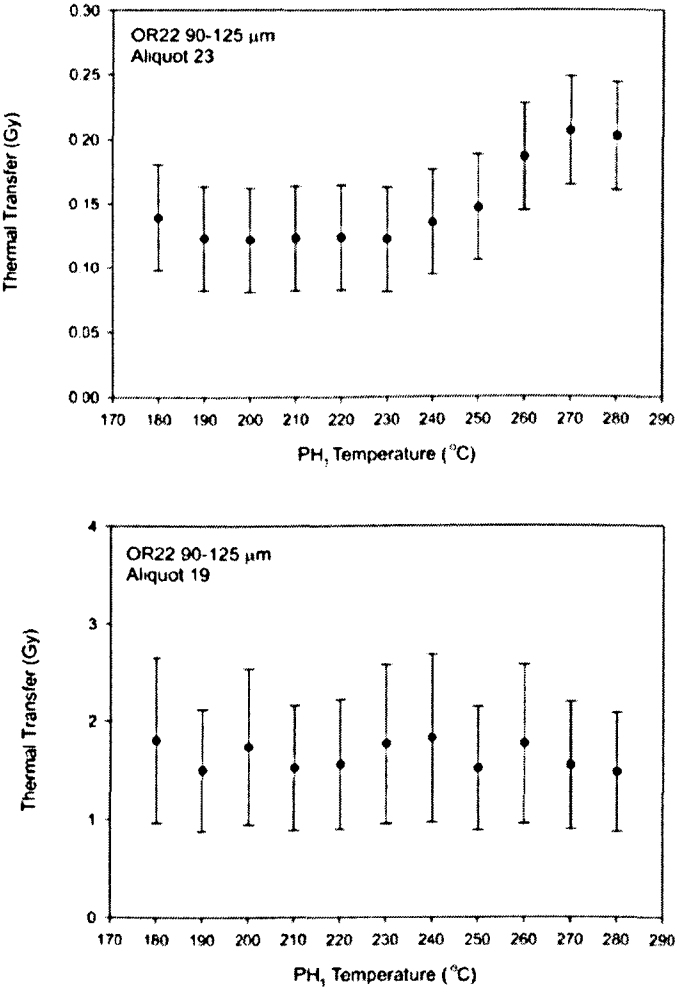

Figure 4.5 *Thermal transfer (Gy) plotted against PH_I temperature. Error bars shown at 1σ level.*

4.3.4 Fast component analysis: OSL decay curve fitting

4.3.4.1 Linearly Modulated OSL (LM-OSL) curve fitting

The results for the background measurement of LM-OSL over 4000 seconds are shown in Figure 4.6. This was determined via the average LM-OSL intensity (counts/2.0s) of three blank stainless steel discs with silicone oil covering ~0.5 mm diameter.

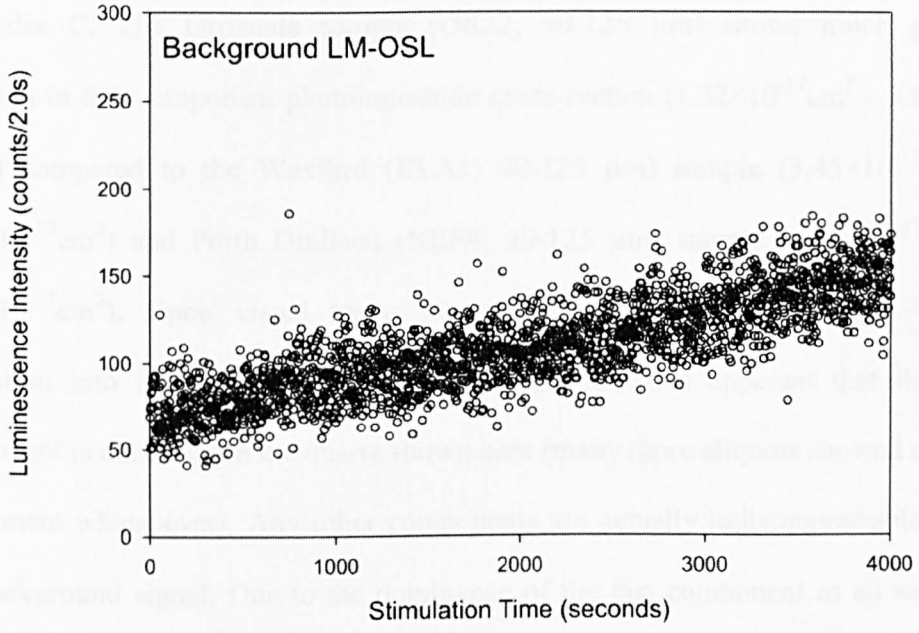

Figure 4.6 *Average LM-OSL from three blank stainless steel discs with ~0.5 mm diameter silicone oil coverage. This was taken as background and subtracted from all subsequent LM-OSL measurements upon quartz.*

Measurements for the natural LM-OSL and their decomposed dataset for the 'best fit' (lowest Chi-squared/degrees of freedom) number of components of two aliquots of each sample are shown in Figure 4.7. Some measurement values are negative due to the background subtraction i.e. the background value was greater than the LM-OSL signal from the quartz. All samples appear to have a common fast component photoionisation cross-section (see caption Figure 4.7) of the same magnitude as those published by others (e.g. Agersnap Larsen, et al., 2000; Jain, et al., 2003b;

Singarayer and Bailey, 2003; 2004; Choi, et al., 2006a; Choi, et al., 2006b; Li and Li, 2006; Demuro, et al., 2008) (see Tables 4.6 and 4.7).

Table 4.7 shows calculated fast component photoionisation cross-sections as a result of applying the LM-OSL technique and subsequent curve deconvolution. Fast component photoionisation cross-sections were calculated using the parameters derived from deconvolution of LM-OSL curves, these parameters are given in Appendix C. The Orrisdale sample (OR22; 90-125 μm) shows much greater variation in fast component photoionisation cross-section ($1.32\times10^{-17}cm^2$ - $3.82\times10^{-17}cm^2$) compared to the Wexford (BLA1; 90-125 μm) sample ($3.45\times10^{-17}cm^2$ - $4.74\times10^{-17}cm^2$) and Porth Dinllaen (NEF4; 90-125 μm) sample ($4.02\times10^{-17}cm^2$ - $4.60\times10^{-17}cm^2$). Upon visual inspection of LM-OSL curves (Figure 4.7) and separation into fast, medium and slow components, it is apparent that the fast component is dominant in the quartz shown here (many more aliquots showed no fast component whatsoever). Any other components are actually indistinguishable from the background signal. Due to the dominance of the fast component in all samples the standard SAR protocol should be suitable for D_e analysis (Murray and Wintle, 2000).

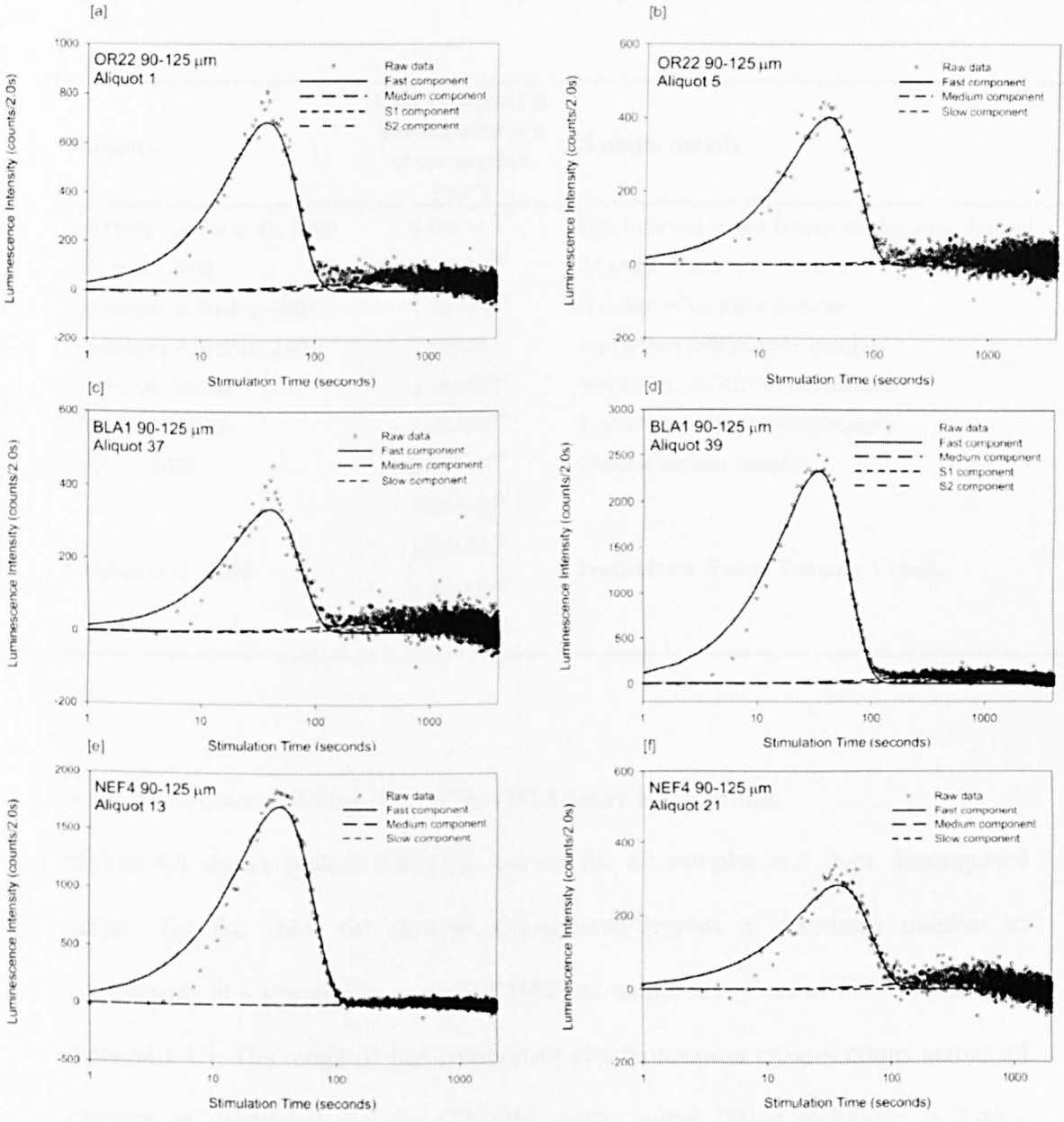

Figure 4.7 *Natural LM-OSL data for (a) Aliquot 1 of sample OR22; 90-125 µm (fast component σ= σ=3.82×10^{-17}cm^2) (b) Aliquot 5 of sample OR22; 90-125 µm (fast component 3.71×10^{-17}cm^2) (c) Aliquot 37 of sample BLA1; 90-125 µm (fast component σ = 3.45×10^{-17}cm^2) (d) Aliquot 39 of sample BLA1; 90-125 µm (fast component σ = 4.74×10^{-17}cm^2) (e) Aliquot 13 of sample NEF4; 90-125 µm (fast component σ = 4.60×10^{-17}cm^2) (f) Aliquot 21 of sample NEF4; 90-125 µm (fast component σ = 4.02×10^{-17}cm^2). For details of other components see Appendix C.*

Table 4.6 Fast component photioionisation cross-sections calculated from different samples published by other authors; use for comparison to Table 4.7.

Authors	Fast component photoionisation cross-section (cm^2)	Sample details
Agersnap Larsen et al., 2000	9.00×10^{-17}	Glaciofluvial quartz from a marine core, Jutland.
Jain et al., 2003	2.32×10^{-17}	Average of multiple samples
Singarayer & Bailey, 2003	2.50×10^{-17}	Average of multiple samples
Singarayer & Bailey, 2004	3.10×10^{-17}	Sri Lankan sedimentary sample
Choi et al., 2006a	2.10×10^{-17}	South Kenyan Rift Valley sample
Choi et al., 2006b	2.00×10^{-17}	South Kenyan Rift Valley sample
Li & Li, 2006	2.30×10^{-17}	Chinese aeolian sample
Demuro et al., 2008	2.04×10^{-17}	Frozen loess, Yukon Territory, Canada
	1.93×10^{-17}	
	2.38×10^{-17}	
	1.66×10^{-17}	

4.3.4.2 Continuous-Wave OSL (CW-OSL) decay curve fitting.

Figure 4.8 shows typical CW-OSL curves for all samples and their decomposed dataset for the 'best fit' (lowest Chi-squared/degrees of freedom) number of components at a stimulation power of 10% and stimulation time of 100 seconds (see Appendix C). The range of fast component photoionisation cross-sections across all samples as calculated via the CW-OSL decay curve fitting technique is 2.48 - 4.21×10^{-17} cm^2 which, once again, fits well within those published by other authors (see Tables 4.6 and 4.7). At all field sites, the majority of grains sampled showed a dominant fast component (Figure 4.8a, b, c and e); with a minority of quartz grains having a more 'intense' medium component (Figure 4.8d and f). The slow component observed in these aliquots may not actually be a true 'component', it is

likely to be an artefact of background signal derived from instrumental error and counting statistics.

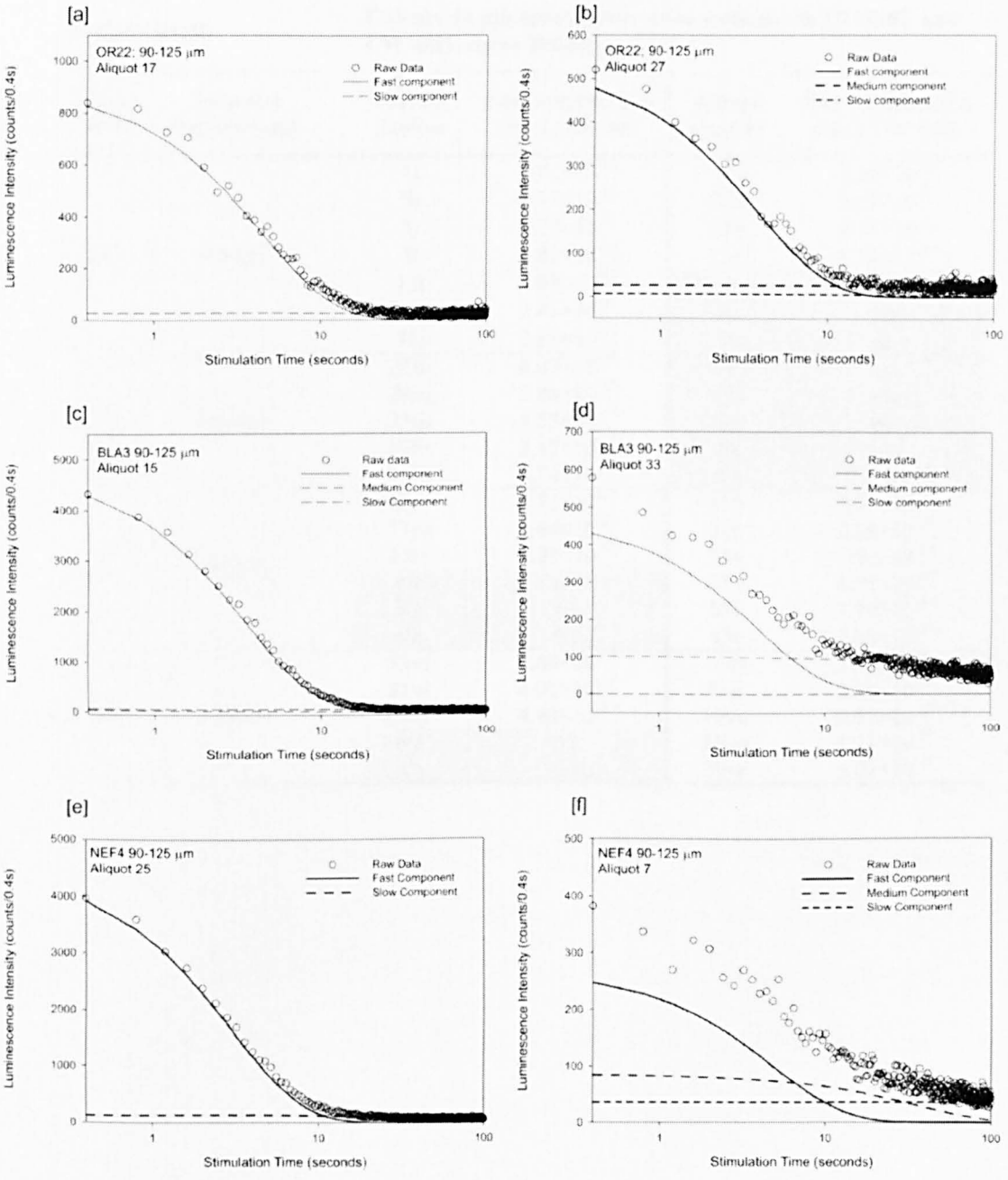

Figure 4.8 *Natural CW-OSL decay curves for (a) Aliquot 17 of sample OR22; 90-125 μm (fast component $\sigma = 2.74\times10^{-17}cm^2$) (b) Aliquot 27 of sample OR22; 90-125 μm (fast component $\sigma = 3.27\times10^{-17}cm^2$) (c) Aliquot 15 of sample BLA3; 90-125 μm (fast component $\sigma = 3.47\times10^{-17}cm^2$) (d) Aliquot 33 of sample BLA3; 90-125 μm (fast component $\sigma = 3.16\times10^{-17}cm^2$) (e) Aliquot 25 of sample NEF4; 90-125 μm (fast component $\sigma = 4.21\times10^{-17}cm^2$) (f) Aliquot 7 of sample NEF4; 90-125 μm (fast component $\sigma = 2.48\times10^{-17}cm^2$). For details of other components see Appendix C.*

Table 4.7 *Fast component photoionisation cross-sections calculated via both methods of decay curve fitting; LM-OSL and CW-OSL for different aliquots of each sample.*

Sample details		**Calculated photoionisation cross-sections via LM-OSL and CW-OSL curve fitting**			
Sample name	Grain size fraction (μm)	Aliquot number	Fast component σ (cm^2) LM-OSL	Aliquot number	Fast component σ (cm^2) CW-OSL
OR22	90-125	1i	3.82×10^{-17}	29ii	3.35×10^{-17}
		5i	3.71×10^{-17}	27ii	3.23×10^{-17}
		3i	3.73×10^{-17}	17ii	2.73×10^{-17}
		7i	1.82×10^{-17}	13ii	1.36×10^{-17}
		13i	1.93×10^{-17}	n/a	n/a
		29i	2.45×10^{-17}	n/a	n/a
		31i	2.83×10^{-17}	n/a	n/a
BLA1	90-125	23iii	4.07×10^{-17}	n/a	n/a
		29iii	3.88×10^{-17}	n/a	n/a
		33iii	4.53×10^{-17}	n/a	n/a
		37iii	3.45×10^{-17}	n/a	n/a
		39iii	4.74×10^{-17}	n/a	n/a
BLA3	90-125	1iv	3.73×10^{-17}	15v	3.47×10^{-17}
		11iv	2.64×10^{-17}	21v	2.85×10^{-17}
		15iv	4.22×10^{-17}	25v	3.72×10^{-17}
		n/a	n/a	31v	3.72×10^{-17}
		n/a	n/a	33v	3.10×10^{-17}
		n/a	n/a	45v	2.98×10^{-17}
NEF4	90-125	13vi	4.60×10^{-17}	3vii	2.98×10^{-17}
		21vi	4.02×10^{-17}	7vii	2.48×10^{-17}
		27vi	4.49×10^{-17}	19vii	3.97×10^{-17}
		n/a	n/a	25vii	4.22×10^{-17}
		n/a	n/a	29vii	4.09×10^{-17}

4.4 Discussion

4.4.1 The combined preheat dose-recovery test

4.4.1.1 Recycling ratios as a function of preheat temperature

For sample OR22; 90-125 μm, the recycling ratios for some aliquots at all PH_1 temperatures up to and including 230°C did not overlap with unity ± 10% within 1σ errors. Therefore in some aliquots the test dose OSL was not accurately accounting for sensitivity change pertained during measurement of the main OSL signal. At PH_1 temperatures of ≥240°C, the test dose OSL was accurately accounting for sensitivity change at both low and high regenerative doses.

This is not the case for BLA1; 90-125 μm and NEF4; 90-125 μm where all recycling ratios are at unity ± 10% within 1σ errors across the full range of PH_1 temperatures. In these samples the test dose was accurately accounting for sensitivity change at all PH_1 temperatures for both low and high regenerative doses. This is an important observation due to the range of regenerative doses used (5.8 – 155.4 Gy) to cover the saturating exponential growth of luminescence with given dose (within which the natural dose lies). It is encouraging to observe that the test dose was able to account for sensitivity change for both the low and very high regenerative doses as such high doses have the potential to induce their own sensitivity changes. The recycling ratios remain important criteria for acceptance/rejection of aliquots and must be monitored during routine SAR procedures.

4.4.1.2 Thermal transfer as a function of preheat temperature

A PH_1 temperature with a low thermal transfer should be used (Murray and Wintle, 2000) to ensure that the calculated D_e results from the natural signal, rather than a

thermally-transferred signal. For sample OR22; 90-125 μm, thermal transfer of >5% of the natural signal became more common in aliquots treated with preheats of 220°C and above. A quartz type was also present which was able to induce high levels (over 15% of the natural signal) of thermal transfer at PH_1 temperatures as low as 180°C. Equally, a quartz type is present that induces very little thermal transfer (<5% of the natural signal) up to PH_1 temperatures of 280°C. This emphasises the importance of thermal transfer as an aliquot rejection criterion, as it is apparent that aliquots containing the quartz type which is sensitive to thermal treatment could have high thermal transfer values at any PH_1 temperature.

For BLA1; 90-125 μm and NEF4; 90-125 μm, thermal transfer is less of an issue in comparison to the Orrisdale sample (i.e. no aliquots displayed 'high' levels of thermal transfer as a percentage of the natural signl), as the majority of aliquots across the full range of PH_1 temperatures induce thermal transfer of ≤5% of the natural signal and in doing so satisfy the acceptance criteria of Murray and Wintle (2000). Thermal transfer must still be monitored and a zero dose point included as part of the routine SAR protocol for D_e determination. This ensured that any aliquots displaying thermal transfer as a significant (>5%) percentage of the natural signal were clearly identified and rejected.

4.4.1.3 Summary of preheat dose-recovery test

The OR22 sample was much more variable in terms of thermal transfer and recycling ratios at all PH_1 temperatures, in comparison to the NEF4 and BLA1 samples which demonstrated acceptable recycling ratios and levels of thermal transfer across the full range of PH_1 temperatures. Therefore, the rejection criteria were rigorously adhered

to. This ensured that the accepted aliquots were giving D_e values unaffected by thermal transfer and sensitivity change. This in turn allowed the most accurate D_e to be determined for subsequent age calculation. The preheat-dose recovery test suggested that a PH_1 temperature of ≤260°C would be satisfactory for sample OR22. However, the analysis of recycling ratios suggests that a PH_1 temperature of ≥240°C would be more applicable. A PH_1 temperature of **250°C** was chosen for the standard SAR protocol for D_e determination purposes for all Orrisdale samples.

For samples BLA1 and NEF4 a preheat temperature of ≤260°C was used; according to the preheat-dose recovery test. These samples were largely unaffected by thermal transfer and sensitivity change could be accounted for by the test dose OSL across the full range of PH_1 temperatures. A PH_1 temperature of **240°C** was chosen for the standard SAR protocol for all samples from both Wexford and Porth Dinllaen.

The results from these tests allowed an appropriate preheat temperature to be determined for quartz at all field sites. The preheat dose-recovery test allowed an assessment to be made upon whether aliquots that would usually be accepted (according to the established rejection criteria) were accurately recovering the known given dose. As this was the case for all samples, further confidence is gained in the rejection criteria.

4.4.2 Thermal transfer calculated according to Jain et al. (2002)

It is difficult to discuss the data derived from this test due to such inter-aliquot variation as shown in Figure 4.5. This is once again related to the luminescence characteristics of the quartz mounted on each aliquot, a type of which has the ability

to induce high levels of thermal transfer. In this test, although thermal transfer can be calculated in Gy, the value is of limited use unless compared to D_e so that the proportion of the natural signal as affected by thermal transfer can also be calculated. The first step of this test is to bleach the quartz to ensure that any signal derived is purely as a result of thermal transfer, and so a D_e cannot be calculated for each aliquot on an individual basis, as the grains have been bleached. This is a downfall of this particular test, and so to enable thermal transfer to be compared to D_e, the average D_e for this sample was used.

In the case of aliquot 23, thermal transfer was as low as ~0.12 Gy which was ~0.2% of the average D_e for this sample and was therefore negligible. Figure 4.5 shows the results for aliquot 19 whose thermal transfer reached ~ 3 Gy (~5% of the average D_e for this sample) at certain PH_1 temperatures. This could have resulted in a significant offset in D_e, especially if the actual calculated D_e was below the average for this sample causing erroneously old ages to be determined, simply because thermal transfer was providing a significant percentage of the calculated D_e. With this in mind, thermal transfer was an important criteria for the rejection of aliquots when final D_e measurements were carried out. Thermal transfer was monitored carefully for each aliquot and if it was greater than 5% of the natural signal, the aliquot must be rejected as an inaccurate palaeodose estimate would ultimately have been achieved.

This test was not carried out on any samples from other field sites due to the lengthy measurement time and low 'value-added' in terms of conclusions that could be drawn from this test. The simpler method of measuring thermal transfer as part of the

preheat-dose recovery test was equally as useful for thermal transfer estimation albeit as a percentage rather than in Gray.

4.4.3 Fast component characterisation summary

LM-OSL and CW-OSL measurements allowed the presence or absence of the fast component to be assessed and to estimate its 'strength' or 'intensity' in relation to other components that were present. The photoionisation cross-section of the fast component was then compared to other published results to check if it sits within the published defined range (see Table 4.6 and 4.7). Both methods of decay curve fitting (LM-OSL and CW-OSL) allow the fast component photoionisation cross-sections to be calculated (and compared to previously published results) and the presence of other medium or slow components to be assessed.

4.4.3.1 LM-OSL curve fitting

It is clear from LM-OSL curve fitting results that the OR22; 90-125 μm showed more variation in calculated fast component photoionisation cross-sections compared to the Wexford (BLA1) and Porth Dinllaen (NEF4) samples. This was possibly due to the provenance of quartz grains in the Orrisdale samples which originated from an area of highly varying bedrock lithology (see Figure 4.9 and Section 4.4.4). The higher variability of bedrock in the source areas for the Orrisdale glaciofluvial complex possibly explains why the fast component photoionisation cross-sections also differ somewhat at the Orrisdale field site; possibility related to varying quartz types. Despite the variation in calculated fast component photoionisation, all aliquots shown in Figure 4.7 had a dominant fast component in terms of luminescence

intensity and so validating the use of the SAR protocol (Murray and Wintle, 2003; Demuro, et al., 2008).

A problem with the LM-OSL method was the inability of the fitting procedure to accurately 'fit' the rising limb of the fast component. It was often the case, as in the aliquots measured here, that the 'fitted' fast component was actually greater (in terms of luminescence intensity) than the raw data within the initial 10 seconds (Figure 4.7). This may be due to the blue LEDs in the Risø machine i.e. at low stimulation powers (the initial 10 seconds), the blue LEDs were not increasing linearly in stimulation power, or, the LEDs were not switching on at the correct time and so the accurate power required at this level was not provided by the stimulation equipment. The stimulation power for the initial 10 seconds of stimulation via LM-OSL was so low (0-0.23%) that errors relating to blue LED stimulation became more apparent. There seemed, therefore, to be a below-linear increase in stimulation power in the initial 10 seconds, creating larger errors at the beginning of the measurement. However, the curve fitting programme was able to capture and accurately replicate the peak in LM-OSL as a result of the peak in fast component OSL emission.

LM-OSL curve fitting was also undertaken after the initial three data channels were excluded (i.e. those affected by inaccurate stimulation power) to see if this made a difference to the calculated fast component photoionisation cross-sections. This procedure made little difference to the photoionisation cross-section values.

4.4.3.2 CW-OSL decay curve fitting

A similar variation in fast component photoionisation cross-section as that obtained via LM-OSL curve fitting was also replicated for aliquots of quartz from each field site as a result of CW-OSL decay curve fitting. The fast component was dominant and no problematic medium or slow components were apparent. For quartz where a stronger medium component was observed, they could be easily recognised via characteristically slower decay in luminescence with time during optical stimulation for D_e determination. These aliquots could subsequently be rejected. The dominant fast component in the majority of aliquots of each sample means that the standard SAR protocol was suitable for D_e determination (Murray and Wintle, 2000; Demuro, et al., 2008).

The CW-OSL decay curve fitting procedure was much quicker in terms of measurement and curve fitting time than the LM-OSL technique and allowed just as high quality data to be obtained (in terms of resolution of the fast component). If, however, samples show the presence of stronger medium or slow components via initial investigations via the LM-OSL method, then the LM-OSL method may be best for subsequent quantitative measurement of their photoionisation cross-sections. This is because at longer measurement times, the resolution of the data from the CW-OSL method reduces rapidly, as 250 data bins are used for CW-OSL measurement. For LM-OSL, a greater number of data bins could be used to improve data resolution over longer measurement times (as would be required if dominant slow components are observed).

The CW-OSL decay curve fitting technique does not appear to have the problem of overestimating the rising limb of the fast component as the LM-OSL method does. This may be due to higher, constant (rather than linearly ramped) initial stimulation power (10%) and better signal to noise ratios in the first seconds of stimulation via the CW-OSL method.

4.4.4 Quartz luminescence characteristics in relation to sediment provenance

The glacial sediments that have been sampled have an Irish Sea Basin provenance, reflecting the passage of ice through the basin from ice caps in the Lake District, Scotland and Northern Ireland. The bedrock geology of the Irish Sea floor (Figure 4.9) affects the quartz types within these glacial sediments, which, in turn, determines the luminescence characteristics of the quartz grains which are used for OSL dating. Poor quartz luminescence characteristics may arise from the freshly eroded nature of sediments (especially those of glacigenic origin) resulting in poor quartz luminescence sensitivity (Lukas, et al., 2007). Low luminescence sensitivity in quartz from glacially-derived sediments has been reported in other studies (Rhodes and Pownall, 1994; Richards, 2000; Spencer and Owen, 2004; Lukas, et al., 2007) and has been attributed to either a fresh bedrock source, a lack of subaerial weathering of the grains (Rhodes and Pownall, 1994) or an insufficient number of bleaching and dosing cycles due to the proximity of the depositional setting to the quartz provenance (Pietsch, et al., 2008).

Figure 4.9 shows the bedrock overridden by glaciers radiating from the Lake District and Scotland and feeding into the Irish Sea Basin. The materials deposited on the Isle of Man, Wexford and Porth Dinllaen, in part, reflect glacial erosion and transport of

such materials from these source areas. In addition, during its passage southwards, the Irish Sea ice-stream will have scoured and transported a considerable amount of sediment from the base of the Irish Sea floor. Figure 4.9 shows that the bedrock lithologies in the North Channel Basin and the Solway Firth Basin are Triassic sandstones. Further south, Permo-Triassic sandstones and Carboniferous materials outcrop, with a further major source of Triassic sandstone in the East Irish Sea Basin. This complex assemblage of source materials which comprises the glacial deposits of the Isle of Man, Wexford and Porth Dinllaen contributes to the complicated mixture of quartz grains within the outwash sands and gravels targeted for this research.

The Wexford and Porth Dinllaen samples provided favourable values for thermal transfer, recycling ratios and dose recovery ratios in comparison to the Orrisdale samples. This may be related to their geographical location, much further south in the Irish Sea Basin. On its passage further south, the ISIS would have scoured the dominantly Triassic and Permo-Triassic sandstones, from the East Irish Sea Basin, the Caernarfon Bay Basin (off-coast of north-west Wales), and the Kish Bank Basin (off-coast of south-west Ireland). These sandstones have been subject to cycles of both aeolian and fluvial transport and deposition in Triassic and Permo-Triassic desert environments (Jackson, et al., 1995) and should therefore provide favourable luminescence sensitivity characteristics. It is these sources of quartz that have been hypothesised to provide favourable luminescence characteristics. However, no direct investigation into quartz provenance and luminescence characteristics has been undertaken to establish this.

The Orrisdale samples did, however, contain certain quartz types that gave favourable values for thermal transfer, recycling ratios and dose recovery ratios; although this quartz was not as dominant as it was in the Wexford and Porth Dinllaen samples. A small-aliquot (~30 quartz grains) approach for D_e determination allowed aliquots containing dominantly 'poor' quartz (in terms of luminescence characteristics; thermal transfer, sensitivity change) to be separated from those containing 'favourable' quartz through application of the rejection criteria used throughout these tests.

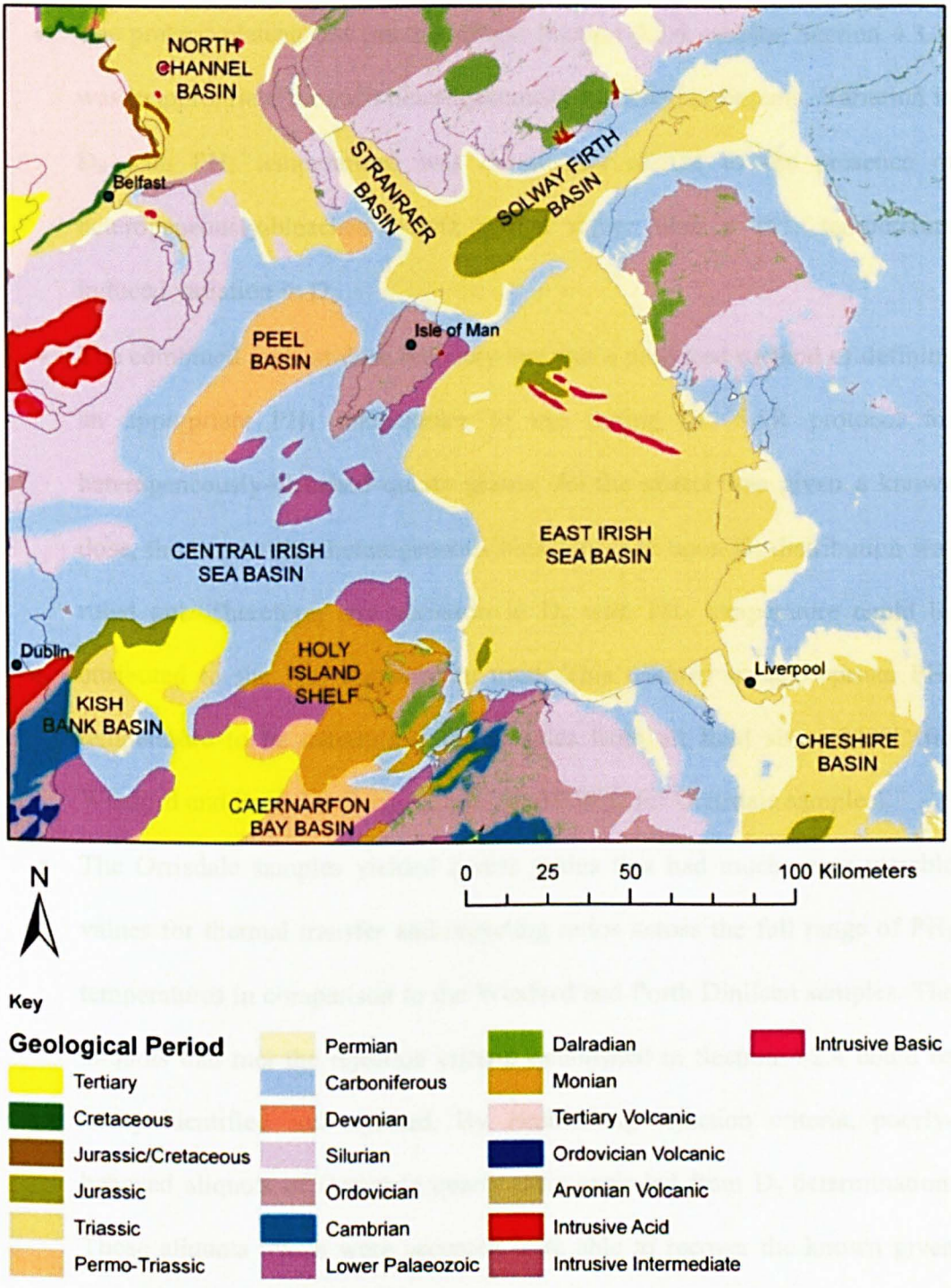

Figure 4.9 *General Pre-Quaternary geology of the Irish Sea. Based on 1:1 000 000 Geology of the United Kingdom, Ireland and the adjacent Continental Shelf (South Sheet). Redrafted from British Geological Survey, The Geology of the Irish Sea (1995).*

4.5 Conclusions

- The preheat plateau test (methodology; Section 4.2.4. results; Section 4.3.1) was inappropriate for such heterogeneously-bleached sediments. Variation in D_e with PH_1 temperatures was dominantly related to the presence of heterogeneously-bleached quartz grains rather than a PH_1 temperature induced variation in D_e.
- The combined preheat-dose recovery test was a preferred method of defining an appropriate PH_1 temperature to use during the SAR protocol for heterogeneously-bleached quartz grains. As the quartz was given a known dose, the impact that heterogeneous bleaching had upon D_e distribution was ruled out. Therefore, any variation in D_e with PH_1 temperature could be attributed to the PH_1 temperature used. This enabled an appropriate PH_1 temperature to be determined for samples from all field sites (240°C for Wexford and Porth Dinllaen samples, and 250°C for Orrisdale samples).
- The Orrisdale samples yielded quartz grains that had much more variable values for thermal transfer and recycling ratios across the full range of PH_1 temperatures in comparison to the Wexford and Porth Dinllaen samples. The aliquots that met the rejection criteria established in Section 4.2.4 could be easily identified and rejected. By establishing rejection criteria, poorly-behaved aliquots of Orrisdale quartz were excluded from D_e determination. Those aliquots which were accepted were able to recover the known given dose with 1σ errors.
- The thermal transfer test, according to Jain et al. (2002) (Section 4.2.6.2) enabled thermal transfer to be calculated in Gray. However, the 'value added', in terms of extra information achieved via the application of this test

was low when the length of measurement and data analysis time were taken into consideration. Thermal transfer could alternatively be calculated as a percentage of the natural signal via an additional zero-dose point at the end of the SAR cycle. This measurement was much more efficient and allowed aliquots to be rejected based on the percentage of the natural signal that was calculated to be as a result of thermal transfer.

- The CW-OSL decay curve fitting procedure was the preferred methodology for component analysis, unless there was a dominant slow component present. If a dominant slow component *was* present, then analysis via LM-OSL over a much longer stimulation time would be required to enable this component to be characterised more accurately by calculating photoionisation cross-section. In the research presented here, initial LM-OSL measurements (over 4000s) showed only a dominant fast component (and in a minority of cases, a weaker medium component) was present in all samples, and so fitting of decay curves could be undertaken through the CW-OSL methodology (stimulation for 100s with blue LEDs at 10% power), which requires less measurement and curve fitting time. By using the CW-OSL methodology, fast component photoionisation cross-sections could be calculated.
- The fast component photoionisation cross-sections calculated fit comfortably within the range of those previously published by others.
- The quartz luminescence characteristics observed from the samples analysed in this chapter may be attributable to the varying provenance of quartz grains. The less favourable luminescence characteristics of the Orrisdale samples (in terms of thermal transfer and luminescence sensitivity) may be related to the relative proximity of the sampling site to the freshly eroded bedrock source

areas of Northern Ireland, Southern Scotland and the Lake District. In comparison, the Wexford and Porth Dinllaen sampling sites are much further south and may be dominantly composed of quartz of Irish Sea Basin provenance i.e. Triassic and Permo-Triassic sandstones which have been subject to cycles of both aeolian and fluvial transport and deposition in Triassic and Permo-Triassic desert environments (Jackson, et al., 1995) and should therefore provide favourable luminescence sensitivity characteristics.

Chapter 5

Testing an approach to OSL dating of late Devensian glaciofluvial sediments of the British Isles

5.1 Introduction

In the British and Irish Isles there has been considerable research effort expended in improving understanding of the expansion and retreat of the last ice-sheet (Marine Isotope Stage 2) (Evans and Ó Cofaigh, 2003b; Clark, et al., 2004a; Ó Cofaigh and Evans, 2007), but the chronological control for the Last Glacial Maximum (LGM) extent of the British and Irish Ice-sheet (BIIS) is poor when compared to the Laurentide Ice-sheet (Miller, et al., 1999; Marsella, et al., 2000; England, et al., 2006; Carlson, et al., 2007). The timing and extent of the advance to maximum limits in the south Irish and Celtic Sea basin, in particular, remains a subject of some controversy. This sector of the BIIS has been identified as fast flowing and named the Irish Sea Ice-Stream (ISIS) which extended south through the Irish Sea Basin (ISB) as far as the Scilly Isles. Here we approach the concept of LGM of Marine Isotope Stage 2 (MIS) from a perspective of glaciers reaching their maximum extent (Thomas and Chiverrell, submitted) rather than global ice volume (Mix, et al., 2001).

Several studies have argued that the ISIS extended far south, past the Scilly Isles into the Celtic Sea (Scourse, 1991a; Scourse, et al., 1991; Ó Cofaigh and Evans, 2001a; Ó Cofaigh and Evans, 2001b; Hiemstra, et al., 2006; Ó Cofaigh and Evans, 2007; Thomas and Chiverrell, submitted) whilst others have proposed a more limited extent into the southern Irish Sea Basin to a line looping from St Davids Head in southwest

Wales to Rosslare in southeast Ireland (Bowen, et al., 2002; Knight, 2004) (Figure 6.1a). Advance to the LGM extent in the Celtic Sea is thought to have been a short-lived and unstable event accomplished by the advance of a fast-flowing and dynamically sensitive Irish Sea ice-stream (ISIS) (Roberts et al., 2007, Thomas and Chiverrell, 2007) whose surging behaviour was determined largely by change in internal, subglacial bedform conditions rather than external, climate and sea-level variation.

In part, the lack of chronology for the timing of maximum extent and subsequent retreat of the BIIS reflects the paucity of material dateable by radiocarbon techniques; however considerable strides have and are being made by applying optical (Duller, 1994; Olley, et al., 2004; Duller, 2006) and cosmogenic (Ballantyne, et al., 2007; Golledge, et al., 2007; Ballantyne, et al., 2008) dating techniques to glacial sediments. The attraction of optical dating lies in that it directly dates the time of deposition using the quartz and feldspars that dominate glaciofluvial sediments.

The optical dating signal itself is acquired by individual minerals (e.g. quartz and feldspar) through exposure to environmental radiation within sedimentary bodies. The signal is reset or bleached through exposure to daylight during transportation processes. Thus optically stimulated luminescence (OSL) dating of sediments attempts to determine the time that has elapsed since burial. Optical dating techniques have been used to date sediments successfully from a wide range of depositional environments; however the application of this technique to glacigenic sediments has proven to be more challenging.

A number of problems arising from the nature of depositional environments constrain the application of optical dating to glaciofluvial deposits. Turbulence and turbidity of the water column means that minerals are often not sufficiently exposed to daylight to enable the optical signal to be completely reset (Ditlefsen, 1992; Rendell, et al., 1994; Sanderson, et al., 2007); this is especially the case during transport by glacial outwash rivers. Many mineral grains therefore have an 'inherited' residual optical signal left behind from the previous burial cycle resulting in heterogeneously-bleached sediments. Optical dating of such sediments may therefore produce ages that are overestimated. These problems are compounded by the short duration of glaciofluvial transport experienced by ice-proximal sediments, which further reduces the opportunity for bleaching (Raukas and Stankowski, 2005). Despite such problems many authors have applied optical techniques to date glacigenic sediments with some being more successful (Almond, et al., 2001; Mangerud, et al., 2001; Owen, et al., 2002; Duller, 2006; Alexanderson and Murray, 2007; Bøe, et al., 2007; Klasen, et al., 2007) than others (Duller, et al., 1995; Raukas and Stankowski, 2005). A further obstacle to successful dating of glacigenic sediments from the British Isles lies in the often poor luminescence characteristics of quartz. This appears to be a function of their bedrock provenance and freshly eroded nature, thus they are unlikely to have experienced the cycles of acquisition and loss of the optical signal (through repeated erosion, transport and deposition) needed to sensitise the quartz.

This chapter presents a methodology that is aimed at improving the success of optical dating of a late MIS stage 2 palaeosandur at Orrisdale on the Isle of Man (Thomas, et al., 1985). The northern plain of the Isle of Man records the northward passage of the

margin of the ISIS during retreat from MIS 2 LGM extent. This retreat was punctuated by numerous ice-marginal oscillations and the glacigenic terrain around Orrisdale comprises a series of moraine ridges and marginal sandur. We applied a directed approach to sediment sampling to evaluate which depositional sub-environments of the glaciofluvial sandur system (e.g. channel, bar-top, back-bar and overbank) were most likely to produce assemblages of quartz grains that had been sufficiently bleached. Within these depositional sub-environments we targeted different grain size fractions present within individual samples to tighten the sediment/process characterised and explore any grain size dependence of OSL resetting.

A range of methodological techniques and statistical models were used to deal with heterogeneous bleaching and poor quartz luminescence characteristics. Several 'age' models have been published which address the problem of deriving the best single-valued estimate of the burial dose from such heterogeneously-bleached equivalent dose (D_e) distributions (Galbraith and Green, 1990; Olley, et al., 1998; Galbraith, et al., 1999) more detail about which is given in Section 5.4.4.3. Bailey and Arnold (2006) produced the first statistically-based decision-protocols to enable the appropriate 'age' model to be used, and this was derived for heterogeneously-bleached fluvial sediments. The applicability of this decision protocol for the Orrisdale glaciofluvial samples was also assessed.

This lithofacies-based approach to OSL sampling described above was then applied to ice-marginal glaciofluvial sediments from two *additional* sites located around the periphery of the Irish Sea Basin, on the Llŷn Peninsula (Northwest Wales) and in Co.

Wexford (Southeast Ireland). Lithologically and sedimentologically well-documented and widely-spaced sites were chosen; a coastal section at Porth Dinllaen on the Llŷn Peninsula which displayed evidence for a lower fan, distal sandur environment (Figure 6.1); and a quarry at Blackwater, Co. Wexford where depositional evidence for ice-contact glaciofluvial sedimentation was observed. The decision protocol of Bailey and Arnold (2006) was then applied to samples from both of these sites, and its applicability was once again tested.

In combination with results concerning the timing of glaciofluvial deposition at Orrisdale on the Isle of Man (Roberts, et al., 2006; Thomas, et al., 2006; Roberts, et al., 2007) the aim is to produce a chronology for the retreat of the ISIS from its maximum LGM extent through the various retreat stage positions recorded in glaciofluvial sediments exposed on the current Irish, Welsh and Manx coasts.

5.2 Lithofacies and bleaching regime

Lithofacies analysis refers to the identification of lithological components, sedimentary structures and the vertical and lateral relationships between them in a sedimentary sequence (Miall, 2006). Understanding the architectural relationships between lithofacies (or architectural element analysis (AEA)) can subdivide sedimentary basin fills into elements (or facies assemblages) on the basis of sedimentary body geometry and lithological composition (Miall, 1985; Brookfield and Martini, 1999; Boyce and Eyles, 2000). These approaches help geologists to constrain the nature of past depositional environments and processes.

Contemporary glaciofluvial environments are typically braided systems characterised by large and rapid discharge fluctuations, an abundance of easily eroded debris, and high rates of sediment transport and deposition (Hammer and Smith, 1983). Fluctuations in meltwater and sediment supply to sandur reflect seasonal, diurnal and stochastic changes, as well as responses to advance or retreat cycles of the source ice masses. All these factors result in a spatially and temporally variable pattern of grain size and sediment structure, which is then preserved in the fossil record as complicated laterally and vertically variable sequences of lithofacies.

Figure 5.1 shows a flow diagram of the main routeways, storage and depositional environments of a proglacial sandur, identifying the transport and storage mechanisms (and associated lithofacies) that provide enhanced opportunities for bleaching of mineral grains. Little bleaching is expected in turbulent and turbid water columns as sunlight cannot effectively penetrate the water column. Depositional sub-environments also influence the degree of bleaching. Those lithofacies deposited in turbid environments proximal to the ice margin such as deep channel (trough cross-stratified sands / gravels; Gt); bar core (massive gravels; *Gm*) and bar growth (planar cross-stratified bedded sands/gravels; *Sp*/*Gp*) have a low bleaching potential. Those deposited during waning flow in shallow, slow flowing or stagnant water columns have the highest chance of bleaching (in comparison to ice-proximal sub-environments) such as bar-top and back-bar deposits (rippled sands; *Sr*, horizontally-laminated sands; *Sh* and finely-laminated sands; *Fl*). Subaerial exposure of these deposits under low flow conditions presents an opportunity for these bar-top and back-bar deposits to be subject to aeolian transport (McGowan, et al., 1996; McGowan and Sturman, 1997). If this occurs during daylight hours then the potential

for complete bleaching of the optical signal is much greater. Aeolian transport provides a mechanism for quartz grains to be bleached and re-distributed across the sandur surface that need not be linked to a certain lithofacies type as individual aeolian-derived strata are rarely preserved and rarely identifiable in the geological record. It is this lithofacies-based approach that forms the basis to sampling for OSL dating undertaken in this research.

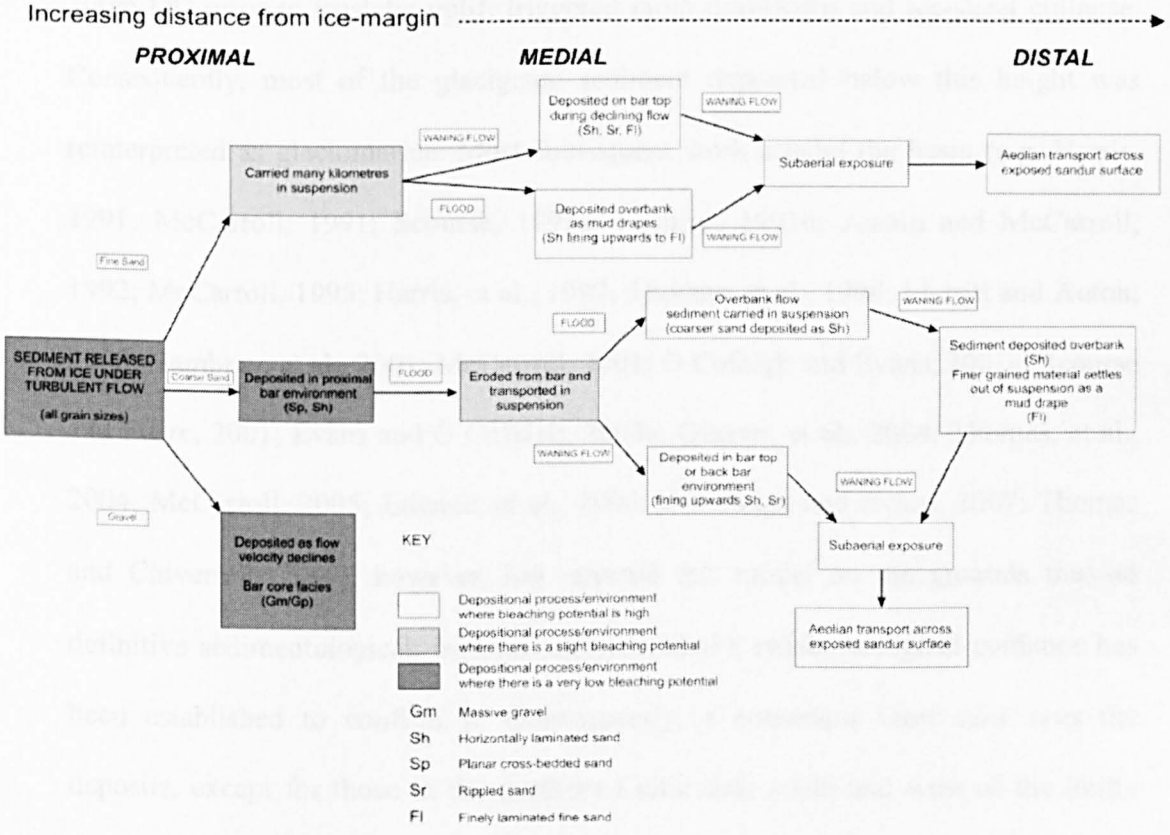

Figure 5.1 *Flow diagram illustrating the main sediment routeways, temporary storage and depositional environments in a proglacial sandur. This model includes a crude separation into fine sand, coarse sand and gravel, although in reality 'gravel' will include coarse sands as well. Processes which are thought to provide an enhanced opportunity for mineral grains exposed to daylight are highlighted. Lithofacies types which result from deposition in certain sub-environments are illustrated in brackets. Aeolian deposits are not linked to a certain lithofacies type as they are rarely preserved in the fossil record. It is more likely that they are deposited across the entire sandur surface and incorporated into a range of different lithofacies types.*

5.3 Depositional setting, field sites and sedimentary sequence

5.3.1 Depositional setting: the glaciomarine debate

Since the days of Tiddeman (1872), authors have accepted that the advance and retreat of the BIIS was accomplished terrestrially. In the 1980's, however, this concept was challenged by Eyles and McCabe (1989) who argued that during Late Devensian expansion ice advanced down the Irish Sea Basin when the floor was isostatically-depressed. During deglaciation re-flooding to relative sea-levels up to 100m OD prior to isostatic uplift triggered rapid drawdown and ice-sheet collapse. Consequently, most of the glacigenic sediment deposited below this height was reinterpreted as glaciomarine. Most subsequent work around the basin (e.g. Harris, 1991; McCarroll, 1991; Scourse, 1991a; Scourse, 1991b; Austin and McCarroll, 1992; McCarroll, 1995; Harris, et al., 1997; Thomas, et al., 1998; Merritt and Auton, 2000; Hambrey, et al., 2001; McCarroll, 2001; Ó Cofaigh and Evans, 2001a; Scourse and Furze, 2001; Evans and Ó Cofaigh, 2003a; Glasser, et al., 2004; Thomas, et al., 2004; McCarroll, 2005; Etienne, et al., 2006; Ó Cofaigh and Evans, 2007; Thomas and Chiverrell, 2007), however, has rejected this model on the grounds that no definitive sedimentological, isostatic or, particularly, palaeontological evidence has been established to confirm it. Consequently, a consensus view now sees the deposits, except for those in the northern Celtic Sea; south and west of the Scilly Isles, as terrestrial in origin. The interpretation of all sites used for dating determination confirms this consensus view and are regarded as of terrestrial glaciofluviatile origin, as described below.

5.3.2 Field site 1; Orrisdale, Isle of Man

The Isle of Man occupies a position in the centre of the Irish Sea (~54°N, 4°W; Figure 5.2a) and has been over-ridden during successive advances of major ice-streams from source areas in western Scotland (Thomas, et al., 2006). The Quaternary geological record on the Isle of Man reflects entirely the LGM advances and retreat cycle in MIS 2, during which the island was overridden by the ISIS issuing from western Scotland, Northern Ireland and the Lake District on route to maximum positions in the Celtic Sea and English Midlands. A series of successive retreat-stage ice-marginal positions are recorded in the Orrisdale area on the west coast of the Isle of Man (Figure 5.2c) during deglaciation, with margin-parallel sandur systems trapped between the northwards retreating ice margin and the lower Palaeozoic bedrock of the Manx Uplands (Thomas, et al., 2006). The ice-marginal sequence around Orrisdale is exposed in 8 km of continuous coastal section, with the glaciofluvial deposits stratigraphically defined as the Bishop's Court Member of the Orrisdale Formation (Figure 5.3) (Chiverrell, et al., 2001; Thomas, et al., 2006). The glacigenic sediments on the Isle of Man reflect their provenance from up-ice source areas in the Irish Sea Basin and the uplands of the Lake District, Scotland and Northern Ireland. The dominant, although not exclusive, bedrock lithologies in the area immediately adjacent to Orrisdale, essentially the floor of the Irish Sea, are Triassic and Permo-Triassic sandstones (Jackson, et al., 1995).

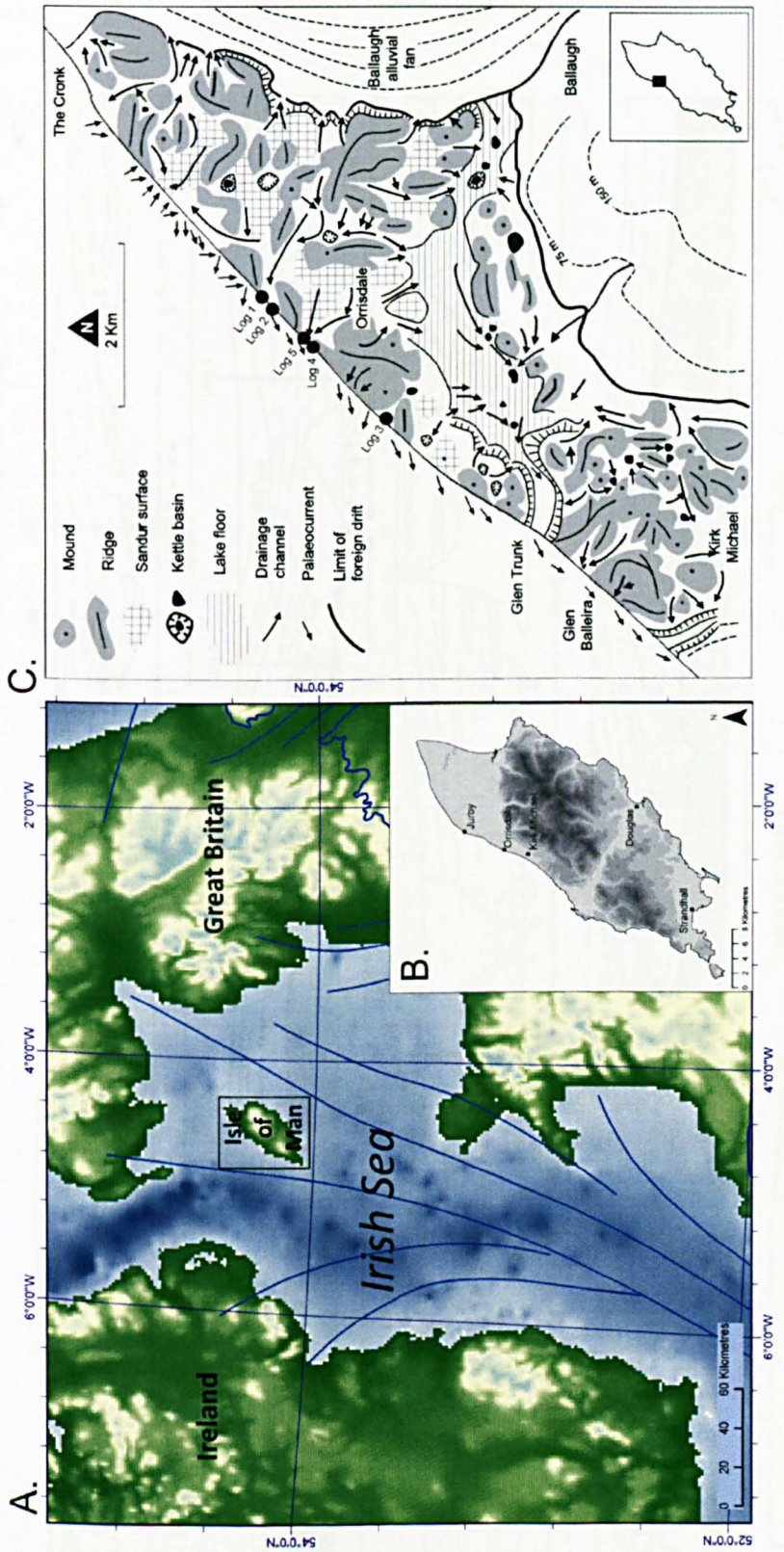

Figure 5.2 *(a) Map showing the location, longitude and latitude of the Isle of Man. Ice flow lines for the ISIS are also indicated. Inset: (b) Map of the Isle of Man showing the localities mentioned in the text. (c) Geomorphological map of the Orrisdale area, between Glen Trunk and The Cronk. Areas of sedimentary logging are labelled (modified from Thomas et al. 2006).*

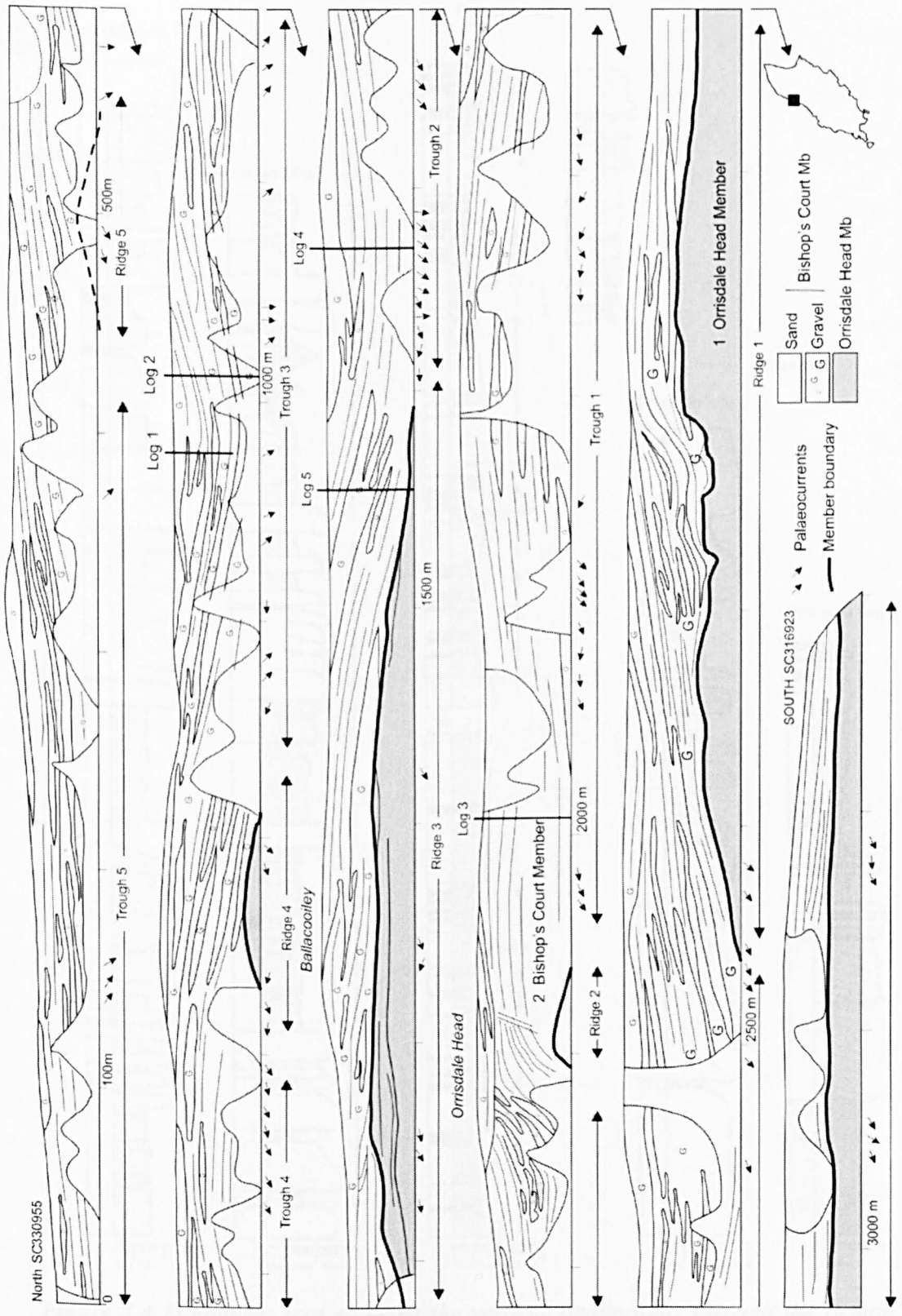

Figure 5.3 *Serial stratigraphy showing lateral exposure of the Bishop's Court Member (redrafted from Thomas et al., 2006). Areas of lithofacies logging are highlighted on the map (see Figure 5.4 for stratigraphic details).*

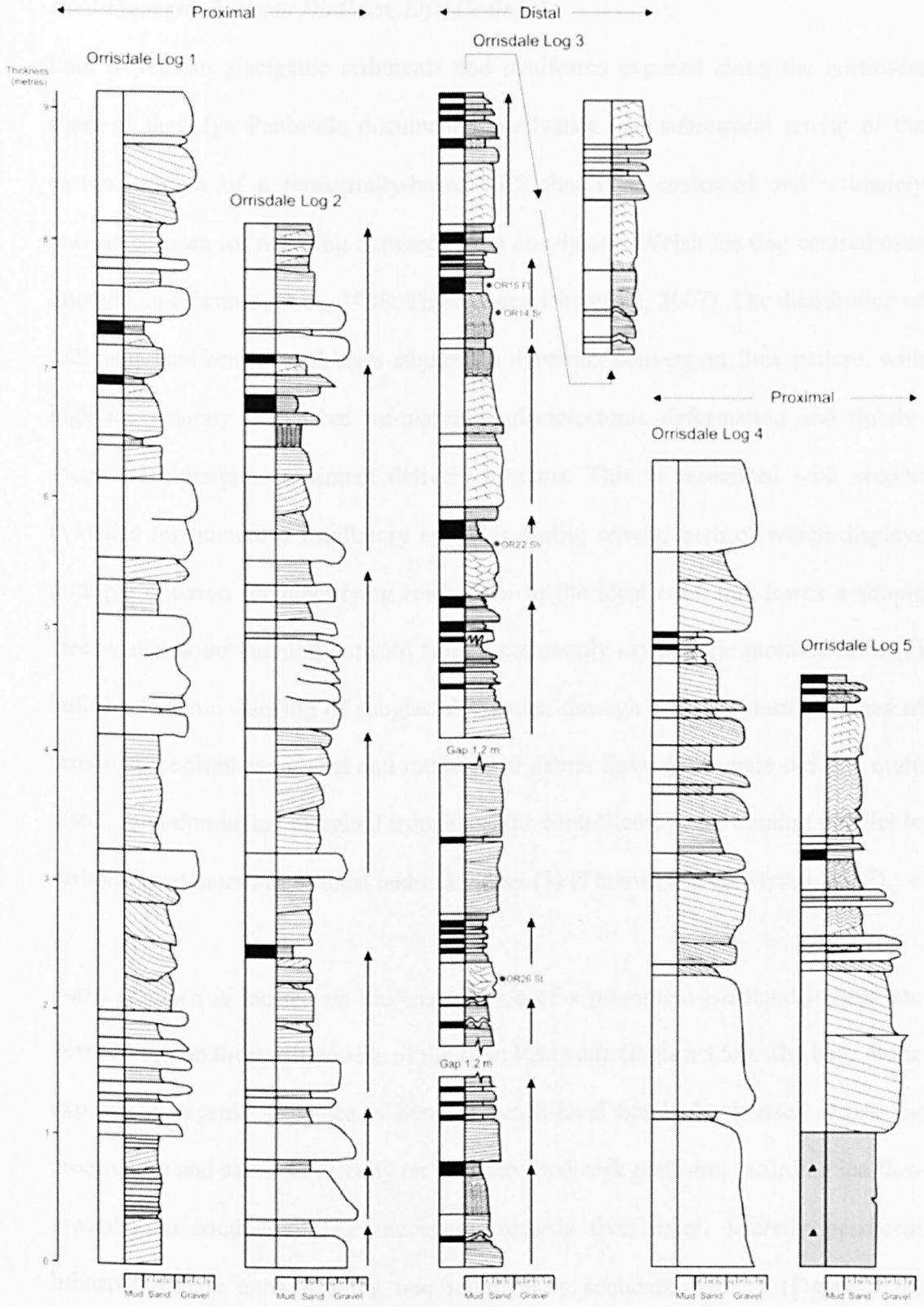

Figure 5.4 *Lithofacies logs showing the vertical stratigraphy through the Bishop's Court Member. Locations of each vertical section are shown in Figure 5.3, x-axis displays grain size. Major fining-up sequences are marked with upwards arrows. Luminescence sampling locations are indicated on Orrisdale Log 3.*

5.3.3 Field site 2; Porth Dinllaen, Llŷn Peninsula

Late Devensian glacigenic sediments and landforms exposed along the northwest coast of the Llŷn Peninsula document the advance and subsequent retreat of the eastern margin of a terrestrially-based ISIS that met, coalesced and ultimately uncoupled from ice radiating outwards from an adjacent Welsh Ice Cap centred over Snowdonia (Thomas, et al., 1998; Thomas and Chiverrell, 2007). The distribution of sediment–landform assemblages suggests a dynamic, convergent flow pattern, with high ice velocity, pervasive ice-marginal glaciotectonic deformation and tightly-focused ice-marginal sediment delivery systems. This is associated with section evidence for numerous oscillatory episodes during retreat, each of which displays multiple criterion for identifying readvance. In the ideal case, this forms a simple three-stage model running outward from a commonly asymmetric moraine form (1) built by tectonic stacking of subglacial diamict, through fronting clastic wedges of proximal ice-front fan gravel and intercalated debris flows (2) to pass out into more distal, sand-dominated marginal trough sandur controlled by and running parallel to earlier retreat moraines or local bedrock ridges (3) (Thomas and Chiverrell, 2007).

Porth Dinllaen is located on the eastern side of a prominent headland jutting into Porth Nefyn on the northern side of the Llŷn Peninsula (Figure 5.5c). The base of the exposed glacigenic sequence is beneath beach-level but bedrock rises across the promontory and sands sit directly on a striated bed-rock platform, recording ice flow towards the southwest. The succession records five major, laterally persistent lithostratigraphic units forming one sedimentary sequence. Unit 1 (Figure 5.5b) overlies bedrock and consists of an upward-fining succession from parallel-laminated and cross- laminated sands into thin, laminated, massive and rippled silts.

It is disconformably overlain by Unit 2, comprising stacked sets of laterally persistent massive pebble gravel and planar and trough cross-stratified granule to pebble gravel. A gradational boundary passes upwards into Unit 3, a thick (~16 m) succession of predominantly parallel laminated sands and thin rippled silts occurring in upward-fining cycles. Unit 4 forms a laterally impersistent sequence of parallel and ripple-laminated fine sands, silts and massive muds. Unit 5 is similar to Unit 1 and sees a return to massive pebble gravel in stacked sets. Palaeocurrent indicators show a consistent flow direction running southwest and are coincident with the ice-movement indications provided by striations.

The sequence is interpreted as recording early passage of Irish Sea ice flowing southwest towards its LGM limit and the contemporaneous subglacial scour of a pre-existing rock headland. No evidence of subglacial diamict associated with this advance is recorded from this site though other, locally-adjacent sections display tectonised Irish Sea Till at the base of the succession do (Thomas and Chiverrell, 2007). The overlying sequence records progressive accumulation in an unconstrained, sand-dominated, lower fan sandur environment, running parallel to the ice-margin towards the WSW, equivalent to stage (3) of the simple model defined above. Accumulation occurred through regular channel avulsion onto sandur surfaces in successive flood events, giving a dominant shallow-water flow that generated widespread rippled sands. Changes in the location of distributary channels after major flood events account for the trough cross-bedded channel gravels and massive and planar cross-bedded gravels in the succession, formed by incision into pre-existing surfaces and the passage of migrating bars. The occurrence of extensive, sometimes thick silt and clay suggests localised ponding of water across large parts

of the sandur surface after major floods and the generation of small lake systems in abandoned parts of the sandur.

5.3.4 Field site 3; Blackwater, Co. Wexford

Thick successions of Late Devensian glacigenic sediment are almost continuously exposed in a 10 km stretch of coastal cliff section running north through the Screen Hills from Blackwater, Co. Wexford (Summers, 1981; Thomas and Summers, 1983; Thomas and Summers, 1984; Thomas and Kerr, 1987; Eyles & McCabe, 1989; Ó Cofaigh and Evans, 2007). The succession (Figure 5.5d) (Thomas and Summers, 1983) passes up from the Macamore Member, a laterally extensive clay-rich diamict equivalent to the Irish Sea Till, seen elsewhere in the basin; through the Knocknasilloge Member, a laterally impersistant sequence of laminated, massive and rippled fine sands, silts and clays, considered to be of lacustrine origin by Thomas and Kerr (1987); disconformably upwards into the Screen Member, a series of distally-thinning clastic wedges showing down-ice passage from gravels into sands. The steep, proximal side of these wedges are formed of distally thinning sheets of Ballinclash Member, a sandy diamict, thrust-over the Screen Member deposits and highly unconformable upon thrust slices of Macamore and Knocknasilloge Member beneath (Thomas and Summers, 1984). The individual wedges of Screen Member sands and gravels record successive ice-marginal still-stand that occurred during deglaciation. Each still-stand was accompanied by override of the ice-contact face of each wedge, resulting in intense glaciotectonism (Thomas and Summers, 1984), accentuation of the resultant ice-marginal moraine form and considerable down-ice compression of the exposed sequence (Thomas and Summers, 1984, Ó Cofaigh and Evans, 2007). In all, nine repeat wedges and associated thrust zones, some

overlapping one another (Thomas and Summers, 1984), have been identified and, together, they represent the first major oscillatory still-stand of the ice stream since retreat from the LGM margin further south. This still-stand may reflect stabilisation of the ice stream as it reached the narrow corridor between the coasts of Wales and southeast Ireland (Ó Cofaigh and Evans, 2007).

Blackwater Quarry is located two kilometres northwest of Blackwater Head (Figure 5.5e), a large tectonised moraine structure that intersects the coast north of Blackwater Harbour. The coastal sections below the headland show, to the rear, a series of thrust planes rising south towards the moraine crest (Figure 5.5d). Each thrust carries-up deformed Macamore Member diamict and associated sand from the roots and is overlain by a thinning, thrust-emplaced sheet of Ballinclash diamict towards the moraine crest. The southernmost thrust marks the ice-contact and immediately in front of it, partially deformed beneath the rising thrust plane, is a large ice-front alluvial fan showing rapid outward passage from stacked sheets of gravel into thinner sheets of sand. The quarry is cut in the outer face of the moraine through a separate but otherwise identical alluvial fan, itself probably forming a set of coalescing fans off the southwest front of the moraine ridge and feeding out onto the floor of a fronting ice-marginal sandur trough (Figure 5.5). The sedimentary succession in the upper part of the quarry is shown in Figure 5.6d. It consists largely of multi-storied sets of upward-fining cycles varying between 0.5 and 2.5 m in thickness, but with the majority averaging less than a metre. Most cycles appear incomplete or truncated but start with either large trough-based gravel channels or laterally persistent massive, sometimes graded, and often large-scale planar cross-bedded gravel bars, scoured into underlying surfaces. These pass rapidly upwards

into planar cross-bedded sands, parallel-laminated sands, trough cross-bedded sands and relatively rare rippled sands and massive and laminated muds. Most of the gravel bars and channels are within outcrop scale and extend laterally for between 30 and 50 m.

The sequence is interpreted as recording the development of a large, relatively high-angled ice-front alluvial fan, fed by a tunnel exit immediately to its rear. Each fining-upward set represents endemic channel switching across the surface of the fan in successive meltwater flood cycles. Each cycle was produced by channel incision into a pre-existing fan surface, followed by deposition of trough cross-stratified channel gravels that pass down-current into massive gravel indicative of migrating bar cores and planar cross-bedded gravels indicative of bar front migration. Bar gravels pass upwards into parallel-laminated sands formed in a variety of sub-environments including bar top, bar margin and channel floor. Parallel laminated sands pass upwards into rippled sands and thence into massive or parallel laminated mud. This fining-upwards passage indicates a vertical accretion sub-environment formed in cut-off channel floors, in shallow scours or in hollows on bar surfaces, either during low flow or by repeated spillage of water across inactive parts of the system.

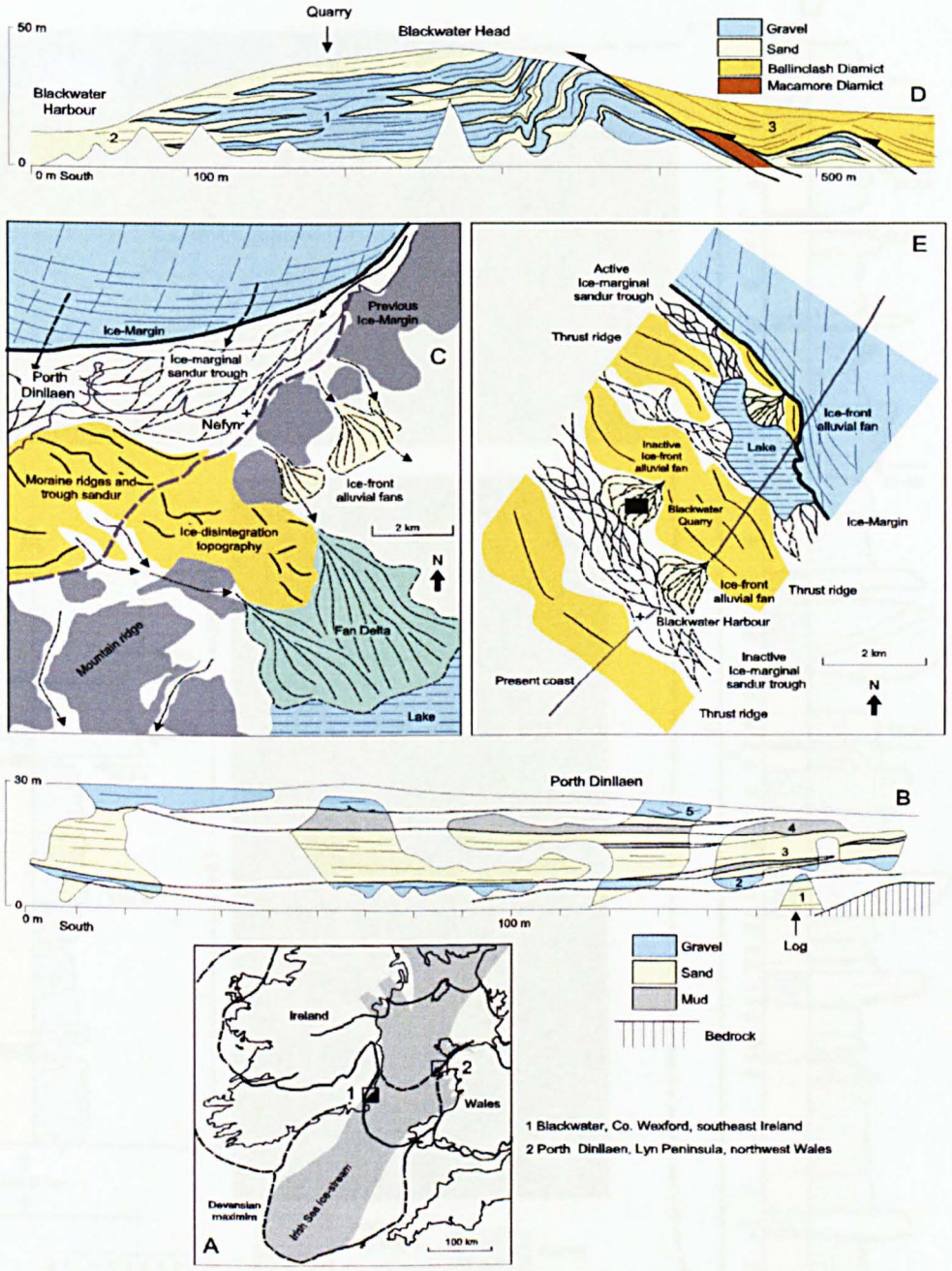

Figure 5.5 *(a) Map of Late Devensian ice limits in the Irish Sea Basin and location of sites examined. Maximum limit after Thomas and Chiverrell (submitted). 1: Blackwater Head, Co, Wexford, Ireland. 2: Porth Dinllaen, Llŷn Peninsula, Wales. (b) Serial section in cliffs at Porth Dinllaen showing location of sampled log profile (after Thomas and Chiverrell, 2007). (c) Cartoon showing palaeogeographical reconstruction of glacial environments around Porth Dinllaen at time of deposition of sediments sampled. (d) Serial sections in cliffs across Blackwater Head (after Thomas and Summers, 1984). Note that quarry is located one kilometre to the rear of the cliff. (e) Cartoon showing palaeogeographic reconstruction of depositional environments around Blackwater at time of deposition of sediments sampled (drafted by GSP Thomas).*

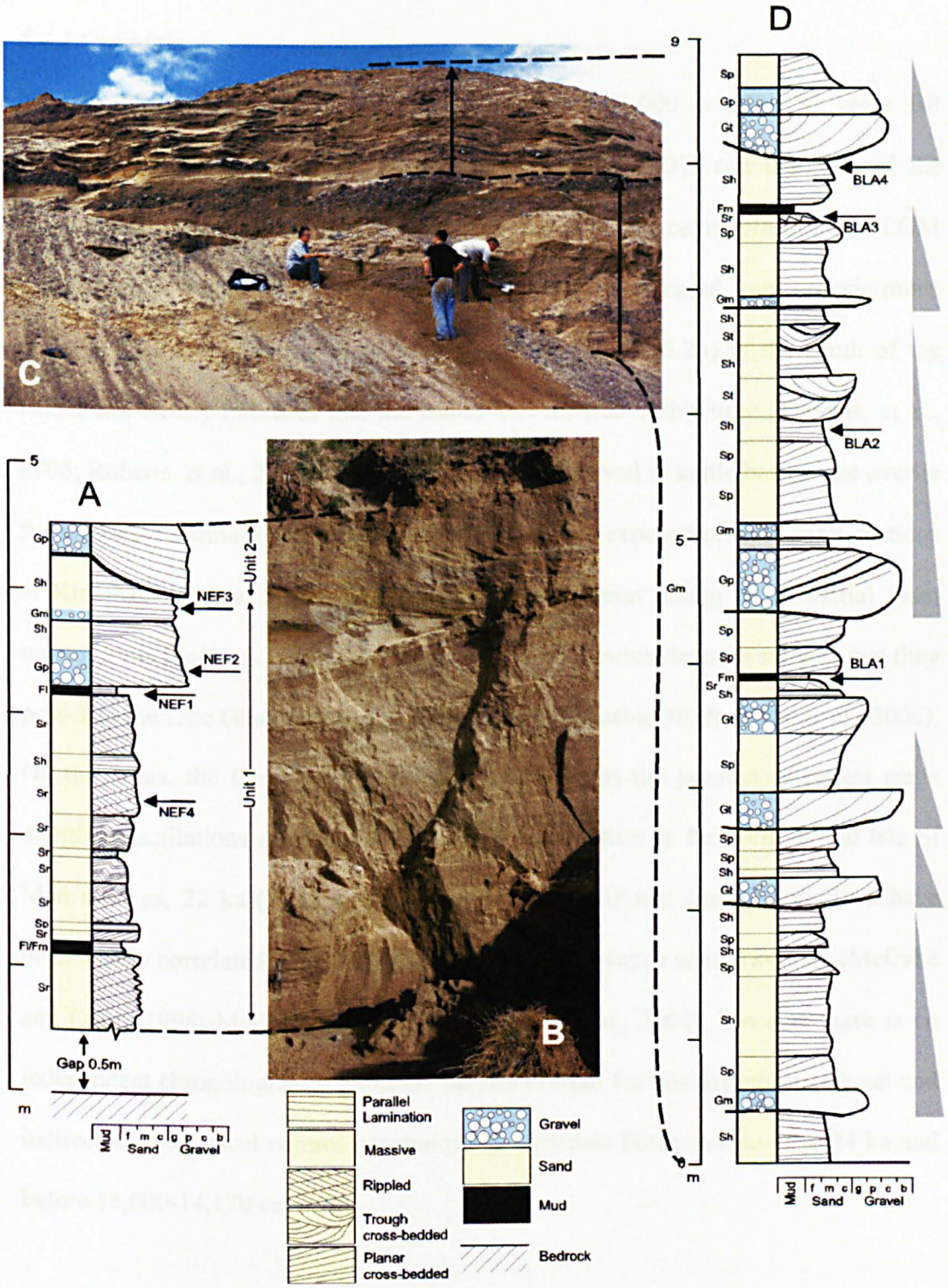

Figure 5.6 *(a) Log profile through Unit 1, Porth Dinllaen, showing location of samples. (b) Photograph of section, Porth Dinllaen. (c) Photographic montage of sections in north wall of quarry at Blackwater showing location of log profile. (d) Log profile showing location of samples, Blackwater Quarry (drafted by GSP Thomas).*

5.4 Existing chronology

5.4.1 Orrisdale

The island was over-ridden at some point after 36,000 ± 670 ^{14}C years BP (uncalibrated) (Thomas, et al., 2006; Roberts, et al., 2007) and the bulk of the glacigenic stratigraphy was lain down during retreat of the ice margin from the LGM limits after 24-21 ka. The above radiocarbon date was obtained from organic muds beneath Shellag Formation diamict at Strandhall (Figure 5.2b) in the south of the island and clearly indicates that the island was ice-free at this time (Thomas, et al., 2006; Roberts, et al., 2007). Organic sediments preserved in kettle basins that overlie the Orrisdale Formation glacigenic sequence and are exposed in west coast sections at Kirk Michael and Jurby (Figure 5.2b). Radiocarbon dating of terrestrial plant macrofossils (*Salix* sp.) from the base of these organic-rich deposits suggest that they post-date the Late Glacial warming at 15,000-14,170 cal-a BP (Roberts, et al., 2006). On this basis, the Orrisdale Formation is regarded as the product of retreat stage marginal oscillations during and after rapid deglaciation as far north as the Isle of Man after ca. 22 ka (Thomas, et al., 2006). Orrisdale and Jurby Formations have been widely correlated with the Heinrich Event 1 readvance at ca. 18-16 ka (McCabe and Clark, 1998; McCabe, et al., 1998; Thomas, et al., 2004); however there is no independent chronological support on the Isle of Man for this hypothesis. Direct and indirect chronological control constrains the Orrisdale Formation to after 24 ka and before 15,000-14,170 cal-a BP.

5.4.2 Porth Dinllaen

There is no direct, previously determined evidence for dating the glacial successions at either Porth Dinllaen or Blackwater. However, radiometric dates from a moss

layer below the Allerød horizon at Glanllynan, some 20 km to the southwest, indicated that the Llŷn Peninsula was ice free by 18,550-16,450 cal. a BP (Coope, et al., 1971) and Thomas and Summers (1983) believed the Screen Hills readvance event, some 150 km southwest in flowline distance, to have occurred around ~18 ka.

Cosmogenic ^{10}Be dates from the Wicklow Mountains (Ballantyne, et al., 2006), eastern Ireland, situated on the western margin of the ISIS enable us to constrain the chronology for the retreat of the ISIS. The Wicklow Mountains, ~70 km to the north of Wexford, were thought to have supported an independent ice cap (Warren, 1993) and to have been completely encircled by thick, converging ice masses from the Irish Midlands and the Irish Sea Basin (the ISIS) during the MIS 2 maximum. This convergence means that retreat of the ISIS to its position off-coast of the Wicklows may have coincided with the subsequent shrinkage and retreat of the Wicklow ice dome. The ^{10}Be dates from palaeonunataks, above the maximum height of the Wicklow ice dome give ages of 46.9 ± 3.0 ka and 95.9 ± 6.1 ka, compared to samples taken from summits thought to have been overrun by warm-based ice during extension to LGM limits which gave cosmogenic ^{10}Be ages of 18.2 ± 1.2, 18.5 ± 1.2 and 19.1 ± 1.2 ka (Ballantyne, et al., 2006). These ages are thought to reflect the emergence of actively glaciated summits from under a cover of erosive warm-based ice and are in agreement with those of Bowen et al. (2002). The ^{10}Be ages from the Wicklows may also reflect retreat and shrinkage of the ISIS off-coast of this location at the same time period. The deglaciation of the Wicklows which are at almost the same latitude as Porth Dinllaen, on the eastern margin of the ISIS, constrains the timing of ISIS retreat at Porth Dinllaen to approximately the same time period (~21-17 ka).

5.4.3 Blackwater

Ó Cofaigh and Evans (2007) collected samples of single shell fragments from the Irish Sea Till (Macamore Member) from sites along the south coast of Ireland for AMS radiocarbon dating. Six ages ranging between 28,072-23,931 cal. a BP (2σ range) demonstrated that the last advance of the ISIS, which deposited the Irish Sea Till along the southeast and south coast of Ireland and in the Scilly Isles, reached its overall maximum southern limit after this. The three youngest ages constrain the precise timing of this advance to after 24,410-23,931 cal. a BP (Ó Cofaigh and Evans, 2007). This interpretation is supported by a radiocarbon age of 27,948-23,612 cal. a BP from organic sediments below the Scilly Member, the stratigraphic correlative of the Irish Sea Till, on the Scilly Isles (Scourse, et al., 1991; Hiemstra, et al., 2006). Subsequent northwards retreat of the ice-stream seems to have been rapid, as suggested by the absence of thick deglacial depocentres recording pinning of the ice stream along the south coast of Ireland. This contrasts with sites further north such as the Screen Hills, where major deglacial sediment accumulations mark still-stand and oscillations of the ice stream margin during overall recession (Thomas and Summers, 1983; McCabe, 1987; Evans and Ó Cofaigh, 2003a; Thomas, et al., 2004). These first major still-stands reflect stabilisation of the ice stream as it reached the narrow corridor between the coasts of Wales and SE Ireland (Ó Cofaigh and Evans, 2007). The glacigenic sediments at Blackwater, including the Screen Member which overlies the Irish Sea till dated by Ó Cofaigh and Evans (2007), are hypothesised to represent terrestrial deposition soon after ~23 cal. a BP, but have not been directly dated. This location offers the potential for securing a chronology for retreat of the ISIS from LGM limits via optical dating of these sediments.

5.5 Field and laboratory methodology

5.5.1 Lithofacies logs and field sampling

The sections at Orrisdale, Porth Dinllaen and Blackwater have been described in some detail (e.g. Thomas and Summers, 1982; 1983; 1984; Thomas, et al., 1985; Thomas and Kerr, 1987; Thomas, et al., 1998; Thomas and Chiverrell, 2003; Thomas, et al., 2004; Thomas, et al., 2006; Thomas and Chiverrell, 2007), and serial stratigraphical sections therein were used as a template to locate appropriate sampling areas (e.g. Figure 5.3). The sequences encountered during field sampling were broadly similar in character to these earlier mapping of the exposures.

Lithofacies- and AEA-based approaches underpinned the sampling methodology for optical dating, with a series of vertical profiles logged, recording grain size, lithofacies and facies architecture. Sampling locations were identified in the deposits of both ice-distal and -proximal palaeo-sandur, discerned using lithofacies assemblages and grain size (Thomas, et al., 1985). These vertical logs (Figure 5.4; Orrisdale, 5.6a; Porth Dinllaen & 5.6d; Wexford) were used to identify appropriate sites for luminescence sampling, targeting a range of lithofacies and interpreted depositional environments. We employed a comprehensive approach, sampling the full range of lithofacies to assess differences in bleaching of the OSL between depositional environments.

Samples of sediment for luminescence analysis were collected by hammering opaque PVC cylinders (7 x 30cm) into the cleaned vertical exposures until they were completely filled with sediment. Upon extrusion from the cliff-face, these cylinders were sealed using thick duct tape. Samples used for optical dating at each field site

are shown in Figures 5.4, 5.6a and 5.6d. The sequence at Orrisdale (Figure 5.4) displays, in parts, what appear to be a series of complete fining-up cycles from bar core (*Gm/Gp*) through to finely-laminated bar-top deposits (*Fl*), elsewhere these cycles are truncated by erosive contacts. In all probability the sequence reflects a series of temporally disconnected events, with more gap than record. Variable preservation appears to have affected and restricted the occurrence of finer grained lithofacies.

At Porth Dinllaen, a shallow-water rippled-sand (*Sr*) lithofacies was targeted for OSL dating (NEF4, Figure 5.6a & b). This *Sr* lithofacies is thought to be deposited in a shallow-water overbank or bar-top environment under declining flow conditions. A finer, overlying mud drape layer was also sampled (NEF1) however, the layer was too thin and insufficient quartz was recovered for luminescence dating.

At Wexford, samples BLA1 (*Fl*) and BLA3 (*Sr*) were used for optical dating purposes (Figure 5.6d). BLA1 forms part of a fining-up sequence (*Gt* → *Sh* → *Sr* → *Fl*) in a back-bar or bar-top slack-water environment, where finer grains potentially have been allowed to settle out of suspension under shallow and waning flow. This sequence was also targeted as it is hoped that the back-bar environment may have been subaerially exposed during declining flows, enabling satisfactory bleaching of quartz grains. Sample BLA3 forms part of a fining-up sequence but this sample is a bar-top, rippled sand (*Sr*) lithofacies thought to be deposited during declining flow. The *Sr* lithofacies indicates that although water is still flowing, it is shallow enough for friction with the surface to cause the formation of shallow-water ripples.

5.5.2 Laboratory methodology

5.5.2.1 Dose-rate measurement

A bulk sample of material was used for dose-rate determination. Radioisotopes of K, U and Th were measured using high-resolution, low-level gamma spectrometry. Samples were packed into air-tight plastic containers and stored for around three weeks in order to achieve secular equilibrium between ^{226}Ra and ^{222}Rn. Dose-rate conversion factors (Adamiec and Aitken, 1998) were used to convert concentrations (ppm) into annual dose rates (Gy/ka). Due to both rapid sediment accumulation during the period of deposition and the depth of sampling locations beneath the present day land surface (>20 metres) the contribution of cosmic radiation (Prescott and Hutton, 1994) is minimal (0.0281 ± 0.0014 Gy/ka) but can contribute a larger proportion of total dose-rate to particularly low-activity samples. Temporal variation in water content is thought to be minimal as the sediments are free-draining sand and gravel. Present day water content was used to calculate beta attenuation due to moisture content. To account for possible post-depositional variations in water content an average water content error of ± 5% was assumed for the samples. Values for dose-rate (Gy/ka) are shown in Table 3.2. Values for radionuclide activities (^{238}U, ^{226}Ra and ^{210}Pb) overlapped within 2σ suggesting that radioactive disequilibrium in the ^{238}U decay chain was not an issue in these samples (see Chapter 3 for details).

5.5.2.2 OSL sample preparation and measurements

The OSL samples were extruded under subdued yellow or red laboratory light and then wet sieved and treated with 30% H_2O_2 and 30% HCl to remove organic matter and carbonates respectively and subsequently immersed in heavy liquids (specific gravity 2.76 g/cm^3 and 2.62 g/cm^3) to achieve a mono-mineralic sample of quartz.

The quartz samples were etched with 48% HF for 40 minutes to remove any remaining feldspars and the outer part of the quartz grains affected by alpha irradiation. Fine sand grains (>90 μm) were mounted onto 9 mm diameter stainless steel discs using silicone oil. A circular area of ca. 0.5 mm diameter was covered with silicone oil and the quartz grains were mounted, ensuring a monolayer of grains covered the area. Typically, the discs contain ca. 30 quartz grains, for a grain size range of 90-125 μm; for coarser grain sizes (150-180 μm, 180-200 μm, 200-250 μm) the area covered by quartz grains was increased appropriately to ensure ~30 grains were present.

All luminescence measurements were performed using automated Risø DA-15 readers, equipped with diodes emitting 470Δ30 nm and an EMI 9235QB photomultiplier. The optical stimulation units delivered ~30 mW cm^{-2} at 90% power. The OSL and signal depletion measurements were carried out at 125°C to prevent retrapping of charge in the trap corresponding to the 110°C TL peak (Murray and Wintle, 1998; Wintle and Murray, 2000). The optical stimulation time used for all the OSL measurements was 40 seconds. The sensitivity-corrected regenerated (L_x) and test dose (T_x) values were derived from the OSL signal counts obtained from the initial 0.8 seconds of the OSL decay curves, minus a background estimate obtained in the last 8 seconds consisting of instrument 'noise' and any remaining slower bleaching signal components.

5.5.3 Quartz characterisation

Glaciofluvial sediments typically pose two significant problems for OSL dating; *poor quartz OSL characteristics* and *poor bleaching*. Poor quartz luminescence

characteristics may arise from the freshly eroded nature of sediments resulting in poor quartz luminescence sensitivity. Low luminescence sensitivity in quartz from glacially-derived sediments has been reported in other studies (Rhodes and Pownall, 1994; Richards, 2000; Spencer and Owen, 2004; Lukas, et al., 2007) and has been attributed to either a fresh bedrock source, a lack of subaerial weathering of the grains (Rhodes and Pownall, 1994) or an insufficient number of bleaching and dosing cycles due to the proximity of the depositional setting to the quartz provenance. Quartz in the sandur sediments at Orrisdale, Porth Dinllaen and Wexford may have acquired luminescence sensitivity during cycles of aeolian and fluvial transport and deposition in Permo-Triassic desert environments as suggested by their bedrock provenance (see Chapter 4, Section 4.4.4) (Jackson, et al., 1995). Nevertheless in settings like formerly glaciated environments, a luminescence dating approach should include characterisation of quartz OSL, details of which are outlined in Chapter 4.

A series of experiments were carried out to ensure the application of the most appropriate Single-Aliquot Regenerative-Dose (SAR) protocol to the samples and to confirm that a fast component (optical dating signal) was both present and *dominant* within the quartz. First, the appropriate preheat temperature for this quartz was investigated via a preheat-dose recovery test (details of which are given in Chapter 4, Section 4.2.5). This allowed the effect of thermal treatment upon D_e to be assessed independently of variations in the natural D_e which are often attributed to heterogeneous bleaching. Secondly, confirmation that the SAR protocol was targeting a dominant 'fast' component was obtained (Murray and Wintle, 2000) via

LM-OSL and CW-OSL decay curve fitting (details given in Chapter 4, Section 4.3.4).

5.5.4 D_e determination

5.5.4.1 The SAR protocol

The standard SAR protocol of Murray and Wintle (2000) was used for D_e determination of small aliquots. The regenerative doses were selected to cover the saturating exponential growth of luminescence with given dose as preliminary measurements of varying sized aliquots indicated that the true D_e lay within this range. Appendix B shows dose-response curves for each of the samples, indicating the range of regenerative doses used and the interpolation method used for burial dose estimation. A high test dose (~19 Gy) was applied to all samples due to the inherently poor luminescence sensitivity of quartz which required this high dose to give a measureable test dose signal and ensure good counting statistics. This test dose was followed by a cutheat of 200°C.

Aliquots were rejected if the criteria for both low and high repeat-point recycling ratios (1.0 ± 10%; *recycling ratio must overlap this range within 1σ errors*) and thermal transfer (<5% of the natural signal) were not met (Murray and Wintle, 2000). An OSL-IR depletion ratio of below one was taken as indicative of feldspar contamination and an acceptance criterion of 1.0 ± 10% was applied (*OSL-IR depletion ratio must overlap this range within 1σ errors*) (Duller, 2003). Additionally, if the dose-response was not described by a single saturating exponential function, the aliquot was also rejected. Aliquots containing quartz that had no natural signal and had a 'weak' fast component or dominant 'medium'

component were also rejected. This was done by simple visual analysis of OSL decay curves; those aliquots containing quartz with a dominant medium component showed a characteristically slower decay in luminescence intensity with time (the OSL signal did not reach background level until after 10 seconds of blue LED stimulation at 90% of total power) and were rejected. Of the aliquots that were rejected, the vast majority (~70%) were rejected in the first place due to the absence of a natural OSL signal. Overall, only ~25% of aliquots that were measured satisfied *all* of the criteria for acceptance.

5.5.4.2 Constructing a 'representative' population of aliquots

In general, the analysis of heterogeneously-bleached samples requires measurement of a greater number of aliquots than for well-bleached sediments to ensure that well-bleached aliquots are present and to produce a representative D_e distribution. To determine the minimum number of values required to characterise a particular D_e distribution the 64 D_e values obtained for sample OR14 (200-250 μm) were analysed. This sample shows evidence of heterogeneous bleaching both in the shape of its distribution (weighted skewness value of 1.6) and overdispersion of 53%. The overdispersion parameter can be described as the spread in a distribution that is in addition to the spread accounted for by the errors on individual D_e values (Galbraith, et al., 1999).

Following the method of Rodnight (2006), 20 random sub-samples of 5, 10, 15, 20, 30, 40, 50 and 60 D_e values were generated (from the original data set of 64 D_e values), and each was tested for normality using the Shapiro-Wilks test (Shapiro and Wilk, 1965). Sample OR14 (200-250 μm) required at least *40* D_e values to obtain a

dataset for all 20 sub-samples that was statistically non-normal. Therefore in this research, at least 50 D_e's were obtained per sample. This required the measurement of large numbers of small aliquots (see Table 5.1), as the majority of aliquots were rejected due to the lack of a natural OSL signal. During subsequent measurement runs, the Risø machines were stopped once natural signals had been measured to allow screening of the natural signals to be undertaken. This was to ensure that the remainder of the SAR protocol was only applied to those aliquots containing quartz with a natural signal and so reducing wasted measurement time. Dose-response curves were therefore only generated for aliquots which displayed a natural signal (see Appendix A and B).

In total, ~250 aliquots needed to be measured per sample, to ensure that at least 50 were finally accepted once all rejection criteria had been applied. Each measurement run of 24 aliquots (measuring at least 6 regenerative dose points, up to a maximum of ~190 Gy) took at least 4 days. However, measurement time was significantly reduced once aliquots displaying no natural signal were rejected.

5.5.4.3 Statistical 'age' models and decision-protocols

Empirical studies of fluvial and glaciofluvial sediments (Murray, et al., 1995; Olley, et al., 1998; Olley, et al., 1999; Lepper, et al., 2000; Olley, et al., 2004; Rodnight, 2006) have reported evidence of asymmetric equivalent dose (D_e) distributions based on single-aliquot and single-grain approaches, where the larger D_e values are attributed to the presence of poorly-bleached grains in the sample. Several schemes have been published which address the problem of deriving a single-value estimate of the burial dose from such positively skewed and overdispersed D_e distributions.

Those listed below have been use to deal with heterogeneously-bleached sediments by other authors (e.g. Olley, et al., 1998; Bailey and Arnold, 2006; Duller, 2006; Rodnight, et al., 2006).

1. *The Minimum Age Model (MAM)* of Galbraith et al. (1999), both the three and four parameter versions (MAM-3 and MAM-4, respectively) state that the distribution of D_e values is approximated by a truncated log-normal distribution, with the truncation point giving the estimate of palaeodose. Via this method, the MAMs attempt to define the minimum D_e acquired by the fully bleached proportion of grains.

2. *The mean of the lowest 5%* (L5%) of D_e values (Olley, et al., 1998) was used upon partially bleached fluvial samples from Australia. By calculating the mean of the lowest 5% of D_e values, Olley et al. (1998) found that burial ages generally increased with depth. In this method, the lowest 5% of aliquots are therefore expected to represent the well-bleached portion of the sample.

The decision protocol of Bailey and Arnold (2006) (Figure 5.7) enables a robust statistically-informed choice to be made as to which 'age' model is the most appropriate for a particular shaped D_e distribution. These protocols were derived for a set of real and modelled D_e distributions from fluvial samples using overdispersion, weighted skewness and kurtosis to characterise the D_e distribution (for further detail see Bailey and Arnold, 2006). This decision process was then tested on empirical data (Arnold, et al., 2007) for samples for which there was independent age control (Bailey and Arnold, 2006). Appropriate 'age' models can now be selected on an

independent basis for statistical reasons, rather than selecting the 'age' model that suits, largely governed by the resulting age output.

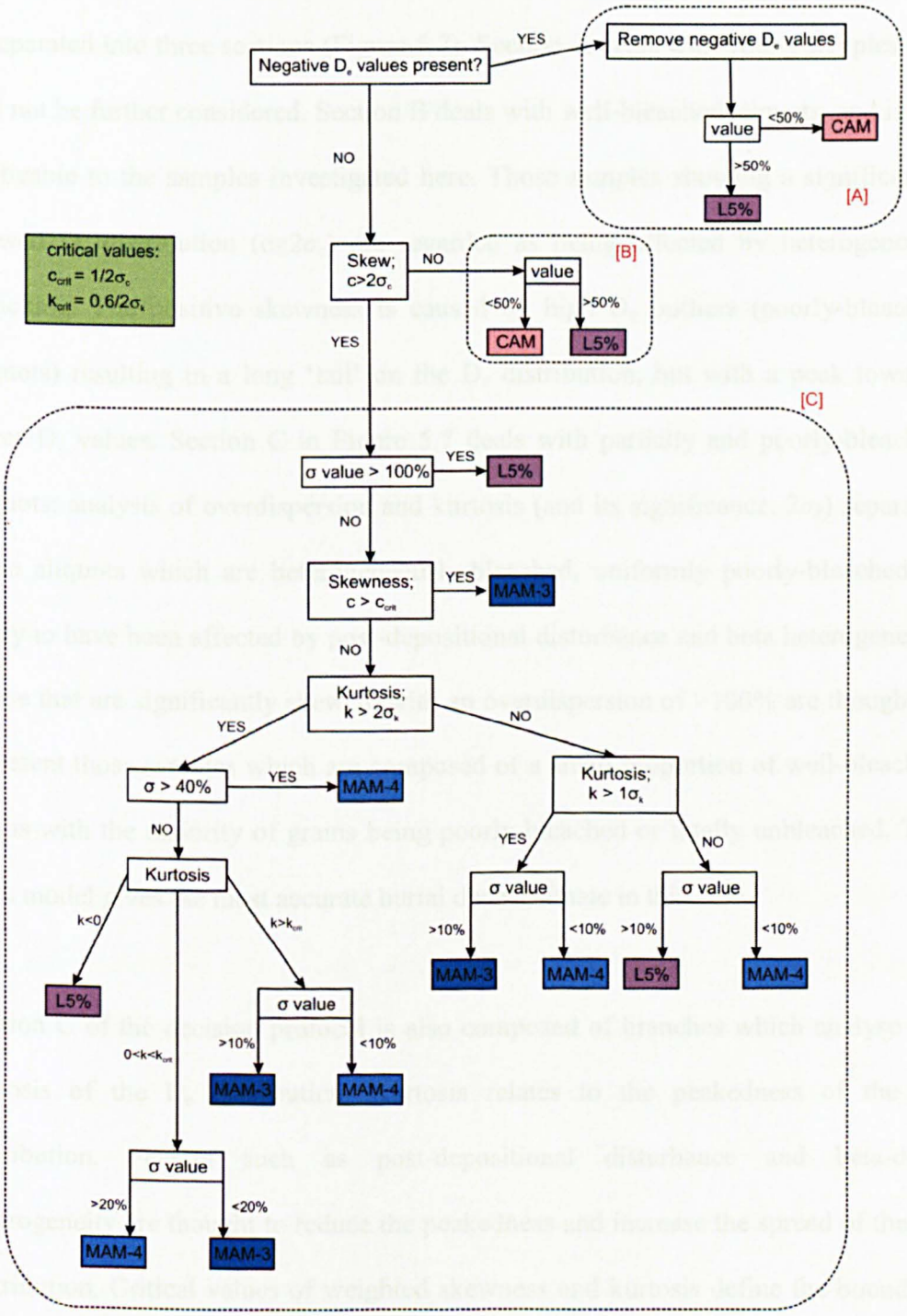

Figure 5.7 *The decision protocol of Bailey and Arnold, 2006. Critical values were derived from Arnold (2006).*

The robust application of independent decision-protocols (Bailey and Arnold, 2006) is imperative for analysis of D_e distributions resulting from heterogeneous bleaching to select appropriate 'age' models. The decision protocol of Bailey & Arnold (2006) is separated into three sections (Figure 5.7). Section A deals with young samples and will not be further considered. Section B deals with well-bleached aliquots, and is not applicable to the samples investigated here. Those samples showing a significantly skewed D_e distribution ($c>2\sigma_c$) are regarded as being affected by heterogeneous bleaching. The positive skewness is caused by high D_e outliers (poorly-bleached aliquots) resulting in a long 'tail' on the D_e distribution, but with a peak towards lower D_e values. Section C in Figure 5.7 deals with partially and poorly-bleached aliquots; analysis of overdispersion and kurtosis (and its significance; $2\sigma_k$) separates those aliquots which are heterogeneously-bleached, uniformly poorly-bleached or likely to have been affected by post-depositional disturbance and beta heterogeneity. Those that are significantly skewed, with an overdispersion of >100% are thought to represent those samples which are composed of a small proportion of well-bleached grains with the majority of grains being poorly-bleached or totally unbleached. The L5% model gives the most accurate burial dose estimate in this case.

Section C of the decision protocol is also composed of branches which analyse the kurtosis of the D_e distribution. Kurtosis relates to the peakedness of the D_e distribution. Factors such as post-depositional disturbance and beta-dose heterogeneity are thought to reduce the peakedness and increase the spread of the D_e distribution. Critical values of weighted skewness and kurtosis define the boundary between selection of the MAM-3 and MAM-4 estimates. In such cases, lower kurtosis values indicate a lack of peakedness (platykurtic) and the MAM-3 model is

most appropriate, as this model usually gives higher D_e estimates than L5% and MAM-4.

The decision-protocol of Bailey and Arnold (2006) was tested to ascertain if it is appropriate for the Orrisdale, Porth Dinllaen, and Wexford samples and to evaluate which statistical 'age' model should be used for each of these samples. To run the decision protocol, weighted skewness (c), kurtosis (k) and overdispersion (σ) were calculated for each D_e distribution (Table 5.1) (Arnold, 2006; Bailey and Arnold, 2006). An approximate test of the statistical significance of c and k was made using the 'standard error of skewness/kurtosis', here σ_c and σ_k, respectively (Tabachnick and Fidell, 1996; Bailey and Arnold, 2006). D_e distributions with c or k values greater than twice the standard error ($2\sigma_c/2\sigma_k$) were regarded as statistically significant. Critical values for c_{crit} ($1/2\sigma_c$) and k_{crit} ($0.6/2\sigma_k$) have been calculated as described by Arnold (2006).

5.6 Results

5.6.1 D_e distributions and age calculation

D_e distributions were plotted as probability histograms (the sum of all the bars on each plot is equal to one) as shown in Figures 5.8 and 5.9 and the bin widths were calculated as the median error of the D_e values for each sample. Inspection of these histograms and radial plots (Figure 5.10) shows that the D_e distributions for all Orrisdale samples are skewed. Table 5.1 lists the statistical parameters necessary for the decision protocol of Bailey and Arnold (2006) to be applied. The weighted skewness values for all the Orrisdale D_e distributions show significant ($>2\sigma_c$) positive skewness and overdispersion values of >39%. Such positive skewness and

high overdispersion values are characteristic of heterogeneously-bleached sediments (Olley, et al., 1999).

The results of applying the decision protocol are given in Table 5.1. For all of the Orrisdale samples, the protocol recommends the application of the MAM-3 for D_e determination and in combination with the environmental dose-rate data (Table 5.1) produced ages in the range of 25.9-14.1 ka (Table 5.1). The ages calculated for the *Sh*, *Sr* and *Fl* lithofacies (samples OR22, OR14 and OR15 respectively) are all in agreement with each other (within 2σ errors). However, the age calculated for the *St* lithofacies is ~10 ka older than the other samples, perhaps indicative of poor bleaching and a resulting age overestimation.

For three of the Wexford and one of the Porth Dinllaen samples (BLA1; 90-125 μm and 180-212 μm, BLA3; 212-250 μm and NEF4; 90-125 μm) the decision protocol recommended the application of MAM-3 whereas for BLA3; 90-125 μm the L5% model was recommended. Resulting age calculations in the range 38-23 ka were obtained for Wexford samples by using the age model as suggested by the decision protocol (Table 5.1). An age of 21.3 ± 2.6 was obtained for the Porth Dinllaen sample by using the MAM-3 as recommended by the decision protocol.

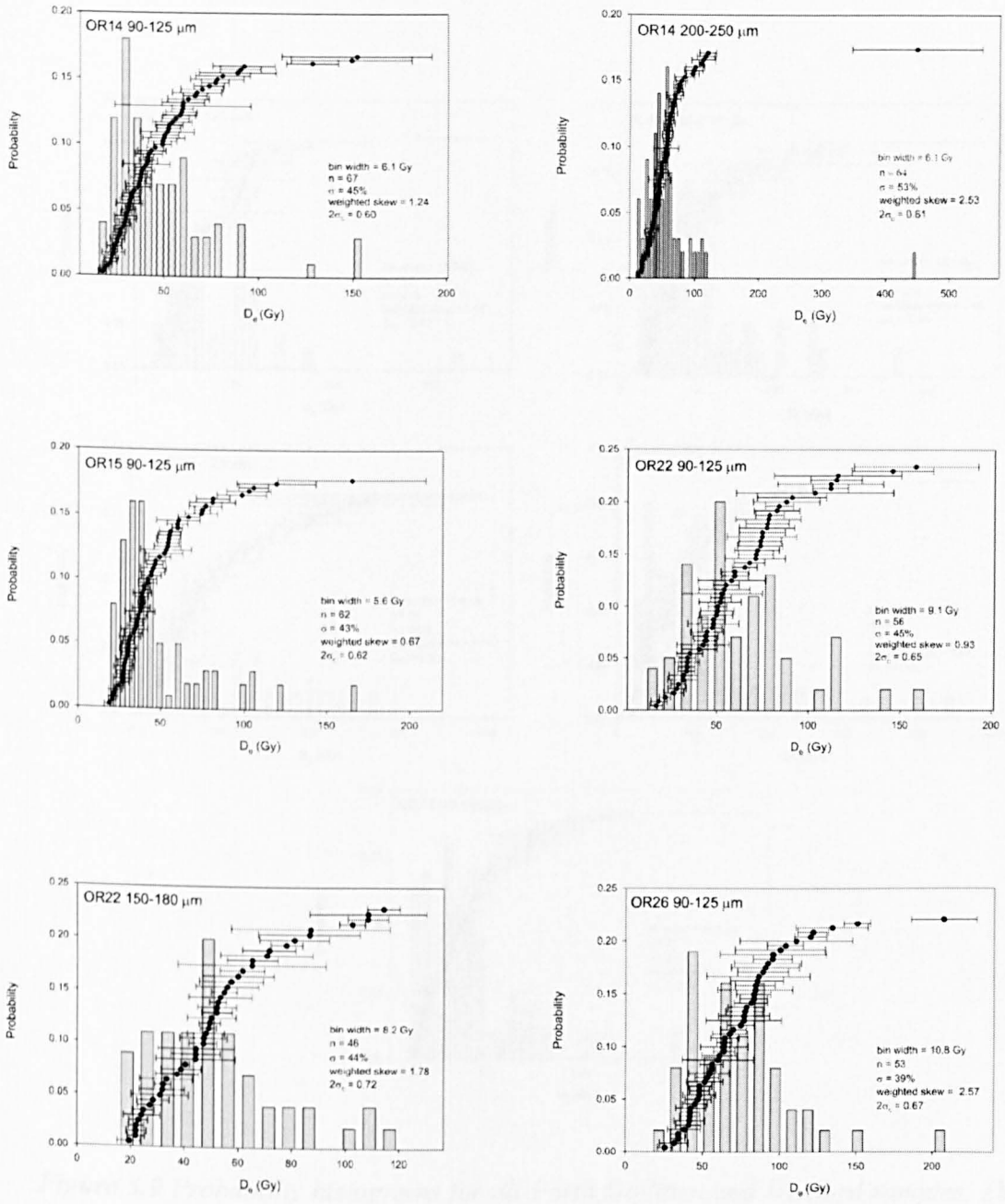

Figure 5.8 *Probability histograms for all Orrisdale samples. Overdispersion (σ), weighted skew and the weighted skewness significance values ($2\sigma_c$) are listed. If weighted skew is greater than the $2\sigma_c$ then the sample D_e distribution is significantly skewed. Bin widths are also listed and calculated as the median error on each of the D_e values within the distribution.*

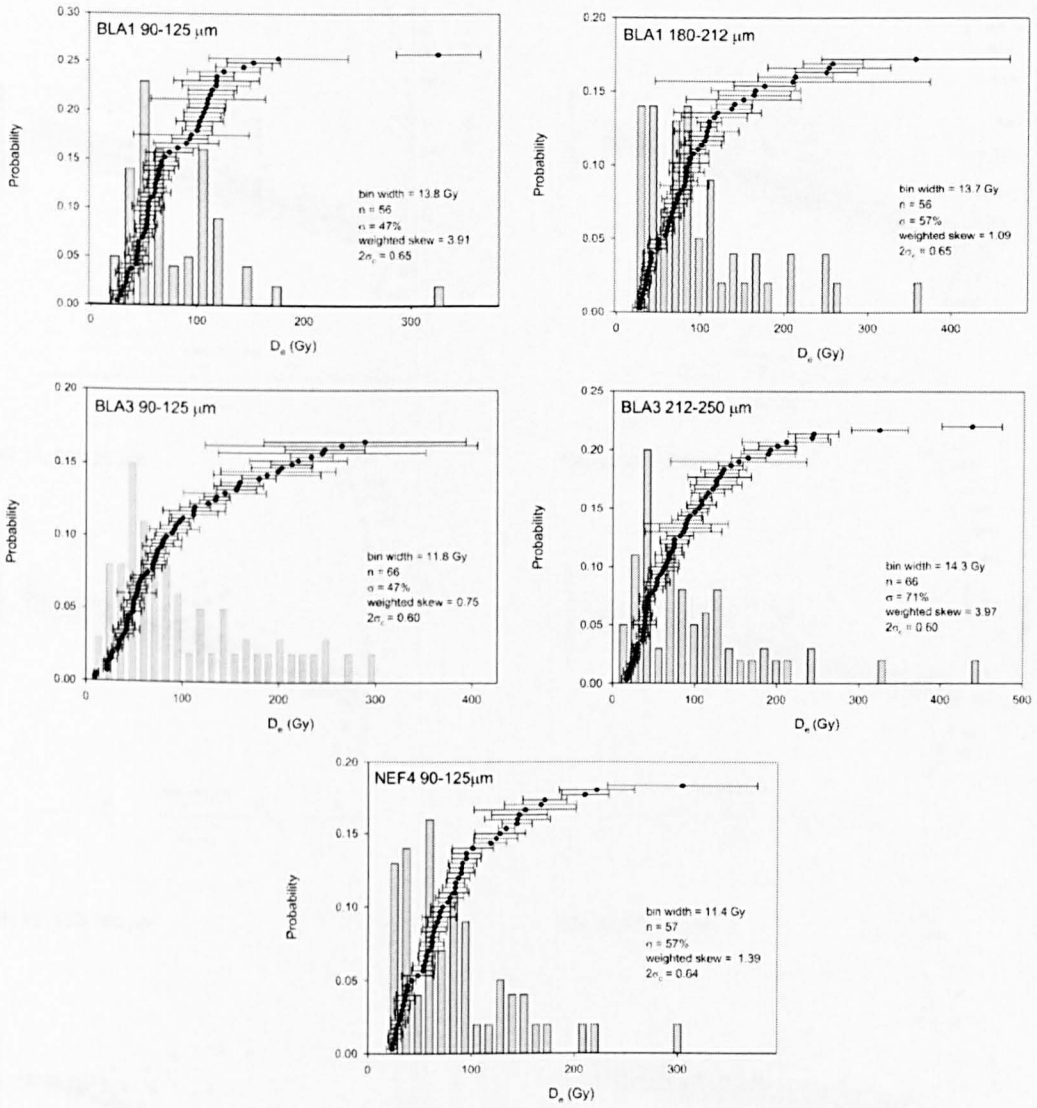

Figure 5.9 *Probability histograms for all Porth Dinllaen and Wexford samples. The number of D_e values (n), overdispersion (σ), weighted skew and weighted skewness significance values ($2\sigma_c$) are listed. If weighted skew is greater than the $2\sigma_c$ significance value, then the sample D_e distribution can be described as significantly skewed.*

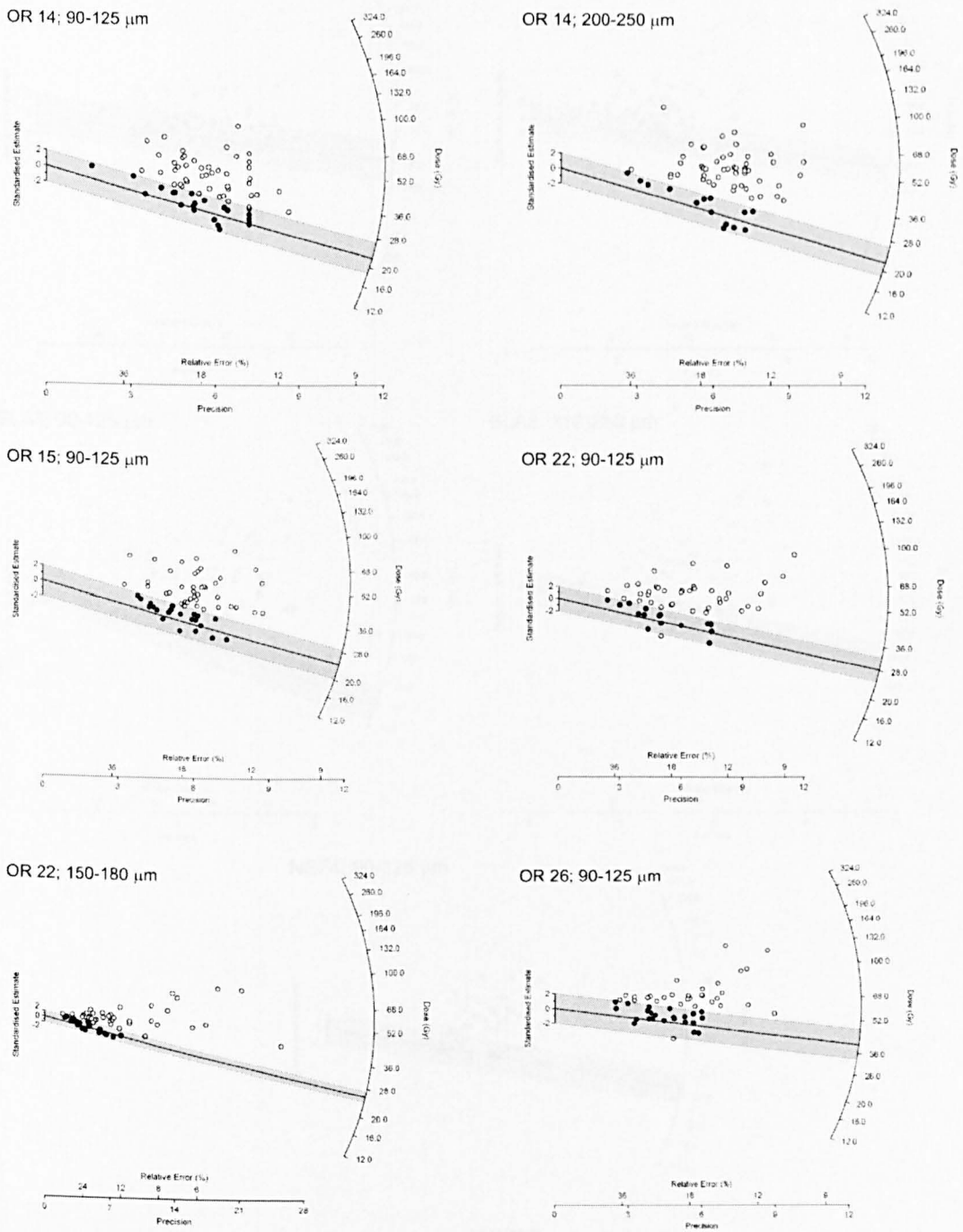

Figure 5.10 *Radial plots for all Orrisdale samples. The 2σ shaded area is centred on the D_e calculated following the age model suggested using the decision protocol of Bailey and Arnold (2006).*

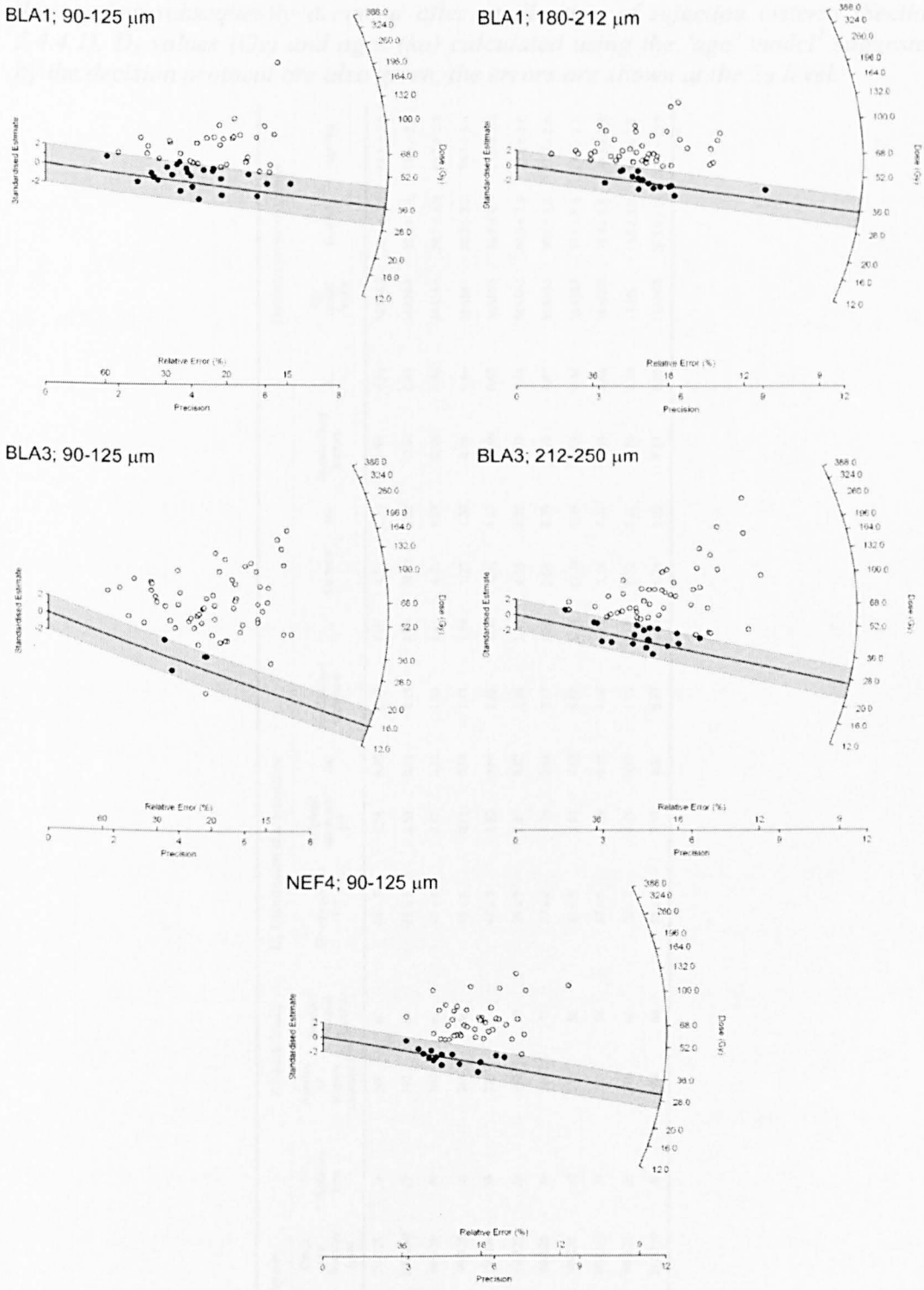

Figure 5.11 *Radial plots for all Porth Dinllaen and Wexford samples. The 2σ shaded area is centred on the D_e calculated using the 'age' model as recommended by the decision protocol of Bailey and Arnold (2006).*

Table 5.1 *Statistical parameters calculated for use during the decision protocol of Bailey and Arnold (2006) with details concerning number of aliquots measured and the number subsequently accepted after application of rejection criteria (Section 5.4.4.1). D_e values (Gy) and ages (ka) calculated using the 'age' model[2] suggested by the decision protocol are also given, the errors are shown at the 2σ level.*

Sample details			Aliquot details		D_e Distribution characteristics									Decision protocol results		
Sample number	Grain size fraction (μm)	Lithofacies type	Number of aliquots measured	Number of valid D_e values	Overdispersion (σ)	Weighted skewness (ε)	$2\sigma_\varepsilon$	Standardised skewness	ε_{crit}	Kurtosis	$2\sigma_k$	Standardised kurtosis	k_{crit}	Age model chosen	D_e (Gy)	Age (ka)
OR14	90-125	*Sr*	240	67	46 ± 5	1.24	0.60	2.07	1.67	4.29	1.20	3.58	0.50	MAM-3	22.4 ± 1.6	14.1 ± 2.6
OR14	200-250	*Sr*	192	64	51 ± 5	2.53	0.61	4.15	1.64	40.03	1.22	32.81	0.49	MAM-3	22.2 ± 3.4	14.4 ± 2.5
OR15	90-125	*Fl*	240	62	43 ± 4	0.67	0.62	1.08	1.61	4.45	1.24	3.59	0.48	MAM-3	24.2 ± 3.8	14.2 ± 2.5
OR22	90-125	*Sh*	264	56	45 ± 5	0.93	0.65	1.43	1.54	1.27	1.30	0.98	0.46	MAM-3	28.3 ± 5.3	16.4 ± 3.4
OR22	150-180	*Sh*	336	59	46 ± 5	1.52	0.64	2.38	1.56	-0.11	1.27	-0.09	0.47	MAM-3	25.5 ± 4.5	15.0 ± 2.9
OR26	90-125	*St*	192	53	39 ± 5	2.57	0.67	3.84	1.49	4.15	1.35	3.07	0.44	MAM-3	40.0 ± 7.3	25.9 ± 5.0
NEF 4	90-125	*Sr*	168	57	57 ± 6	1.39	0.64	2.17	1.56	3.81	1.29	2.95	0.47	MAM-3	30.4 ± 3.2	21.3 ± 2.6
BLA1	90-125	*Fl*	240	56	47 ± 5	3.91	0.65	6.02	1.54	11.24	1.30	8.65	0.46	MAM-3	37.1 ± 8.8	37.7 ± 9.1
BLA1	180-212	*Fl*	288	56	57 ± 6	1.09	0.65	1.68	1.54	3.18	1.30	2.45	0.46	MAM-3	35.4 ± 6.8	36.8 ± 7.2
BLA3	90-125	*Sr*	216	66	73 ± 7	0.75	0.60	1.25	1.67	0.32	1.21	0.26	0.50	L5%	15.8 ± 1.6	23.6 ± 2.5
BLA3	212-250	*Sr*	288	66	71 ± 7	3.97	0.60	6.62	1.67	6.26	1.21	5.17	0.50	MAM-3	26.5 ± 10.1	40.9 ± 15.8

[2] For samples BLA1 (90-125 μm and 180-212 μm) and BLA3 (212-250 μm) the L5% model was also applied, giving D_e values of 27.3 ± 4.7, 28.7 ± 3.6 and 19.7 ± 2.5 Gy respectively. In combination with dose rate data (Table 3.2), ages of 27.8 ± 5.0, 29.9 ± 3.9 and 30.4 ± 4.1 ka respectively were then calculated.

5.7 Discussion

5.7.1 Appropriateness of Bailey and Arnold's decision protocol

The decision protocol of Bailey and Arnold (2006) was created using a combination of modelled and empirical data, but was ultimately tailored for use with single grains of quartz deposited in a fluvial environment. In the approach used here, small aliquots consisting of approximately 30 grains of quartz were used. Due to the lack of OSL signal yielded from the majority of quartz grains in the aliquots of the Orrisdale, Porth Dinllaen and Wexford samples (~60% of all aliquots observed a natural OSL signal that was undetectable above the machine background), it was thought that analysis was on an 'almost single-grain level' with only one or two grains per aliquot yielding a detectable OSL signal (Duller, 2008). Therefore, the boundaries used for weighted skewness, kurtosis and overdispersion (which would otherwise be dependent upon aliquot size) used in the original protocol were applied to the samples investigated here.

However, the critical values of c_{crit} ($1/2\sigma_c$) and k_{crit} ($0.6/2\sigma_k$) were alternatively taken from Arnold (2006) as these were derived purely from modelled data, rather than those published in Bailey and Arnold (2006) which were tailored for fluvial samples and derived by 'trial and error' (Bailey and Arnold, 2006). The modelling procedure incorporated the impact that varying bleaching conditions, geological dose magnitude and the spread of the burial dose (due to spatial heterogeneity of radioisotopes) would have upon D_e distributions. To determine a value for these critical values a well-bleached sample from each field site would be required and its D_e distribution analysed and statistical parameters compared to a poorly- or heterogeneously-bleached sample from the same field site. This allows the spread in

the D_e distribution which is *not* due to bleaching, but due to factors such as beta-dose heterogeneity or post-depositional disturbance to be analysed. Quantitative estimates of skewness, kurtosis and overestimation could then be compared to those of a poorly-bleached sample, allowing critical values to be established which can successfully distinguish between the samples. This is not possible for the samples under investigation here as a naturally well-bleached sample does not, at present, exist and so the next best option is to use those derived from purely modelled data as in Arnold (2006).

5.7.2 Impacts of depositional environment upon optical dating

The OSL ages obtained for the Bishop's Court Member proglacial ice-marginal sandur deposits at Orrisdale range over 16.4-14.1 ka, for samples OR14, OR15 and OR22 (Table 5.1). The *Sr*, *Fl* and *Sh* lithofacies sampled a series of stacked bar-forms and targeted a waning flow regime (samples OR14, OR15 and OR22 respectively). The ages produced by these lithofacies are broadly similar and overlap within their 2σ error ranges. The *Sr, Fl* and *Sh* were taken from fining-up sequences, suggestive of a waning and shallower water flow, perhaps with a less turbid water column, allowing more efficient bleaching of a sufficient proportion of the quartz grains. Subaerial exposure of the bar-top environment is also possible as part of both the annual and diurnal flow cycle. Once subaerially exposed, transport via aeolian processes is possible, enhancing the opportunity for sufficient bleaching (McGowan, et al., 1996; McGowan and Sturman, 1997).

The *St* lithofacies (OR26) sampled is part of a laterally extensive (>10 m), deep sandur channel and produced an age estimation ~ 10 ka older (according to the

MAM-3) than the other lithofacies. Trough cross-bedded sets (Figure 5.4) were interpreted as reflecting higher energy in-channel settings and are clearly distinguishable from the cycles of *Sp, Sh, Sr* and *Fl* which displayed clear bar-form sediment architecture. These lithofacies can also occur within channels, but they reflect a lower energy flow regime. The calculated 2σ age (31-21 ka) falls in the same time frame as the LGM extent (during MIS 2) when the ISIS margin was much further south, in the Celtic Sea (Scourse and Furze, 2001; Scourse, et al., 2004; Hiemstra, et al., 2006; Scourse, et al., 2006; Ó Cofaigh and Evans, 2007) and is therefore a distinct age overestimation. The age overestimation of the *St* lithofacies perhaps reflects the dominant poorly-bleached nature of the quartz grains carried in this deep, fast flowing and sediment-laden channel as reflected in the significantly skewed (>2σ_c) D_e distribution. However, the overdispersion value for this sample is the lowest of all the samples (although they do overlap within errors), and so it would appear to be the best bleached based on overdispersion alone. This type of outlier shows that OSL dating of these types of sediment should be underpinned by the analysis of multiple samples, without this comparison there are no reasons to question this age determination.

For all Wexford samples where the MAM-3 was applied (BLA1; 90-125 μm and 180-212 μm and BLA3; 212-250 μm), distinct age overestimations were produced, when compared to the constraining age control (e.g. Coope, et al., 1971; Scourse and Furze, 2001; Scourse, et al., 2004; Scourse, et al., 2006; Ó Cofaigh and Evans, 2007). This is likely to be related to the poorly-bleached nature of quartz in this ice-contact alluvial fan environment. Although the samples were taken from fining-up sequences, indicating waning flow, it is likely that the ice-contact alluvial fan

environment, from which these samples originate, was a permanently sediment-laden, turbid environment not conducive to satisfactory bleaching. It was hoped that the bar-top deposit (BLA1 – *Fl*) would have been subaerially exposed at some point during its depositional history, resulting in satisfactory bleaching of a 'population' of quartz grains. However, the fan environment at this location may never have undergone such low flow conditions for the bar-top to be exposed above the water level. This contrasts with the distal sandur environments sampled on the Isle of Man which appeared to provide a more favourable bleaching environment allowing a dominantly well-bleached population of quartz grains to be sampled from a variety of lithofacies.

The extent of partial bleaching is revealed when overdispersion and weighted skewness are analysed (Table 5.1). For the Wexford samples overdispersion values ranging from 47-73% were calculated, in comparison to 39-51% for the same parameter calculated for Orrisdale samples. This higher and wider range of overdispersion values together with the significantly positively skewed D_e distributions indicates that the spread in the data, assumed to be due to heterogeneous bleaching, is greater for the ice-contact Wexford samples.

In comparison, the ice-distal Porth Dinllaen sandur sample (NEF4; 90-125 μm) yielded a reasonable 2σ age estimate of 23.9-18.7 ka, based upon a dominantly well-bleached population of quartz grains targeted using the MAM-3. As with samples from more ice-distal glaciofluvial lithofacies at Orrisdale, the rippled sand (*Sr*) lithofacies appears to have been used successfully for OSL dating. This *Sr* lithofacies was interpreted as having been deposited in a shallow water environment where the

ripples formed due to friction between the sandy bed and the water surface. The lithofacies succession is typical of a waning flow regime, which has allowed sufficient light to penetrate the water column for a population of quartz grains to be completely bleached upon deposition.

The entire sequence at Porth Dinllaen was dominated by sandy lithofacies (Figures 5.5 and 5.6) deposited in a distal proglacial sandur environment and the dominant well-bleached component of the quartz perhaps reflects the sufficient duration of transport from the ice-margin. The diurnal water flow variation in ice-marginal sandar and the cyclical process of erosion and deposition potentially allows bar-tops to be subaerially-exposed during low flow, creating further opportunity for bleaching. During peak water flows, these bar top deposits are submerged and often the quartz grains re-eroded and deposited further down the sandur. The stratigraphy of sandar typically contain more gap than record, thus bleaching appears to be a function of the exposure to sunlight in the ultimate depositional setting and prior exposure during sediment recycling shortly before deposition. The distal sandur environment on both counts appears the most appropriate location from which to sample for optical dating.

5.7.3 Impacts of grain size upon optical dating

Varying the grain size fraction of a sample selected for analysis appears to have little impact on age determination. The coarser grain sizes in samples OR14 (200-250 μm) and OR22 (150-180 μm) provide slightly younger ages, however, they overlap within the 2σ error limits. The coarser grain size fraction in sample BLA3 (212-250 μm) provided a slightly younger age than the 90-125 μm grain size fraction when the

L5% model was applied to both, however, they also overlap within the 2σ error limits (see Table 5.1). This is in contrast to other published work on fluvial (e.g. Olley, et al., 1998; Wallinga, 2002) and gully samples (e.g. Lang and Mauz, 2006). These authors observed much younger ages from coarser grain size fractions of the same sample. The D_e distributions for the all samples show that glaciofluvial sandur systems act as an efficient 'mixer' of sediment grains, allowing some to be well-bleached and others to be poorly-bleached, with no bias towards preferential bleaching of a particular grain size fraction. This is perhaps due to the turbid and fast flowing nature of the transport environment, meaning that all grain sizes are not exposed to sufficient light to result in all grains of a particular grain size fraction to be completely bleached. All grain size fractions are heterogeneously-bleached, with no particular grain size fraction being preferentially bleached over another. This needs to be tested on a wider range of samples from different depositional subenvironments for a firm conclusion to be made.

5.7.4 Performance of the statistical 'age' model decision protocol

Although successful application at Orrisdale is apparent (based upon the agreement of the OSL ages with the constraining chronology), the decision protocol is not as yet validated for broader application at other field sites. Further testing on other heterogeneously-bleached glaciofluvial sediments OSL dated by this methodology is required.

For the Wexford sample (BLA3; 90-125 μm) where the decision protocol identified the L5% model as most appropriate for D_e determination, a 2σ age range of 26.1-21.1 ka was calculated. This age is in close agreement with the constraining chronology

from other sites around the Celtic Sea (e.g. Scourse, et al., 2004; Scourse, et al., 2006; Ó Cofaigh and Evans, 2007). Ó Cofaigh and Evans (2007) obtained a series of ^{14}C ages (24.9-23.9 cal. a BP) from marine shells reworked into Irish Sea till (Macamore Member) which provide maximal ages for ice advance across the south coast of Ireland. These till deposits underlie the Screen Member (Ó Cofaigh and Evans, 2001) and the ages obtained here conform to the stratigraphy, particularly for the lower half of the error range. However, for the remainder of the Wexford samples, the decision protocol recommended the use of the MAM-3 (Table 5.1) which resulted in the calculation of optical ages in the range of 37-41 ka; significant age overestimations in comparison to the constraining chronology of Ó Cofaigh and Evans (2007).

The L5% model was applied to these remaining Wexford samples to establish whether this model, (which usually gives the lowest D_e estimates in comparison to the other 'age' models), would give more realistic age estimates. The results of this are shown in Table 5.1 and calculated ages are in the range 34-23 ka. Age overestimations are therefore *still* observed which suggests that the lowest D_e values targeted also represent quartz grains that were not completely bleached. *Any* of the statistical age models outlined in this chapter could be applied to these samples and age overestimations would still result as the small aliquot methodology used in this research could not detect quartz grains that were completely bleached within a population of over 50 D_e values.

For the Porth Dinllaen sample the use of the MAM-3 model gave a realistic age estimate (2σ age estimate of 23.9-18.7 ka). Although there is a lack of chronological

control at this field site, the calculated age is younger than that for the Wexford samples and older than the samples from Orrisdale and this conforms with northwards retreat of the ISIS. The decision protocol appears to provide a robust independent basis for the generation of age estimates, but to confirm its wider applicability; the 'age' model decision protocol needs testing on a wider range of samples from different depositional environments.

5.7.5 Interpretation of optical ages

In terms of Quaternary stratigraphy of the Isle of Man (Thomas, et al., 1985; Chiverrell, et al., 2001; Thomas, et al., 2004; Thomas, et al., 2006) the Orrisdale Formation was lain down during retreat from LGM limits and so post dates 24-21 ka. Interstadial flora and fauna dated in kettlehole sediments show that the Orrisdale area was ice free by at least 15,000-14,170 cal a BP (Roberts, et al., 2006). The calculated OSL ages (Table 5.1) overlap with the earlier part of this age range and suggest that the Orrisdale Formation was deposited as a result of the Killard Point Stadial readvance 18-15 ka. Ages in the range of 17-14 ka (Table 5.1) have been obtained which agree with the geologically-constrained chronology. The Orrisdale Formation therefore thought to be contemporaneous with the Killard Point Stadial identified in eastern Ireland ~16.4 ka.

The 2σ OSL age range for the Screen Member at Wexford (26.1-21.1 ka) overlaps with the younger AMS radiocarbon ages for shells incorporated within the Irish Sea till (24.9-23.9 cal. ka BP) (Ó Cofaigh and Evans, 2007). The Irish Sea Till was deposited at this location during advance after 24.4-23.9 cal. ka BP to margins in the ISIS that extended as far south as the north of the Scilly Isles in the south Celtic Sea.

Notwithstanding that the optical age for the Screen Member must be regarded as maximal because it is still possible that the aliquots used to derive the age estimate were not completely bleached, the younger end of the age range *is* plausible for the Screen Member. In combination these ages imply that the advance of the ISIS to the LGM position in the south Celtic Sea and subsequent retreat to the Screen Hills occurred extremely rapidly. Using a maximum age difference of 3.8 ka this implies a minimum retreat rate of ~75 m per annum (based on a maximum distance of ~280 km between Celtic Sea maximum limits and St. Georges Channel). By taking the central age from each 2σ range, a maximum retreat rate of ~350 m per annum is calculated (based on a minimum age difference of 0.8 ka). From this point northwards, it is hypothesised that the ISIS stabilised and adopted a slow and oscillatory retreat (Thomas and Chiverrell, 2007). The presence of glaciotectonically-deformed sediments along the coastlines of Wexford and North Wales reinforces the view of staccato retreat punctuated by ice-marginal oscillation. These cycles of advance and retreat oscillations account for the more or less ubiquitous evidence for glaciotectonic deformation.

The glaciofluvial sequence at Porth Dinllaen reflects a large scale meltwater outwash plain trapped between the retreating ice-margin and the bedrock ridge of the Llŷn Peninsula. From a retreat limit some distance north of Nefyn, the ice-margin re-advanced to a limit that ran from Nefyn westwards across the headland of Penrhyn Nefyn (Thomas and Chiverrell, 2007). The readvance caused widespread deformation of underlying sediment and the creation of a large ice-front alluvial fan at Nefyn and extensive distal sandur sedimentation out beyond it (Thomas and Chiverrell, 2007). This readvance episode now has an optical age of 21.3 ± 2.6 ka

(2σ error). It is likely that the real age sits within the lower portion of the 2σ range due to the likelihood that this age range incorporates estimates from some heterogeneously bleached quartz grains. By taking the lower end of the 2σ age range, a retreat of c. 100 km from the coastline of Co. Wexford, in ~2 ka, or an average of 50 m per annum (slower than that from the LGM position in the south Celtic Sea) is suggested.

The younger end of the 2σ optical age calculated for glaciofluvial sediments at Porth Dinllaen is ~4.8 ka younger than the youngest AMS radiocarbon date calculated for glacially-transported marine shells from the Irish Sea Till in southeastern Ireland (Ó Cofaigh and Evans, 2007). The ISIS retreated ~380 km from its maximum extent in the Celtic Sea to a position off the north coast of the Llŷn Peninsula in north Wales in this time period. Previous investigations into the sedimentology of the Irish Sea Till and correlative deposits elsewhere in the Celtic Sea have proposed that the advance to LGM limits was unstable and short-lived and was facilitated in part by a saturated substrate of marine mud (Scourse, et al., 1990; Scourse, et al., 1991; Ó Cofaigh and Evans, 2001a; Ó Cofaigh and Evans, 2001b; Evans and Ó Cofaigh, 2003a; Hiemstra, et al., 2006). The chronology presented here conforms to this theory of rapid ISIS retreat from LGM extent.

Further to the north within the Irish Sea Basin, optical ages of between 17-14 ka from ice-marginal sandur at Orrisdale suggest that ice then retreated rapidly from Porth Dinllaen at 21.3 ± 2.6 ka to a position to the north of the Isle of Man, and subsequently re-advanced onto the northern plain of the Isle of Man during the Killard Point Stadial ~18-14 ka. These ages and estimated rates of marginal retreat

enhance the argument for a rapid and dynamic retreat of the ISIS from LGM limits in the Celtic Sea, which was probably conditioned by both external (climate/sea level) and internal (subglacial bed conditions) forcing.

5.8 Conclusions

(i) Targeting specific lithofacies in fossil glaciofluvial sediment sequences improves the chance of successful dating using OSL methodologies. These lithofacies should reflect the depositional subenvironments most likely to yield well-bleached quartz grains, notwithstanding the general tendency of glaciofluvial deposits to yield positively skewed and heterogeneously-bleached D_e distributions.

(ii) As a recommendation, it is logical for sampling for luminescence dating of glaciofluvial sediments to target well-displayed bar forms and the fining-up sequences exemplified here for sand dominated 'distal-flow' lithofacies assemblages, especially finely laminated sands (bar-top) and rippled sand lithofacies. The bar-top deposits are more likely to have been subaerially exposed during waning flow, improving chances for efficient bleaching. The rippled sand deposits are formed in shallow water where light penetration through the water column is sufficient enough to create a well-bleached population of grains within a remaining population of partially/poorly-bleached grains.

(iii) Factors such as heterogeneous bleaching and poor quartz characteristics (due to sediment provenance) can be overcome by measuring large numbers (~200-300) of small aliquots (~30 grains), to enable a statistically sufficient number (~50) of aliquots to be accepted, having satisfied all of the acceptance criteria.

(iv) The well-bleached 'population' of quartz grains can be statistically extracted from the remaining partially/poorly-bleached population by using appropriate 'age' models. The 'age' model to use can be chosen by the decision protocol of Bailey and Arnold (2006), originally designed for single-grain analysis, can be applied to heterogeneously-bleached sediments where small-aliquots (~30 grains) have been used for D_e determination where only one or two grains in that aliquot contribute to the OSL signal.

(v) Previously, researchers have encountered repeated problems during luminescence dating of glacigenic sediments, and these include *heterogeneous bleaching* (Duller, et al., 1995; Raukas and Stankowski, 2005; Alexanderson and Murray, 2007; Lukas, et al., 2007), *poor quartz luminescence sensitivity* (Rhodes and Pownall, 1994; Richards, 2000; Spencer and Owen, 2004) and the lack of a dateable *fast component* (Lukas, et al., 2007). In the approach followed here, these problems have either been avoided or overcome to produce a chronology:

1) Poor quartz luminescence sensitivity can perhaps be avoided by investigating quartz provenance. The previously cycles and sensitised quartz of the Triassic and Permo-Triassic sandstones in the Irish Sea Basin appear to provide favourable luminescence characteristics.
2) Characterising the optical components and identifying the presence of a fast component using CW-OSL decay curves confirm that the sampled quartz is applicable for the SAR protocol.

3) Heterogeneous bleaching was evident in all Orrisdale samples and was overcome by targeting glaciofluvial lithofacies more conducive to efficient bleaching. Using small aliquots and appropriate 'age' models allowed the extraction of the true D_e from the well-bleached 'population' of quartz grains.

(vi) The approaches used to determine OSL ages for the glaciofluvial deposits under investigation here have met with some success, but the process of obtaining ages is significantly lengthier than for more easy to date samples such as those that are uniformly well-bleached. Heterogeneously-bleached samples of this nature require the use of more material and numbers of aliquots, previous attempts (Duller, et al., 1995; Owen, et al., 2002; Raukas and Stankowski, 2005) may have struggled or been deterred by apparent poor performance/difficulties. In addition to the analysis of large amounts of material, heterogeneously-bleached materials of this nature require robust protocols and methodologies to streamline and improve laboratory efficiency.

(vii) As a result of the application of the OSL dating procedures mentioned here, ages in the range of 17-14 ka have been obtained for the Orrisdale which agree with the geologically-constrained chronology. The Orrisdale Formation therefore thought to be contemporaneous with the Killard Point Stadial identified in eastern Ireland ~16.4 ka.

(viii) OSL ages calculated using the 'Lowest 5%' model for an ice-contact alluvial fan at Blackwater, Wexford, are in chronostratigraphical agreement with the constraining radiocarbon and OSL chronology from elsewhere in southern Ireland and on the Scilly Isles (Ó Cofaigh and Evans, 2007; Scourse, 2006; Scourse et al.

2004). Ice-contact, ice-proximal type sediments such as those from Wexford are not ideal for the application of optical dating due to the poor bleaching characteristics evident even in the finer grain size fraction of fining-up sequences that indicate waning flow. The MAM is inappropriate for such samples as it gives distinct age overestimations, although the L5% model did give a realistic age estimate for one such sample. The decision protocol used here to select the appropriate 'age' model for the Wexford samples is not necessarily applicable to the majority of these very poorly-bleached sediments, where minimal aliquots contain quartz grains that are completely bleached. In all but one of these samples all 'age' model output gives an overestimation. By taking the younger end of the 2σ error age range as calculated by the L5% model applied to the D_e distribution of sample BLA3; 90-125 μm, we have concluded that the Screen Member of the Blackwater formation has an optical age of 23.6 ± 2.5 ka. This has allowed maximum and minimum rates of retreat for the ISIS from LGM limits to be calculated in conjunction with other chronological information.

(xi) In comparison, the distal sandur lithofacies (*Sr*) targeted for OSL dating at Porth Dinllaen yielded a well-bleached population of quartz grains that allowed an optical age to be calculated via the use of MAM-3 for D_e determination. The younger end of the OSL age calculated from the Porth Dinllaen sample using the MAM-3 (21.3 ± 2.6 ka) is younger than the constraining AMS radiocarbon chronology of Ó Cofaigh and Evans (2007) which constrains the timing of advance to LGM limits to after 24.9-23.9 cal. a BP. This enhances the argument that the ISIS retreated in a rapid and dynamic fashion from LGM limits in the Celtic Sea to the coast of Wales from where it adopted a slower and oscillatory retreat pattern northwards as indicated by the

evidence documented most recently by Thomas and Chiverrell (and earlier by Whittow and Ball, 1970; Addison, 1990; Chambers, et al., 1995).

(xii) This protocol for OSL dating of glaciofluvial sediments has the potential for much wider application to high latitude or temperate areas where there is an abundance of such sediments that are well preserved in the geological record.

Chapter 6

The chronology and palaeoglaciology for the retreat of the late Devensian Irish Sea Ice-Stream

6.1 Introduction

Ice-streams are relatively narrow, fast-flowing zones (10-100 km in width) of concentrated ice flow surrounded by otherwise slow-flowing inter-stream zones. Flow velocities are typically an order of magnitude larger than in inter-stream zones. Fast ice-streams have broad catchment areas from which large fluxes are discharged to the ice-sheet margin by a relatively narrow stream. They play an important role in regulating ice-sheet behaviour, discharging as much as 85% of the ice mass in the case of modern-day Antarctica (Boulton, et al., 2001; Boulton and Hagdorn, 2006). Ice-streams exert a fundamental control on the stability and dynamics of modern ice-sheets and they are thought to have played a similarly important role in regulating the dynamics of middle and high-latitude Quaternary ice-sheets. Stokes and Clark (2001) proposed the Irish Sea Basin (ISB) as a location for a large ice-stream within the British and Irish Ice-sheet (BIIS) referred to as the Irish Sea Ice-stream (ISIS) (Figure 6.1) (Merritt and Auton, 2000; Evans and Ó Cofaigh, 2003a; Hiemstra, et al., 2006).

The time period focussed upon in this research is the Last Glacial Maximum (LGM) of MIS 2, defined by EPILOG (Environmental Processes of the Ice age: Land, Oceans, Glaciers) as the most recent interval during MIS 2 when global ice-sheets reached their maximum integrated volume and is currently identified as centred

around 21 cal. ka BP (Mix, et al., 2001). Thomas and Chiverrell (submitted) reviewed evidence for the LGM in Britain and Ireland and found an increasingly repeatable two phase sequence, with ice advance broadly after 30 cal. ka BP and maximum extension reached early between 30 and 24 cal. ka BP, with a retreat and subsequent readvance in the period 24-20 cal. ka BP. However, this is not to say that all sectors of the BIIS reached maximum volume at the same time. Indeed, the evidence presented in this research argues for asynchrony within the BIIS with the timing of ISIS advance to its maximum extent across southern Ireland and to the Scilly Isles being placed within the younger supposedly less extensive readvance phase of the BIIS.

The late MIS 2 glaciation in Britain began after ~30 ka with extensive growth of glaciers in the mountains of the Western Highlands and Southern Uplands of Scotland, Lake District. These centres of ice accumulation expanded until the dominant ice from the Scottish Highlands became confluent with Southern Upland, Lake District and Northern Irish ice in a large stream moving southwards through the northern Irish Sea Basin. At its maximum extent, ice in the northern basin extended over 500 km and reached the southern Celtic Sea (Scourse, et al., 1990; Scourse, et al., 1991; Scourse and Furze, 2001; Ó Cofaigh and Evans, 2007), although the limits of the maximum extent of the ISIS are still debated (Bowen, et al., 2002; Knight, 2004). On the basis of offshore evidence, Scourse and Furze (2001) suggested that grounded ice, as part of the ISIS, deposited subglacial till as far as 300 km south of St. Georges Channel, into the Celtic Sea, with glaciomarine deposits occurring to the south of this terrestrial glacial limit. The presence of erratic-bearing glacigenic

sediments on the northern shores of the Scilly Isles is also testimony to the presence of an ice-stream margin (Hiemstra, et al., 2006).

Modelled computer simulations (e.g. Boulton and Hagdorn, 2006) also argue for the presence of an ice-stream occupying the Irish Sea Basin which was able to draw down the ice-sheet surface, allowing agreement with the low profile and low summit elevation models of the last ice-sheet over the British Isles (Ballantyne and Sutherland, 1987; Boulton, et al., 1991; Lambeck, 1993b; Boulton and Hagdorn, 2006). The simulations demonstrate the glaciological probability of a major stream/lobe in the southern Irish Sea or Celtic Sea and the modelled data readily created a major fixed ice-stream in the Irish Sea, similar to that proposed by Scourse and Furze (2001) which, during MIS 2, reached the latitude of the Scilly Isles. Deforming bed conditions (or a 'soft' bed) were thought to be the driver behind the expansion to maximum extent of the ISIS (Ó Cofaigh and Evans, 2001a; Ó Cofaigh and Evans, 2001b).

The flow dynamics and flow phasing of this sector of the BIIS remain poorly understood because of the fragmentary nature of the field evidence and poor chronostratigraphic control (Roberts, et al., 2007). Detailed research into the sedimentary stratigraphy of glacigenic deposits left behind as a result of the advance and retreat phases of the ISIS (e.g. Thomas and Summers, 1983; Thomas, 1984; Thomas and Summers, 1984; Thomas, et al., 1985; McCabe, 1987; Eyles and McCabe, 1989; McCabe, et al., 1998; Ó Cofaigh and Evans, 2001b; Scourse and Furze, 2001; Evans and Ó Cofaigh, 2003a; Thomas, et al., 2004; Hiemstra, et al., 2006; Roberts, et al., 2007; Thomas and Chiverrell, 2007) has enabled reconstruction

of the sedimentary environments of deposition at the various marginal positions and marginal oscillations during ice retreat.

A lack of organic material available for dating via radiocarbon techniques within these deposits has hindered the resolution of the chronology for the advance and retreat of the ISIS. Radiocarbon ages are often available from peat samples taken from infilled kettle holes which overlie glacigenic sequences and these are often Bølling/Allerød ages, but direct evidence from glacial sediments themselves is somewhat lacking. This contrasts with North America where organic material is widespread, enabling the extent of the Laurentide ice-sheet to be reconstructed accurately. Without appropriate organic samples for radiocarbon ages, most sectors of the MIS 2 ice-sheet lack adequate chronological control. Considerable strides have been made by applying optical (e.g. Duller, 2004; Olley, et al., 2004; Duller, 2006), cosmogenic (e.g. Ballantyne, et al., 2006; Ballantyne, et al., 2007; Golledge, et al., 2007; Ballantyne, et al., 2008) and Accelerator Mass Spectrometry (AMS) radiocarbon (e.g. McCabe and Clark, 1998; Scourse and Furze, 2001; Ó Cofaigh and Evans, 2007) dating techniques to glacigenic deposits of the UK and as a result, the present day ISIS advance and retreat chronology is gradually becoming more complete.

This chapter presents a synthesis of and evaluates the chronological data for sediments associated with the ISIS during MIS 2. Bayesian techniques have been used to test models of relative order of events by assessing the conformability of relative order models as informed by the interpretation of geomorphology and sedimentology (Buck, et al., 1991; Blockley, et al., 2004; Bronk Ramsey, 2008b;

Chiverrell, et al., 2008). This approach allowed the identification of contexts or materials that were out of sequence and focused attention on problem materials (e.g. those affected by reworking or poor bleaching) and errors in interpretation (outlier ages) (Chiverrell, et al., 2008; Foster, et al., In Press). Probability-based age estimates for the advance and retreat stages of the ISIS were then calculated and used to estimate rates of retreat for the ISIS.

6.2 Constraining the timing of glacial landforms

The nature of the record (landforms and sediments) used to discern the advance and retreat of the ISIS is challenging, and much of our understanding is underpinned by geomorphological reasoning of the relative order of events. Bayesian analysis offers a robust methodology to validate the depositional models that comprise a myriad of forms of geochronological control (Chiverrell, et al., 2008). Radiocarbon, cosmogenic isotope (rock exposure) and optically stimulated luminescence (OSL) have been applied to glacigenic sedimentary sequences to constrain the timing of advance and retreat of the ISIS. The application of these approaches is constrained in that, for various reasons, the materials dated need not be contemporaneous with the geomorphological question. However, even if the contexts are not contemporaneous with environmental changes, older, *terminus ante quem* (TAQ) or younger than constraint, *terminus post quem* (TPQ) can be equally important. In summary it is critical that the contemporaneity relationships between the dated context and dated materials, and the event under study are well defined. This section reviews the application and limitations of the dating techniques in relation to securing the timing of retreat for the ISIS.

6.2.1 Radiocarbon dating

The aim here is not to review radiocarbon dating (see Bronk Ramsey, 2008b, for example) but to outline how the technique has been used to constrain the timing of glacigenic sequences associated with the ISIS. Glacigenic sediments are typically lacking in fossil organic material due to the cold and ice-covered environments which are not conducive to the presence of abundant flora or fauna. Therefore, radiocarbon techniques have more often been adopted to date fossils, organic muds, peat and kettle hole fills either directly underlying or overlying the glacigenic deposit, and those bracket the timing of deposition rather than determine a direct age (e.g. Coope, et al., 1971; Chambers, et al., 1995; Scourse and Furze, 2001; Roberts, et al., 2006; Roberts, et al., 2007). In this sense they can only give 'older than' (*minimum*) or 'younger than' (*maximum*) ages, but in conjunction with other dating techniques, can provide powerful chronological information. For example, on the Isle of Man, the timing of deposition for MIS 2 glaciation is constrained by radiocarbon dates from basal organic muds overlain by diamict and from organic material taken from kettle holes which overlie the glacigenic sequence (Roberts, et al., 2006; Roberts, et al., 2007).

Other applications of radiocarbon dating techniques include the dating of marine shells found within the Irish Sea Tills on the south coast of Ireland (e.g. Ó Cofaigh and Evans, 2007). Although the shells were not deposited *in situ*, but deposited and subsequently remobilised by the advancing ISIS, their AMS radiocarbon dating provides constraining *maximum* ages for the sediment within which they lie (Ó Cofaigh and Evans, 2007). Foraminiferal shells found in situ within fossiliferous glaciomarine muds from north-eastern Ireland constrain readvance episodes during

retreat from LGM extent (e.g. McCabe, 1996; McCabe and Clark, 1998; McCabe, et al., 1998; Clark, et al., 2004b; McCabe, et al., 2005).

6.2.2 Cosmogenic isotope dating

Cosmogenic nuclides are produced in rocks at the surface of the Earth by the action of cosmic radiation (Cerling and Craig, 1994; Gosse and Phillips, 2001). A detailed review of the theory and application of cosmogenic isotope dating is given in Gosse and Phillips (2001). Most of the cosmic ray flux is attenuated within the top one to two metres of the surface of the solid Earth, therefore, processes such as glaciations that scour rock from greater depths and deposit it on the surface can be dated by measuring the subsequent accumulation of cosmogenic nuclides. The most widely used cosmogenic nuclides are ^{3}He, ^{10}Be, ^{14}C, ^{21}Ne, ^{26}Al and ^{36}Cl and their physical and chemical properties make it possible to apply surface exposure dating methods on rock surfaces of almost any lithology at any latitude and altitude for exposures ranging from 10^{2} to 10^{7} years (Gosse and Phillips, 2001). Ballantyne et al. (2006) used ^{10}Be concentrations within the surface of upstanding rock outcrops to establish the vertical dimensions and age of the Wicklow Mountains ice dome which fed into the western margin of the ISIS.

6.2.3 Optically Stimulated Luminescence (OSL) dating

There are relatively few techniques for the direct dating of the time of deposition of sediments (Aitken, 1998). The luminescence methods are dominant in this respect and approaches such as OSL present an opportunity to date the dominant constituents of the sediment itself (quartz and feldspar). The history of the exposure to environmental radiation over time is carried by electrons (charge) trapped within

mineral grains; the total number of electrons in these traps will increase with burial time, but the charge is released when the mineral grains are exposed to daylight during depositional processes. This process of detrapping charge by light exposure is referred to as *bleaching*. The amount of trapped charge forms a clock that starts ticking at the moment the mineral is buried and shielded from light (Aitken, 1998; Wallinga, 2002). The luminescence signal used for dating reflects the amount of charge trapped, and hence the irradiation dose the sample has received since burial.

The application of this technique to glacigenic sediments has proven to be challenging due to the lack of opportunity for minerals to be exposed to daylight as the majority of glacigenic sediments are transported and deposited by a glacier or ice-sheet or are deposited in turbid proglacial sandur environments (see Chapter 2). However, methodologies have been established to help to overcome problems associated with heterogeneous bleaching, making OSL a viable technique for the direct dating of glacigenic deposits (e.g. Duller, 2006). OSL has been applied successfully to glacigenic sediments in the Scilly Isles (Scourse and Furze, 2001; Scourse, et al., 2004; Hiemstra, et al., 2006), south-eastern Ireland, north-western Wales and the Isle of Man (see Chapter 5).

6.2.4 Sequence models

Bayesian modelling offers a robust methodology for integrating dating control and assessing the relative order of events. Buck et al. (1996) and Bronk Ramsey (2008a) provide a thorough summary of the application of Bayesian statistical methods to archaeological and various other depositional settings. Increasingly, Bayesian methods are applied to sets of closely spaced, stratigraphically related samples (e.g.

radiocarbon ages for lake sediment cores), and these relationships are used to restrict the overlapping uncertainty distribution in the age estimates (Blockley, et al., 2006; Blockley, et al., 2008). For example, a sample lower in a section cannot actually be younger than one above it, given certain assumptions about the sediment i.e. that it was deposited layer upon layer and has not been disturbed (Rhodes, et al., 2003). This prior information can be used to modify the independent uncertainty distribution of each subsequent sample, specifically to restrict the range of possible values allowed by the uncertainty distribution of individual samples when several overlapping distributions occur for closely spaced samples. The advantages of this method are a reduction in the uncertainty of the date estimate and an analysis of the correspondence between the stratigraphical and the scientific dating information. Bayesian approaches also provide a sound method for combining the age information from different dating techniques (Rhodes, et al., 2003). A disadvantage is that assumptions about depositional processes have a direct in influence on the result (Rhodes, et al., 2003). As a landscape system, the former ISIS is considerably more complicated than a lake basin, with the database of age control for the advance and retreat stages increasingly quite extensive (Table 6.1), based on several different techniques and spanning multiple locations.

Here we have employed Bayesian approaches (Buck, et al., 1996; Blockley, et al., 2004) implemented using OxCal *v. 3.10* (Bronk Ramsey, 2001) to test a hypothetical 'relative order' model of the expected chronological order of the dating control (Chiverrell, et al., 2008). Details of the Markov Chain Monte Carlo sampling and the algorithms employed in OxCal for this are available from Bronk Ramsey (2008a). The construct of the model is outlined in the following section, but comprised a

younging sequence with events arranged into a pseudo-stratigraphical order (e.g. Figure 6.2). Lack of conformity in these relative order models of ages either implied problems with individual age determinations or that our relative order model was flawed and that the discrepancies need explaining. These sequence models contain dating information arranged into an expected order (oldest first) and underpinned by one event preceding another, with prior information affecting the resultant probability distributions. Within the 'Sequence' model, ages for which no relative order information was assumed are grouped as *Phases*, and these shared similar relationships with other items in the sequence model. Using a combination of Sequences and Phases allowed OxCal to produce probability age ranges for events (Geomorphological changes) that have not been directly dated using the relative order model. These are either Boundaries or Event queries in the Sequence model. It must be stressed that these estimates are clearly interpretative, and will change as further data are added or if modelled from a different perspective or in a different order.

Complications arise due to the direct comparison between ages calculated by different dating techniques i.e. their errors are calculated differently and incorporate different parameters. For radiocarbon ages to be directly compared to OSL ages, the OSL errors need to be those arising from 'measurement precision' i.e. those derived solely from the propagation of measurement uncertainties which come from counting statistics on each parameter measured (equivalent dose and dose rate determination), fitting uncertainties in equivalent dose estimation and variation between equivalent dose values from different aliquots of the same sample (Rhodes, et al., 2003). These precision-only errors do not provide a realistic estimation of overall uncertainty in

the OSL age, which is also subject to systematic errors. Errors relating to the calibration of the beta source (for irradiation of OSL samples), errors in the estimation of water content, cosmic ray contribution (for dose rate determination) and the contribution of internal dose rate (thought to be almost negligible e.g. Mejdahl, 1987; Murray and Funder, 2003) are all ignored in this Bayesian approach to allow comparability with all methods of age determination. In most cases, the observed variation between the equivalent doses of different aliquots provides the greater proportion of the 'precision-only errors'. This method could only be applied to OSL ages calculated by the author (see Chapter 5). Precision-only errors for OSL age estimates provided by other authors could not be calculated. For cosmogenic isotope dating, the errors given include uncertainty in the value of the ^{10}Be production rate, to allow comparison between the exposure ages and dates obtained by other methods (Ballantyne, et al., 2006).

All the radiocarbon ages were calibrated either during or prior to the running of the Sequence model in OxCal (Bronk Ramsey, 2001). For the running of the Bayesian model, all ages suffixed with ka (Table 6.1) (OSL, TL and cosmogenic ages) were adapted to ka BP (i.e. before AD 1950) for comparability with the radiocarbon dating. A number of the radiocarbon ages are towards the upper limit of the INTCAL04 (Reimer, et al., 2004) calibration curve, which covers the period 0-21,341 ^{14}C years BP. As a consequence radiocarbon ages older than ~21,000 ^{14}C years were calibrated before incorporation within OxCal using the Fairbanks et al. (2005) calibration curves and software. Throughout this chapter all radiocarbon ages are suffixed by cal. a BP with present defined as AD 1950 and presented as the 2 sigma age range. For all other geochronological methodologies the ages are clearly

identified and suffixed with ka. In OxCal radiocarbon ages to be calibrated during the Bayesian analysis were entered in uncalibrated ^{14}C years BP, and any pre-calibrated radiocarbon ages and ages obtained by all other dating techniques were entered as calendar ages in years BP (before AD 1950).

Table 6.1 *Chronological information derived from different sources using a variety of dating techniques (OSL, TL, AMS radiocarbon, cosmogenic isotopes). All radiocarbon ages are shown using uncalibrated and calibrated ranges. All age information derived by other chronological techniques is given as ka.*

Reference	Location	Dating method	Material	Laboratory code	Age (1σ precision only errors)	Units	Calibrated 2σ radiocarbon age range (cal-yr BP)
Basal (advance) ages							
Roberts et al. (2007)	Strandhall, Isle of Man	AMS ^{14}C	Basal organic muds	Beta-178163	36 000 ± 670	yr BP	40,008: 42,500*
Chambers et al. (1995)	Pen-y-bryn, NW Wales	AMS ^{14}C	Organic matter underlying glacigenic sequence	SRR-3151	41 160 ± 850	yr BP	44,205: 47,281*
				SRR-3149	31 170 ± 350	yr BP	35,777: 37,297*
				SRR-3150	40 570 ± 820	yr BP	43,740: 46,712*
Scourse & Furze (2001)	Scilly Isles	AMS ^{14}C	Organic matter of Porthloo Breccia	Q2410	34 500 ± 843	yr BP	38,200: 41,508*
				Q2358	21 500 ± 845	yr BP	23,612: 27,948*
Scourse et al. (2006)	Scilly Isles	OSL	Porthloo Breccia	n/a	49.0 ± 3.0	ka	n/a
Maximum extent ages							
Ó Cofaigh & Evans (2007)	Ardmore Bay, Co. Waterford	AMS ^{14}C	Single shell fragments from the Irish Sea Till	Beta-215771	20 185 ± 70	yr BP	23,931: 24,410*
				Beta-215772	20 775 ± 80	yr BP	24,644: 25,390*
				Beta-222304	21 135 ± 130	yr BP	24,999: 25,238*
				Beta-222305	20 295 ± 120	yr BP	23,937: 24,612*
	Whiting Bay, Co. Waterford	AMS ^{14}C	Single shell fragments from the Irish Sea Till	Beta-222306	23 025 ± 150	yr BP	27,200: 28,072*
	Garryvoe, Co. Cork	AMS ^{14}C	Single shell fragments from the Irish Sea Till	Beta-215778	22 075 ± 90	yr BP	26,258: 26,850*
Scourse & Furze (2001)		TL	Old Man Sandloess	QTL1d	18.6 ± 3.7	ka	n/a
				QTL1f	18.6 ± 3.7	ka	n/a
		OSL	Old Man Sandloess	738al	20.0 ± 3.5	ka	n/a
				741al	26.0 ± 4.8	ka	n/a
Scourse et al. (2006)			Tregarthen Gravel	n/a	25.1 ± 2.2	ka	n/a
				n/a	22.7 ± 0.9	ka	n/a
Retreat phase ages							
Thrasher (Chapter 5, this volume)	Blackwater, Co. Wexford	OSL	Glaciofluvial outwash from Screen Mb	BLA1(90-125)	27.8 ± 2.5	ka	n/a
				BLA1(180-212)	29.9 ± 1.9	ka	n/a
				BLA3(90-125)	23.6 ± 1.2	ka	n/a
				BLA3(212-250)	30.4 ± 2.0	ka	n/a
Ballantyne et al. (2006)	Wicklow Mountains, Co. Wicklow	Cosmogenic ^{10}Be	Upstanding rock outcrops	DJ01	19.1 ± 1.2	ka	n/a
				KAN01	18.2 ± 1.2	ka	n/a
				SCA01	18.5 ± 1.2	ka	n/a
Bowen et al. (2002)	Mottee Stone, Co. Wicklow	Cosmogenic ^{36}Cl	Glacial erratic boulders and glacially smoothed bedrock	n/a	22.3 ± 2.0	ka	n/a
	Lough Nahanagan, Co. Wicklow			n/a	17.1 ± 0.9	ka	n/a
Thrasher (Chapter 5, this volume)	Porth Dinllaen, NW Wales	OSL	Glaciofluvial outwash	NEF4(90-125)	21.3 ± 1.2	ka	n/a
Readvance ages							
McCabe et al. (2005)	Linns, NE Ireland	AMS ^{14}C	Benthonic foraminifera	AA-56700	14 157 ± 69	yr BP	16,450: 17,350
	Rathcor Bay, NE Ireland			AA-56701	14 250 ± 130	yr BP	16,450: 17,650
	Cranfield Point, NE Ireland			AA-21818	14 705 ± 130	yr BP	17,150: 18,550
	Cooley Point, NE Ireland			AA-17693	15 020 ± 110	yr BP	18,000: 18:700
				AA-17694	15 390 ± 110	yr BP	18,580: 18,910
	Kilkeel, NE Ireland			AA-17695	15 400 ± 140	yr BP	18,520: 18,960
				AA-21819	15 605 ± 140	yr BP	18,650: 19,080
	Kilkeel, NE Ireland			AA-22351	16 760 ± 130	yr BP	19,550: 20,200
				AA-22352	16 750 ± 160	yr BP	19,500: 20,250
Clark et al. (2004b)	Kilkeel, NE Ireland	AMS ^{14}C	Benthonic foraminfera	CAMS89688	17 370 ± 190	yr BP	20,050: 21,100
				CAMS89687	16 940 ± 70	yr BP	19,890: 20,270
				CAMS89686	17 040 ± 70	yr BP	19,960: 23,360
	Killard Point, NE Ireland			AA-22820	13 795 ± 115	yr BP	15,950: 16,900
				AA-22821	13 995 ± 105	yr BP	16,200: 17,100
Thrasher (Chapter 5, this volume)	Orrisdale, Isle of Man	OSL	Glaciofluvial outwash from Bishops Court Member	OR14(90-125)	14.1 ± 1.2	ka	n/a
				OR14(200-250)	14.4 ± 1.1	ka	n/a
				OR15(90-125)	14.2 ± 1.2	ka	n/a
				OR22(90-125)	16.4 ± 1.5	ka	n/a
				OR22(150-180)	15.0 ± 1.3	ka	n/a
				OR26(90-125)	25.9 ± 2.4	ka	n/a
Post- Readvance ages							
McCabe & Clark (1998)	Rough Island, NE Ireland	AMS ^{14}C	Benthonic foraminifera	AA-21822	12 740 ± 95	yr BP	14,650: 15,400
Roberts et al. (2006)	Glen Balleira, Isle of Man	AMS ^{14}C	Plant macrofossils	SUERC3037	12 492 ± 95	yr BP	14,150: 15,000
	Jurby, Isle of Man			SUERC3282	12 276 ± 45	yr BP	13,950: 14,600
Coope et al. (1971)	Glanllynnau, NW Wales	Radiocarbon	Coleoptera	Birm-212	14 468 ± 300	yr BP	16,450: 18,550

* *AMS radiocarbon ages calibrated using software of Fairbanks et al. (2005) and then input to OxCal as calendar dates (C_dates). All other AMS radiocarbon ages were calibrated directly in OxCal according to Reimer et al. (2004). The 2σ calibrated range is given for all AMS radiocarbon ages.*

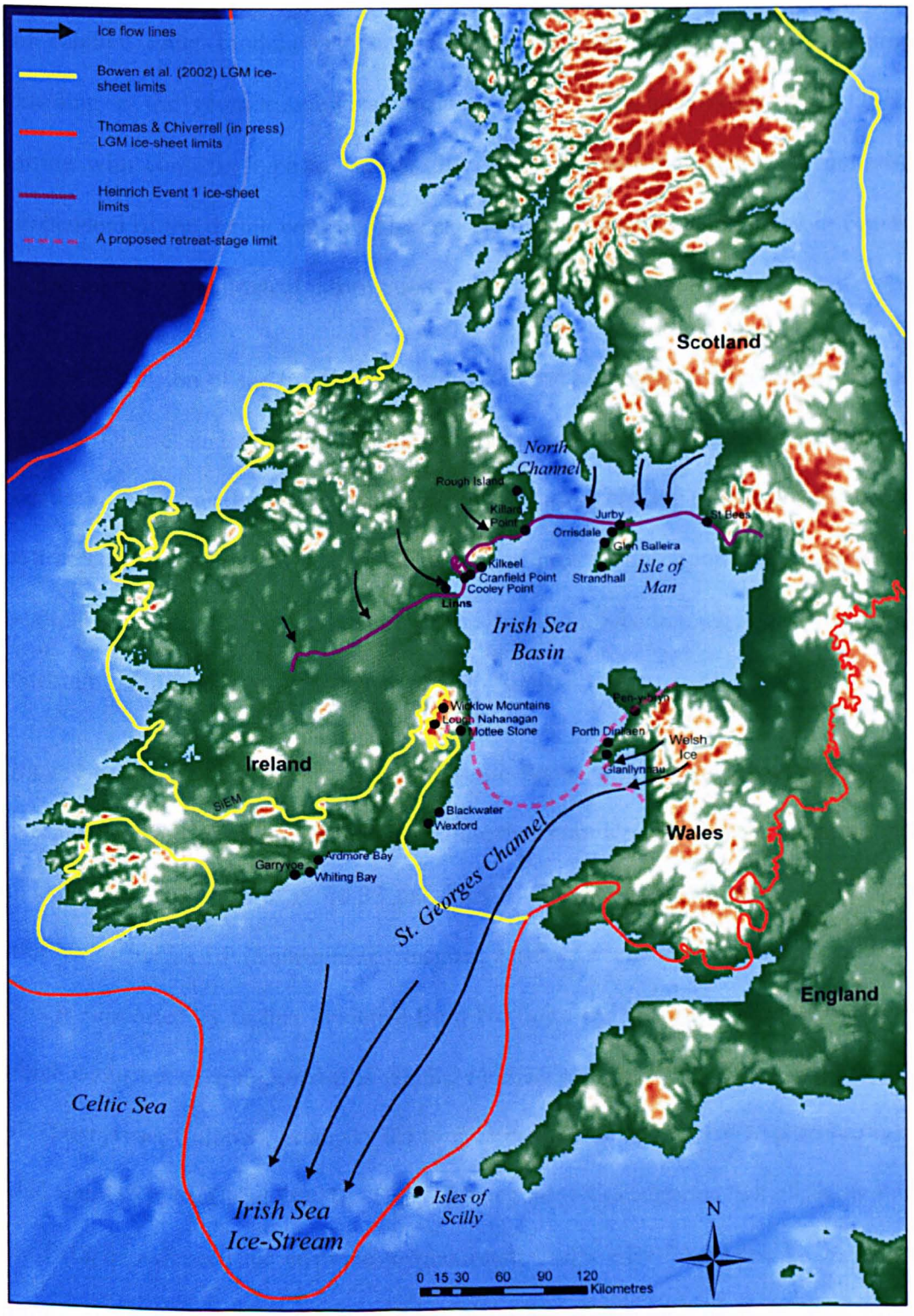

Figure 6.1 *Map showing the LGM limits of the ISIS (red) and the limits previously proposed by Bowen et al. (2002) (yellow). The Heinrich Event 1 readvance limits are also shown (purple). A proposed retreat-stage ice marginal limit is also highlighted (pink). Locations referred to in the text are marked on the map.*

6.3 Dating the advance and retreat of the ISIS

The relative order model was constructed by arranging the dating information according to the geomorphological sequence of advance and retreat of the ISIS, starting with contexts hypothesised as the oldest and finishing with the youngest, independent of the dating control. The relative order model is summarised in Figure 6.2 and all the chronological information is given in Table 6.1.

The last expansion of ice from source regions in the mountains of Scotland, Ireland, the Lake District and Wales is recorded in thick sequences of glacigenic sediments. Locally buried beneath these deposits accumulations of organic mud and peat record ice-free conditions prior to this ice advance, and provide an opportunity to generate maximal ages for this ice advance. These basal radiocarbon ages provide TPQ constraint on the onset of the advance to LGM limits.

Organic deposits which lie beneath glacigenic deposits in the mountain ice-source areas, such as the Scottish Highlands and the Southern Uplands constrain the timing of glacier expansion to after 40-33 cal. ka BP (Balglass; Brown, et al., 2007) and after 39-34 cal. ka BP (Sourie near Glasgow; Jardine, et al., 1988; Bos, et al., 2004). This is supported by further evidence from Northern Ireland where organic deposits which occur between regional tills yielded radiocarbon ages ranging from 31 cal. ka BP (Derryvree; Colhoun, et al., 1972) to greater than 48 cal. ka BP (Aghnadarragh; McCabe, 1987; McCabe, 2008b). This evidence therefore suggests that all sectors of the BIIS experienced ice advance to maximum limits after 35-30 cal. ka BP. The timing of ice advance for the ISIS itself is further constrained by basal ages from sites around the perimeter of the ISB as reviewed in this section.

6.3.1 Basal (advance) ages

The Isle of Man, in the centre of the Irish Sea, has been buried during successive advances of ice from source areas in western Scotland during the Quaternary (Thomas, et al., 2006), though the surface geology reflects entirely the late MIS 2 advances and retreat cycle of the ISIS. Organic mud beneath MIS 2 Irish Sea diamict at Strandhall (see Figure 6.1) reflects period of ice-free conditions dated to 42,500-40,008 cal. a BP (Thomas, et al., 2006; Roberts, et al., 2007), and this provides TPQ constraint on the expansion of ice out from source areas in Scotland. On the flanks of the mountains of north-west Wales most of the glacial sediments were deposited during late MIS 2 and reflect the actions of locally-sourced Welsh ice and the ISIS (Whittow and Ball, 1970; Addison, 1990; Chambers, et al., 1995; Thomas and Chiverrell, 2007). During this period, the ISIS abutted against the mountain front of Snowdonia to a height of at least 200 metres and overran much of Anglesey and the Llŷn Peninsula (Thomas and Chiverrell, 2003). The MIS 2 glacigenic sediments and landforms along the north-west coast of Wales document the advance and subsequent retreat of the eastern margin of the ISIS and the zone of coalescence between the eastern margin of the ISIS and the adjacent Welsh ice-sheet (Thomas, et al., 1998; Thomas and Chiverrell, 2007). A sequence of organic deposits (including wood) buried by glacigenic sediments at Pen-y-bryn, Lower (Welsh) Till; Intermediate Gravels (proglacial outwash) and Upper (Irish Sea) Till (Addison, 1990; Addison and Edge, 1992), are at present unique in Wales (Chambers, et al., 1995). Radiocarbon dating of these organic remains produced age determinations between 60-40 cal. ka BP (see Table 6.1 for details) (Chambers, et al., 1995), and are therefore thought to be of Early Devensian age, before the ISIS had reached this location.

6.3.2 Maximum extent ages

There has been much debate over the maximum extent of the BIIS in the Celtic Sea during MIS 2, some holding that the ISIS extended far south into the Celtic Sea reaching the Scilly Isles (Scourse, 1991a; Scourse, et al., 1991; Ó Cofaigh and Evans, 2001a; Ó Cofaigh and Evans, 2001b; Hiemstra, et al., 2006; Ó Cofaigh and Evans, 2007), whilst others have suggested a more restricted extent (Bowen, et al., 2002; Knight, 2004). Advance to the maximum southern limit in the Celtic Sea is thought to have been a short-lived and unstable event facilitated by subglacial bed conditions rather than a response of the ice-sheet to climate forcing alone (Ó Cofaigh and Evans, 2007).

6.3.2.1 The Scilly Isles

Vibrocores from the UK sector of the Celtic Sea showed marine sands overlying thin glacigenic sediments which drape the sand ridges (Scourse, et al., 1991). The glacigenic sediments comprise two facies. The northern, or Melville Till, consists of clast-rich, over-consolidated till or proximal glaciomarine sediment with a sparse, reworked microfauna and an erratic suite consistent with derivation from the north. It extends out for a hundred km beyond the Scilly Isles and is correlated with the on-shore till of the northern Scilly Isles. The southern facies, which extends as far as the shelf break are distal glaciomarine silty clays with an abundant, in-situ, cold water microfauna (Scourse and Furze, 2001). Together these facies confirm the margin of a large, terrestrially-based ice-stream running from the southern Irish Sea Basin, to the west of the Scilly Isles, through a grounding line some 100 km from the shelf edge, out into deeper water. The outer, eastern edge of this stream is marked by a moraine that crosses the north-western Isles of Scilly (Scourse and Furze, 2001; Scourse, et

al., 2006). The MIS 2 stratigraphy present on the northernmost islands of the Scilly Isles has attracted some controversy (Eyles and McCabe, 1989; Scourse, 1991a) although opinion has converged on terrestrial rather than marine glacigenic origin for the Scilly Till (correlative of the Irish Sea Till).

Organic deposits that predate lithological units associated with the glacial advance (Scilly Till, Tregarthen Gravel, Hell Bay Gravel and the Old Man Sandloess) have yielded radiocarbon ages (Q-2410; 41,508-38,200 cal. a BP and Q-2358; 27,948-23,612 cal. a BP) and provide TPQ constraint on the timing of advance of the ISIS into LGM limits in the Celtic Sea (Scourse, et al., 2004; Scourse, et al., 2006). OSL ages from periglacial soliflucted material (Porthloo Breccia) are affected by incomplete bleaching of the quartz and provide only *maximum* ages of 49.0 ± 3.0 ka (Scourse, et al., 2004; Hiemstra, et al., 2006). OSL ages for samples taken from the Scilly Till and associated glaciofluvial sands (Tregarthen Gravel) are also affected by incomplete bleaching probably due to the glaciofluvial depositional environment, thus age estimates were based on minimum equivalent dose values and were calculated as 25.1 ± 2.2 ka and 22.7 ± 0.9 ka (Scourse, et al., 2004; Scourse, et al., 2006). The geochronological control obtained for the glacigenic sequence on the Scilly Isles confirms its association with advance of the ISIS to its maximum southern limit and constrains its timing (Scourse, et al., 2006).

6.3.2.2 Southern Ireland

The stratigraphy and sedimentology of the Quaternary succession along the south coast of Ireland has been well documented (Synge, 1978; Warren, 1985; Ó Cofaigh and Evans, 2001a). In summary, Irish Sea Till overlies a raised marine platform

which was deposited at a time of raised relative sea level. Overlying the marine platform are local provenance periglacial deposits which in turn buried the glacigenic stratigraphy. The glacigenic sequence had long been regarded as pre Late MIS 2 or older based on the grounds that the deposits lie well beyond the traditional LGM limit at the Southern Ireland End Moraine (SIEM; see Figure 6.1) (Bowen, et al., 2002). However, recently it has been suggested that the BIIS was more extensive during the LGM advance and may have covered most of Ireland (Scourse, 1991a; Scourse, et al., 1991; Ó Cofaigh and Evans, 2001b; Ó Cofaigh and Evans, 2001a). Ó Cofaigh and Evans (2007) regard the Irish Sea Till as having been deposited as sub-glacial diamict during this advance and as a corollary of the Scilly Till found in the northern Scilly Isles. This muddy Irish Sea diamict contains a variety of reworked marine macro- and micro-fauna. These shells were reworked by a grounded ISIS during its last advance into the Celtic Sea from marine sediments either subglacially (scoured from the sea floor by the advancing ice-stream) or glaciotectonically (stacked and thrusted during basal glacial transport) (Van der Meer, et al., 1994; Ó Cofaigh and Evans, 2001a; Evans and Ó Cofaigh, 2003a; Ó Cofaigh and Evans, 2007). The radiocarbon dating of the shells would therefore provide a *maximum* age (TPQ) for the timing of the advance of the ISIS to its maximum hypothesised limits. A population of 26 radiocarbon ages were obtained by dating of individual shell fragments, and they range in age from ~23 cal. ka BP to a maximum of 47.5 ^{14}C ka BP (out of calibration range) (Ó Cofaigh and Evans, 2007). The youngest three radiocarbon ages were taken as providing maximum age information (see Table 6.1), with a calibrated age range of 28.1-23.9 cal. ka BP.

6.3.3 Retreat stages

6.3.3.1 Co. Wexford, south-eastern Ireland

In south-eastern Ireland the glacigenic stratigraphy has been well documented (e.g. Thomas and Summers, 1982; 1983; Thomas and Kerr, 1987; Evans and Ó Cofaigh, 2003a). The most extensive exposure of the stratigraphy occurs along the Co. Wexford coastline which coincides with the Screen Hills; a kame and moraine complex riddled with kettleholes (Figure 6.1). The broad glacial stratigraphy consists of the Irish Sea Till (*Macamore Member*) overlain by laminated silts and clays (*Knocknasilloge Member*) and a sequence of thick and widely exposed sands and gravels deposited by braided proglacial outwash streams (*Screen Member*) (Thomas and Summers, 1983). The stratigraphy reflects the rapid retreat of the ISIS margin from its maximum limits in the Celtic Sea to the coast of south-eastern Ireland where it appeared to stabilise due to the narrow passage of St George's Channel helping to promote comparative ice-sheet stability, slower retreat and numerous ice-marginal oscillations as represented by the frequently glaciotectonised deposits exposed along this section of coastline (Thomas and Summers, 1983; McCabe, 1987; Evans and Ó Cofaigh, 2003a; Thomas, et al., 2004; Ó Cofaigh and Evans, 2007). OSL dating of the proglacial outwash at Blackwater (Figure 6.1) encountered problems associated with poor bleaching of the OSL signal. As a consequence the ages provide a *maximum* age for deposition of the Screen Member (see Chapter 5) and it is a plausible hypothesis that had a dominant population of well-bleached grains been present the ages may have been younger. The youngest of the four OSL ages (see Table 6.1) constrains the ice marginal sandur to 23.6 ± 2.4 ka.

6.3.3.2 Co. Wicklow, eastern Ireland

The Wicklow mountains are some 20km inland of the coastline of eastern Ireland and further 30 km north from the Screen Hills ice marginal terrain. During the MIS 2 glaciation the Wicklows supported an independent ice cap that interacted with inland and Irish Sea ice (Warren, 1993; Ballantyne, et al., 2006).

Geochronological investigations in this region focused on ice retreat and the exposure of 'fresh' bedrock or eroded boulder surfaces, as these can be dated by cosmogenic ^{10}Be and ^{36}Cl isotope techniques (Bowen, et al., 2002; Ballantyne, et al., 2006). Bowen et al. (2002) targeted a glacial erratic granitic boulder (the Mottee Stone) for ^{36}Cl dating southeast of the Wicklow Mountains in the lowlands and produced exposure ages of 22.3 ± 2.0 ka. Ballantyne et al. (2006) dated glacially-scoured bedrock producing ^{10}Be exposure ages of 46.9 ± 3.0 ka and 95.9 ± 6.1 ka from high altitude sites, probable nunataks above putative LGM trimlines of the Wicklow ice-dome. There remains some uncertainty as to whether these 'trim-lines' reflect the former ice-sheet surface or horizontal thermal boundaries within the ice (eg: base of cold-based and non-erosive ice). Lower altitude sites that were overrun by ice yielded a narrow range of ^{10}Be exposure ages of 18.2 ± 1.2, 18.5 ± 1.2 and 19.1 ± 1.2 ka (1σ errors), all of which were consistent with emergence of actively glaciated summits from under a cover of erosive ice after the LGM (Ballantyne, et al., 2006).

6.3.3.3 North-western Wales

A more fragmentary chronology exists for the glacial succession in north-west Wales. The generalised glacial sequence observed in the exposed cliff sections of the

Llŷn Peninsula coastal area consists of a threefold succession of Irish Sea Till overlain by an Intermediate Series of sands and gravels and an Upper Till of Welsh upland origin. Radiometric dates from a moss layer embedded in grey silty clay below the Allerød horizon at Glanllynan indicated that the Llŷn Peninsula was ice free by 18,550-16,450 cal. a BP (Coope, et al., 1971), thereby giving a *minimum* age (TAQ) for the overlying Devensian glacial succession. At Porth Dinllaen on the Llŷn Peninsula, the Intermediate Series of sands and gravels have been interpreted by Thomas and Chiverrell (2007) as representing an unconstrained lower fan sandur environment located some distance from the direct influence of a feeding ice margin. These ice-distal proglacial deposits have been dated via OSL techniques to 21.3 ± 1.2 ka (see Chapter 5).

6.3.4 Readvance stages; Killard Point Stadial

The Killard Point Stadial has been linked to North Atlantic cooling as a result of Heinrich Event 1 (McCabe and Clark, 1998; McCabe, et al., 1998; McCabe, et al., 2005) and the readvance was associated with fast ice flow, drumlinization and subglacial sediment transfer to a prominent moraine system that was inferred to extend from the Bride Moraine on the Isle of Man to St Bees on the Cumbrian coast and Killard Point on the Irish coast. The age of this readvance has been constrained by an array of AMS radiocarbon dates from north-eastern Ireland, and OSL and AMS radiocarbon dating of associated glacigenic sediments on the Isle of Man. Unfortunately, little chronological work has been undertaken in Cumbria, and so limiting our knowledge of the timing and maximum extent of the eastern margin of the ISIS at this time.

6.3.4.1 North-eastern Ireland

One of the richest areas for chronological information related to the MIS 2 glacial succession is the north-eastern Irish coast due to the abundant exposure of glacigenic deposits hypothesised to be related to the Heinrich Event 1/Killard Point Stadial. A variety of ice-contact landforms are evident on the margins of Dundalk Bay (Figure 6.1) and Carlingford Lough where moraines and ice-contact deltas overlie interstadial muds and mark the former extent of grounded ice lobes that are thought to have ended in shallow marine settings (McCabe and Clark, 1998). The age of this readvance is constrained by AMS radiocarbon dating of benthonic foraminifera (*Elphidium clavatum*) from marine mud below and interbedded with ice-contact outwash deposits at sites along the ice limit in north-eastern Ireland; Rough Island, Killard Point, Cranfield Point, Cooley Point and Kilkeel (see Figure 6.1 and Table 6.1). This ice-sheet readvance, the Killard Point Stadial, occurred ~18.8-16.4 cal. ka BP, (McCabe and Clark, 1998; McCabe, et al., 1998) and represents a major glacial readvance between the LGM and the Younger Dryas Stadial. At the Killard Point type locality, the readvance is marked by terminal outwash deposits with AMS radiocarbon ages of 16,900-15,950 cal. a BP (McCabe, et al., 1998). Further AMS radiocarbon dates from benthonic foraminifera have been calculated for this region which are in agreement with those of McCabe and Clark (1998a) and provide further constraint for the timing of this readvance (e.g. Clark, et al., 2004b; McCabe, et al., 2005).

6.3.4.2 Isle of Man

A series of ice marginal oscillations are recorded on the northern plain of the Isle of Man and have tentatively been correlated with the Killard Point readvance in north-

eastern Ireland (Thomas, et al., 2004). The presence of the promenant Bride Moraine towards the northern plain of the island provides a maximum ice-marginal limit for this readvance (Figure 6.1). The lack of organic matter within the glacigenic sediments themselves has limited further refinement of this chronology. AMS radiocarbon dating of terrestrial plant macrofossils from kettleholes at Orrisdale and Jurby suggested the readvance occurred before 15.0-14.2 cal. ka BP (Roberts, et al., 2006). During deglaciation, the Orrisdale area on the west coast of the Isle of Man (Figure 6.1) was the location for a series of successive ice-marginal positions with margin-parallel sandur systems trapped between the northwards retreating ice margin and the lower Palaeozoic bedrock of the Manx Uplands (Thomas, et al., 2006). The stratigraphy at Orrisdale is exposed in 8 km of continuous coastal section, with the glaciofluvial deposits stratigraphically defined as the Bishop's Court Member of the Orrisdale Formation (Thomas, et al., 1985; Chiverrell, et al., 2001; Thomas, et al., 2006). OSL dating of the ice-marginal glaciofluvial deposits produced five OSL ages ranging from 16.4 ± 1.5 ka to 14.1 ± 1.2 ka, and these span the hypothesised timing for the Killard Point readvance (~16 ka).

6.4 Testing the relative order model

Our proposed relative order model of dated contexts is summarised in Figure 6.2, with the ages arranged entirely based on interpretation of stratigraphical and geomorphological information. The relative order model consists of eight Phases. Each Phase relates to a period of glacigenic deposition at geographical locations through the ISB and are ordered from south to north, underpinned by the assumption that marginal retreat occurred in a northwards direction. Exceptions to this structure are that Phases 1 and 8 provide TPQ and TAQ control respectively for the MIS 2

glacial event as a whole and are therefore not limited to one geographical location. Each Phase is separated by a Boundary which represents a time period of ice stream retreat to the subsequent Phase and whilst these Boundaries cannot be dated directly the Bayesian approach allows calculation of probability-based age estimates using the Sequence of age control.

The conformability of this model has been tested using Bayesian approaches in OxCal (Buck, et al., 1996; Bronk Ramsey, 2001; 2008a; Chiverrell, et al., 2008; Foster, et al., In Press), a process that helps to identify outlier ages and contexts that are out of sequence. Sequence models can be regarded as conformable if the agreement index exceeds 60%; the process and justification for this threshold, albeit a little arbitrary, are summarised below (after Bronk Ramsey, 2008). The agreement index is calculated for both the model as a whole and for each modelled age, and in simplest terms it reflects the area of overlap between the prior un-modelled data and (modelled) posterior density functions, expressed as a percentage. The lower the percentage overlap, the lower the agreement between the data and the imposed relative order model, and where the agreement index is lower than 60%, this highlights problem ages that either require re-evaluation of the relative order model or that the problematic ages need explaining.

For initial runs (not shown) all ages (Table 6.1) were incorporated producing an agreement index of 2.3%, which reflects that certain ages do not conform with our relative order model. The ages that had low individual agreement indices included OSL ages BLA3 (212-250), BLA1 (90-125), BLA1(180-212) from Co. Wexford and OR26(90-125) from the Isle of Man. The BLA samples were taken from an ice-

contact glaciofluvial alluvial fan system; the implications of this being a high likelihood of poor-bleaching with a resulting significant age overestimate. Sample OR26 (90-125) was taken from a deep glaciofluvial sandur palaeo-channel and is also thought to have been insufficiently bleached upon transport and deposition within a turbid and turbulent water column, resulting in age overestimation (Chapter 5). The radiocarbon age (Birm-212), taken from organic deposits overlying the glacigenic sequence at Glanllynnau (northwestern Wales), should be younger than all the ages obtained for the Killard Point Stadial readvance, however its 2σ age range of 18.5-16.4 cal. ka BP is actually older and is therefore out of sequence. This radiocarbon assay was obtained from a moss-rich layer from the base of a kettlehole sequence, but some of the dated moss fragments may have been from aquatic species and thus subject to hard water errors (Coope and Brophy, 1972). Wider comparison in this age sequence supports this conclusion identifying clear age overestimation. All these age determinations were excluded from subsequent Bayesian assessment of the relative order model.

Assessment of the revised relative order model (Figure 6.3), excluding these ages produced considerable improvement of the agreement index to 76.9% (see Figure 6.3); higher than the 60% threshold suggestive of a 'conformable sequence'. This indicates that our chronological framework now sits well within the stratigraphical, geomorphological and geographical evidence. For each phase, a probability-based boundary age which brackets that phase has been calculated (see Figure 6.3) and this information helps to constrain the timing of significant phases in the retreat history of the ISIS.

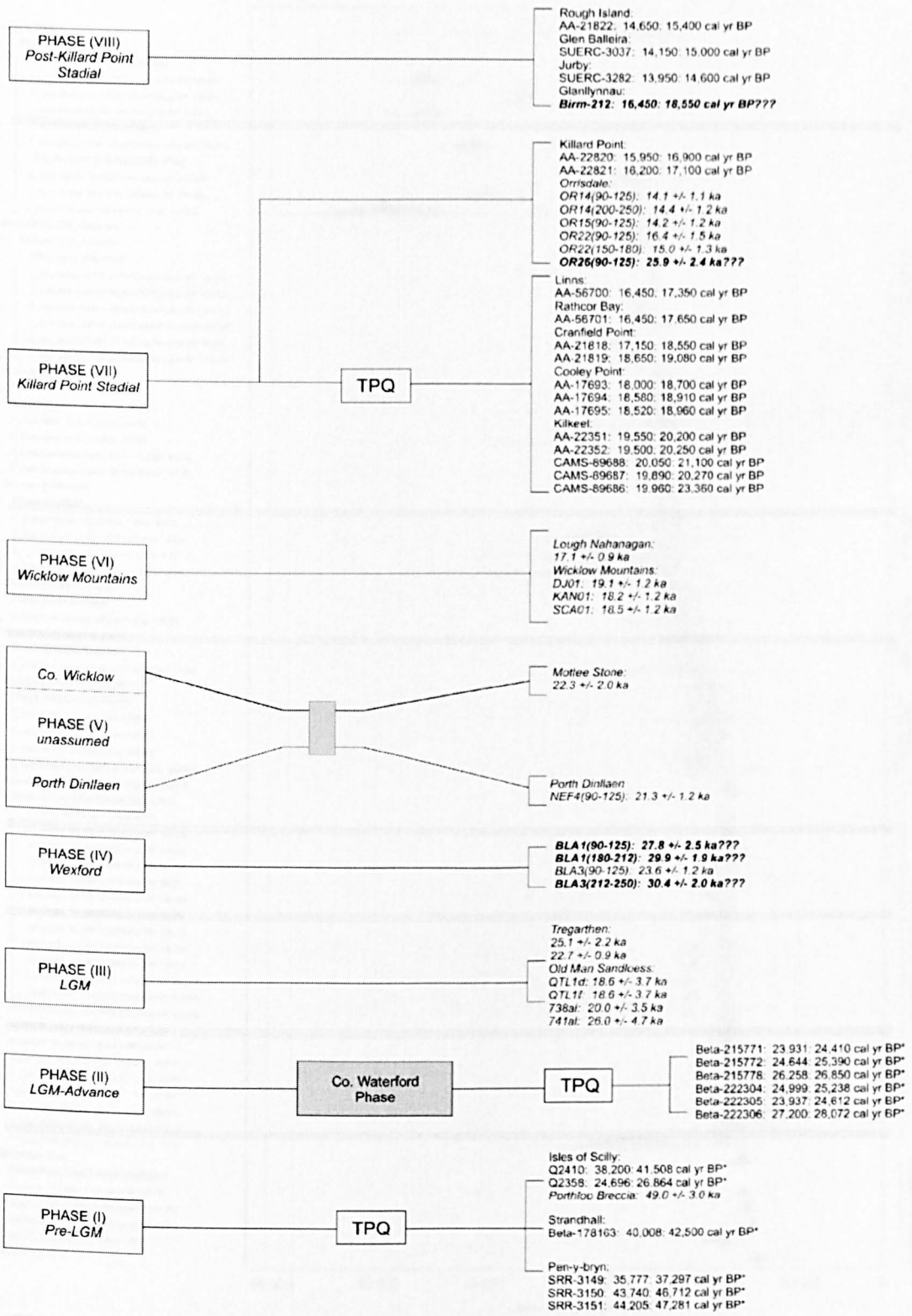

Figure 6.2 *Relative order model for retreat of the ISIS input to OxCal v.3.10. TPQ and TAQ ages which constrain the timing of each phase are clearly indicated. Those dates in bold followed by ??? yielded a low agreement index and were subsequently rejected from Bayesian analysis. Ages marked with * were calibrated using Fairbanks et al. (2005) before being input as calendar dates (C_dates). For further chronological information see Table 6.1.*

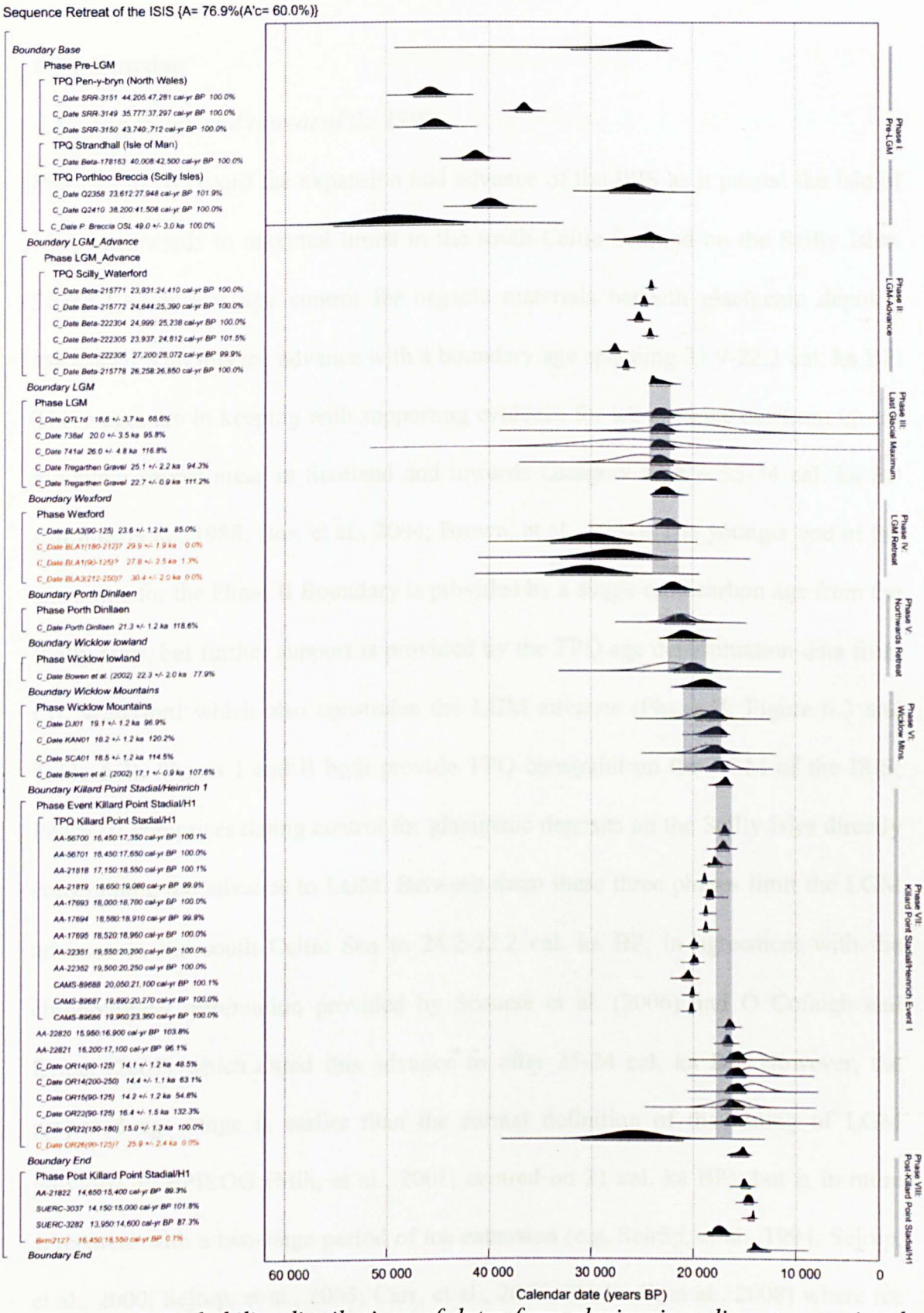

Figure 6.3 *Probability distributions of dates from glacigenic sediments associated with the advance and retreat of the ISIS. Each distribution represents the relative probability that an event occurs at a particular time in cal. a BP. In this sequence, the dates with a low (<60%) agreement index are queried and not included in the Bayesian model (those shown in red). The agreement index of 76.9% is above the acceptance threshold of 60% and shows that the dates within the sequence form an ordered sequence. Each phase is highlighted by grey vertical bars.*

6.5 Discussion

6.5.1 Expansion and retreat of the ISIS

Phases I to III record the expansion and advance of the ISIS as it passed the Isle of Man southwards to maximal limits in the south Celtic Sea and on the Scilly Isles. Phase I comprises age control for organic materials beneath glacigenic deposits associated with this ice advance with a boundary age spanning 31.9-22.2 cal. ka BP. These ages are in keeping with supporting evidence for ice advance out from up-ice mountain source areas in Scotland and towards Glasgow after ~ 35-34 cal. ka BP (Jardine, et al., 1988; Bos, et al., 2004; Brown, et al., 2007). The younger end of the age range for the Phase II Boundary is provided by a single radiocarbon age from the Scilly Isles, but further support is provided by the TPQ age determination data from Co. Waterford which also constrains the LGM advance (Phase II; Figure 6.3 and Table 6.2). Phases I and II both provide TPQ constraint on the LGM of the ISIS; Phase III comprises dating control for glacigenic deposits on the Scilly Isles directly constraining the advance to LGM. Between them these three phases limit the LGM advance in the south Celtic Sea to 24.2-22.2 cal. ka BP, in agreement with the chronological information provided by Scourse et al. (2006) and Ó Cofaigh and Evans (2007) which dated this advance to after 25-24 cal. ka BP. However, the proposed age range is earlier than the formal definition of the timing of LGM provided by EPILOG (Mix, et al., 2001; centred on 21 cal. ka BP), but is in more agreement with a two-stage period of ice extension (e.g. Sejrup, et al., 1994; Sejrup, et al., 2000; Sejrup, et al., 2005; Carr, et al., 2006; Bradwell, et al., 2008) where ice reached a maximum early between 30-24 cal. ka BP, with a retreat and subsequent readvance in the period 24-20 cal. ka BP (Thomas and Chiverrell, submitted). The ISIS is proposed to have reached its maximum extent into the Celtic Sea during this

later phase of readvance. This argues for asynchrony within the BIIS, with North Sea and north of Scotland maximum ice limits being reached much earlier (30-25 cal. kyr BP; Carr, et al., 2006; Bradwell, et al., 2008). This asynchrony is thought to be part-driven by local factors such as variation in the ice-marginal environment (marine or terrestrial termination), sedimentary bed conditions (easily deformable) and the internal dynamics of ice-streams and ice-lobes (Thomas and Chiverrell, submitted).

Phase IV relates to when the ISIS margin had retreated from LGM extent and was positioned along the Co. Wexford coastline and has been be constrained to between 23.9-21.4 cal. ka BP (Table 6.2). To some extent the overlap between the LGM of the ISIS and Phase IV is a function of the errors associated with some of the ages. Nevertheless, the overlap is also suggestive of rapid retreat of the ISIS margin from its LGM position to the coastline of Wexford. The oldest age for Phase III (24.2 cal. ka BP; maximum extent of ISIS, see Table 6.2) and the youngest plausible age for the period of sedimentary deposition at Co. Wexford (21.4 cal. ka BP; Table 6.2) were taken to calculate the maximum possible time frame (2800 years) in which the ISIS retreated ~280 km from the Celtic Sea to the present-day coast of southeastern Ireland. Alternatively, if mid-range age estimates are taken for Phases III and IV, an approximate minimum retreat period of 600 years is calculated. These estimates range encompass retreat rates of ~100-470 metres per annum. These are in agreement with the proposition that the outlet lobes which drained the BIIS, such as the ISIS, responded rapidly to a glacio-eustatic sea-level rise driven by Laurentide Ice-sheet (LIS) ice-berg discharges, whereby positive feedbacks caused destabilisation of ice-sheets at, or close to, sea-level elsewhere (Scourse, et al., 2000; Scourse and Furze, 2001). Rapid wastage of the ISIS margin in a glaciomarine environment at its

maximum extent is further corroborated by evidence from Ice-Rafted Detritus (IRD) records from the continental slope of the Goban Spur, south of the Porcupine Sea Bight (Hall and McCave, 1998b; a) which contain chalk of a Celtic Sea bed origin which implicates the Celtic Sea lobe of the ISIS as the source material. This indicates that the ISIS contributed to IRD fluxes to the North Atlantic and took part in Heinrich Event 2 destabilisation of the ice-margin, resulting in rapid retreat rates as calculated above. The lack of thick deglacial sediment depocentres along the coastline of southern Ireland, also indicate that the retreat of the ISIS was rapid (Ó Cofaigh and Evans, 2007).

Phase V comprises the 'northwards' retreat of the ISIS from Wexford (Figure 6.3) and consists of two sub-phases probably of similar timing; the deglaciation of the lowland Wicklow area and of the Llŷn Peninsula in North Wales. These sites are on opposite sides of the Irish Sea Basin and formed the western and eastern margins of the ISIS. Figure 6.1 shows the proposed retreat stage ice-margin limit. Retreat from Co. Wexford to this retreat-stage position in the Wicklows and at Porth Dinllaen (~100 km) is constrained to the period 23.3-18.7 cal. ka BP (see Table 6.2). This time range spans the EPILOG definition of LGM (centred on 21 cal. ka BP) and thus emphasises the asynchrony with global ice volume given the ISIS sector of the BIIS had retreated almost 420 km during the last global ice volume maximum (Mix et al., 2001).

The ages for deposition at Co. Wexford (23.9-21.4 cal. ka BP) and Llŷn/Wicklow (23.3-18.7 cal. ka BP) are suggestive of marginal retreat rates of between ~20 and 65 metres per annum covering distances of ~100 km; an order of magnitude slower than

that from LGM to Wexford, which perhaps reflects the stabilisation of the ice-stream between the narrow corridor of Ireland and Wales. This slower rate, resulting from a grounded ISIS (Van Landeghem, et al., 2008) retreat is supported by sedimentological evidence from along the coastlines of southeastern Ireland (e.g. Thomas and Summers, 1982; 1983; 1984; Thomas and Kerr, 1987; Evans and Ó Cofaigh, 2003a), eastern Ireland (north of Dublin) (Eyles and McCabe, 1989; McCabe, 2008b) northwestern Wales (Harris, et al., 1995; Harris, et al., 1997; Thomas, et al., 1998; Thomas and Chiverrell, 2003; Thomas and Chiverrell, 2007) which are characterised by glaciotectonic deformation structures (closely-spaced thrust ridges) indicative of multiple small-scale readvances or oscillations of the ice-margin during overall retreat. The Wicklow Mountains themselves deglaciated later than the surrounding lowland area and an age range for this phase (Phase VI) is calculated as 20.9-17.2 cal. ka BP, younger than that of Phase V, probably a function of local ice source areas, the Wicklow ice dome (Charlesworth, 1928; Warren, 1993; Ballantyne, et al., 2006).

Northwards from Llŷn/Wicklow there is a considerable geographical gap before the next published dating of ice marginal positions/limits and these are in the north ISB on the Isle of Man and on the northeastern coast of Ireland. This region has been proposed as the location of a substantial re-advance episode during the decline of the last BIIS and the sequence of events has been correlated with drivers in the North Atlantic and Heinrich Event 1 (McCabe, 1996; McCabe and Clark, 1998; McCabe, et al., 1998; McCabe, et al., 2005). Phase VII contains all the chronological information that constrains and directly dates this readvance. The abundance of AMS radiocarbon and OSL ages for this phase means that it is tightly constrained to between 17.7-16.2

cal. ka BP. There is now significant evidence to suggest that the Killard Point Stadial readvance occurred contemporaneously across north-western Ireland and across the northern plain of the Isle of Man, despite differing ice-source areas, with the readvance limit extending from Killard Point, across the Irish Sea Basin and the northern plain of the Isle of Man (Figure 6.1). The presence of the prominent Bride Moraine across the northern plain of the Isle of Man (Thomas, 1984) together with OSL-dated glaciofluvial outwash deposits to the south of this feature provide evidence for this. This argues for a basin-wide ISIS response to North Atlantic cooling; although rapid wastage of the ISIS is not recorded in North Atlantic IRD records as the glacially derived material was no longer able to bypass the shelf to the continental slope due to either very shallow water (resulting in ice-berg grounding) or a Celtic shelf landbridge connecting mainland Britain with Ireland at this time (Scourse and Furze, 2001), so preventing transfer via ice rafting. Unfortunately, no chronological information is available for the Cumbria sediments (e.g. Trotter, et al., 1937; Huddart, 1971; 1977; 1991; 1994; Thorne, et al., 1997; Merritt and Auton, 2000) that are also thought to be associated with the Killard Point Stadial, as indicated by the presence of the St. Bees Moraine. Further refinement of the timing and geographical extent of this phase could be achieved by dating ice marginal contexts across the Carlisle lowlands. Notwithstanding considerable gaps in our chronological understanding, this Bayesian modelling approach has allowed the sequence of deglaciation to be more tightly defined and offers considerable scope for maintenance and robust assessment of this database of chronological information to which further age control can be added.

Table 6.2 Probability-based boundary age estimates derived from Bayesian analysis using OxCal (v.3.10).

Phase Number	Phase Name	Probability-derived boundary age (cal. ka BP)	Mid-range age (cal. ka BP)
I	Pre-LGM	31.9-22.4	-
II	LGM-Advance	26.7-22.4	-
III	LGM	24.2-22.2	23.2
IV	Wexford	23.9-21.4	22.6
V	Northwards retreat [1]	23.3-18.7	21.0
VI	Wicklow Mountains	20.9-17.2	19.0
VII	Heinrich Event 1	17.7-16.2	16.9
VIII	Post-Heinrich Event 1	16.3-14.5	-

[1] 'Northwards retreat' phase consists of two ages from different locations on the perimeter of the Irish Sea Basin; Mottee Stone (eastern Ireland) and Porth Dinllaen (northwestern Wales). During Bayesian analysis, contemporaneous deposition at each location was ***not*** assumed. However, the similarity of the probability-derived boundary age suggests that glacigenic deposition at the aforementioned locations was indeed contemporaneous (representing the eastern and western margins of the ISIS) and has subsequently been merged into one phase. See Figure 6.1 for a hypothesised retreat-stage ice-marginal limit at these locations.

6.5.2 Wider implications: palaeoglaciology and sea-level modelling

The geochronological control for the last ISIS highlights rapid advance from source areas after 35-34 cal ka BP and expansion over 400 km to maximal limits in the south Celtic Sea. Retreat from these maximal limits appears to have been accomplished equally rapidly. The land-system approach and interpretation of glacial bedforms (Clark and Stokes, 2001) supports the identification of palaeo-icestreaming in the Irish Sea Basin. High resolution swath-bathymetry for the floor of the Irish Sea just north of Anglesey shows a series of subglacial bedforms; drumlins, flutes and bedrock streamlining, that are all associated with faster ice converging towards the central Irish Sea Basin (Van Landeghem, et al., 2008). The rapidity of ice advance and retreat implicit in the available chronology agrees with the apparent geomorphological evidence for ice-streaming. The 'slippery bed' BIIS

models derived by Boulton and Hagdorn (2006) also support the presence of a rapidly advancing and retreating ISIS, with retreat rates of up to ~330 metres per annum during deglaciation of the Irish Sea Basin. However, the timing of the ISIS maximum differs as the ice-sheet model is forced by global ice volume maximum of Mix et al. (2001) and cannot take into account asynchrony between and within ice-sheets.

The ISB has attracted considerable debate over whether during the advance and retreat from LGM limits the ISIS interacted with a marine or terrestrial margin. Some authors believe that the deglaciation of the Irish Sea Basin was dominated by a glaciomarine environment with an actively-carving tide-water margin (Eyles and Eyles, 1984; McCabe, 1986; McCabe, 1987; McCabe, et al., 1987; Eyles and McCabe, 1989) whereas others believe that retreat of the ISIS was characterised by a grounded ice-margin (Thomas, et al., 1998; Scourse and Furze, 2001; Hiemstra, et al., 2006). The controversy stems from the proposition that the Irish Sea tills, exposed in sections around the shores of the present-day Irish Sea Basin represent glaciomarine sediments rather than terrestrially deposited till (Eyles and McCabe, 1989). Other authors have held that the depressed eustatic sea-levels during the LGM period (114-135 m below OD) (Fairbanks, 1989) requires improbable glacio-isostatic depression of the earth's crust to produce such a high relative sea-level and resultant glaciomarine sedimentation (Scourse and Furze, 2001). Indeed, substantial evidence for a terrestrially-based and/or grounded ice-stream is present across the entire ISB (e.g. Harris, 1991; McCarroll, 1991; Scourse, 1991a; Scourse, 1991b; Austin and McCarroll, 1992; McCarroll, 1995; Harris, et al., 1997; Thomas, et al., 1998; Merritt and Auton, 2000; Hambrey, et al., 2001; McCarroll, 2001; Ó Cofaigh and Evans,

2001a; Scourse and Furze, 2001; Evans and Ó Cofaigh, 2003a; Glasser, et al., 2004; Thomas, et al., 2004; McCarroll, 2005; Etienne, et al., 2006; Ó Cofaigh and Evans, 2007; Thomas and Chiverrell, 2007; Van Landeghem, et al., 2008). However, glaciomarine models remain controversial at the present time with wide differences in opinion regarding timing, magnitude and causes of deglacial changes in relative sea-level (Eyles and Eyles, 1984; Eyles and McCabe, 1989; McCabe, et al., 1998; McCarroll, 2001; McCabe, et al., 2005). McCabe (2008b) suggested that radiocarbon dated marine cores taken from between the Isle of Man and the coast of Co. Down (Kershaw, 1986) ***suggest*** that a marine seaway developed along the central trough of the Irish Sea Basin between 23-24 cal. ka BP. However, the marine cores analysed showed extensive evidence of bioturbation which may have influenced the distribution of natural and sellafield-derived (plutonium and americium) radionuclides throughout the upper 180 cm of the core. Additionally, a marine carbon reservoir correction was not undertaken. Both such factors would potentially result in erroneous age determinations.

In addition, swath-bathymetry data from the northern sector of the ISB notes the extensive presence of iceberg pits and ploughing marks offshore of north Wales. However, the evidence was inconclusive as to whether this indicated full glaciomarine conditions or the presence of a glaciolacustrine setting (Van Landeghem, et al., 2008). More extensive analysis of this type needs to be undertaken to evaluate the spatial pattern of grounded-ice deforming bed conditions and glaciomarine indicators which are critical for understanding the evolution of the ISIS during advance and subsequent retreat stages. The rapid rates of retreat calculated here for the initial stage of deglaciation of the Celtic Sea/Irish Sea Basin

suggest that ice-marginal termination in a water body is possible (Scourse and Furze, 2001). The slower rates of retreat calculated from St. Georges Channel northwards indicated a more stable, grounded ice stream with ice-marginal termination in a terrestrial environment. This could be related to the raised terrain across St. Georges Channel which prevented further incursion of the shallow marine environment.

The past 30 years has seen a plethora of models for glacio-isostatic adjustment for the British Isles (e.g. Lambeck, 1991; 1993a; b; Lambeck, et al., 1996; Peltier, et al., 2002; Shennan, et al., 2006; Brooks, et al., 2008). These models combine eustatic and isostatic components of sea level adjustment and they are geophysical in part, driven by an Earth model (to simulate deformation of the solid Earth to surface loading), an ice model (to define the global distribution of grounded ice thickness over time) and the sea-level model (which generates sea-level predictions based on input from the Earth and ice models) (Brooks, et al., 2008). In the south Celtic Sea and ISB they show relative sea level of ~ 50-60 metres *below* OD during the period 20-15 ka (Brooks, et al., 2008). It must be stressed these models are constrained by a series of sea level index points entirely from the Holocene, with little or no direct constraint for the deglacial period. A conflicting sea level record is provided by McCabe (2008b) who presents relative sea-level as 10-20 metres *above* OD in the period 20-15 ka, based upon a series of marine muds situated above present sea-level in northeastern Ireland. Given growing evidence for discrepancies between glaciological and sedimentological evidence and sea-level models, it appears that both need critical re-evaluation. Glaciologically we need definitive evidence marine or otherwise and more extensive data from the sea floor (e.g. Van Landeghem, et al., 2008) to further establish the exact environment of deglaciation of the ISB. Sea-level

modellers require more accurate glacial reconstructions in order to predict the timing and magnitude of glacial rebound and its implications for relative sea-level. It is necessary to know the size (thickness and extent) of the ice-sheet and how much the ice-sheet has changed in size over time i.e. its retreat stages (Brooks, et al., 2008). The results from this research will hopefully be able to inform sea-level modellers as to timing of retreat of the ISIS which can then be incorporated into complex sea-level models with the aim of resolving the wider debate concerning relative sea-levels since LGM. If predictions of sea level using better icesheet geometries fail to provide a better match with the increasingly robust evidence for glaciomarine conditions, though further corroboration on that is still required, then surely the problems must lie elsewhere within the models (McCabe, 2008a)

6.6 Conclusions

This chapter reviews the chronological control available for the advance of the ISIS to LGM limits, and subsequent retreat and readvances episodes. The chronology is composed of a variety of published OSL, TL, radiocarbon and cosmogenic isotope ages and a series of new OSL ages obtained during this research. These varied and widely distributed chronological data have been put into context by analysis of their stratigraphical, geomorphological and geographical inter-relationships. This led to the construction of a relative order model for the chronological control underpinning the advance and retreat of the last ISIS, and the conformability of this was tested using Bayesian techniques to determine the level of agreement with the physical evidence. The Bayesian approach highlighted OSL and radiocarbon ages that did not conform to the relative order model, producing an initial low overall model agreement index of 2.3%. Problem ages were excluded from subsequent Bayesian

modelling, and the agreement index between the chronology and the relative order model increased to 76.9%. This approach also produced probability-based age estimates for each of the boundaries between Phases allowing constraint of the timing of retreat stages of the ISIS.

The timing of the LGM phase which resulted in deposition of Irish Sea Till in southern Ireland and the Scilly Isles is constrained to between 24.2-22.2 cal. a BP. The timing of the Co. Wexford retreat phase is constrained to 23.9-21.4 cal. a BP, which suggests that the ISIS retreated in an extremely rapid manner (between ~100-470 metres per annum) from LGM limits in the Celtic Sea to the coastlines of southeastern Ireland and Wales where it then adopted a much slower retreat (between ~20-65 metres per annum) probably due to the stabilising effect of the narrow corridor between Wales and Ireland (St. Georges Channel). Whether this retreat was characterised entirely by a glaciomarine or terrestrial environment is still under debate. It is known that the terminus of the ISIS at its maximum extent is likely to have been glaciomarine in nature (Scourse and Furze, 2001) but whether sustained retreat in a glaciomarine environment occurred is, at present, unfounded. In reality, it is likely that a variety of ice-marginal retreat environments existed at different periods throughout the deglaciation of the ISB, with the possibility of extensive proglacial lakes or very shallow connecting marine environments, allowing the discharge of icebergs and creation of iceberg scours seen off the coast of north Wales.

The abundance of age determinations for the Killard Point Stadial in the Irish Sea Basin, have allowed the timing of this phase to be constrained to between 17.7-16.2

cal. a BP. Evidence from the Isle of Man confirmed that this readvance limit extended across the Irish Sea Basin. No chronological data is presently available for the hypothesised eastern margin of the Killard Point Stadial readvance limit at St. Bees in Cumbria and so this should be a future priority, to enable the timing and extent to be constrained further. A dearth of chronological evidence is also apparent along the eastern coastline of Ireland, just north of the Wicklow Mountains. McCabe (2008b) present detailed sedimentological stratigraphy for this region and so further dating efforts should be directed towards this area.

Chapter 7

GENERAL CONCLUSIONS & WIDER IMPLICATIONS

7.1 Introduction

Knowledge of the retreat rates of past ice-sheets, glaciers and ice-streams as a response to past climate warming is increasingly important as this is one way by which we can predict the response of present day ice-sheets and glaciers to the expected future climate warming. During MIS 2, the Irish Sea Basin was occupied by the ISIS; a major ice-stream of the last BIIS which was controlled by multiple sources (Southern Uplands, Lake District, north-eastern Ireland and Wales) and acted as an outlet for a large volume of ice which had accumulated in other areas of the BIIS. It has been established that there is considerable controversy concerning the dynamic nature of the ISIS, its maximum extent, how rapidly it retreated and implications that this has for past sea-level reconstructions for the Irish Sea Basin.

Here, OSL dating has been applied to small aliquots of glaciofluvial quartz from three field locations on the present-day Irish Sea perimeter, in an attempt to produce a robust chronology for the MIS 2 retreat of the ISIS. Robust methods and analytical techniques were developed due to challenges associated with poor quartz luminescence characteristics and heterogeneous bleaching of the quartz grains used for OSL dating. These procedures included establishing rejection criteria to identify aliquots containing quartz with dominantly poor luminescence characteristics as well as the use of a statistically-based decision-protocol (Bailey and Arnold, 2006) which allowed the objective selection of an appropriate statistical 'age' model to apply to

D_e datasets for final age determination. Such a decision-protocol is useful when D_e distributions are complicated by significant skewness and overdispersion as a direct result of the heterogeneously-bleached nature of the quartz grains. The palaeoglaciology and retreat chronology for the ISIS has been discussed and interpreted in relation to the constraining chronology provided by other authors. This chapter summarises and outlines the main conclusions and wider implications of this research and suggests future work priorities.

7.2 Summary and conclusions

To determine the rate of retreat of the ISIS, OSL dating was used to assess the age of glaciofluvial sediments which were deposited as a *direct* result of the melting and retreat of terrestrial sectors of the ice-stream margin. Three field sites (*Wexford*, *Porth Dinllaen* and *Orrisdale*), located on a likely retreat path of the ISIS, displayed extensive vertical and lateral exposure of glaciofluvial sediments which allowed an assessment of stratigraphy and lithofacies relationships to be made.

At Orrisdale, a variety of lithofacies that reflected different depositional sub-environments within a distal (sand-dominated) glaciofluvial sandur system were sampled and different grain size fractions extracted from each to investigate the impact that depositional environment and grain size may have had upon the potential for complete bleaching of the optical signal. Sampling was directed towards fining-up sequences (horizontally laminated sand, rippled sand and finely laminated sand) of longitudinal braid bars which were preserved in section. Such lithofacies architecture is associated with waning water flow and as a result, their higher potential for exposure to daylight enables bleaching of a proportion of quartz grains.

The investigation employed at Orrisdale acted as a 'test field site' for the lithofacies approach. The results identified the 'best' depositional sub-environments and resulting lithofacies (in terms of the dominant bleaching status of the assemblage of quartz grains) and this then informed a more directed sampling strategy for optical dating at Wexford and Porth Dinllaen which targeted rippled sands (*Sr*) and finely-laminated sands (*Fl*) of the finer bar-top sequences.

Quartz luminescence characterisation was a necessary step for OSL analysis to enable an appropriate thermal treatment to be determined and to evaluate whether a dominant fast component, as determined by the photoionisation cross-section, was present to validate use of the SAR protocol. Aliquots which showed the presence of quartz grains with a natural-OSL signal were dominated by the fast component in the initial part of the CW-OSL decay curve under blue light stimulation, allowing for application of the SAR protocol. The SAR protocol was used to obtain D_e's from small aliquots (consisting of ~30 grains) of each sample. A preheat of 250°C (10s duration) was applied to Orrisdale samples and 240°C (10s duration) for Wexford and Porth Dinllaen samples. A cutheat of 200°C was used for all samples.

The quartz characteristics of all samples in this research were complex and varied (in terms of thermal transfer, fast component presence) and appeared to be related to the complex nature of their quartz provenance. The numerous lithologies that the quartz could have been derived from (Irish Sea Basin, Northern Ireland, Lake District, Southern Uplands) seems to have caused such widely varying luminescence characteristics. In such samples with complex luminescence characteristics, small aliquots are required for analysis as it enables the different quartz types to be

separated and analysed on an almost individual basis enabling 'isolation' of 'good' quartz i.e. that with favourable luminescence characteristics.

A large percentage of aliquots were rejected due to the lack of any natural optical signal. Many more aliquots were rejected as they did not satisfy the remaining criteria for acceptance. For each sample at least 50 D_e values were obtained to ensure the extent of heterogeneous-bleaching, as indicated by skewness and overdispersion values, was adequately observed. Two gamma spectrometers; a HPGe detector (Pop Top type) and an Ultralow-level Canberra BE50 detector were used to determine the activities used in environmental dose-rates calculation for the samples. The higher efficiency BE50 detector (relative efficiency at 1.33 MeV of 50%) was used for particularly low-activity Wexford samples (<1Gy/ka) to enable a quicker measurement time, increased precision and this also allowed reproducibility of results to be checked. Comparisons were made between the results from both detectors, the results from which confirmed reproducibility of the measured data.

All lithofacies types from the Orrisdale field site showed evidence of heterogeneous-bleaching via significantly skewed D_e distributions (>$2\sigma_c$) with high overdispersion values (39-51%). This is related to the nature of the depositional environment; even though samples were taken from environments relatively distal to the ice margin, the permanently turbid nature of the water column was not conducive to complete bleaching of *all* quartz grains.

A variety of statistical 'age' models (e.g. Galbraith and Green, 1990; Olley, et al., 1998; Galbraith, et al., 1999) have been used to handle the populations of D_e values;

each designed to extract the well bleached proportion of quartz grains in an otherwise heterogeneously-bleached population. Once >50 D_e values had been obtained for each sample, a decision protocol (Bailey and Arnold, 2006) was applied to determine which statistical 'age' model is most appropriate for final D_e estimation and age calculation.

For all of the Orrisdale samples, the MAM-3 was appropriate for D_e determination (after running the decision-protocol) and subsequent age calculation resulted in agreement (within 2σ errors) with the age of *Killard Point Stadial (~16 cal. ka BP)* sediments from north-eastern Ireland (McCabe, et al., 1998). Not all lithofacies types yielded the same age, with the *St* (trough cross-bedded sand) lithofacies producing an age estimation ~10 ka older (according to the MAM-3) than the other lithofacies. The age overestimation of the *St* lithofacies perhaps reflects the dominant poorly-bleached nature of the quartz grains carried in this deep, fast flowing and sediment-laden channel as reflected in the significantly skewed ($>2\sigma_c$) D_e distribution. However, the overdispersion value for this sample is the lowest of all the samples (although they do overlap within errors), and so it would appear to be the best bleached based on overdispersion alone. This type of outlier shows that OSL dating of these types of sediment should be underpinned by the analysis of multiple samples, although this was not possible at Porth Dinllaen.

Varying the grain size fraction of a sample selected for analysis appears to have had little impact on age determination. The D_e distributions for the Orrisdale samples show that glaciofluvial sandur systems have acted as an efficient 'mixer' of sediment grains, and allowed some to be well-bleached and others to be poorly-bleached, with

no bias towards preferential bleaching of a particular grain size fraction. This is perhaps due to the turbid and fast flowing nature of the transport environment; all grain size fractions are heterogeneously-bleached, with no particular grain size fraction being preferentially bleached over another.

For Wexford samples, both grain size fractions of the rippled sand (*Sr*) and finely-laminated sand (*Fl*) lithofacies sampled from the upper part of fining-up sequences in a longitudinal braid bar within proximal-type sediments of the Screen Member showed evidence of heterogeneous-bleaching; overdispersion values were the highest of all samples (47-73%) and D_e distributions were all significantly skewed ($>2\sigma_c$). The application of the decision protocol resulted in the MAM-3 being applied to all D_e distributions apart from that of the 90-125 μm grain size fraction of the *Sr* lithofacies (BLA3) where the L5% was most appropriate. All ages calculated using the MAM-3 gave significant age overestimations in comparison to the constraining chronology for timing of the LGM extent (Bowen, et al., 1986; Bowen, et al., 2002; Scourse, et al., 2004; Scourse, et al., 2006; Ó Cofaigh and Evans, 2007). The age calculated using the L5% model was more realistic (23.6 ± 2.5 ka) and was in stratigraphical agreement with the constraining chronology. Glaciofluvial sedimentation at Wexford, resulting in the deposition of the Screen Member is therefore concluded to have occurred shortly after LGM extent was reached, once the ice-stream had stabilised along the coastline of south-eastern Ireland as indicated by the presence of frequently glaciotectonised stratigraphy exposed in section at this field site. The glaciotectonised stratigraphy occurred as a result of the oscillating ice-margin characterised by small-scale (metres) advances and retreats.

Proximal sandur sediments such as those from Wexford are not recommended for the application of optical dating due to the poor bleaching characteristics evident even in the finer grain size fraction of fining-up sequences. The MAM is inappropriate for such samples as it gives distinct age overestimations. The decision protocol used here to select the appropriate 'age' model is not necessarily applicable to these very poorly-bleached sediments, where only a few of the lowest aliquots appear to represent the real age of the sample. In these samples all 'age' model output gives an overestimation apart from the L5%. Once again, varying the grain size fraction appears to have little difference on the calculated age with each overlapping with one another (within 2σ errors) from the same sample.

At Porth Dinllaen a rippled-sand (*Sr*) was sampled from dominantly ice-distal (sand-dominated) sediments and used for optical dating due to the success of results from using this lithofacies at the other field sites. The D_e distribution of this sample was significantly skewed and had a high overdispersion value (57%) indicative of heterogeneous-bleaching which appears to reflect *most*, if not, *all* glaciofluvial sediments. The application of the decision protocol resulted in the use of the MAM-3 and subsequent age calculation yielded an age of 21.3 ± 2.6 ka. This is younger than the constraining age for the LGM extent (Ó Cofaigh and Evans, 2007) and indeed the optical dates obtained from Wexford. This indicates the timing of deposition at Porth Dinllaen as the ISIS retreated northwards.

In combination with previously published chronological information, OSL dating has enabled a chronology to be established for the ISIS that constrains the timing of retreat phases from LGM position (24.2-22.2 cal. ka BP) and subsequent readvance

into the northern Irish Sea Basin during the Killard Point Stadial (17.7-16.2 cal ka BP) (e.g. McCabe, 1996; McCabe and Clark, 1998; McCabe, et al., 1998; Clark, et al., 2004b). Rapid retreat rates (~100-470 metres per annum) were calculated from LGM limits in the Celtic Sea to St. Georges Channel, northwards of which, retreat of the ice-margin slowed considerably (~20-65 metres per annum). The retreat chronology and inferred rates of retreat during different phases are useful to researchers investigating how contemporary ice-streams (such as those in the Antarctic and Greenland ice-sheets) may respond as a result of predicted future climate warming. Understanding the dimensions of the BIIS during various retreat stages is also critical information for ice-sheet modellers and those investigating the impact of glacio-isostatic rebound upon past sea level changes in the Irish Sea Basin (e.g. Lambeck, 1991; 1993a; b; Lambeck, et al., 1996; Peltier, et al., 2002; Shennan, et al., 2006; Brooks, et al., 2008; McCabe, 2008a; b).

7.3 Future work

The optical dating technique has been successfully applied to distal glaciofluvial sediments and offers considerable scope for future research into constraining the extent and timing of LGM and its subsequent retreat and readvance stages. Although there are a variety of challenges associated with the glaciofluvial sediments analysed in this research (heterogeneous bleaching, poor quartz luminescence characteristics, large numbers of aliquots to be analysed, long measurement times, statistical challenges), an approach has been devised to enable these challenges to be overcome. This approach emphasised the use of lithofacies analysis to aid OSL sample selection, highlighted the importance of investigating sample bedrock provenance and the influence that certain bedrock lithologies may have upon quartz

OSL characteristics. Emphasis was also placed upon the value of detailed quartz OSL characterisation before age determination is undertaken. This optical dating approach can be applied to other localities exhibiting sedimentation as a result of the retreating ISIS margin, allowing the timing of its flow phases to be constrained further.

The Devensian glacial stratigraphy along the north-western Cumbrian coastline has been well documented in the past (Trotter, et al., 1937; Huddart, 1971; 1977; 1991; 1994; Thorne, et al., 1997; Merritt and Auton, 2000) but controversy concerning the timing of stratigraphic formation is ongoing. Some authors (Trotter, et al., 1937; Thorne, et al., 1997; Merritt and Auton, 2000) believe the Late Devensian deposits at St Bees were the product of two oscillations of the ISIS (the earlier Gosforth Oscillation and the later Scottish Readvance) and others (Huddart, 1971; Huddart and Tooley, 1972; Huddart, 1977; 1991; 1994; Huddart and Glasser, 2002) believe it to be a result of a single readvance (the Scottish Readvance) (Williams, et al., 2001).

The stratigraphy at St Bees, Cumbria consists of the Lowca Till; the basal till of the main Late Devensian glaciation which is overlain by the St Bees Silts and Clays, thought to have been deposited in a proglacial lake as a result of damming of regional drainage. The silts and clays are overlain by a coarsening upwards succession of the St Bees Sands and Gravels; the lower part of which indicates low energy, distal, proglacial sandur sedimentation. The upwards-coarsening succession indicates gradual advance of ice towards the St Bees area with the gravel lithofacies representing proximal proglacial sandur sedimentation. The gravels are succeeded by the St Bees Till and the sandy clay, which are considered to be subglacial facies

deposited from the readvance of the ISIS causing vast glaciotectonic deformation (Huddart, 1994).

The presence of the distal proglacial sandur sedimentation facies (the St Bees Sands and Gravels) at this location presents an opportunity to constrain the chronology of the Late Devensian succession via the optical dating techniques applied in this research, and perhaps solve the ongoing debate as to the number of ice advances thought to have produced the glacial stratigraphy observed at St Bees. Together with chronological information from northeastern Ireland and the Isle of Man, a more complete regional picture of ice-sheet readvance during the Killard Point Stadial could then be achieved.

A similar opportunity exists at Kirkham, central Lancashire where the presence of the extensive (~25 km) Kirkham moraine is thought to represent the stacking of glacigenic sediments due to ice-marginal oscillations just before the terminal decline of the BIIS, when rapid ice wastage and ice-marginal retreat denoted the transition to the warm conditions of the late-Glacial interstadial (the Windermere Interstadial) (Thomas, et al., submitted). The moraine displays a complex morphology of glaciotectonised ridges, intervening margin-parallel sandur troughs and ice disintegration ridges and kettle-hole basins (Thomas, et al., submitted). The presence of glaciofluvial sandur sedimentation preserved within the moraine provides an opportunity to date the material using OSL. Although optical age determination would not yield an age relating to when the Kirkham moraine was created, it would give a *maximum* age, as to when the ice-stream margin extended to this area.

There is further scope for the application of optical dating to glaciofluvial sediments along the north-western coast of Wales. As documented by Thomas and Chiverrell (2007), the glacigenic stratigraphy exposed in section along this coastline is dominated by evidence of multiple ice-marginal oscillations for example, at Dinas Dinlle. Thomas and Chiverrell (2007) identified 11 possible readvance episodes with the possibility of many more which are presently obscured due to buried moraines. Further sampling for optical dating of distal glaciofluvial sediments along the coastline of north-western Wales could allow a comprehensive OSL chronology to be achieved as to the timing of these ice-marginal oscillations. This would give an indication as to whether ice-marginal oscillations occurred frequently during a rapid retreat of the ISIS or whether they occurred over a longer period of sustained retreat.

Although the success of the optical dating technique was limited at Wexford due to the extremely poorly-bleached nature of the quartz from these proximal glaciofluvial sediments giving only maximum ages for the Screen Member; this could present an opportunity to test the single-grain methodology to observe if there are any *individual* grains that show evidence of complete bleaching. The single-grain technique could allow these well-bleached grains to be isolated and taken into consideration when undertaking D_e analysis and applying the appropriate statistical 'age' model. Although the small aliquot methodology used in this research was thought to have been on an *'almost single-grain level of analysis'*, based upon the number of aliquots that yielded a natural OSL signal and the number of grains upon each aliquot (Duller, 2008), it is apparent that in *such* poorly-bleached sediments, the single-grain technique itself should allow further scope for the individual identification of well-bleached grains in comparison to the single-aliquot method

used here. It is clear, however, that the application of the single-grain methodology would require vast quantities of data analysis in extracting the well-behaved (in terms of quartz luminescence characteristics) and well-bleached grains from a population of otherwise poorly-bleached grains.

The decision protocol of Bailey and Arnold (2006), used for application with the samples in this research to enable the most appropriate statistical 'age' model to be selected needs to be tested elsewhere to confirm its broader applicability. Especially important in this regard is the determination of the 'critical values of skewness/kurtosis' that were derived from the modelled data of Arnold (2006). These critical values may indeed differ for sediments of varying depositional environment or quartz types. Ideally, a well-bleached sample D_e distribution should be obtained to evaluate levels of skewness, kurtosis and overdispersion enabling a benchmark to be determined with which other heterogeneously-bleached samples can be compared. Due to the very nature of the depositional environment of glacial sediments, the presence of a well-bleached sample to use in this manner is extremely unlikely and so the critical values determined from modelled data are the best to work with at the present time.

One of the outcomes of quartz characterisation tests was that complex and widely varying luminescence characteristics were observed between aliquots/grains of the same sample and that this could be related to the complex provenance of the quartz under investigation. A more detailed investigation could be undertaken to establish exactly which bedrock lithologies in areas such as the Lake District, Scottish Highlands, Southern Uplands, Northern Ireland and the Irish Sea Basin itself,

actually provides sampling areas with 'good' quartz luminescence characteristics (low thermal transfer, dominant fast component, accountable sensitivity change). This could be done by sampling the bedrock itself, undertaking luminescence sensitivity tests, thermal transfer tests and LM- and CW-OSL curve fitting. If certain bedrock lithologies can be linked to 'good' quartz then this would allow future preliminary investigations to be undertaken to establish whether the quartz is derived from an area with typically 'good' quartz bedrock lithologies. This should enhance the success of luminescence techniques and allow certain sampling areas to be avoided or specifically targeted, based upon bedrock lithology quartz characteristics.

For example, in Buchan, north-eastern Scotland, the quartz used for OSL dating of glacigenic sediments (e.g. Duller, 2006; Gemmell, et al., 2007) was adequately bleached, had reasonable quartz luminescence characteristics (e.g. sensitivity, fast component) and gave reliable age data. In comparison, OSL dating of glacial moraines within the Younger Dryas limit in the north-western Scottish Highlands (e.g. Lukas, et al., 2007) was unsuccessful due to poor quartz luminescence sensitivity and the lack of a dominant fast component. Bedrock lithology is thought to have played an important role in the success/failure of OSL dating at these locations. The area surrounding Buchan is composed of a variety of lithologies including Devonian Sandstones ('Old Red Sandstone'), acidic and basic igneous intrusive bodies and quartzose mica-schists (Lukas, et al., 2007). The Devonian Sandstones were initial deposited in a warm, semiarid Devonian climate when this region lay 15° to 25° south of the equator (Jackson, et al., 1995) giving plenty of scope for multiple transport events via aeolian and fluvial processes. The previous cycling (erosion, transport, bleaching and deposition) of this sediment is likely to

have contributed to its favourable quartz luminescence sensitivity characteristics and ability to derive reliable age data. The area surrounding the north-western Highlands is dominantly composed of metamorphic schistose rocks which are unlikely to have been cycled in this way. Additionally, a lack of lithological variety means that no minor quartz component is present that could have been identified via single-grain analysis to have provided favourable luminescence characteristics. Such investigations into sediment provenance could be undertaken previous to OSL dating to ensure that a 'favourable' lithological type contributed to the quartz present at the locality under investigation.

The techniques adopted in this research have enabled the successful application of optical dating to sediments that were previously thought of as 'un-dateable' via this method. It is hoped that the output from this research will stimulate further efforts into providing accurate reconstructions of the earth's glacial history. With the rapid development of the optical dating technique, which has enabled it to be applied successfully to an increasingly wider range of depositional environments, chronologies for Quaternary glacial environments should become more frequently available and more tightly constrained as a result.

Bibliography

Adamiec, G. and Aitken, M. J. (1998). Dose-rate conversion factors: update. *Ancient TL* **16,** 37-50.

Adamiec, G. (2005). OSL decay curves - relationship between single- and multiple-grain aliquots. *Radiation Measurements* **39,** 63-75.

Addison, K. (1990). Pen-y-bryn, Caernarfon in Addison, K., Edge, M. J. and Watkins, R. (Eds), *The Quaternary of North Wales: Field Guide*, Quaternary Research Association, pp. 108-116.

Addison, K. and Edge, M. J. (1992). Early Devensian interstadial and glacigenic sediments in Gwynedd, North Wales. *Geological Journal* **27,** 181-190.

Agersnap Larsen, N., Bulur, E., Bøtter-Jensen, L. and McKeever, S. W. S. (2000). Use of the LM-OSL technique for the detection of partial bleaching in quartz. *Radiation Measurements* **32,** 419-425.

Aitken, M. J., Tite, M. S. and Reid, J. (1964). Thermoluminescent Dating of Ancient Ceramics. *Nature* **202,** 1032-1033.

Aitken, M. J., Zimmerman, D. W. and Fleming, S. J. (1968). Thermoluminscent Dating of Ancient Pottery. *Nature* **219,** 442-445.

Aitken, M. J. (1985). *Thermoluminescence Dating*. Academic Press.

Aitken, M. J. and Xie, J. (1990). Moisture correction for annual gamma dose. *Ancient TL* **8,** 6-9.

Aitken, M. J. (1998). *An Introduction to Optical Dating: The Dating of Quaternary Sediments by the Use of Photon-stimulated Luminescence.* Oxford University Press.

Alexanderson, H. and Murray, A. S. (2007). Was southern Sweden ice free at 19-25 ka, or were the post LGM glacifluvial sediments incompletely bleached? *Quaternary Geochronology* **2,** 229-236.

Almond, P. C., Moar, N. T. and Lian, O. B. (2001). Reinterpretation of the glacial chronology of South Westland, New Zealand. *New Zealand Journal of Geology & Geophysics* **44,** 1-15.

Arnold, L. J. (2006). Optical dating and computer modelling of arroyo epicycles in the American Southwest, *Unpublished D Phil thesis*, University of Oxford.

Arnold, L. J., Bailey, R. M. and Tucker, G. E. (2007). Statistical treatment of fluvial dose distributions from southern Colorado arroyo deposits. *Quaternary Geochronology* **2,** 162-167.

Auclair, M., Lamothe, M. and Huot, S. (2003). Measurement of anomalous fading for feldspar IRSL using SAR. *Radiation Measurements* **37,** 487-492.

Austin, W. E. N. and McCarroll, D. (1992). Foraminifera from the Irish Sea glacigenic deposits at Aberdaron, western Lleyn, North Wales: palaeoenvironmental implications. *Journal of Quaternary Science* **7,** 311-317.

Bailey, R. (1997). Optical detrapping of charge from the 110°C quartz TL region. *Ancient TL* **15,** 7-10.

Bailey, R. M., Smith, B. W. and Rhodes, E. J. (1997). Partial bleaching and the decay form characteristics of quartz OSL. *Radiation Measurements* **27,** 123-136.

Bailey, R. M. (2000a). The interpretation of quartz optically stimulated luminescence equivalent dose versus time plots. *Radiation Measurements* **32,** 129-140.

Bailey, R. M. (2000b). The slow component of quartz optically stimulated luminescence. *Radiation Measurements* **32,** 233-246.

Bailey, R. M., Singarayer, J. S., Ward, S. and Stokes, S. (2003). Identification of partial resetting using D_e as a function of illumination time. *Radiation Measurements* **37,** 511-518.

Bailey, R. M. and Arnold, L. J. (2006). Statistical modelling of single grain quartz D_e distributions and an assessment of procedures for estimating burial dose. *Quaternary Science Reviews* **25,** 2475-2502.

Ballantyne, C. K. and Sutherland, D. G. (1987). *Wester Ross Field Guide.* Quaternary Research Association.

Ballantyne, C. K., McCarroll, D. and Stone, J. O. (2006). Vertical dimensions and age of the Wicklow Mountains ice dome, Eastern Ireland, and implications for the extent of the last Irish Ice Sheet. *Quaternary Science Reviews* **25,** 2048-2058.

Ballantyne, C. K., McCarroll, D. and Stone, J. O. (2007). The Donegal ice dome, northwest Ireland: Dimensions and chronology. *Journal of Quaternary Science* **22,** 773-783.

Ballantyne, C. K., Stone, J. O. and McCarroll, D. (2008). Dimensions and chronology of the last ice sheet in Western Ireland. *Quaternary Science Reviews,* 185-200.

Balson, P. S. and Jeffrey, D. H. (1991). The glacial sequence of the southern North Sea in Ehlers, J., Gibbard, P. L. and Rose, J. (Eds), *Glacial Deposits in Great Britain and Ireland*, Balkema, pp. 245-253.

Bateman, M. D. (1995). Thermoluminescence dating of the British coversand deposits. *Quaternary Science Reviews* **14,** 791-798.

Bateman, M. D. (1998). The origin and age of coversand in North Lincolnshire, UK. *Permafrost and Periglacial Processes* **9,** 313-325.

Bateman, M. D. and Murton, J. B. (2006). The chronostratigraphy of Late Pleistocene glacial and periglacial aeolian activity in the Tuktoyaktuk Coastlands, NWT, Canada. *Quaternary Science Reviews* **25,** 2552-2568.

Bell, W. T. (1979). Attenuation factors for the absorbed radiation dose in quartz inclusions for thermoluminescence dating. *Ancient TL* **8,** 2-13.

Benn, D. I. and Evans, D. J. A. (1998). *Glaciers & Glaciation*. Arnold.

Berger, G. W. (1984). Thermoluminescence dating studies of glacial silts from Ontario. *Canadian Journal of Earth Science* **21,** 1393-1399.

Berger, G. W. (1990). Effectiveness of the natural zeroing of the thermoluminescence in sediments. *Journal of Geophysical Research* **95,** 12375-12397.

Blockley, S. P. E., Lowe, J. J., Walker, M. J. C., Asioli, A., Trincardi, F., Coope, G. R., Donahue, R. E. and Pollard, A. M. (2004). Bayesian analysis of radiocarbon chronologies: Examples from the European Late-glacial. *Journal of Quaternary Science* **19,** 159-176.

Blockley, S. P. E., Blockley, S. M., Donahue, R. E., Lane, C. S., Lowe, J. J. and Pollard, A. M. (2006). The chronology of abrupt climate change and Late Upper Palaeolithic human adaptation in Europe. *Journal of Quaternary Science* **21,** 575-584.

Blockley, S. P. E., Bronk Ramsey, C. and Higham, T. F. G. (2008). The Middle to Upper Paleolithic transition: dating, stratigraphy, and isochronous markers. *Journal of Human Evolution* **55,** 764-771.

Bøe, A.-G., Murray, A. S. and Olaf Dahl, S. (2007). Resetting of sediments mobilised by the LGM ice-sheet in southern Norway. *Quaternary Geochronology* **2,** 222-228.

Bond, G. C. and Lotti, R. (1995). Iceberg discharges into the North Atlantic on millennial time scales during the last glaciation. *Science* **267,** 1005.

Boothroyd, J. C. and Ashley, G. M. (1975). Process, bar morphology and sedimentary structures on braided outwash fans, northeastern gulf of Alaska in Jopling, A. V. and McDonald, B. C. (Eds), *Glaciofluvial and Glaciolacustrine sedimentation*, Society of Economic Paleontologists and Mineralogists, Tulsa (Okla.), **23**, pp. 193-222.

Bos, J. A. A., Dickson, J. H., Coope, G. R. and Jardine, W. G. (2004). Flora, fauna and climate of Scotland during the Weichselian Middle Pleniglacial - Palynological, macrofossil and coleopteran investigations. *Palaeogeography, Palaeoclimatology, Palaeoecology* **204,** 65-100.

Bøtter-Jensen, L. and Duller, G. A. T. (1992). A new system for measuring optically stimulated luminescence from quartz samples. *Nuclear Tracks and Radiation Measurements* **20,** 549-533.

Bøtter-Jensen, L., Duller, G. A. T., Murray, A. S. and Banerjee, D. (1999). Blue light emitting diodes for optical stimulation of quartz in retrospective dosimetry and dating. *Radiation Protection Dosimetry* **84,** 335-340.

Bøtter-Jensen, L., Bulur, E., Duller, G. A. T. and Murray, A. S. (2000). Advances in luminescence instrument systems. *Radiation Measurements* **32,** 523-528.

Bøtter-Jensen, L., Andersen, C. E., Duller, G. A. T. and Murray, A. S. (2003). Developments in radiation, stimulation and observation facilities in luminescence measurements. *Radiation Measurements* **37,** 535-541.

Boulton, G. S. (1974). Processes and patterns of glacial erosion in Coates, D. R. (Ed), *Glacial Geomorphology*, State University.

Boulton, G. S., Jones, A. S., Clayton, K. M. and Kenning, M. J. (1977). A British ice-sheet model and patterns of glacial erosion and deposition in Britain in Shotton, F. W. (Ed), *British Quaternary Studies: Recent Advances*, Clarendon Press.

Boulton, G. S., Peacock, J. D. and Sutherland, D. G. (1991). Quaternary. in Craig, G. Y. (Ed), *Geology of Scotland*, The Geological Society, pp. 503-543.

Boulton, G. S., Dongelman, P. W., Punkari, M. and Broadgate, M. (2001). Palaeoglaciology of an ice sheet through the Weichselian. *Quaternary Science Reviews* **20,** 591-625.

Boulton, G. S. and Hagdorn, M. (2006). Glaciology of the British Isles Ice Sheet during the last glacial cycle: form, flow, streams and lobes. *Quaternary Science Reviews* **25,** 3359-3390.

Bowen, D. Q., Rose, J., McCabe, A. M. and Sutherland, D. G. (1986). Correlation of quaternary glaciations in England, Ireland, Scotland and Wales. *Quaternary Science Reviews* **5,** 299-340.

Bowen, D. Q., Phillips, F. M., McCabe, A. M., Knutz, P. C. and Sykes, G. A. (2002). New data for the Last Glacial Maximum in Great Britain and Ireland. *Quaternary Science Reviews* **21,** 89-101.

Boyce, J. I. and Eyles, N. (2000). Architectural element analysis applied to glacial deposits: Internal geometry of a late Pleistocene till sheet, Ontario, Canada. *Bulletin of the Geological Society of America* **112,** 98-118.

Bradwell, T., Stoker, M. S., Golledge, N. R., Wilson, C. K., Merritt, J. W., Long, D., Everest, J. D., Hestvik, O. B., Stevenson, A. G., Hubbard, A. L., Finlayson, A. G. and Mathers, H. E. (2008). The northern sector of the last British Ice Sheet: Maximum extent and demise. *Earth Science Reviews* **88,** 207-226.

Bronk Ramsey, C. (2001). Development of the radiocarbon calibration program OxCal. *Radiocarbon* **43,** 355-363.

Bronk Ramsey, C. (2008a). Deposition models for chronological records. *Quaternary Science Reviews* **27,** 42-60.

Bronk Ramsey, C. (2008b). Radiocarbon dating: Revolutions in understanding. *Archaeometry* **50,** 249-275.

Brookfield, M. E. and Martini, I. P. (1999). Facies architecture and sequence stratigraphy in glacially influenced basins: Basic problems and water-level/glacier input-point controls (with an example from the Quaternary of Ontario, Canada). *Sedimentary Geology* **123,** 183-197.

Brooks, A. J., Bradley, S. L., Edwards, R. J., Milne, G. A., Horton, B. and Shennan, I. (2008). Postglacial relative sea-level observations from Ireland and their role in glacial rebound modelling. *Journal of Quaternary Science* **23,** 175-192.

Brown, E. J., Rose, J., Coope, R. G. and Lowe, J. J. (2007). An MIS 3 age organic deposit from Balglass Burn, central Scotland: Palaeoenvironmental significance and implications for the timing of the onset of the LGM ice sheet in the vicinity of the British Isles. *Journal of Quaternary Science* **22,** 295-308.

Bryant, I. D. (1983). The utilization of Arctic river analogue studies in the interpretation of periglacial river sediments from southern Britain in Gregory, K. J. (Ed), *Background to Palaeohydrology*, John Wiley & Sons Ltd.

Buck, C. E., Kenworthy, J. B., Litton, C. D. and Smith, A. F. M. (1991). Combining archaeological and radiocarbon information: a Bayesian approach to calibration. *Antiquity* **65,** 808-821.

Buck, C. E., Cavanagh, W. G. and Litton, C. D. (1996). *The Bayesian Approach to Interpreting Archaeological Data*. Wiley.

Bulur, E. (1996). An alternative technique for optically stimulated luminescence (OSL) experiment. *Radiation Measurements* **26,** 701-709.

Bulur, E., Bøtter-Jensen, L. and Murray, A. S. (2000). Optically stimulated luminescence from quartz measured using the linear modulation technique. *Radiation Measurements* **32,** 407-411.

Bulur, E., Duller, G. A. T., Solongo, S., Bøtter-Jensen, L. and Murray, A. S. (2002). LM-OSL from single grains of quartz: a preliminary study. *Radiation Measurements* **35,** 79-85.

Buylaert, J. P., Murray, A. S., Vandenberghe, D., Vriend, M., De Corte, F. and Van den haute, P. (2008). Optical dating of Chinese loess using sand-sized quartz: Establishing a time frame for Late Pleistocene climate changes in the western part of the Chinese Loess Plateau. *Quaternary Geochronology* **3,** 99-113.

Cant, D. J. and Walker, R. G. (1978). Fluvial processes and facies sequences in the sandy braided South Saskatchwan River, Canada. *Sedimentology* **25,** 625-648.

Carlson, A. E., Clark, P. U., Raisbeck, G. M. and Brook, E. J. (2007). Rapid Holocene deglaciation of the labrador sector of the Laurentide Ice Sheet. *Journal of Climate* **20,** 5126-5133.

Carr, S. J., Holmes, R., Van der Meer, J. J. M. and Rose, J. (2006). The Last Glacial Maximum in the North Sea: micromorphological evidence of extensive glaciation. *Journal of Quaternary Science* **21,** 131-153.

Cerling, T. E. and Craig, H. (1994). Geomorphology and in-situ cosmogenic isotopes. *Annual Review of Earth & Planetary Sciences* **22,** 273-317.

Chambers, F. M., Addison, K., Blackford, J. J. and Edge, M. J. (1995). Palynology of organic beds below Devensian glacigenic sediments at Pen-y-bryn, Gwynedd, North Wales. *Journal of Quaternary Science* **10,** 157-173.

Charlesworth, J. K. (1928). The glacial retreat from central and southern Ireland. *Quaterly Journal of the Geological Society of London* **84,** 293-344.

Chiverrell, R. C., Thomas, G. S. P. and Harvey, A. M. (2001). Late Devensian and Holocene landscape change in the uplands of the Isle of Man. *Geomorphology* **40,** 219-236.

Chiverrell, R. C., Plater, A. J. and Thomas, G. S. P. (Eds) (2004). *The Quaternary of the Isle of Man & North West England.*, Quaternary Research Association.

Chiverrell, R. C., Foster, G. C., Thomas, G. S. P., Marshall, P. and Hamilton, D. (2008). Robust chronologies for landform development. *Earth Surface Processes and Landforms.*

Choi, J. H., Murray, A. S., Cheong, C. S., Hong, D. G. and Chang, H. W. (2003a). The resolution of stratigraphic inconsistency in the luminescence ages of marine terrace sediments from Korea. *Quaternary Science Reviews* **22,** 1201-1206.

Choi, J. H., Murray, A. S., Jain, M., Cheong, C. S. and Chang, H. W. (2003b). Luminescence dating of well-sorted marine terrace sediments on the southeastern coast of Korea. *Quaternary Science Reviews* **22,** 407-421.

Choi, J. H., Duller, G. A. T. and Wintle, A. G. (2006a). Analysis of quartz LM-OSL curves. *Ancient TL* **24,** 9-20.

Choi, J. H., Duller, G. A. T., Wintle, A. G. and Cheong, C.-S. (2006b). Luminescence characteristics of quartz from the Southern Kenyan Rift Valley: Dose estimation using LM-OSL SAR. *Radiation Measurements* **41,** 847-854.

Clark, C., Evans, D. J. A., Khatwa, A., Bradwell, T., Jordan, C. J., Marsh, S. H., Mitchell, W. A. and Bateman, M. D. (2004a). Map and GIS database of glacial landforms and features related to the last British Ice Sheet. *Boreas* **33,** 359-375.

Clark, C. D. and Stokes, C. R. (2001). Extent and basal characteristics of the M'Clintock Channel Ice Stream. *Quaternary International* **86,** 81-101.

Clark, P. U., McCabe, A. M., Mix, A. C. and Weaver, A. J. (2004b). Rapid rise of sea level 19.000 years ago and its global implications. *Science* **304,** 1141-1144.

Clifford, N. J., Richards, K. S., Brown, R. A. and Lane, S. N. (1995). Scales of variation of suspended sediment concentration and turbidity in a glacial meltwater stream. *Geografiska Annaler. Series A, Physical Geography* **77,** 45-65.

Colhoun, E. A., Dickson, J. H., McCabe, A. M. and Shotton, F. (1972). A middle Midlandian freshwater series at Derryvree, Maguiresbridge, Co Fermanagh, Northern Ireland. *Proceedings of the Royal Society of London, series B* **180,** 274-292.

Collins, D. N. (1996). Sediment transport from glacierized basins in the Karakoram mountains. Erosion and sediment yield: global and regional perspectives. *Proceedings of the Exeter Symposium, July 1996*, pp. 85-96.

Connaughton, M. (1986). Fluvial architecture and facies models of Pleistocene sandur sequences, University of Liverpool, Unpublished PhD Thesis.

Coope, G. R., Morgan, A. and Osbourne, P. J. (1971). Fossil coleoptera as indicators of climatic fluctuations during the last glaciation in Britain. *Palaeogeography, Palaeoclimatology, Palaeoecology* **10,** 87-101.

Coope, G. R. and Brophy, J. A. (1972). Late Glacial environmental changes indicated by a coleopteran succession from North Wales. *Boreas* **1,** 97-142.

Dackombe, R. V. and Thomas, G. S. P. (1991). Glacial deposits and Quaternary stratigraphy of the Isle of Man. *Glacial deposits in Great Britain and Ireland*, 333-344.

Dansgaard, W., Johnsen, S. J., Clausen, H. B., Dahl-Jensen, D., Gundestrup, N. S., Hammer, C. U., Hvidberg, C. S., Steffensen, J. P., Sveinbjörnsdottir, A. E., Jouzel, J. and Bond, G. (1993). Evidence for general instability of past climate from a 250-kyr ice-core record. *Nature* **364,** 218.

Dawson, M. R. and Bryant, I. D. (1987). Three-dimensional facies geometry in Pleistocene outwash sediments, Worcestershire, U.K. in Ethridge, F. G., Flores, R. M. and Harvey, M. D. (Eds), *Recent developments in fluvial sedimentology: Contributions from the Third International Fluvial Sedimentology Conference*, Society of Economic Paleontologists and Mineralogists.

Demuro, M., Roberts, R. G., Froese, D. G., Arnold, L. J., Brock, F. and Ramsey, C. B. (2008). Optically stimulated luminescence dating of single and multiple grains of quartz from perennially frozen loess in western Yukon Territory, Canada: Comparison with radiocarbon chronologies for the late Pleistocene Dawson tephra. *Quaternary Geochronology* **3,** 346-364.

Ditlefsen, C. (1992). Bleaching of K-feldspars in turbid water suspensions: a comparison of photo- and thermoluminescence signals. *Quaternary Science Reviews* **11,** 33-38.

Divigalpitiya, W. M. R. (1982). Thermoluminescence dating of sediments, *MSc. thesis*, Simon Fraser University.

Duller, G. A. T. (1994). Luminescence dating of poorly bleached sediments from Scotland. *Quaternary Geochronology (Quaternary Science Reviews)* **13,** 521-524.

Duller, G. A. T., Wintle, A. G. and Hall, A. M. (1995). Luminescence dating and its application to key pre-late Devensian sites in Scotland. *Quaternary Science Reviews* **14,** 495-519.

Duller, G. A. T., Bøtter-Jensen, L., Kohsiek, P. and Murray, A. S. (1999). A high-sensitivity optically stimulated luminescence scanning system for measurement of single sand-sized grains. *Radiation Protection Dosimetry* **84,** 325-330.

Duller, G. A. T. (2003). Distinguishing quartz and feldspar in single grain luminescence measurements. *Radiation Measurements* **37,** 161-165.

Duller, G. A. T. (2004). Luminescence dating of Quaternary sediments: recent advances. *Journal of Quaternary Science* **19,** 183-192.

Duller, G. A. T. (2006). Single grain optical dating of glacigenic deposits. *Quaternary Geochronology* **1,** 296-304.

Duller, G. A. T. and Augustinus, P. C. (2006). Reassessment of the record of linear dune activity in Tasmania using optical dating. *Quaternary Science Reviews* **25,** 2608-2618.

Duller, G. A. T. (2008). Single-grain optical dating of Quaternary sediments: why aliquot size matters in luminescence dating. *Boreas* **37,** 589-612.

Edwards, R., Brooks, A., Shennan, I., Milne, G. and Bradley, S. (2008). Reply: Postglacial relative sea-level observations from Ireland and their role in glacial rebound modelling. *Journal of Quaternary Science* **23,** 1-5.

England, J., Atkinson, N., Bednarski, J., Dyke, A. S., Hodgson, D. A. and Ó Cofaigh, C. (2006). The Innuitian Ice Sheet: configurations, dynamics and chronology. *Quaternary Science Reviews* **25,** 689-703.

Etienne, J. L., Jansson, K. N., Glasser, N. F., Hambrey, M. J., Davies, J. R., Waters, R. A., Maltman, A. J. and Wilby, P. R. (2006). Palaeoenvironmental interpretation of an ice-contact glacial lake succession: an example from the late Devensian of southwest Wales, UK. *Quaternary Science Reviews* **25,** 739-762.

Evans, D. J. and Ó Cofaigh, C. (2003a). Depositional evidence for marginal oscillations of the Irish Sea ice stream in southeast Ireland during the last glaciation. *Boreas* **32,** 76-101.

Evans, D. J. A. and Ó Cofaigh, C. (2003b). Depositional evidence for marginal oscillations of the Irish Sea ice stream in southeast Ireland during the last glaciation. *Boreas* **32,** 76-101.

Evans, D. J. A., Clark, C. D. and Mitchell, W. A. (2005). The last British Ice Sheet: A review of the evidence utilised in the compilation of the Glacial Map of Britain. *Earth-Science Reviews* **70,** 253-312.

Eyles, C. H. and Eyles, N. (1984). Glaciomarine sediments of the Isle of Man as a key to late Pleistocene stratigraphic investigations in the Irish Sea Basin. *Geology* **12,** 359-364.

Eyles, N., Eyles, C. H. and Miall, A. D. (1983). Lithofacies types and vertical profile models; an alternative approach to the description and environmental interpretation of glacial diamict and diamictite sequences. *Sedimentology* **30,** 393-410.

Eyles, N. and McCabe, A. M. (1989). The Late Devensian (<22,000 BP) Irish Sea Basin: The sedimentary record of a collapsed ice sheet margin. *Quaternary Science Reviews* **8,** 307-351.

Fairbanks, R. G. (1989). A 17,000-year glacio-eustatic sea level record: Influence of glacial melting rates on the Younger Dryas event and deep-ocean circulation. *Nature* **342,** 637-642.

Fairbanks, R. G., Mortlock, R. A., Chiu, T.-C., Cao, L., Kaplan, A., Guilderson, T. P., Fairbanks, T. W. and Bloom, A. L. (2005). Marine Radiocarbon Calibration Curve Spanning 0 to 50,000 Years B.P. Based on Paired $^{230}Th/^{234}U/^{238}U$ and ^{14}C Dates on Pristine Corals. *Quaternary Science Reviews* **24,** 1781-1796.

Ferguson, R. I. (1984). Sediment load of the Hunza River in Miller, K. (Ed), *International Karakoram Project,* Cambridge University Press, pp. 374-382.

Fitzsimmons, K. E., Rhodes, E. J., Magee, J. W. and Barrows, T. T. (2007). The timing of linear dune activity in the Strzelecki and Tirari Deserts, Australia. *Quaternary Science Reviews* **26,** 2598-2616.

Foster, G. C., Chiverrell, R. C., Thomas, G. S. P., Marshall, P. and Hamilton, D. (In Press). Fluvial development and the sediment regime of the lower Calder, Ribble catchment, northwest England. *Catena.*

Galbraith, R. F. and Green, P. F. (1990). Estimating the component ages in a finite mixture. *Nuclear Tracks and Radiation Measurements* **17,** 197-206.

Galbraith, R. F., Roberts, R. G., Laslett, G. M., Yoshida, H. and Olley, J. M. (1999). Optical dating of single and multiple grains of quartz from Jinmium rock shelter, Northern Australia: Part I, experimental design and statistical models. *Archaeometry* **41,** 339-364.

Galbraith, R. F., Roberts, R. G. and Yoshida, H. (2005). Error variation in OSL palaeodose estimates from single aliquots of quartz: a factorial experiment. *Radiation Measurements* **39,** 289-307.

Gemmell, A. M. D. (1985). Zeroing of the TL signal of sediment undergoing fluvial transportation: A laboratory experiment. *Nuclear Tracks* **10,** 695-702

Gemmell, A. M. D. (1988a). Zeroing of the TL signal in sediment undergoing fluvioglacial transport. An example from Austerdalen, Western Norway. *Quaternary Science Reviews* **7,** 339-345.

Gemmell, A. M. D. (1988b). Thermoluminescence dating of glacially transported sediments: some considerations. *Quaternary Science Reviews* **7,** 277-285.

Gemmell, A. M. D. (1997). Fluctuations in the thermoluminescence signal of suspended sediment in an alpine glacial meltwater stream. *Quaternary Geochronology (Quaternary Science Reviews)* **16,** 281-290.

Gemmell, A. M. D. (1999). IRSL from fine-grained glacifluvial sediment. *Quaternary Geochronology (Quaternary Science Reviews)* **18,** 207-215.

Gemmell, A. M. D., Murray, A. S. and Connell, E. R. (2007). Devensian glacial events in Buchan (NE Scotland): A progress report on new OSL dates and their implications. *Quaternary Geochronology* **2,** 237-242.

Glasser, N. F., Etienne, J. L., Hambrey, M. J., Davies, J. R., Waters, R. A. and Wilby, P. R. (2004). Glacial meltwater erosion and sedimentation as evidence for multiple glaciations in west Wales. *Boreas* **33,** 224-237.

Glasser, N. F., Harrison, S., Ivy-Ochs, S., Duller, G. A. T. and Kubik, P. (2006). Evidence from the Rio Bayo valley on the extent of the North Patagonian Icefield during the Late-Pleistocene-Holocene transition. *Quaternary Research* **65,** 70-77.

Godfrey-Smith, D. I., Huntley, D. J. and Chen, W.-H. (1988). Optical dating studies of quartz and feldspar sediment extracts. *Quaternary Science Reviews* **7,** 373-380.

Golledge, N. R., Fabel, D., Everest, J. D., Freeman, S. and Binnie, S. (2007). First cosmogenic 10Be age constraint on the timing of Younger Dryas glaciation and ice cap thickness, western Scottish Highlands. *Journal of Quaternary Science* **22,** 785-791.

Gosse, J. C. and Phillips, F. M. (2001). Terrestrial in situ cosmogenic nuclides: theory and application. *Quaternary Science Reviews* **20,** 1475-1560.

Greenwood, S. L., Clark, C. D. and Hughes, A. L. C. (2007). Formalising an inversion methodology for reconstructing ice-sheet retreat patterns from meltwater channels: Application to the British Ice Sheet. *Journal of Quaternary Science* **22,** 637-645.

Hall, A. M. (1997). Quaternary stratigraphy: the terrestrial record in Gordon, J. E. (Ed), *Reflections on the Ice Age in Scotland*, Scottish Natural Heritage, pp. 59-71.

Hall, A. M. and Connell, E. R. (2000). Howe of Byth Quarry in Merritt, J. W., Connell, E. R. and Bridgland, D. R. (Eds), *The Quaternary of the Banffshire Coast and Buchan Field Guide*, Quaternary Research Association.

Hall, I. R. and McCave, I. N. (1998a). Glacial-interglacial variation in organic carbon burial on the slope of the NW European continental margin (40°-50°N). *Progress in Oceanography* **42,** 37-60.

Hall, I. R. and McCave, I. N. (1998b). Late Glacial to Recent accumulation fluxes of sediments at the shelf edge and slope of NW Europe, 48-50°N. *Special Publication of the Geological Society of London* **129,** 339-350.

Hambrey, M. J., Davies, J. R., Glasser, N. F., Waters, R. A., Dowdeswell, J. A., Wilby, P. R., Wilson, D. and Etienne, J. L. (2001). Devensian glacigenic sedimentation and landscape evolution in the Cardigan area of southwest Wales. *Journal of Quaternary Science* **16,** 455-479.

Hammer, K. M. and Smith, N. D. (1983). Sediment production and transport in a proglacial stream: Hilda Glacier, Alberta, Canada. *Boreas* **12,** 91-106.

Hansen, L., Funder, S., Murray, A. S. and Mejdahl, V. (1999). Luminescence dating of the last Weichselian Glacier advance in East Greenland. *Quaternary Science Reviews* **18,** 179-190.

Harris, C. (1991). Glacial deposits at Wylfa Head, Anglesey, North Wales: evidence for late Devensian deposition in a non-marine environment. *Journal of Quaternary Science* **6,** 67-77.

Harris, C., Williams, G., Brabham, P., Eaton, G. and McCarroll, D. (1997). Glaciotectonized Quaternary sediments at Dinas Dinlle, Gwynedd, North Wales, and their bearing on the style of deglaciation in the eastern Irish Sea. *Quaternary Science Reviews* **16,** 109-127.

Harris, C. A., Brabham, P. and Williams, G. (1995). Glaciotectonic structures and their relation to topography at Dinas Dinlle, Arvon, northwest Wales. *Journal of Quaternary Science* **10,** 397-399.

Hart, J. K. (1999). Glacial sedimentology: A case study from Happisburgh, Norfolk. in Jones, A. P., Tucker, M. E. and Hart, J. K. (Eds), *The description & analysis of Quaternary stratigraphic field sections*, Quaternary Research Association, pp. 209-234.

Hein, F. J. and Walker, R. G. (1977). Bar evolution and development of stratification in the gravelly, braided Kicking Horse River, British Columbia. *Canadian Journal of Earth Science* **14,** 562-570.

Hiemstra, J. F., Evans, D. J. A., Scourse, J. D., McCarroll, D., Furze, M. F. A. and Rhodes, E. (2006). New evidence for a grounded Irish Sea glaciation of the Isles of Scilly, UK. *Quaternary Science Reviews* **25,** 299-309.

Hodson, A. J. and Ferguson, R. I. (1999). Fluvial suspended sediment transprt from cold and warm-based glaciers in Svalbard. *Earth Surface Processes and Landforms* **24,** 957-974.

Huddart, D. (1971). Textural distinction of Main Glaciation and Scottish Readvance tills in the Cumberland lowland. *Geological Magazine* **108,** 317-324.

Huddart, D. and Tooley, M. J. (1972). *The Cumberland Lowland handbook.* Quaternary Research Association.

Huddart, D. (1977). Gutterby Spa-Annaside Banks Moraine and St. Bees Moraine. in Tooley, M. J. (Ed), *The Isle of Man, Lancashire coast and Lake District*, Guidebook for excursion A4, X INQUA Congress, Geo Abstracts, Norwich, pp. 38-40.

Huddart, D. (1991). The glacial history and glacial deposits of the North and West Cumbrian lowlands in Ehlers, J., Gibbard, P. L. and Rose, J. (Eds), *Glacial Deposits in Great Britain and Ireland*, A.A. Balkema, pp. 151-167.

Huddart, D. (1994). The Late Quaternary Glacigenic Sequence: Landforms and Environments in Coastal Cumbria. in Boardman, J. and Walden, J. (Eds), *Cumbria Field Guide*, Quaternary Research Association, pp. 59-77.

Huddart, D. and Glasser, N. F. (2002). *Quaternary of Northern England.* Joint Nature Conservation Committee.

Huntley, D. J., Godfrey-Smith, D. I. and Thewalt, M. L. W. (1985). Optical dating of sediments. *Nature* **313,** 105-107.

Huntley, D. J. and Lamothe, M. (2001). Ubiquity of anomalous fading in K-feldspars and the measurement and correction for it in optical dating. *Canadian Journal of Earth Sciences* **38,** 1093-1106.

Huntley, D. J. (2006). Thoughts arising from "Choi, Duller and Wintle: Analysis of quartz LM-OSL curves. Ancient TL 24, 9-20 (2006)". *Ancient TL* **24,** 69-70.

Hütt, G., Jaek, I. and Tchonka, J. (1988). Optical dating: K-feldspars optical response stimulation spectra. *Quaternary Science Reviews* **7,** 381-385.

Hütt, G. and Jungner, H. (1992). Optical and TL dating on glaciofluvial sediments. *Quaternary Science Reviews* **11,** 161-163.

Jackson, D. I., Jackson, A. A., Evans, D., Wingfield, R. T. R., Barnes, R. P. and Arthur, M. J. (1995). United Kingdom offshore regional report: the geology of the Irish Sea.

Jacobs, Z., Duller, G. A. T. and Wintle, A. G. (2006). Interpretation of single grain D_e distributions and calculation of D_e. *Radiation Measurements* **41,** 264-277.

Jain, M. and Singhvi, A. K. (2001). Limits to depletion of blue-green light stimulated luminescence in feldspars: implications for quartz dating. *Radiation Measurements* **33,** 883-892.

Jain, M., Bøtter-Jensen, L., Murray, A. and Jungner, H. (2002). Retrospective dosimetry: Dose evaluation using unheated and heated quartz from a radioactive waste storage building. *Radiation Protection Dosimetry* **101,** 525-530.

Jain, M., Bøtter-Jensen, L. and Singhvi, A. K. (2003a). Dose evaluation using multiple-aliquot quartz OSL: test of methods and a new protocol for improved accuracy and precision. *Radiation Measurements* **37,** 67-80.

Jain, M., Murray, A. S. and Bøtter-Jensen, L. (2003b). Characterisation of blue-light stimulated luminescence components in different quartz samples: implications for dose measurement. *Radiation Measurements* **37,** 441-449.

Jardine, W. G., Dickson, J. H., Haughton, P. D. W., Harkness, D. D., Bowen, D. Q. and Sykes, G. A. (1988). A late Middle Devensian interstadial site at Sourlie, near Irvine, Strathclyde. *Scottish Journal of Geology* **24,** 288-295.

Kars, R. H., Wallinga, J. and Cohen, K. M. (2008). A new approach towards anomalous fading correction for feldspar IRSL dating - tests on samples in field saturation. *Radiation Measurements* **43,** 786-790.

Kershaw, P. J. (1986). Radiocarbon Dating of Irish Sea Sediments. *Estuarine, Coastal and Shelf Science* **23,** 295-303.

Klasen, N., Fiebig, M., Preusser, F. and Radtke, U. (2006). Luminescence properties of glaciofluvial sediments from the Bavarian Alpine Foreland. *Radiation Measurements* **41,** 866-870.

Klasen, N., Fiebig, M., Preusser, F., Reitner, J. M. and Radtke, U. (2007). Luminescence dating of proglacial sediments from the Eastern Alps. *Quaternary International* **164-165,** 21-32.

Knight, J. (2004). Sedimentary evidence for the formation mechanism of the Armoy moraine and Late Devensian glacial events in the north of Ireland. *Geological Journal* **39,** 403-417.

Krbetschek, M. R., Rieser, U., Zöller, L. and Heinicke, J. (1994). Radioactive disequilibria in palaeodosimetric dating of sediments. *Radiation Measurements* **23,** 485-489.

Kuhns, C. K., Agersnap Larsen, N. and McKeever, S. W. S. (2000). Characteristics of LM-OSL from several different types of quartz. *Radiation Measurements* **32,** 413-418.

Lai, Z., Wintle, A. G. and Thomas, D. S. G. (2007). Rates of dust deposition between 50 ka and 20 ka revealed by OSL dating at Yuanbao on the Chinese Loess Plateau. *Palaeogeography, Palaeoclimatology, Palaeoecology* **248,** 431-439.

Lambeck, K. (1991). Glacial rebound and sea-level change in the British Isles. *Terra Nova* **3,** 379-389.

Lambeck, K. (1993a). Glacial rebound of the British Isles - II. A high-resolution, high- precision model. *Geophysical Journal International* **115,** 960-990.

Lambeck, K. (1993b). Glacial rebound of the British Isles - I. Preliminary model results. *Geophysical Journal International* **115,** 941-959.

Lambeck, K., Johnston, P., Smither, C. and Nakada, M. (1996). Glacial rebound of the British Isles - III. Constraints on mantle viscosity. *Geophysical Journal International* **125,** 340-354.

Lambeck, K. and Purcell, A. P. (2001). Sea-level change in the Irish Sea since the Last Glacial Maximum: constraints from isostatic modelling. *Journal of Quaternary Science* **16,** 497-506.

Lamothe, M. and Auclair, M. (1999). A solution to anomalous fading and age shortfalls in optical dating of feldspar minerals. *Earth and Planetary Science Letters* **171,** 319-323.

Lang, A., Hatte, C., Rousseau, D. D., Antoine, P., Fontugne, M., Zoller, L. and Hambach, U. (2003). High-resolution chronologies for loess: Comparing AMS ^{14}C and optical dating results. *Quaternary Science Reviews* **22,** 953-959.

Lang, A. and Mauz, B. (2006). Towards chronologies of gully formation: optical dating of gully fill sediments from Central Europe. *Quaternary Science Reviews* **25,** 2666-2675.

Lepper, K., Agersnap Larsen, N. and McKeever, S. W. S. (2000). Equivalent dose distribution analysis of Holocene eolian and fluvial quartz sands from Central Oklahoma. *Radiation Measurements* **32,** 603-608.

Li, B. and Li, S.-H. (2006). Comparison of D_e estimates using the fast component and the medium component of quartz OSL. *Radiation Measurements* **41,** 125-136.

Lian, O. B., Hu, J., Huntley, D. J. and Hicock, S. R. (1995). Optical dating of Quaternary organic-rich sediments from southwestern British Columbia and northwestern Washington State. *Canadian Journal of Earth Science* **32,** 1194-1207.

Lian, O. B. and Roberts, R. G. (2006). Dating the Quaternary: progress in luminescence dating of sediments. *Quaternary Science Reviews* **25,** 2449-2468.

Lukas, S., Spencer, J. Q., Robinson, R. A. J. and Benn, D. I. (2007). Problems associated with luminescence dating of Late Quaternary glacial sediments in the NW Scottish Highlands. *Quaternary Geochronology* **2,** 243-248.

Maizels, J. (1993). Lithofacies variations within sandur deposits: the role of runoff regime, flow dynamics and sediment supply characteristics. *Sedimentary Geology* **85,** 299-325.

Mangerud, J., Astakhov, V. I., Murray, A. and Svendsen, J. I. (2001). The chronology of a large ice-dammed lake and the Barents-Kara Ice Sheet advances, Northern Russia. *Global and Planetary Change* **31,** 321-336.

Marsella, K. A., Bierman, P. R., Thompson Davis, P. and Caffee, M. W. (2000). Cosmogenic 10Be and 26Al ages of the Last Glacial Maximum, Eastern Baffin Island, Arctic Canada. *Bulletin of the Geological Society of America* **112,** 1296-1312.

Mauz, B., Bode, T., Mainz, E., Blanchard, H., Hilger, W., Dikau, R. and Zoller, L. (2002). The luminescence dating laboratory at the University of Bonn: equipment and procedures. *Ancient TL* **20,** 53-61.

McCabe, A. M. (1986). Glaciomarine facies deposited by retreating tidewater glaciers. An example from the Late Pleistocene of Northern Ireland. *Journal of Sedimentary Petrology* **56,** 880-894.

McCabe, A. M. (1987). Quaternary deposits and glacial stratigraphy in Ireland. *Quaternary Science Reviews* **6,** 259-299.

McCabe, A. M., Dardis, G. F. and Hanvey, P. M. (1987). Sedimentation at the margins of a Late-Pleistocene ice-lobe terminating in shallow marine environments, Dundalk Bay, eastern Ireland. *Sedimentology* **34,** 473-493.

McCabe, A. M. (1996). Dating and rhythmicity from the last deglacial cycle in the British Isles. *Journal of the Geological Society, London.* **153,** 499-502.

McCabe, A. M. and Clark, P. U. (1998). Ice-sheet variability around the North Atlantic Ocean during the last deglaciation. *Nature* **392,** 373-377.

McCabe, A. M., Clark, P. U. and Clark, J. (2005). AMS ^{14}C dating of deglacial events in the Irish Sea Basin and other sectors of the British-Irish ice sheet. *Quaternary Science Reviews* **24,** 1673-1690.

McCabe, A. M. (2008a). Comment: Postglacial relative sea-level observations from Ireland and their role in glacial rebound modelling. *Journal of Quaternary Science* **23,** 175-192.

McCabe, A. M. (2008b). *Glacial Geology and Geomorphology: the landscapes of Ireland.* Dunedin Press.

McCabe, M., Knight, J. and McCarron, S. (1998). Evidence for Heinrich event 1 in the British Isles. *Journal of Quaternary Science* **13,** 549-568.

McCarroll, D. (1991). Ice directions in western Lleyn and the status of the Gwynedd readvance of the last Irish Sea glacier. *Geological Journal* **26,** 137-143.

McCarroll, D. and Harris, C. (1992). The glacigenic deposits of western Lleyn, north Wales: terrestrial or marine? *Journal of Quaternary Science* **7,** 19-29.

McCarroll, D. (1995). Geomorphological evidence from the Lleyn Peninsula constraining models of the magnitude and rate of isostatic rebound during deglaciation of the Irish Sea Basin. *Geological Journal* **30,** 157-163.

McCarroll, D. (2001). Deglaciation of the Irish Sea Basin: a critique of the glaciomarine hypothesis. *Journal of Quaternary Science* **16,** 393-404.

McCarroll, D. (2005). North-west Wales. *The Glaciations of Wales and Adjacent Areas,* 27-40.

McGowan, H. A., Sturman, A. P. and Owens, I. F. (1996). Aeolian dust transport and deposition by foehn winds in an alpine environment, Lake Tekapo, New Zealand. *Geomorphology* **15,** 135-146.

McGowan, H. A. and Sturman, A. P. (1997). Characteristics of aeolian grain transport over a fluvio-glacial lacustrine braid delta, Lake Tekapo, New Zealand. *Earth Surface Processes and Landforms* **22,** 773-784.

Mejdahl, V. (1979). Thermoluminescene dating: Beta-dose attenuation in quartz grains. *Archaeometry* **21,** 61-72.

Mejdahl, V. (1987). Internal radioactivity in quartz and feldspar grains. *Ancient TL* **5,** 10-17.

Mejdahl, V. and Christiansen, H. H. (1994). Procedures used for luminescence dating of sediments. *Quaternary Geochronology (Quaternary Science Reviews)* **13,** 403-406.

Merritt, J. W. and Auton, C. A. (2000). An outline of the lithostratigraphy and depositional history of Quaternary deposits in the Sellafield district, west Cumbria. *Proceedings of the Yorkshire Geological Society* **53,** 129-154.

Miall, A. D. (1977). A review of the braided-river depositional environment. *Earth-Science Reviews* **13,** 1-62.

Miall, A. D. (1978). Lithofacies types and vertical profile models in braided river deposits: A summary. in Miall, A. D. (Ed), *Fluvial Sedimentology,* Canadian Society of Petroleum Geologists, pp. 597-604.

Miall, A. D. (1985). Architectural-element analysis: a new method of facies analysis applied to fluvial deposits. *Recognition of fluvial depositional systems and their resource potential,* 33-81.

Miall, A. D. (2006). Reconstructing the architecture and sequence stratigraphy of the preserved fluvial record as a tool for reservoir development: A reality check. *American Association of Petroleum Geologists Bulletin* **90,** 989-1002.

Miller, G. H., Mode, W. N., Wolfe, A. P., Sauer, P. E., Bennike, O., Forman, S. L., Short, S. K. and Stafford Jr, T. W. (1999). Stratified interglacial lacustrine sediments from Baffin Island, Arctic Canada: Chronology and paleoenvironmental implications. *Quaternary Science Reviews* **18,** 789-810.

Mix, A. C., Bard, E. and Schneider, R. (2001). Environmental processes of the ice age: land, oceans, glaciers (EPILOG). *Quaternary Science Reviews* **20,** 627-657.

Murray, A. S., Olley, J. M. and Caitcheon, G. G. (1995). Measurement of equivalent doses in quartz from contemporary water-lain sediments using optically stimulated luminescence. *Quaternary Science Reviews* **14,** 365-371.

Murray, A. S., Roberts, R. G. and Wintle, A. G. (1997). Equivalent dose measurement using a single aliquot of quartz. *Radiation Measurements* **27,** 171-184.

Murray, A. S. and Roberts, R. G. (1998). Measurement of the equivalent dose in quartz using a regenerative-dose single-aliquot protocol. *Radiation Measurements* **29,** 503-515.

Murray, A. S. and Wintle, A. G. (1998). Factors controlling the shape of the OSL decay curve in quartz. *Radiation Measurements* **29,** 65-79.

Murray, A. S. and Wintle, A. G. (2000). Luminescence dating of quartz using an improved single-aliquot regenerative-dose protocol. *Radiation Measurements* **32,** 57-73.

Murray, A. S. and Olley, J. M. (2002). Precision and accuracy in the optically stimulated luminescence dating of sedimentary quartz: a status review. *Geochronometria* **21,** 1-16.

Murray, A. S. and Funder, S. (2003). Optically stimulated luminescence dating of a Danish Eemian coastal marine deposit: A test of accuracy. *Quaternary Science Reviews* **22,** 1177-1183.

Murray, A. S. and Wintle, A. G. (2003). The single aliquot regenerative dose protocol: potential for improvements in reliability. *Radiation Measurements* **37,** 377-381.

Murton, J. B., Bateman, M. D., Baker, C. A., Knox, R. and Whiteman, C. A. (2003). The Devensian periglacial record on Thanet, Kent, UK. *Permafrost and Periglacial Processes* **14,** 217-246.

Nathan, R. P. and Mauz, B. (2008). On the dose-rate estimate of carbonate-rich sediments for trapped charge dating. *Radiation Measurements* **43,** 14-25.

Ó Cofaigh, C. and Evans, D. J. A. (2001a). Sedimentary evidence for deforming bed conditions associated with a grounded Irish Sea glacier, southern Ireland. *Journal of Quaternary Science* **16,** 435-454.

Ó Cofaigh, C. and Evans, D. J. A. (2001b). Deforming bed conditions associated with a major ice stream of the last British ice sheet. *Geology* **29,** 795-798.

Ó Cofaigh, C. and Evans, D. J. A. (2007). Radiocarbon constraints on the age of the maximum advance of the British-Irish Ice Sheet in the Celtic Sea. *Quaternary Science Reviews* **26,** 1197-1203.

Ollerhead, J., Huntley, D. J. and Berger, G. W. (1994). Luminescence dating of sediments from Buctouche Spit, New Brunswick. *Canadian Journal of Earth Sciences* **31,** 365-371.

Olley, J. M., Murray, A. and Roberts, R. G. (1996). The effects of disequilibria in the Uranium and Thorium decay chains on burial dose rates in fluvial sediments. *Quaternary Geochronology (Quaternary Science Reviews)* **15,** 751-760.

Olley, J. M., Roberts, R. G. and Murray, A. S. (1997). Disequilibria in the uranium decay series in sedimentary deposits at Allen's Cave, Nullarbor Plain, Australia: implications for dose rate determinations. *Radiation Measurements* **27,** 433-443.

Olley, J. M., Caitcheon, G. G. and Murray, A. S. (1998). The distribution of apparent dose as determined by optically stimulated luminescence in small aliquots of fluvial quartz: implications for dating young sediments. *Quaternary Science Reviews* **17,** 1033-1040.

Olley, J. M., Caitcheon, G. G. and Roberts, R. G. (1999). The origin of dose distributions in fluvial sediments, and the prospect of dating single grains from fluvial deposits using optically stimulated luminescence. *Radiation Measurements* **30,** 207-217.

Olley, J. M., Pietsch, T. and Roberts, R. G. (2004). Optical dating of Holocene sediments from a variety of geomorphic settings using single grains of quartz. *Geomorphology* **60,** 337-358.

Osmond, J. K. and Cowart, J. B. (1982). Groundwater in Ivanovich, M. and Harmon, R. S. (Eds), *Uranium Series Disequilibrium: Applications to Environmental Problems*, Clarendon Press.

Owen, L. A., Bailey, R. M., Rhodes, E. J., Mitchell, W. A. and Coxon, P. (1997). Style and timing of glaciation in the Lahul Himalaya, northern India: A framework for reconstructing late Quaternary palaeoclimatic change in the western Himalayas. *Journal of Quaternary Science* **12,** 83-109.

Owen, L. A., Kamp, U., Spencer, J. Q. and Haserodt, K. (2002). Timing and style of Late Quaternary glaciation in the eastern Hindu Kush, Chitral, northern Pakistan: a review and revision of the glacial chronology based on new optically stimulated luminescence dating. *Quaternary International* **97/98,** 41-55.

Pawley, S. M., Bailey, R. M., Rose, J., Moorlock, B. S. P., Hamblin, R. J. O., Booth, S. J. and Lee, J. R. (2008). Age limits on Middle Pleistocene glacial sediments from OSL dating, north Norfolk, UK. *Quaternary Science Reviews* **27,** 1363-1377.

Peltier, W. R., Shennan, I., Drummond, R. and Horton, B. (2002). On the postglacial isostatic adjustment of the British Isles and the shallow viscoelastic structure of the Earth. *Geophysical Journal International* **148,** 443-475.

Pietsch, T. J., Olley, J. M. and Nanson, G. C. (2008). Fluvial transport as a natural luminescence sensitiser of quartz. *Quaternary Geochronology* **3,** 365-376.

Prescott, J. R. and Hutton, J. T. (1994). Cosmic ray contributions to dose rates for luminescence and ESR dating: large depths and long-term time variation. *Radiation Measurements* **23,** 497-500.

Punning, J. M. and Raukas, A. (1983). The age of tills: problems and methods in Evenson, E. B., Schlüchter, C. and Rabassa, J. (Eds), *Tills and related deposits*, pp. 357-364.

Raukas, A. and Stankowski, W. (2005). Influence of sedimentological composition on OSL dating of glaciofluvial deposits: examples from Estonia. *Geological Quarterly* **49,** 463-470.

Reimer, P., Baillie, M., Bard, E., Bayliss, A., Beck, J., Bertrand, C., Blackwell, P., Buck, C., Burr, G., Cutler, K., Damon, P., Edwards, R., Fairbanks, R., Friedrich, M., Guilderson, T., Hughen, K., Kromer, B., McCormac, F., Manning, S., BronkRamsey, C., Reimer, R., Remmele, S., Southon, J., Stuiver, M., Talamo, S., Taylor, F., Plicht, J. v. d. and Weyhenmeyer, C. (2004). *Radiocarbon* **46,** 1029-1058.

Rendell, H. M., Webster, S. E. and Sheffer, N. L. (1994). Underwater bleaching of signals from sediment grains: new experimental data. *Quaternary Geochronology (Quaternary Science Reviews)* **13,** 433-435.

Rhodes, E., Bronk Ramsey, C., Outram, Z., Batt, C., Willis, L., Dockrill, S. and Bond, J. (2003). Bayesian methods applied to the interpretation of multiple OSL dates: high precision sediment ages from Old Scatness Broch excavations, Shetland Isles. *Quaternary Science Reviews* **22,** 1231-1244.

Rhodes, E. J. and Pownall, L. (1994). Zeroing of the OSL signal in quartz from young glaciofluvial sediments. *Radiation Measurements* **23,** 581-585.

Rhodes, E. J. and Bailey, R. M. (1997). The effect of thermal transfer on the zeroing of the luminescence of quartz from recent glaciofluvial sediments. *Quaternary Geochronology (Quaternary Science Reviews)* **16,** 291-298.

Rhodes, E. J. (2000). Observations of thermal transfer OSL signals in glacigenic quartz. *Radiation Measurements* **32,** 595-602.

Richards, B. W. M. (2000). Luminescence dating of Quaternary sediments in the Himalaya and High Asia: a practical guide to its use and limitations for constraining the timing of glaciation. *Quaternary International* **65/66,** 49-61.

Roberts, D., Dackombe, R. V. and Thomas, G. S. P. (2007). Palaeo-ice streaming in the central sector of the British-Irish Ice Sheet during the Last Glacial Maximum: evidence from the northern Irish Sea Basin. *Boreas* **36,** 115-129.

Roberts, D. H., Chiverrell, R. C., Innes, J. B., Horton, B. P., Brooks, A. J., Thomas, G. S. P., Turner, S. and Gonzalez, S. (2006). Holocene sea levels, Last Glacial Maximum glaciomarine environments and geophysical models in the northern Irish Sea Basin, UK. *Marine Geology* **231,** 113-128.

Roberts, H. M., Muhs, D. R., Wintle, A. G., Duller, G. A. T. and Bettis Iii, E. A. (2003). Unprecedented last-glacial mass accumulation rates determined by luminescence dating of loess from western Nebraska. *Quaternary Research* **59,** 411-419.

Rodnight, H. (2006). Developing a luminescence chronology for late Quaternary fluvial change in South African floodplain wetlands, *Unpublished PhD thesis*, University of Wales, Aberystwyth.

Rodnight, H., Duller, G. A. T., Wintle, A. G. and Tooth, S. (2006). Assessing the reproducibility and accuracy of optical dating of fluvial deposits. *Quaternary Geochronology (Quaternary Science Reviews)* **1,** 109-120.

Roesch, W. C. and Attix, F. H. (1968). Basic concepts of dosimetry in Attix, F. H., Roesch, W. C. and Tochilin, E. (Eds), *Radiation Dosimetry*, Academic Press.

Rust, B. R. (1972). Structure and process in a braided river. *Sedimentology* **18,** 221-245.

Sambrook Smith, G. H. (2000). Small-scale cyclicity in alpine proglacial fluvial sedimentation. *Sedimentary Geology* **132,** 217-231.

Sanderson, D. C. W., Bishop, P., Stark, M., Alexander, S. and Penny, D. (2007). Luminescence dating of canal sediments from Angkor Borei, Mekong Delta, Southern Cambodia. *Quaternary Geochronology* **2,** 322-329.

Scourse, J., Austin, W. E. N., Bateman, R. M., Catt, J. R., Evans, C. D. R., Robinson, J. E. and Young, J. R. (1990). Sedimentology and micropalaeontology of glacimarine sediments from the central and southwestern Celtic Sea. in Dowdeswell, J. A. and Scourse, J. (Eds), *Glacimarine Environments: Processes and Sediments*, Geological Society (London) Special Publication.

Scourse, J. (1991a). Glacial deposits of the Isles of Scilly. *Glacial deposits in Great Britain and Ireland*, 291-300.

Scourse, J., Robinson, E. and Evans, C. (1991). Glaciation of the central and southwestern Celtic Sea. *Glacial deposits in Great Britain and Ireland*, 301-310.

Scourse, J. D. (1991b). Late Pleistocene stratigraphy and palaeobotany of the Isles of Scilly. *Philosophical Transactions - Royal Society of London, B* **334,** 405-448.

Scourse, J. D., Hall, I. R., McCave, I. N., Young, J. R. and Sugdon, C. (2000). The origin of Heinrich layers: evidence from H2 for European precursor events. *Earth and Planetary Science Letters* **182,** 187-195.

Scourse, J. D. and Furze, M. F. A. (2001). A critical review of the glaciomarine model for Irish sea deglaciation: evidence from southern Britain, the Celtic shelf and adjacent continental slope. *Journal of Quaternary Science* **16,** 419-434.

Scourse, J. D., Evans, D. J. A., Hiemstra, J. F., McCarroll, D. and Rhodes, E. J. (2004). Late Devensian glaciation of the Isles of Scilly: QRA Research Fund Report. *Quaternary Newsletter* **102,** 49-54.

Scourse, J. D., Evan, D. J. A., Hiemstra, J. F., McCarroll, D., Rhodes, E. and Furze, M. F. A. (2006). Pleistocene stratigraphy, geomorphology and geochronology in Scourse, J. D. (Ed), *The Isles of Scilly: Field Guide*, Quaternary Research Association.

Sejrup, H. P., Haflidason, H., Aarseth, I., King, E., Forsberg, C. F., Long, D. and Rokoengen, K. (1994). Late Weichselian glaciation history of the northern North Sea. *Boreas* **23.**

Sejrup, H. P., Larsen, E., Landvik, J., King, E. L., Haflidason, H. and Nesje, A. (2000). Quaternary glaciations in southern Fennoscandia: Evidence from southwestern Norwary and the northern North Sea region. *Quaternary Science Reviews* **19,** 667-685.

Sejrup, H. P., Hjelstuen, B. O., Dahlgren, K. I. T., Haflidason, H., Kuijpers, A., Nygaard, A., Praeg, D., Stoker, M. S. and Vorren, T. O. (2005). Pleistocene glacial history of the NW European continental margin. *Marine and Petroleum Geology* **22,** 1111-1129.

Shapiro, S. S. and Wilk, M. B. (1965). An analysis of variance test for normality (complete samples). *Biometrika* **52,** 591-611.

Shennan, I., Bradley, S., Milne, G., Brooks, A., Bassett, S. and Hamilton, S. (2006). Relative sea-level changes, glacial isostatic modelling and ice-sheet reconstructions from the British Isles since the Last Glacial Maximum. *Journal of Quaternary Science* **21,** 585-599.

Siegenthaler, C. and Huggenberger, P. (1993). Pleistocene Rhine gravel: deposits of a braided river system with dominant pool preservation. *Braided rivers,* 147-162.

Singarayer, J. and Bailey, R. (2003). Further investigations of the quartz optically stimulated luminescence components using linear modulation. *Radiation Measurements* **37,** 451-458.

Singarayer, J. and Bailey, R. (2004). Component-resolved bleaching spectra of quartz optically stimulation luminescence: preliminary results and implications for dating. *Radiation Measurements* **38,** 111-118.

Smart, P. L. and Frances, P. D. (Eds) (1991). *Quaternary dating methods - a user's guide. Technical Guide 4.*, Quaternary Research Association.

Smith, B. W. and Rhodes, E. J. (1994). Charge movements in quartz and their relevance to optical dating. *Radiation Measurements* **23,** 329-333.

Smith, N. D. (1974). Sedimentology and bar formation in the Upper Kicking Horse River, a braided outwash stream. *Journal of Geology* **82,** 205-223.

Spencer, J. Q. and Owen, L. A. (2004). Optically stimulated luminescence dating of Late Quaternary glaciogenic sediments in the upper Hunza valley: validating the timing of glaciation and assessing dating methods. *Quaternary Science Reviews* **23,** 175-191.

Spooner, N. A. (1994). The anomalous fading of infrared-stimulated luminescence from feldspars. *Radiation Measurements* **23,** 625-632.

Stokes, C. R. and Clark, C. (2001). Palaeo-ice streams. *Quaternary Science Reviews* **20,** 1437-1457.

Stokes, S. (1992). Optical dating of young (modern) sediments using quartz: results from a selection of depositional environments. *Quaternary Science Reviews* **11,** 153-159.

Summers, A. J. (1981). Succession and sedimentation of glacigenic deposits in eastern County Wexford, Ireland., University of Liverpool, Unpublished PhD Thesis.

Synge, F. M. (1978). Pleistocence events in Davies, G. L. and Stephens, N. (Eds), *Ireland*, Methuen and Co Ltd., pp. 115-180.

Synge, F. M. (1981). Quaternary glaciation and changes of sea level in the south of Ireland. *Geologie en Mijnbouw* **60,** 305-315.

Tabachnick, B. G. and Fidell, L. S. (1996). *Using multivariate statistics*, 3rd ed. edn. Harper Collins.

Telfer, M. W., Bateman, M. D., Carr, A. S. and Chase, B. M. (2008). Testing the applicability of a standardized growth curve (SGC) for quartz OSL dating: Kalahari dunes, South African coastal dunes and Florida dune cordons. *Quaternary Geochronology* **3,** 137-142.

Thomas, G. S. P. (1977). The Quaternary of the Isle of Man. in Kidson, C. and Tooley, M. J. (Eds), *Quaternary History of the Irish Sea.*

Thomas, G. S. P. and Summers, A. J. (1982). Drop-stone and allied structures from Pleistocene waterlain till at Ely House, County Wexford. *Journal of Earth Science Royal Dublin Society* **4,** 109-119.

Thomas, G. S. P. and Summers, A. J. (1983). The Quaternary Stratigraphy between Blackwater Harbour and Tinnaberna, County Wexford. *Journal of Earth Science Royal Dublin Society* **5,** 121-134.

Thomas, G. S. P. (1984). The origin of the glacio-dynamic structure of the Bride Moraine, Isle of Man. *Boreas* **13,** 355-364.

Thomas, G. S. P. and Summers, A. J. (1984). Glaciodynamic structures from the Blackwater Formation, Co. Wexford, Ireland. *Boreas* **13,** 5-12.

Thomas, G. S. P. (1985). The Quaternary of the northern Irish Sea Basin. in Johnson, R. H. (Ed), *The geomorphology of north-west England.*, Manchester University Press.

Thomas, G. S. P., Connaughton, M. and Dackombe, R. V. (1985). Facies variation in a Late Pleistocene supraglacial outwash sandur from the Isle of Man. *Geological Journal* **20,** 193-213.

Thomas, G. S. P. and Dackombe, R. V. (1985). Comment on "Glaciomarine sediments of the Isle of Man as a key to late Pleistocene stratigraphic investigations in the Irish Sea Basin". *Geology* **13,** 445-446.

Thomas, G. S. P. and Kerr, P. (1987). The stratigraphy, sedimentology and palaeontology of the Pleistocene Knocknasilloge Member, Co. Wexford, Ireland. *Geological Journal* **22,** 67-82.

Thomas, G. S. P., Chester, D. K. and Crimes, P. (1998). The Late Devensian glaciation of the eastern Lleyn Peninsula, North Wales: evidence for terrestrial depositional environments. *Journal of Quaternary Science* **13,** 255-270.

Thomas, G. S. P. and Chiverrell, R. C. (2003). The sand and gravel resources of North West Wales, Report to the Welsh Assembly Government, 77pp. plus 7 Appendices.

Thomas, G. S. P., Chiverrell, R. C. and Huddart, D. (2004). Ice-marginal depositional responses to readvance episodes in the Late Devensian deglaciation of the Isle of Man. *Quaternary Science Reviews* **23,** 85-106.

Thomas, G. S. P., Chiverrell, R. C., Huddart, D., Long, D. and Roberts, D. (2006). The Ice Age. in Chiverrell, R. C. and Thomas, G. S. P. (Eds), *A New History of the Isle of Man: The Evolution of the Natural Landscape*, Liverpool University Press.

Thomas, G. S. P. and Chiverrell, R. C. (2007). Structural and depositional evidence for repeated ice-marginal oscillation along the eastern margin of the Late Devensian Irish Sea Ice Stream. *Quaternary Science Reviews* **26,** 2375-2405.

Thomas, G. S. P. and Chiverrell, R. C. (submitted). Extent and timing of the Last Glacial Maximum (LGM) in Britain and Ireland. *QRA Special Issue.*

Thomas, G. S. P., Chiverrell, R. C. and Foster, G. C. (submitted). The morphology and structure of the Late Devensian Kirkham moraine system, central Lancashire, England.

Thorne, M. C., Merritt, J. W., Wingfield, R. T. R., Tooley, M. J. and Clayton, K. M. (1997). *Quaternary evolution of the Sellafield Area, Cumbria.* Nirex Science Report.

Tiddeman, R. H. (1872). On the evidence for the ice sheet in north Lancashire and adjacent parts of Yorkshire and Westmoreland. *Quaterly Journal of the Geological Society of London* **28,** 471-489.

Trotter, F. M., Hollingworth, S. E., Eastwood, T. and Rose, W. C. C. (1937). *The geology of the Gosforth District.* Memoir of the Geological Survey of the United Kingdom.

Tsukamoto, S., Asahi, K., Watanabe, T. and Rink, W. J. (2002). Timing of past glaciations in Kanchenjunga Himal, Nepal by optically stimulated luminescence dating of tills. *Quaternary International* **97-98,** 57-67.

Tsukamoto, S., Rink, W. J. and Watanuki, T. (2003). OSL of tephric loess and volcanic quartz in Japan and an alternative procedure for estimating De from a fast OSL component. *Radiation Measurements* **37,** 459-465.

Van der Meer, J. J. M., Verbers, A. and Warren, W. P. (1994). The micromorphological character of the Ballycroneen Formation (Irish Sea Till): a first assessment in Warren, W. P. and Croot, D. (Eds), *Formation and Deformation of Glacial Deposits*, Balkema, pp. 39-49.

Van Landeghem, K. J. J., Wheeler, A. J. and Mitchell, N. C. (2008). Seafloor evidence for palaeo-ice streaming and calving of the grounded Irish Sea Ice Stream: Implications for the interpretation of its final deglaciation phase. *Boreas* **38,** 119-131.

Wallinga, J., Murray, A. and Duller, G. (2000). Underestimation of equivalent dose in single-aliquot optical dating of feldspars caused by preheating. *Radiation Measurements* **32,** 691-695.

Wallinga, J. (2002). Optically stimulated luminescence dating of fluvial deposits: a review. *Boreas* **31,** 303-322.

Warren, W. P. (1985). Stratigraphy in Edwards, K. J. and Warren, W. P. (Eds), *The Quaternary History of Ireland*, Academic Press, pp. 35-65.

Warren, W. P. (1993). *Wicklow in the Ice Age: an Introduction and Guide to the Glacial Geology of the Wicklow District.* Geological Survey of Ireland Publication.

Whittow, J. B. and Ball, D. F. (1970). North-west Wales in Lewis, C. A. (Ed), *The Glaciations of Wales and Adjoining Regions*, Longman, pp. 21-58.

Williams, G. D., Brabham, P. J., Eaton, G. P. and Harris, C. (2001). Late Devensian glaciotectonic deformation at St Bees, Cumbria: a critical wedge model. *Journal of the Geological Society, London.* **158,** 125-135.

Williams, P. F. and Rust, B. R. (1969). The sedimentology of a braided river. *Journal of Sedimentary Petrology* **39,** 649-679.

Wintle, A. G. (1973). Anomalous fading of thermo-luminescence in mineral samples. *Nature* **245,** 143-144.

Wintle, A. G. and Catt, J. A. (1985). Thermoluminescence dating of Dimlington Stadial deposits in eastern England. *Boreas* **14,** 231-234.

Wintle, A. G. (1990). A review of current research on TL dating of loess. *Quaternary Science Reviews* **9,** 385-397.

Wintle, A. G. (1997). Luminescence dating: Laboratory procedures and protocols. *Radiation Measurements* **27,** 769-817.

Wintle, A. G. and Murray, A. S. (2000). Quartz OSL: Effects of thermal treatment and their relevance to laboratory dating procedures. *Radiation Measurements* **32,** 387-400.

Wintle, A. G. and Murray, A. S. (2006). A review of quartz optically stimulated luminescence characteristics and their relevance in single-aliquot regeneration dating protocols. *Radiation Measurements* **41,** 369-391.

Zhou, Y. L., Lu, H. Y., Mason, J., Miao, X. D., Swinehart, J. and Goble, R. (2008). Optically stimulated luminescence dating of aeolian sand in the Otindag dune field and Holocene climate change. *Science in China, Series D: Earth Sciences* **51,** 837-847.

Zimmerman, D. W. (1971). Thermoluminescence dating using fine grains from pottery. *Archaeometry* **13,** 29-52.

APPENDIX A

OSL DECAY CURVES

The figures below show natural-OSL decay curves for a selection of both *accepted* and *rejected* small aliquots of each sample. Stimulation time was 40 seconds and stimulation power was ~30 mW cm^{-2} (90% power of the Risø blue LEDs). Sensitivity-corrected regenerated (L_x) and test dose (T_x) values were derived from the OSL signal counts obtained from the initial 0.8 seconds of the OSL decay curves, minus a background estimate obtained in the last 8 seconds consisting of instrument 'noise' and any remaining slower bleaching signal components. *See Appendix B for dose-response curves for each of the aliquots illustrated here.* Varying intensity of OSL is observed from aliquot to aliquot together with differing rates of decay of OSL with time, indicative of either a medium/slow component or feldspar contamination.

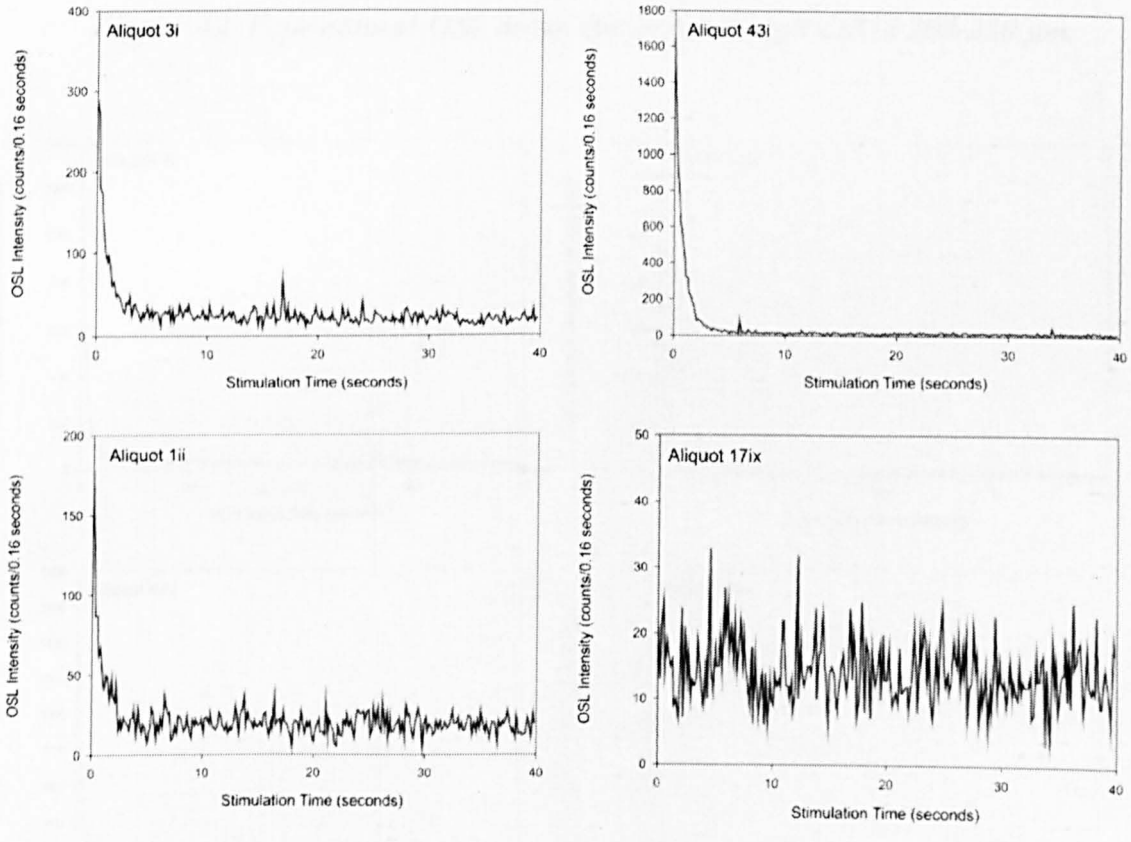

Figure A1 *Four natural-OSL decay curves for sample OR14 90-125 μm.*

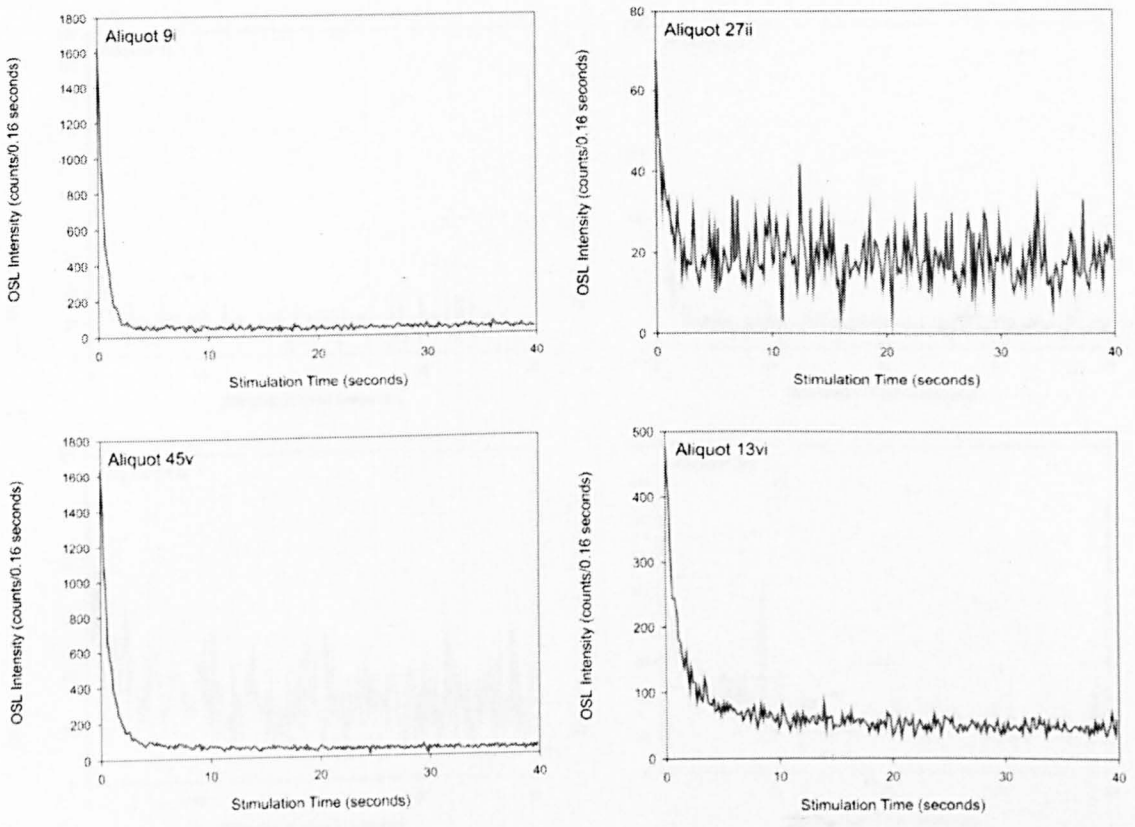

Figure A2 *Four natural-OSL decay curves for sample OR14 200-250 µm.*

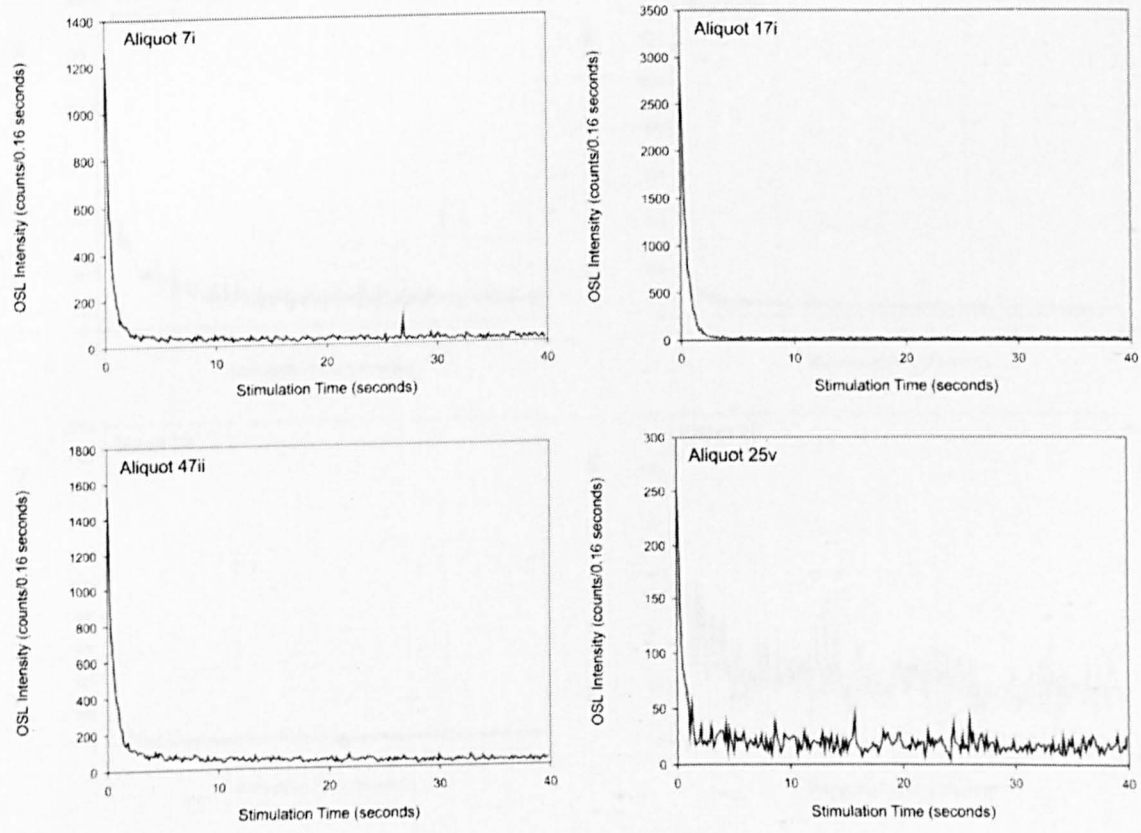

Figure A3 *Four natural-OSL decay curves for sample OR15 90-125 µm.*

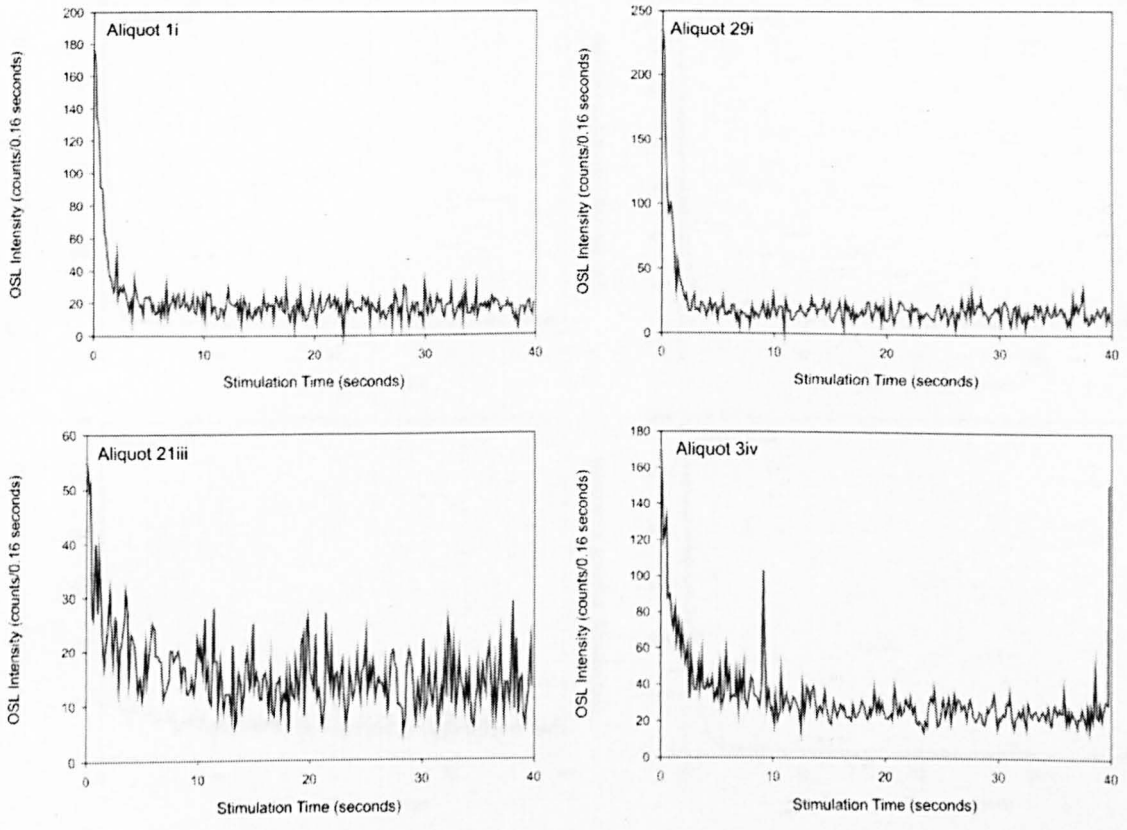

Figure A4 *Four natural-OSL decay curves for sample OR22 90-125 μm.*

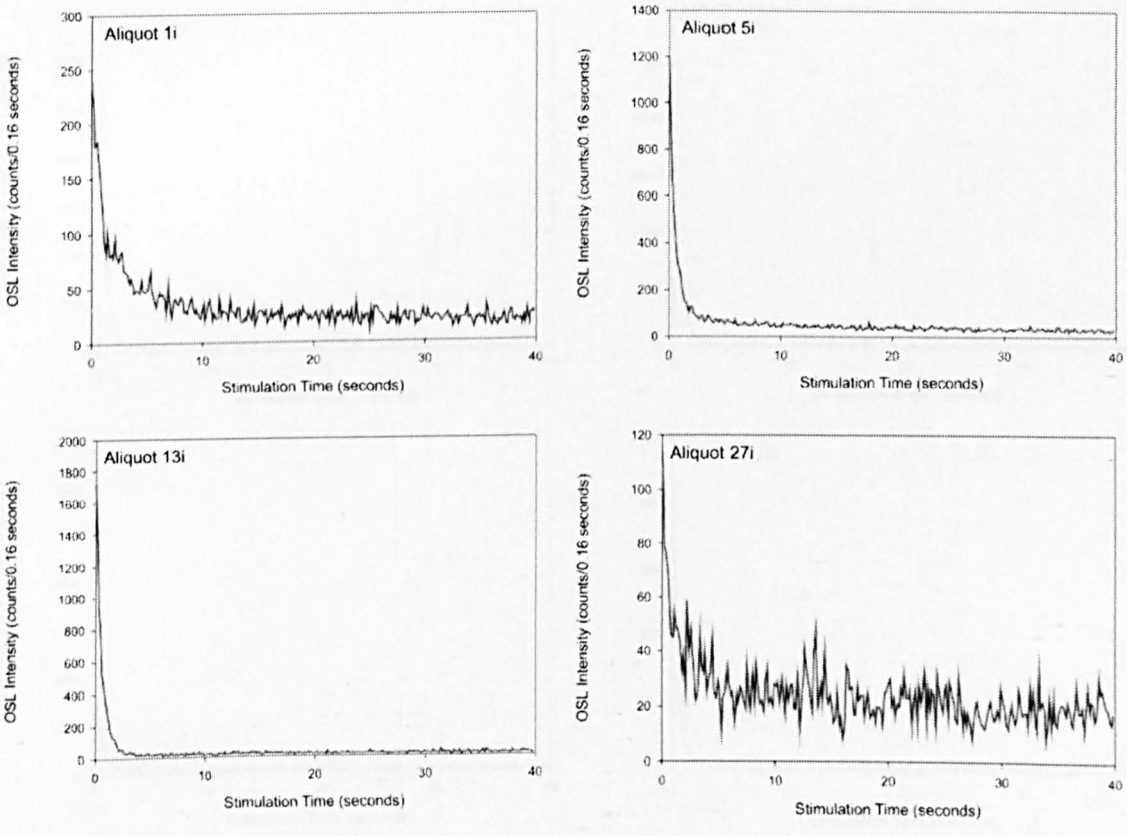

Figure A5 *Four natural-OSL decay curves for sample OR22 150-180 μm.*

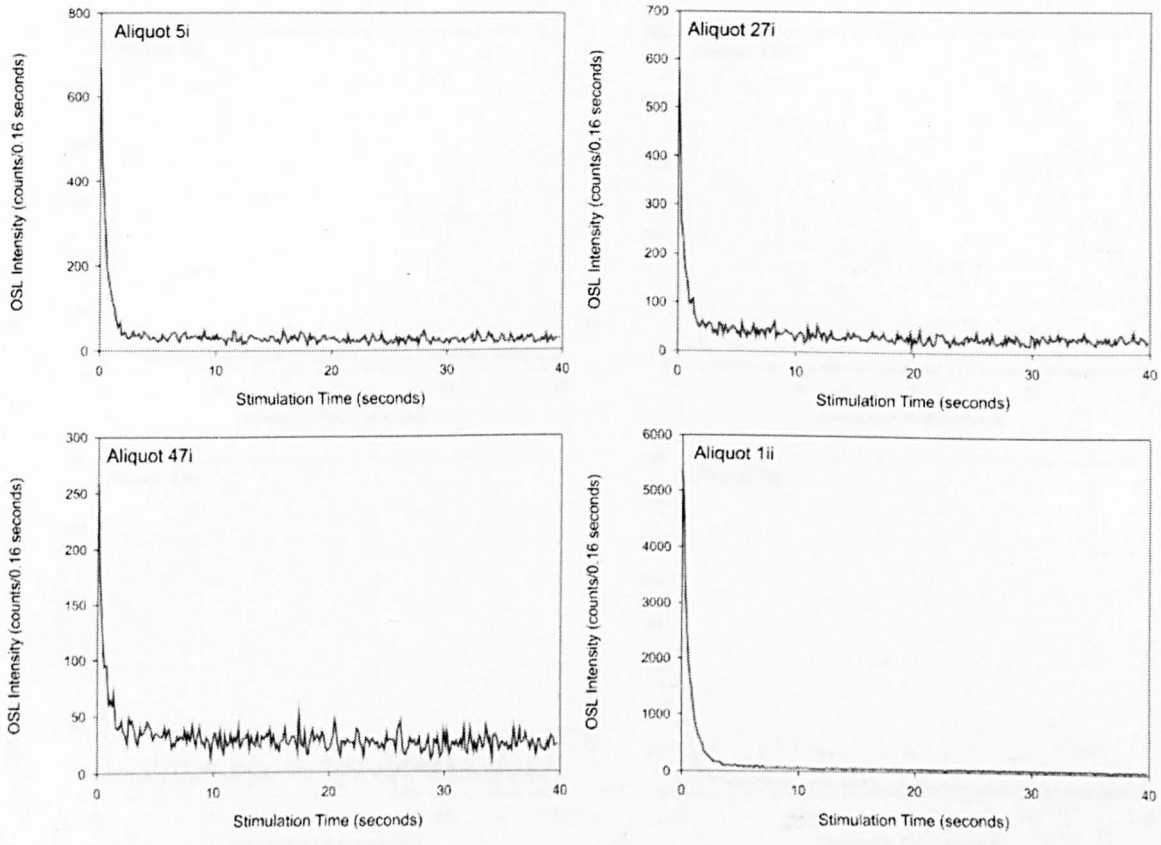

Figure A6 *Four natural-OSL decay curves for sample OR26 90-125 μm.*

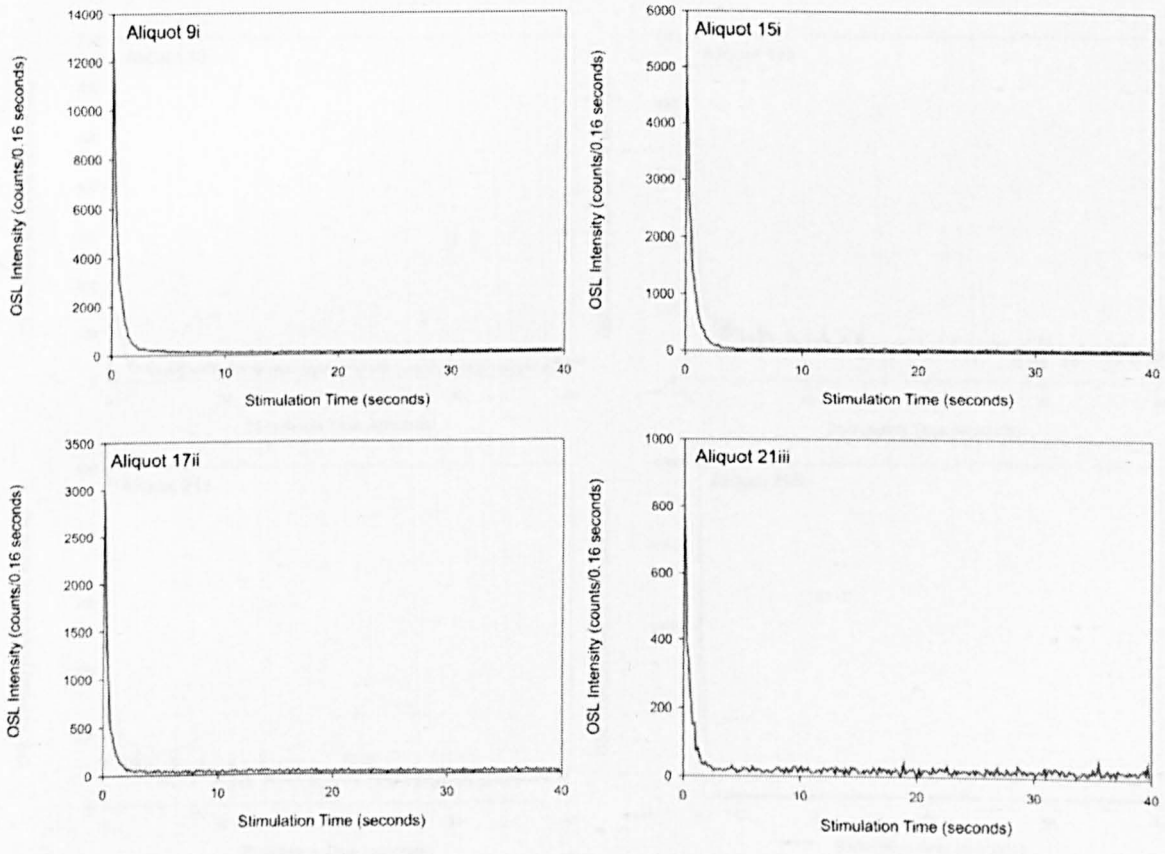

Figure A7 *Four natural-OSL decay curves for sample BLA1 90-125 μm.*

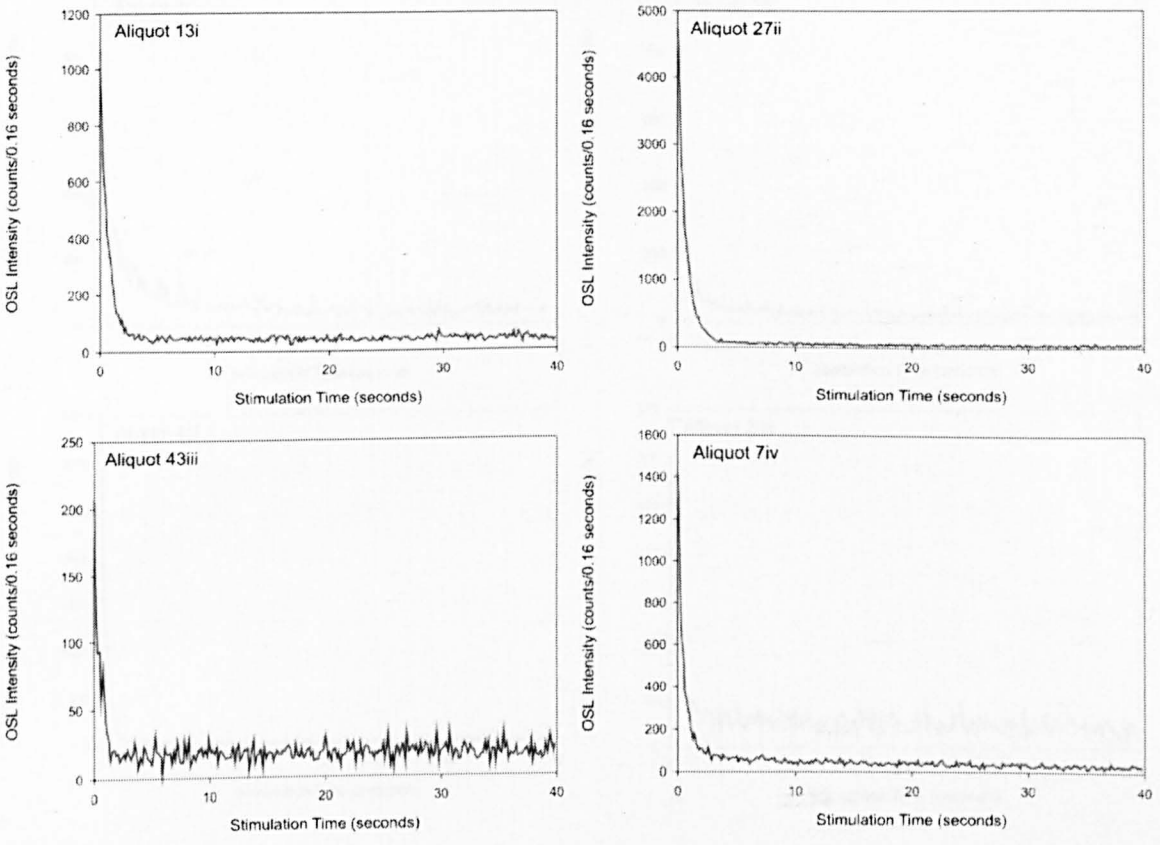

Figure A8 *Four natural-OSL decay curves for sample BLA1 180-212 μm.*

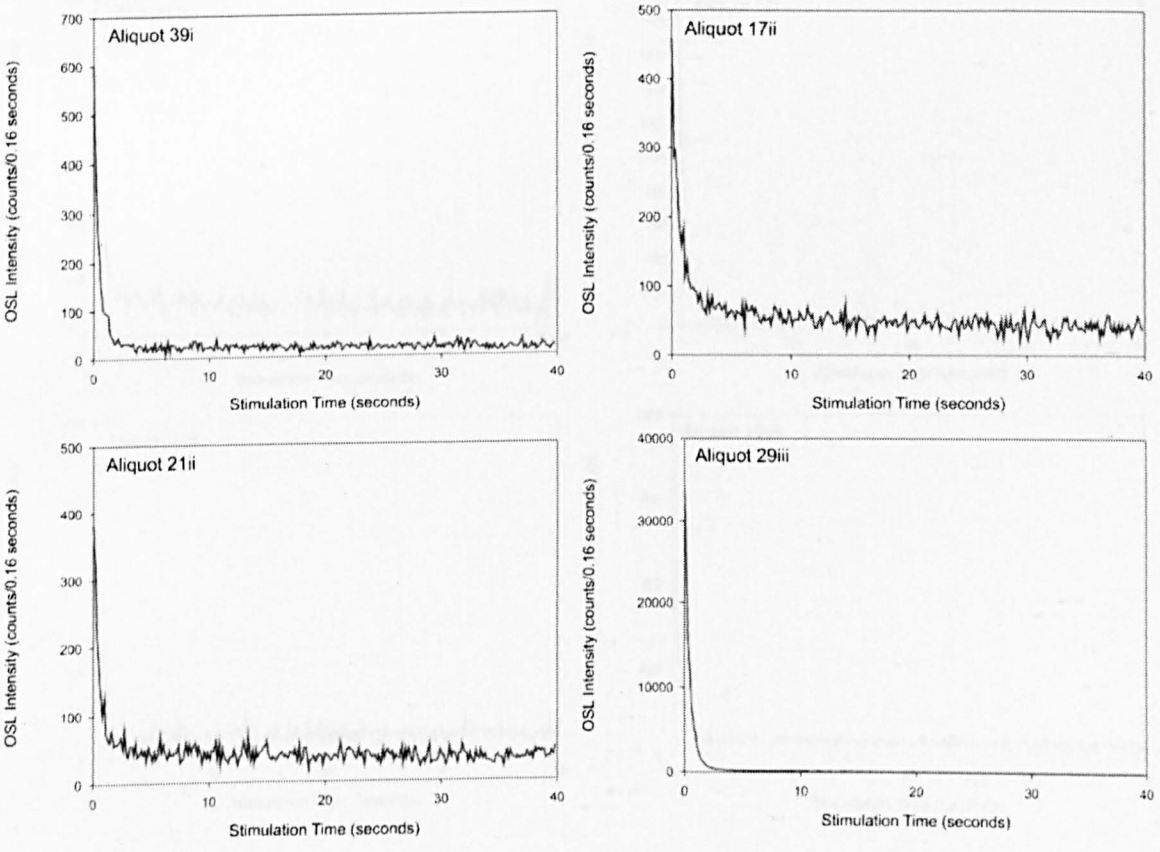

Figure A9 *Four natural-OSL decay curves for sample BLA3 90-125 μm.*

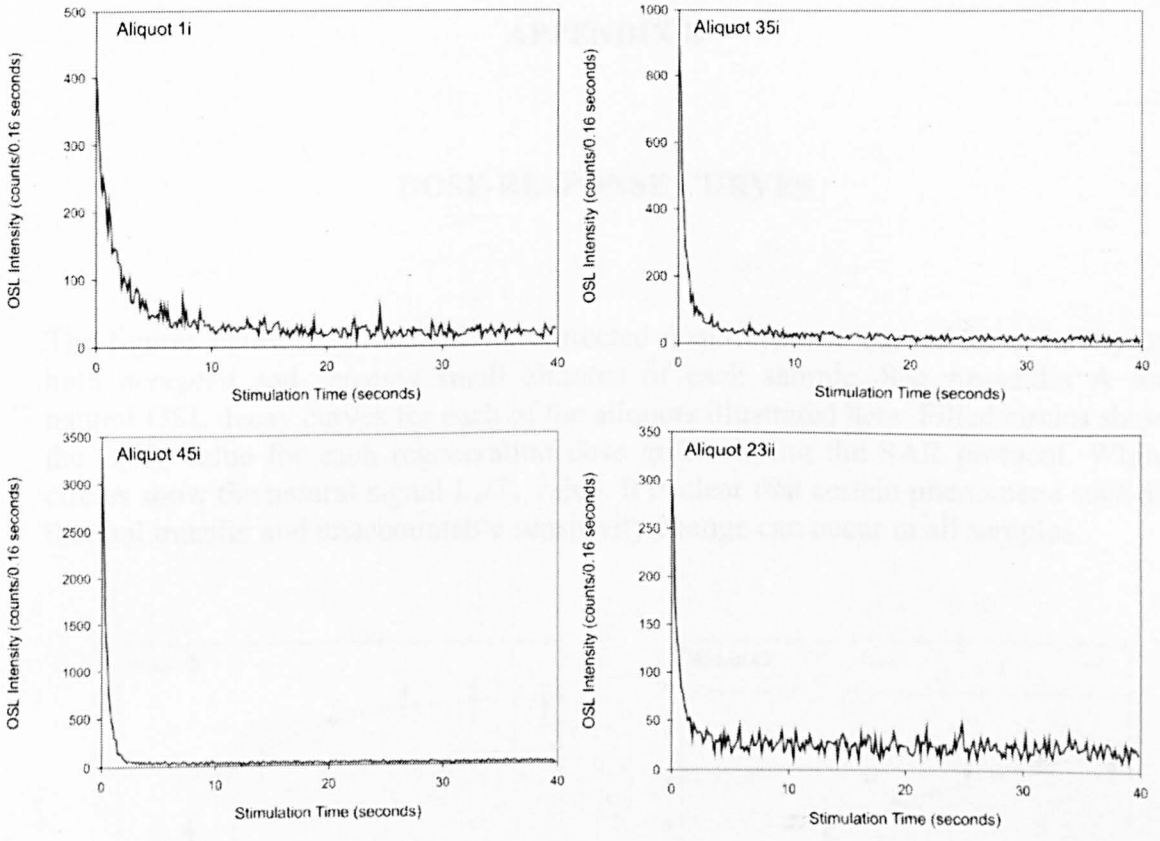

Figure A10 *Four natural-OSL decay curves for sample BLA3 212-250 μm.*

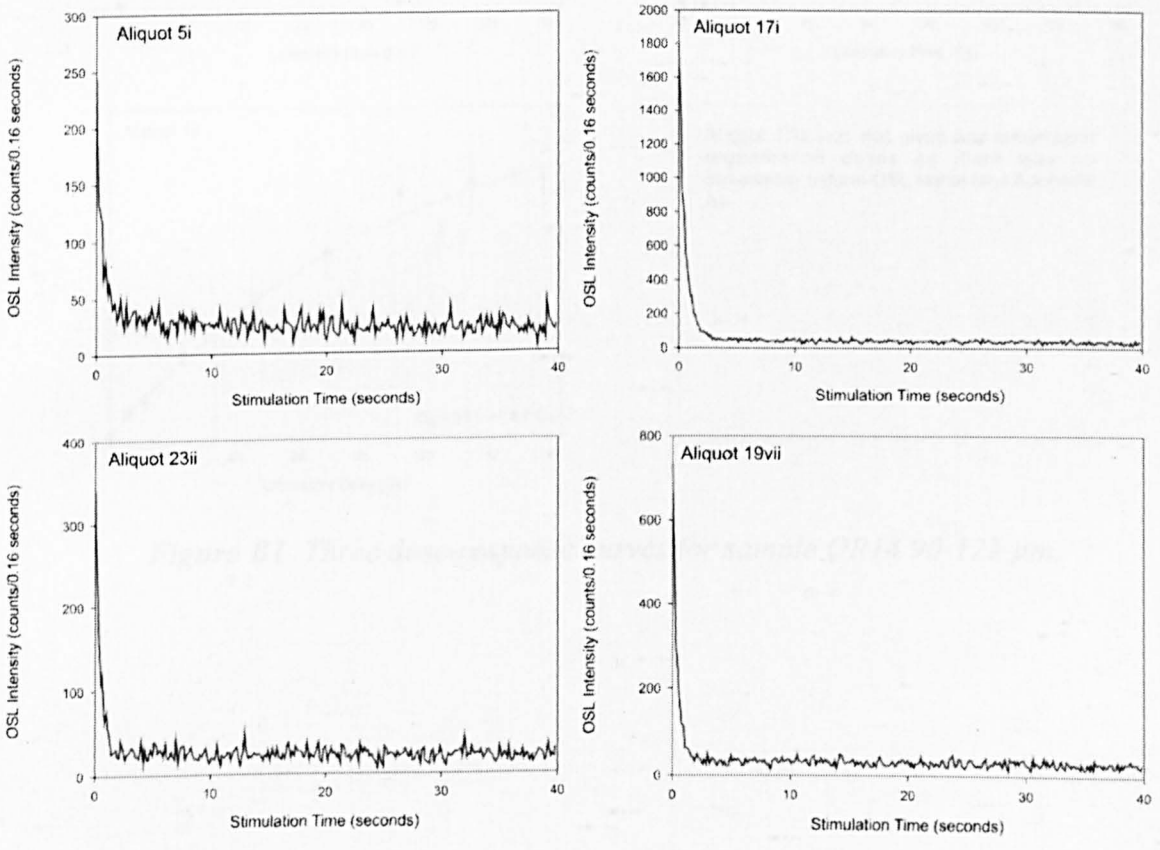

Figure A11 *Four natural-OSL decay curves for sample NEF4 90-125 μm.*

APPENDIX B

DOSE-RESPONSE CURVES

The figures below show sensitivity-corrected dose-response curves for a variety of both *accepted* and *rejected* small aliquots of each sample. See Appendix A for natural-OSL decay curves for each of the aliquots illustrated here. Filled circles show the L_x/T_x value for each regeneration dose given during the SAR protocol. White circles show the natural signal L_x/T_x value. It is clear that certain phenomena such as thermal transfer and unaccountable sensitivity change can occur in all samples.

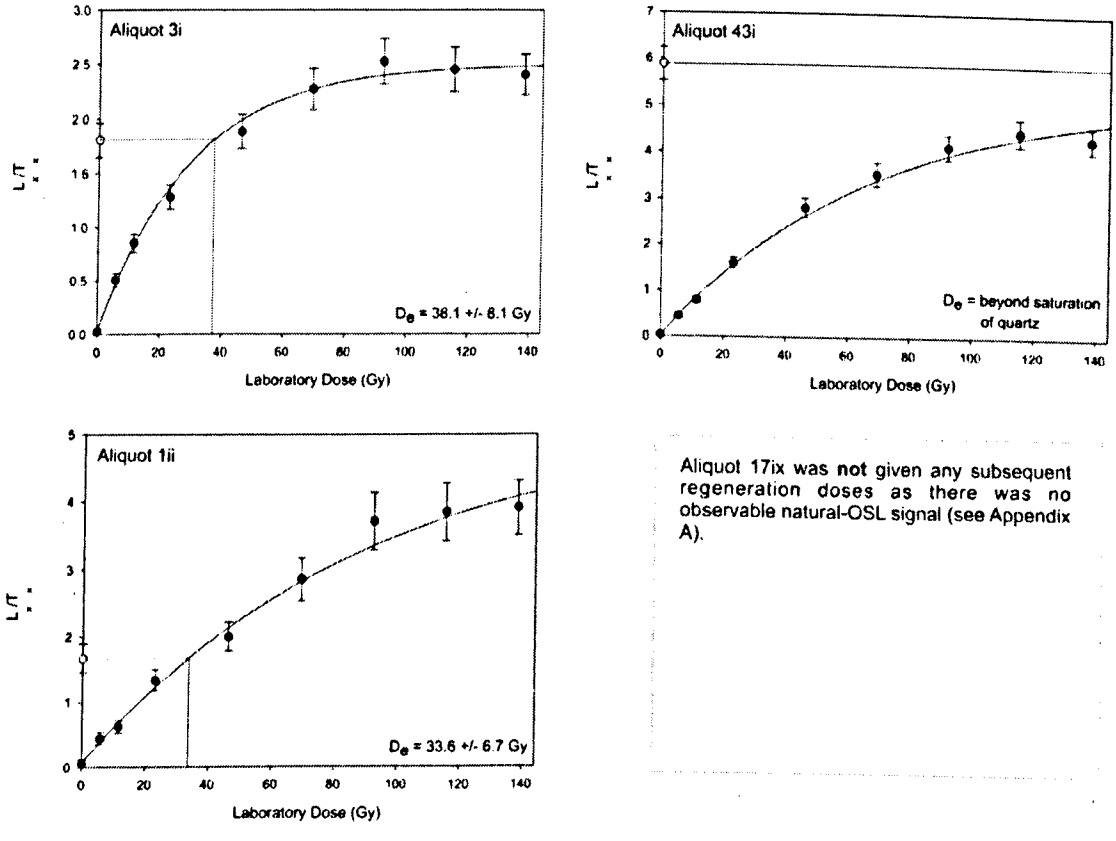

Figure B1 *Three dose-response curves for sample OR14 90-125 μm.*

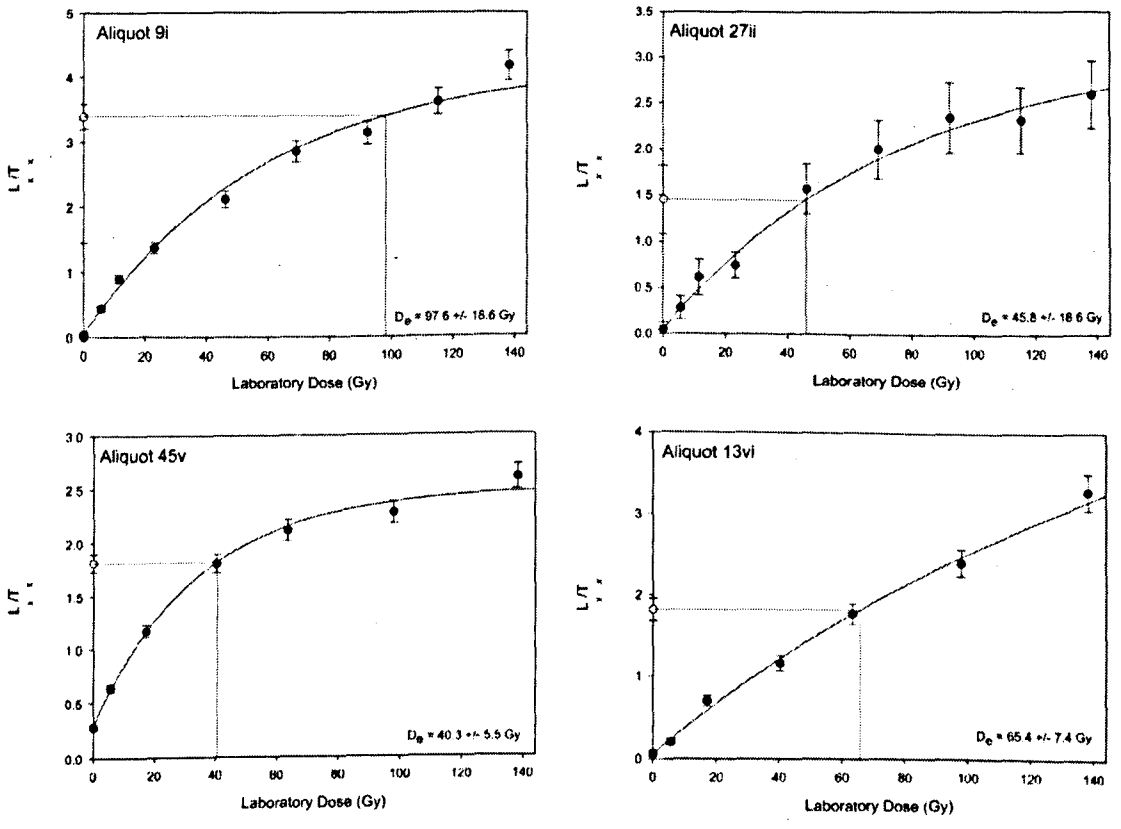

Figure B2 *Four dose-response curves for sample OR14 200-250 μm.*

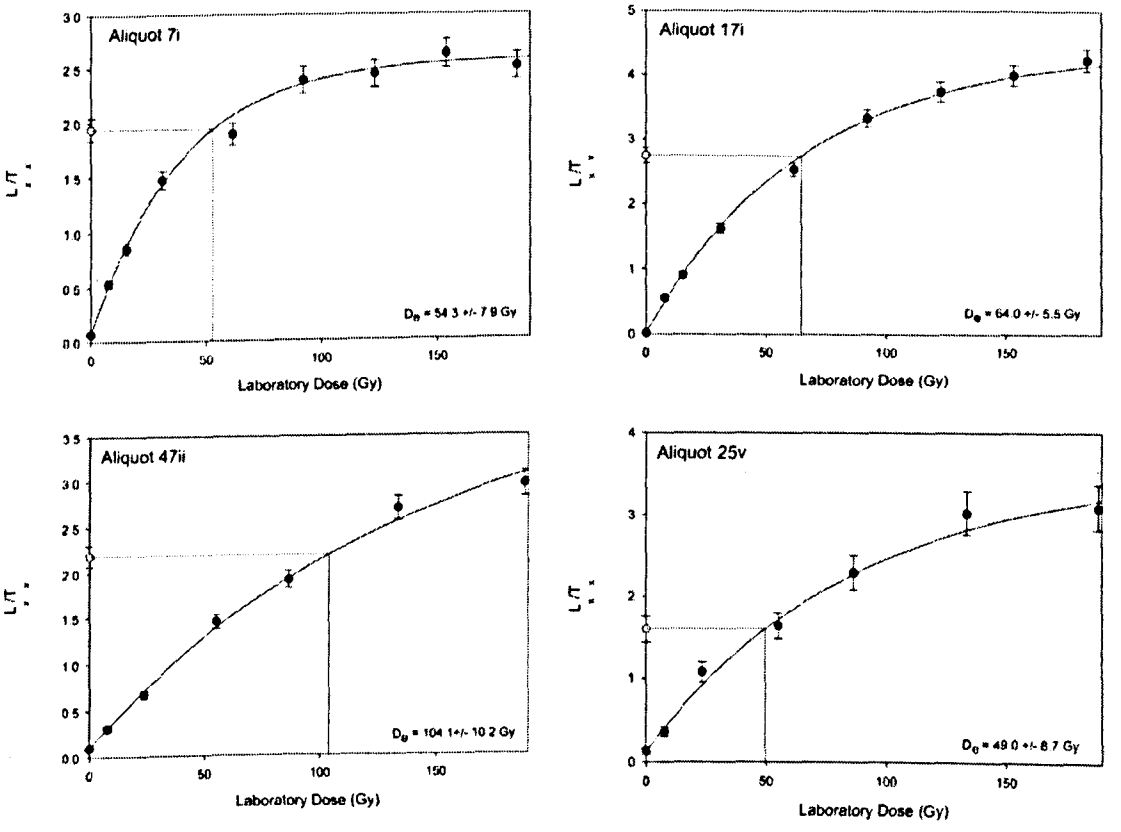

Figure B3 *Four dose-response curves for sample OR15 90-125 μm.*

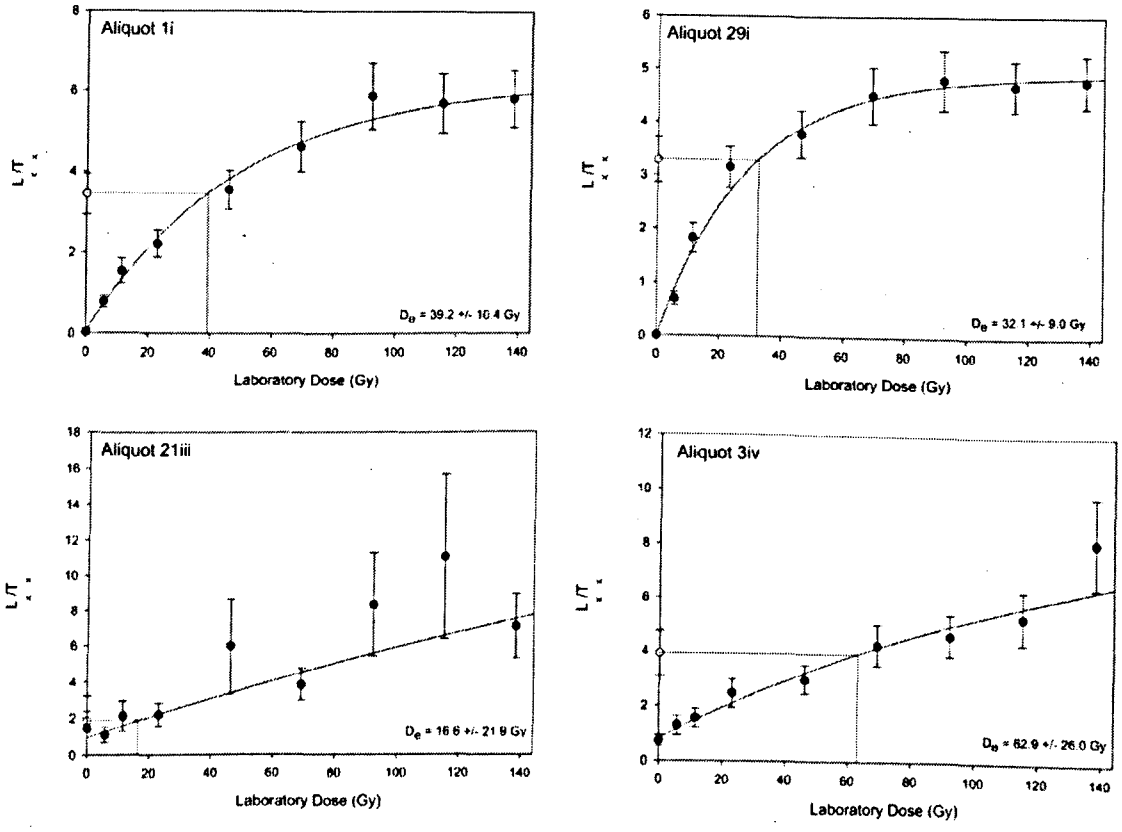

Figure B4 *Four dose-response curves for sample OR22 90-125 μm.*

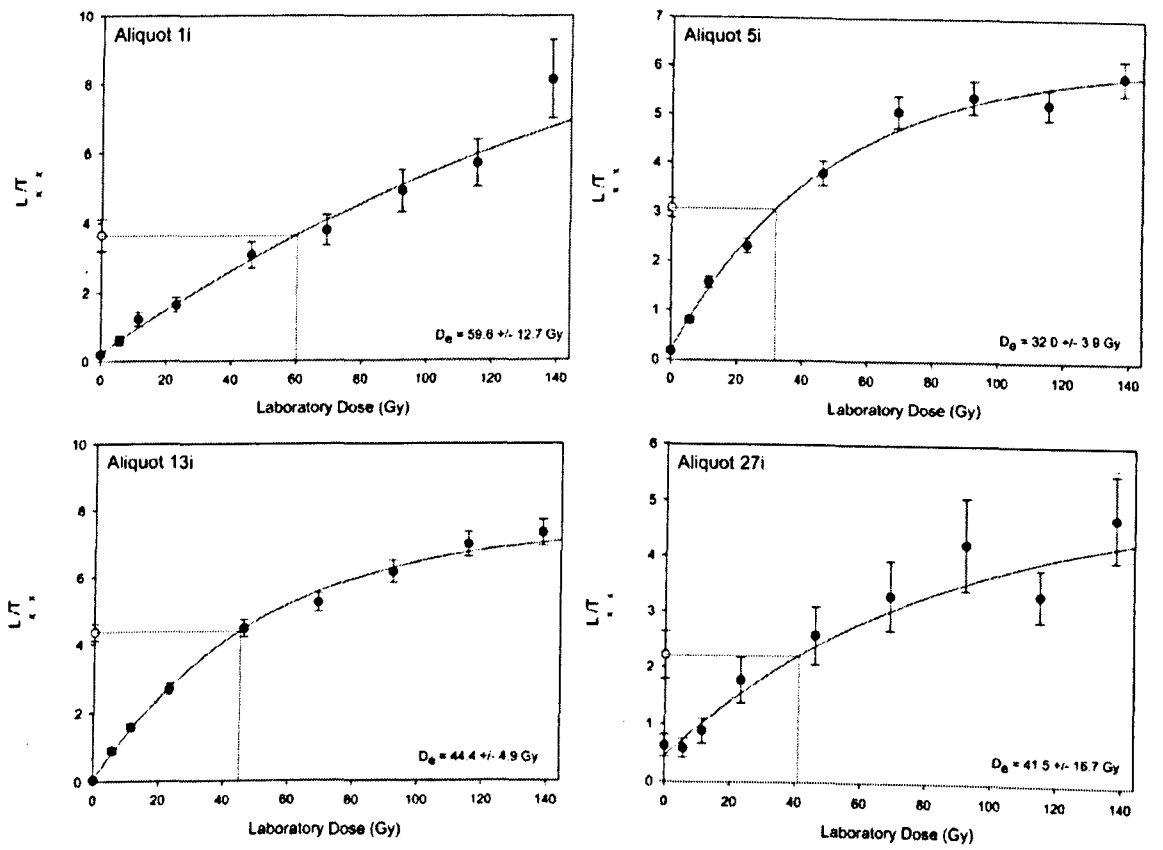

Figure B5 *Four dose-response curves for sample OR22 150-180 μm.*

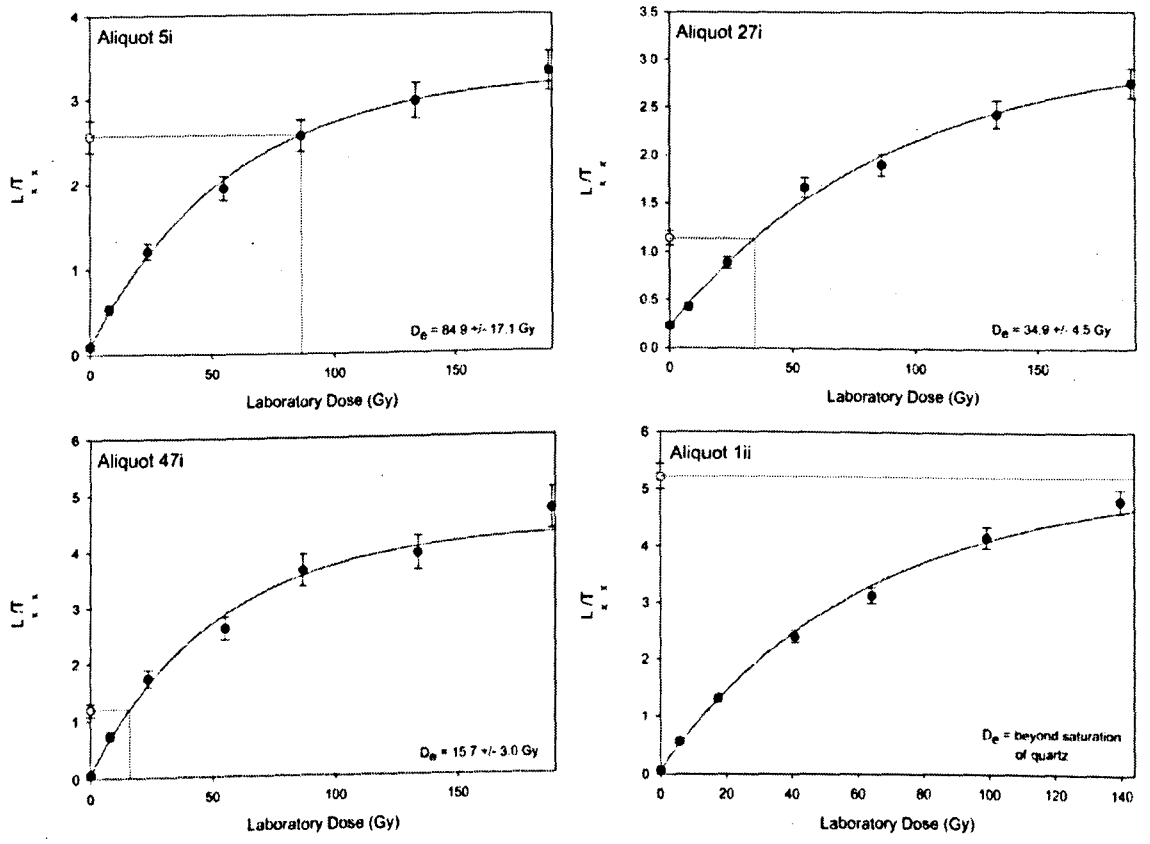

Figure B6 *Four dose-response curves for sample OR26 90-125 μm.*

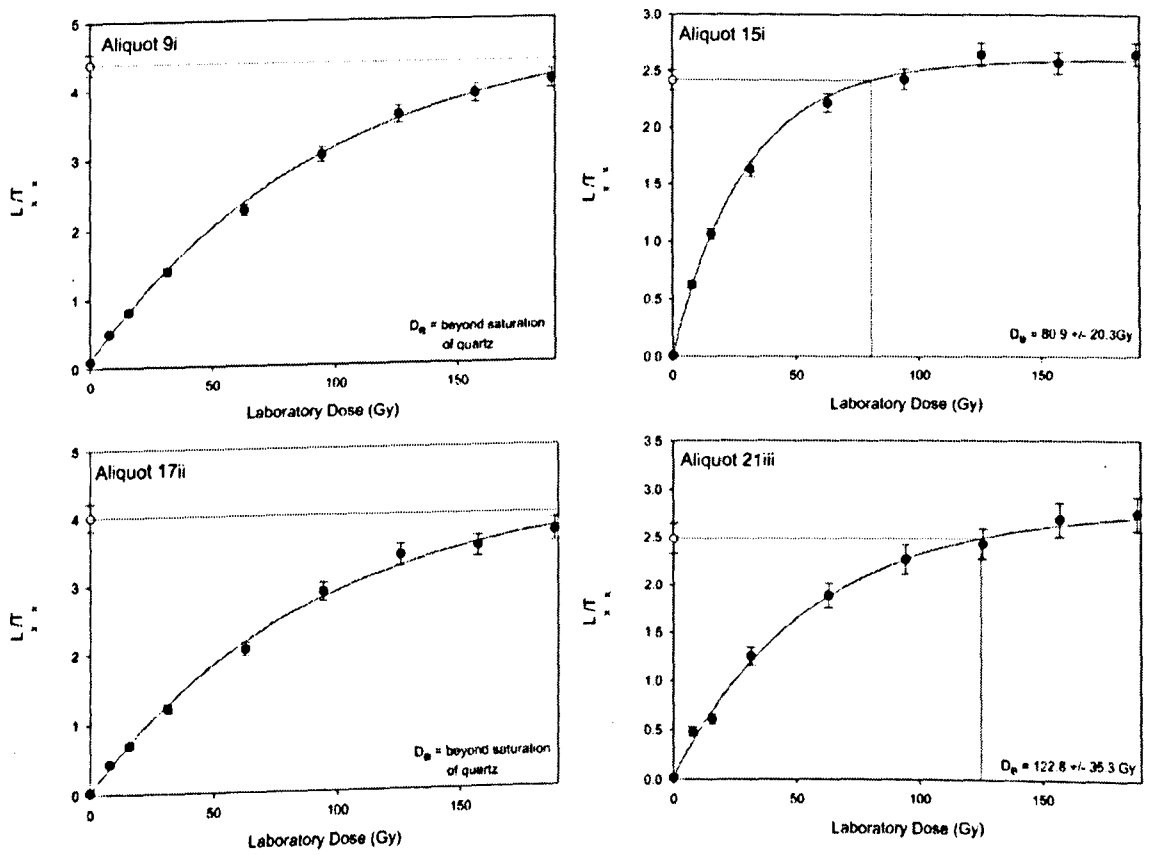

Figure B7 *Four dose-response curves for sample BLA1 90-125 μm.*

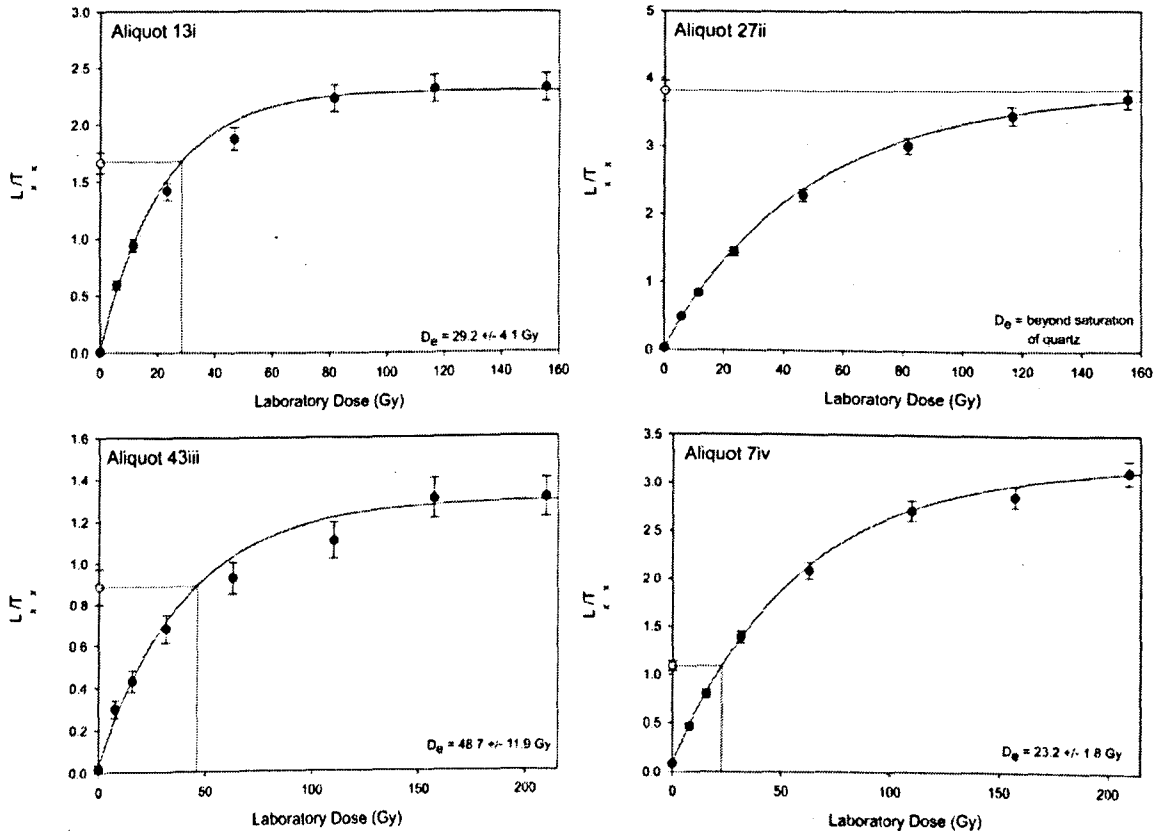

Figure B8 *Four dose-response curves for sample BLA1 180-212 μm.*

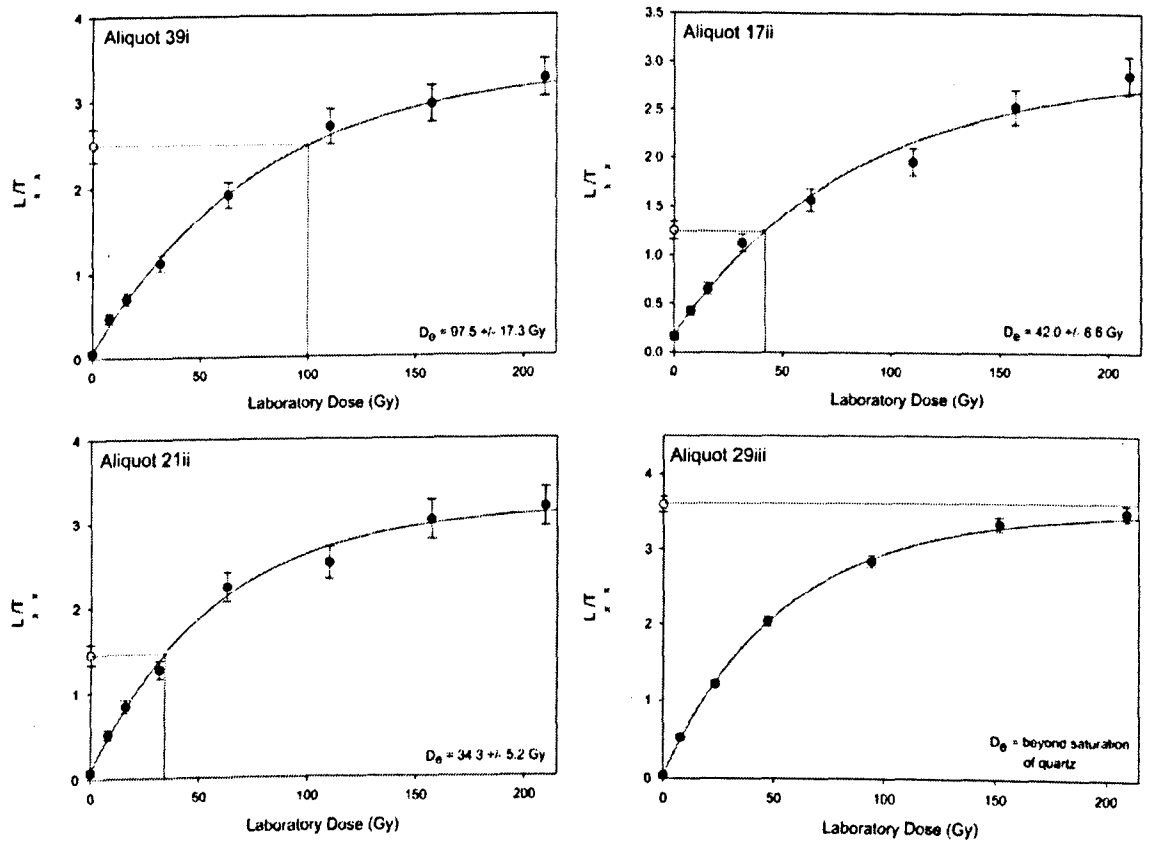

Figure B9 *Four dose-response curves for sample BLA3 90-125 μm.*

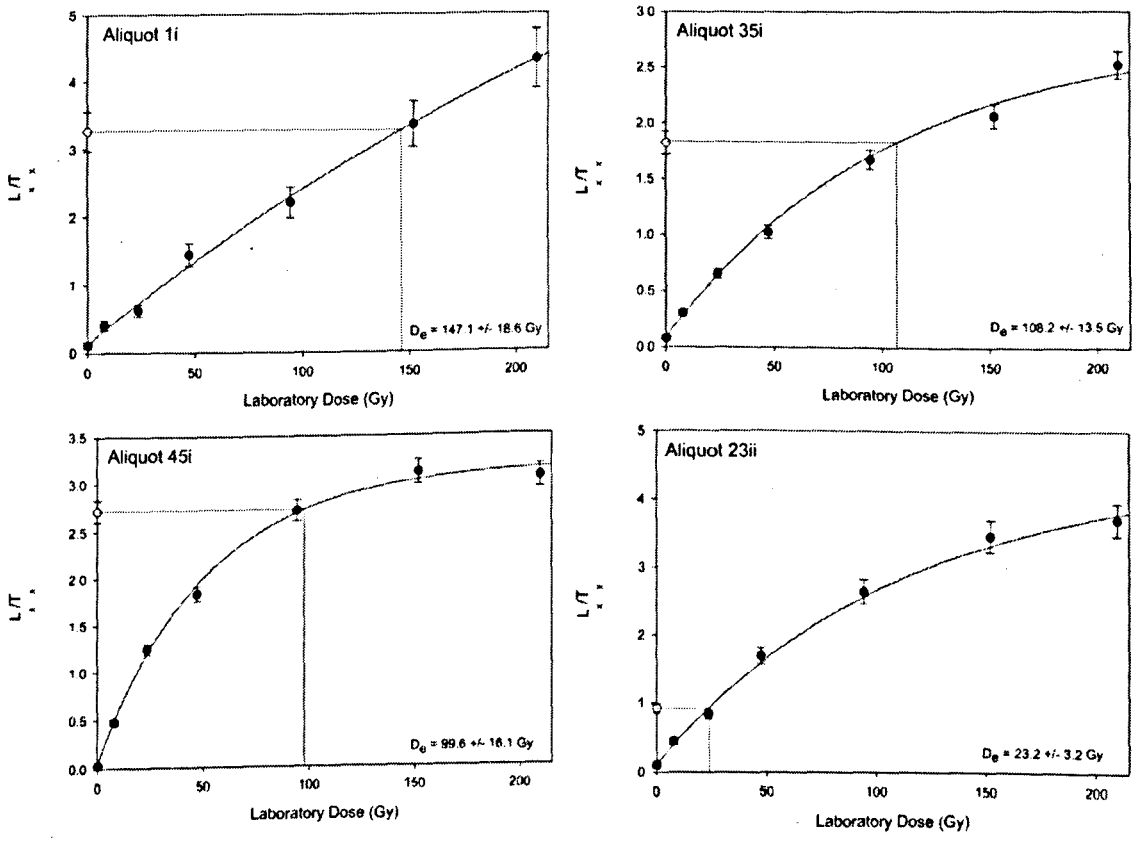

Figure B10 *Four dose-response curves for sample BLA3 212-250 μm.*

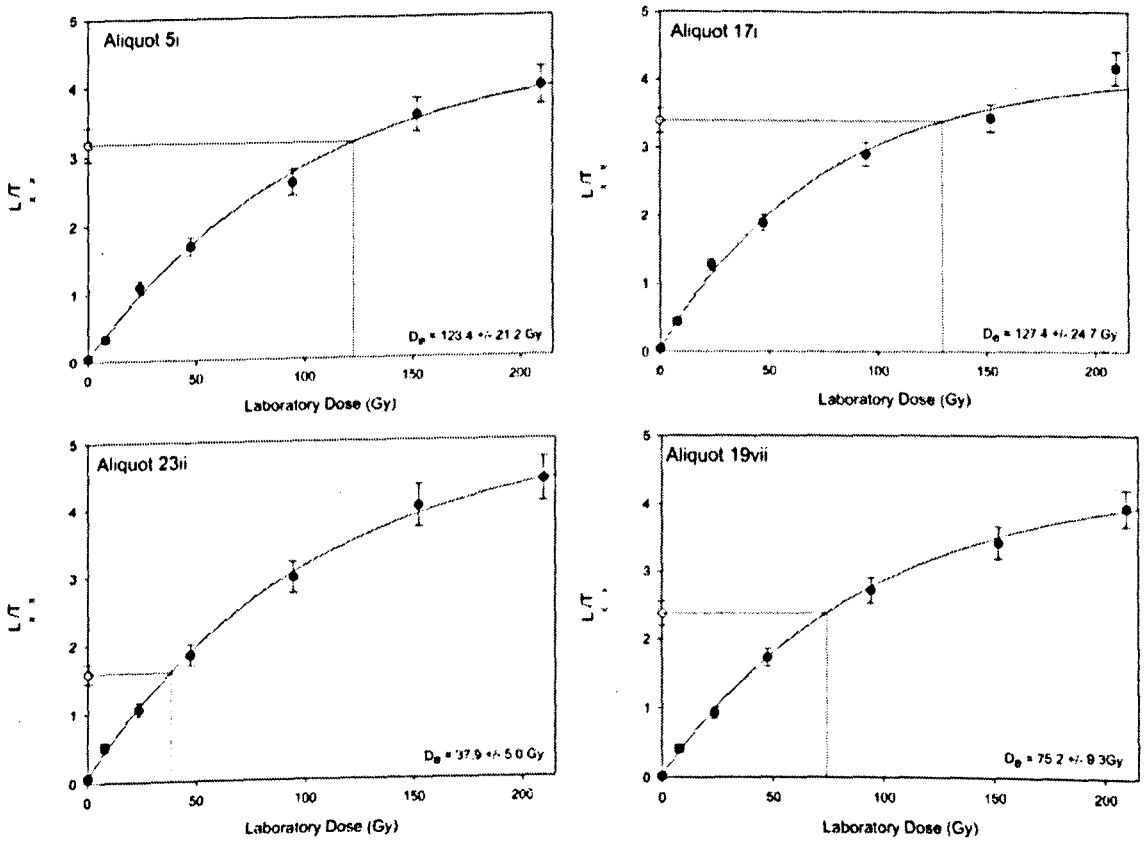

Figure B11 *Four dose-response curves for sample NEF4 90-125 μm.*

APPENDIX C

LM-OSL & CW-OSL CURVE FITTING PARAMETERS

The following tables (C1 – C6) contain the parameters derived from deconvolution of the LM-OSL curves shown in Figure 4.7, detailing the number of trapped electrons (n) and the detrapping probability (b) for each component. The best fit number of components is highlighted in bold. Individual component photoionisation cross-sections can be calculated by using the dividing the detrapping probability (b) by maximum stimulation light intensity (7.3×10^{16} .s^{-1}.cm^{-2}).

Table C1 *OR22; 90-125 μm (AL1i)*

Number of components	2	3	4	5
r^2	0.864	0.895	**0.897**	0.897
n1	4.5×10^4	4.3×10^4	**4.3×10^4**	4.2×10^4
b1	2.6045	2.7075	**2.7935**	2.8043
n2	1.1×10^5	2.8×10^4	**5.6×10^3**	4.4×10^3
b2	0.0028	0.0339	**0.2296**	0.3063
n3		1.1×10^5	**2.8×10^4**	2.4×10^4
b3		0.0019	**0.0235**	0.0304
n4			**1.0×10^5**	8.1×10^4
b4			**0.0017**	0.0025
n5				5.3×10^4
b5				0.0004

Table C2 OR22; 90-125 μm (AL5i)

Number of components	2	3	4
r^2	0.724	**0.742**	0.742
n1	2.6×10^4	**2.5×10^4**	2.5×10^4
b1	2.6267	**2.7110**	2.7172
n2	7.5×10^4	**1.2×10^4**	1.0×10^4
b2	0.0009	**0.0317**	0.0379
n3		**7.9×10^4**	2.8×10^4
b3		**0.0007**	0.0019
n4			1.6×10^7
b4			1.0235×10^{-6}

Table C3 BLA1; 90-125 μm (AL37iii)

Number of components	2	3	4
r^2	0.690	**0.708**	0.708
n1	2.3×10^4	**2.2×10^4**	2.2×10^4
b1	2.3864	**2.5207**	2.5207
n2	6.2×10^4	**1.1×10^4**	1.1×10^4
b2	0.0034	**0.0543**	0.0543
n3		**5.8×10^4**	4.3×10^4
b3		**0.0029**	0.0029
n4			1.6×10^4
b4			0.0029

Table C4 BLA1; 90-125 μm (AL39iii)

Number of components	2	3	4	5
r^2	0.970	0.979	**0.981**	0.981
n1	1.3×10^5	1.3×10^5	$\mathbf{1.3 \times 10^5}$	1.3×10^5
b1	3.3630	3.4128	**3.4368**	3.4609
n2	2.3×10^5	4.9×10^4	$\mathbf{2.8 \times 10^4}$	7.8×10^3
b2	0.0020	0.0279	**0.0629**	0.2077
n3		2.2×10^5	$\mathbf{9.0 \times 10^4}$	2.8×10^4
b3		0.0014	**0.0048**	0.0359
n4			$\mathbf{2.0 \times 10^5}$	1.0×10^5
b4			**0.0007**	0.0037
n5				1.9×10^5
b5				0.0005

Table C5 NEF4; 90-125 μm (AL13vi)

Number of components	2	3	4
r^2	0.970	**0.971**	0.971
n1	9.7×10^4	$\mathbf{9.7 \times 10^4}$	5.5×10^4
b1	2.2393	**3.3662**	3.3607
n2	2.2×10^4	$\mathbf{2.0 \times 10^4}$	4.0×10^5
b2	0.0114	**0.0147**	2.5×10^9
n3		$\mathbf{2.8 \times 10^3}$	4.2×10^4
b3		**0.0679**	3.3610
n4			2.2×10^4
b4			0.0171

Table C6 NEF4; 90-125 (AL21vi)

Number of components	2	3	4
r^2	0.673	**0.674**	0.674
n1	1.7×10^4	**1.7×10^4**	1.6×10^4
b1	1.9639	**2.9475**	2.9798
n2	1.8×10^4	**1.8×10^4**	2.8×10^4
b2	0.0172	**0.0258**	1.2×10^{10}
n3		**1.3×10^{-9}**	2.7×10^3
b3		**7.8×10^{-16}**	0.0904
n4			1.6×10^4
b4			0.0216

The tables below contain the parameters derived from deconvolution of the CW-OSL curves shown in Figure 4.8, detailing the number of trapped electrons (n) and the detrapping probability (b) for each component. The best fit number of components is highlighted in bold. Individual component photoionisation cross-sections can be calculated by using the dividing the detrapping probability (b) value by maximum stimulation light intensity (8.06×10^{15} .s^{-1}.cm^{-2}).

Table C7 OR22; 90-125 μm (AL17ii)

Number of components	2	3
r^2	**0.994**	0.994
n1	**4.1×10^3**	4.1×10^3
b1	**0.2212**	0.2212
n2	**8.5×10^3**	8.5×10^3
b2	**0.0031**	0.0031
n3		5.1×10^{-7}
b3		1.8380

Table C8 *OR22; 90-125 μm (AL27ii)*

Number of components	2	3	4
r^2	0.985	**0.986**	0.986
n1	2.0×10^3	**2.0×10^3**	2.0×10^3
b1	0.2626	**0.2640**	0.2626
n2	1.3×10^4	**3.7×10^2**	1.3×10^4
b2	0.0020	**0.0187**	0.0020
n3		**1.3×10^6**	2.1×10^{-4}
b3		**0.00002**	1.1×10^{-12}
n4			1.0×10^{-3}
b4			1.7×10^{-11}

Table C9 *BLA3; 90-125 (AL15v)*

Number of components	2	3	4
r^2	0.998	**0.999**	0.999
n1	1.7×10^4	**1.7×10^4**	1.7×10^4
b1	0.2778	**0.2799**	0.2778
n2	1.1×10^4	**6.6×10^2**	1.1×10^4
b2	0.0067	**0.0589**	0.0067
n3		**1.5×10^4**	2.9×10^{-4}
b3		**0.0041**	1.1×10^{-12}
n4			1.0×10^{-3}
b4			1.7×10^{-11}

Table C10 *BLA3; 90-125 (AL33v)*

Number of components	2	3	4
r^2	0.972	**0.973**	0.972
n1	1.9×10^3	**1.9×10^3**	1.9×10^3
b1	0.2545	**0.2545**	0.2483
n2	1.3×10^4	**1.3×10^4**	1.5×10^4
b2	0.0076	**0.0077**	0.0067
n3		**1.0×10^{-3}**	1.6×10^{-6}
b3		**1.1×10^{-10}**	3.0×10^{-38}
n4			3.4×10^{-32}
b4			6.0×10^7

Table C11 *NEF4; 90-125 μm (AL25vii)*

Number of components	2	3
r^2	**0.971**	0.971
n1	**1.4×10^3**	1.4×10^3
b1	**0.3348**	0.3348
n2	**9.9×10^3**	9.9×10^3
b2	**0.0047**	0.0047
n3		1.0×10^{-3}
b3		1.1×10^{-10}

Table C12 NEF4; 90-125 μm (AL7vii)

Number of components	2	3	4
r^2	0.954	**0.956**	0.954
n1	1.7×10^3	**1.3×10^3**	1.7×10^3
b1	0.1758	**0.2045**	0.1758
n2	1.0×10^4	**2.9×10^3**	1.0×10^4
b2	0.0090	**0.0293**	0.0090
n3		**3.5×10^6**	1.0×10^{-3}
b3		**0.00001**	1.7×10^{-11}
n4			2.2×10^{-4}
b4			1.1×10^{-12}